

*J. Green*



BEHAVIOR CLASSIFICATION OF SHORT REINFORCED CONCRETE  
COLUMNS SUBJECTED TO CYCLIC DEFORMATIONS

APPROVED BY SUPERVISORY COMMITTEE:

James J. Gusa  
John E. Green  
Richard Klugner  
Clive H. Lynn  
Karl A. Frank

TO MY PARENTS

BEHAVIOR CLASSIFICATION OF SHORT REINFORCED CONCRETE  
COLUMNS SUBJECTED TO CYCLIC DEFORMATIONS

by

KYLE ANDREW WOODWARD, B.S.C.E., M.S.C.E.

DISSERTATION

Presented to the Faculty of the Graduate School of

The University of Texas at Austin

in Partial Fulfillment

of the Requirements

for the Degree of

DOCTOR OF PHILOSOPHY

THE UNIVERSITY OF TEXAS AT AUSTIN

May 1980



## A C K N O W L E D G M E N T S

The support of the National Science Foundation through Grants ENV75-00192 and ENV77-20816 is gratefully acknowledged. The investigation was conducted at the Phil M. Ferguson Structures Laboratory, The University of Texas at Austin, Texas.

The writer wishes to thank the staff at the Laboratory for their assistance in all phases of the investigation. The writer especially thanks Gorham Hinckley, George Moden, Dick Marshall, Dan Perez, and Maxine DeButts. The writer also thanks fellow students Doug Baker, Robert Tyler, Hidetaka Umehara, and Mohammad Taraboulsi for their help during the fabrication, casting, and testing of the specimens. The writer extends his sincerest thanks to fellow graduate student Sam Burguieres for his patience, insight, and common sense. His contributions to the writer's personal and professional development are warmly acknowledged.

The writer wishes to express his appreciation to Dr. James Jirsa, supervising professor, Dr. John Breen, Dr. Karl Frank, Dr. Richard Klingner, and Dr. Ching-Hsie Yew for serving on the dissertation committee. Their guidance and assistance during the preparation of the dissertation were invaluable. The writer would like to offer his warmest thanks to Dr. Jirsa for his guidance and friendship during and before the writer's graduate studies.

K A W

Austin, Texas

# T A B L E O F C O N T E N T S

Part		Page
1	INTRODUCTION . . . . .	1
	1.1 Overview . . . . .	1
	1.2 Background . . . . .	3
	1.3 Outline of Investigation . . . . .	7
	1.4 Past Research . . . . .	10
	1.5 Scope and Objective . . . . .	11
	1.6 Organization . . . . .	11
2	LOADING HISTORY AND TEST SPECIMEN . . . . .	13
	2.1 Introduction . . . . .	13
	2.2 Loading History and Deformation Path . . . . .	13
	Loading History . . . . .	14
	Deformation Path . . . . .	14
	Axial Load . . . . .	14
	Variations . . . . .	14
	2.3 Series Design . . . . .	19
	2.3.1 Overview . . . . .	19
	Shear Resistance . . . . .	20
	Flexural Resistance . . . . .	20
	2.3.2 Specimen Design . . . . .	20
	General Specimen Configuration . . . . .	21
	86 Series Specimens . . . . .	23
	84 Series Specimens . . . . .	27
	2.4 Description of Test Specimens . . . . .	27
	2.5 Notation . . . . .	28
3	LOADING SYSTEM, INSTRUMENTATION, AND DATA REDUCTION . . . . .	33
	3.1 Introduction . . . . .	33
	3.2 Loading System . . . . .	33
	Reaction Frame . . . . .	33
	Hydraulic System . . . . .	36
	3.3 Instrumentation . . . . .	39
	Load Cells . . . . .	42
	Linear Potentiometers . . . . .	42
	Strain Gages . . . . .	42
	3.4 Computer-Based Load Control System . . . . .	45
	3.5 Data Reduction . . . . .	48

Part		Page
4	DESCRIPTION OF SPECIMEN PERFORMANCE . . . . .	50
	4.1 Introduction . . . . .	50
	4.2 Specimen O-86-14-DM . . . . .	56
	4.3 Specimen C-86-14-DM . . . . .	60
	4.4 Specimen O-86-32-D . . . . .	64
	4.5 Specimen C-86-32-D . . . . .	68
	4.6 Specimen C-86-21-D . . . . .	71
	4.7 Specimen O-86-14-D . . . . .	74
	4.8 Specimen C-86-14-D . . . . .	77
	4.9 Specimen C-86-09-D . . . . .	81
	4.10 Specimen C-86-03-D . . . . .	84
	4.11 Specimen C-84-32-D . . . . .	87
	4.12 Specimen C-84-21-D . . . . .	91
	4.13 Specimen C-84-14-D . . . . .	94
5	COMPARISON OF TEST RESULTS . . . . .	98
	5.1 Introduction . . . . .	98
	5.2 Background and Nomenclature . . . . .	98
	5.3 Computed Lateral Loads . . . . .	102
	5.3.1 Flexural Capacity . . . . .	102
	5.3.2 Shear Capacity . . . . .	106
	Length-to-depth Ratio and	
	Loading Condition . . . . .	108
	Loading History . . . . .	108
	Diagonal Loading . . . . .	111
	5.4 Measured Lateral Loads . . . . .	117
	5.5 Effect of Compressive Axial Load . . . . .	117
	5.6 Effect of Cyclic Deformations . . . . .	128
	5.7 Effect of Transverse Reinforcement	
	Spacing . . . . .	128
	5.8 Effect of Longitudinal Bar Diameter . . . . .	136
	5.9 Summary of Observations . . . . .	144
	5.10 Classification Guide . . . . .	146
	5.10.1 Overview . . . . .	146
	5.10.2 Principal Criteria . . . . .	147
	5.10.3 Initial Steps . . . . .	151
	5.10.4 Shear Dominated Behavior . . . . .	151
	5.10.5 Flexure Dominated Behavior . . . . .	152
	5.10.6 Summary . . . . .	153

Part		Page
6	EXPANDED GUIDE TO BEHAVIOR CLASSIFICATION . . . . .	155
6.1	Introduction . . . . .	155
6.2	Japanese Investigations . . . . .	156
6.3	Outline of Predictive Guide . . . . .	160
6.4	Predictive Guide Criteria . . . . .	162
6.4.1	Flexural Capacity - $V_{ff}$ . . . . .	163
6.4.2	Concrete Shear Capacity <sup>ff</sup> - $V_{csc}$ . . . . .	165
	Principal Stress Concept . . . . .	168
	Shear-Friction Concept . . . . .	171
	Modified Shear-Friction Concept . . . . .	173
6.4.3	After Cracking Capacity - $V_{acc}$ . . . . .	177
	Shear Transfer Across Inclined Crack . . . . .	178
	Derivation of $V_{acc}$ . . . . .	179
6.4.4	Core Confinement <sup>acc</sup> - $Z_n$ . . . . .	184
6.4.5	Longitudinal Bar Buckling . . . . .	187
6.4.6	Bond Degradation . . . . .	190
	Test Results . . . . .	192
	Test Parameters . . . . .	192
	Minimum Development Length--Bond Degradation . . . . .	203
	Failure Patterns . . . . .	205
6.5	Expanded Predictive Guide . . . . .	209
	Primary Branches . . . . .	209
	Diagonal Tension Failure . . . . .	212
	Minimum Transverse Reinforcement . . . . .	222
	Secondary Branches . . . . .	223
	Shear Behavior . . . . .	224
	Flexural Behavior . . . . .	225
6.6	Predictive Guide Applied to Current Investigation . . . . .	226
6.7	Implications of Guide to Design . . . . .	229
6.8	Summary . . . . .	232
7	SUMMARY AND CONCLUSIONS . . . . .	234
7.1	Summary of the Investigation . . . . .	234
7.1.1	Experimental Investigation . . . . .	234
	Test Specimen . . . . .	234
	Deformation Path and Loading History . . . . .	235
	Instrumentation . . . . .	235
7.1.2	Supplemental Research . . . . .	236

Part	Page
7.2 Observations--Experimental Investigation . . .	236
Axial Load . . . . .	236
Loading History . . . . .	237
Transverse Reinforcement . . . . .	237
Longitudinal Reinforcement . . . . .	238
7.3 Needed Future Research . . . . .	239
Loading History . . . . .	239
Specimen Geometry . . . . .	239
Axial Load . . . . .	240
Confinement . . . . .	240
Bond . . . . .	240
Shear Capacity . . . . .	240
7.4 Conclusions . . . . .	240
7.5 Predictive Guide . . . . .	243
APPENDICES . . . . .	245
A. REVIEW OF RELEVANT RESEARCH . . . . .	246
B. FLEXURAL CAPACITY COMPUTER PROGRAM . . . . .	301
C. TRANSVERSE REINFORCEMENT CALCULATIONS . . . . .	304
D. MATERIAL PROPERTIES . . . . .	312
E. GEOMETRY CORRECTION . . . . .	318
REFERENCES . . . . .	324

L I S T   O F   T A B L E S

Table		Page
2.1	Test Specimens . . . . .	29
5.1	Computed Lateral Load Capacities for Test Specimens . . . . .	105
5.2	Computed and Observed Lateral Load Capacities . . .	118
5.3	Percentage Loss in Lateral Load between First and Third Cycles . . . . .	119
5.4	Computed Longitudinal Bar Development Lengths (Tension) . . . . .	143
6.1	Specimen Characteristics for Bond Comparison . . .	193
6.2	Example Specimens in Expanded Guide . . . . .	213
6.3	Guide Criteria for Test Specimens . . . . .	227
D.1	Specimen Concrete Strengths . . . . .	314
D.2	Reinforcement Properties . . . . .	315

## L I S T   O F   F I G U R E S

Figure		Page
1.1	Load-deflection behaviors . . . . .	2
1.2	Captive columns . . . . .	5
1.3	Fixed-end member . . . . .	6
2.1	Deformation paths used by Maruyama . . . . .	15
2.2	Column movement in earthquake . . . . .	17
2.3	Diagonal bidirectional loading history, current investigation . . . . .	18
2.4	Maruyama and Ramirez test specimen . . . . .	22
2.5	Axial load vs. moment interaction curve . . . . .	25
2.6	86 series tie spacings . . . . .	30
2.7	84 series tie spacings . . . . .	31
3.1	Principal loading directions . . . . .	34
3.2	Floor-wall reaction system . . . . .	35
3.3	Test setup . . . . .	37
3.4	Loading rams . . . . .	38
3.5	Restraining rams . . . . .	40
3.6	Coupled restraining rams . . . . .	41
3.7	Linear potentiometer locations . . . . .	43
3.8	Linear potentiometer mounting frame . . . . .	44
3.9	Strain gage locations . . . . .	46
3.10	Load control system . . . . .	47
4.1	Deformation path . . . . .	52
4.2	Axes of measurement and deformation . . . . .	53
4.3	Computation of resultant measurements . . . . .	54
4.4	First and second diagonals . . . . .	55
4.5	Specimen 0-86-14-DM load-deflection curve (half cycle) . . . . .	57

Figure		Page
4.6	Specimen 0-86-14-DM crack patterns . . . . .	58
4.7	Crack wrap around effect . . . . .	59
4.8	Specimen C-86-14-DM load-deflection curve (half cycle) . . . . .	61
4.9	Specimen C-86-14-DM load-deflection curves . . . . .	62
4.10	Specimen C-86-14-DM crack patterns . . . . .	63
4.11	Specimen 0-86-32-D load-deflection curves . . . . .	65
4.12	Specimen 0-86-32-D crack patterns . . . . .	66
4.13	Specimen C-86-32-D load-deflection curves . . . . .	69
4.14	Specimen C-86-32-D crack patterns . . . . .	70
4.15	Specimen C-86-21-D load-deflection curves . . . . .	72
4.16	Specimen C-86-21-D crack patterns . . . . .	73
4.17	Specimen 0-86-14-D load-deflection curves . . . . .	75
4.18	Specimen 0-86-14-D crack patterns . . . . .	76
4.19	Specimen C-86-14-D load-deflection curves . . . . .	79
4.20	Specimen C-86-14-D crack patterns . . . . .	80
4.21	Specimen C-86-09-D load-deflection curves . . . . .	82
4.22	Specimen C-86-09-D crack patterns . . . . .	83
4.23	Specimen C-86-03-D load-deflection curves . . . . .	85
4.24	Specimen C-86-03-D crack patterns . . . . .	86
4.25	Specimen C-84-32-D load-deflection curves . . . . .	89
4.26	Specimen C-84-32-D crack patterns . . . . .	90
4.27	Specimen C-84-21-D load-deflection curves . . . . .	92
4.28	Specimen C-84-21-D crack patterns . . . . .	93
4.29	Specimen C-84-14-D load-deflection curves . . . . .	95
4.30	Specimen C-84-14-D crack patterns . . . . .	96
5.1	Test specimen geometry . . . . .	99
5.2	Deformation path . . . . .	101
5.3	Peak deflection symbols . . . . .	103



Figure	Page
5.4	Examples of peak deflection symbols . . . . . 104
5.5	Deep beams . . . . . 109
5.6	Compression strut in specimen . . . . . 110
5.7	Unilateral vs. bilateral loading . . . . . 112
5.8	Shear capacity calculation . . . . . 116
5.9	Effect of axial load (monotonic) . . . . . 121
5.10	Effect of axial load (cyclic tests) . . . . . 122
5.11	Effect of axial load on cracking . . . . . 124
5.12	Tie strains (ties at 1-1/8 in.) . . . . . 125
5.13	Tie strains (ties at 2.57 in.) . . . . . 126
5.14	Effect of loading history . . . . . 129
5.15	Measured vs. computed lateral load capacities (86 series) . . . . . 132
5.16	Measured vs. computed lateral load capacities (84 series) . . . . . 133
5.17	Effect of tie spacing on hysteresis degradation . . 135
5.18	Specimen 0-86-32-D load-deflection curves . . . . . 139
5.19	Shape change observed in hysteresis loops . . . . . 140
5.20	Sliding shear . . . . . 142
5.21	Available development lengths . . . . . 145
5.22	Predictive guide . . . . . 148
5.23	Action of ties . . . . . 150
5.24	Load-deflection relations for guide examples . . . 154
6.1	Typical Japanese test specimen . . . . . 157
6.2	B.R.I. loading system . . . . . 158
6.3	Schematic of expanded predictive guide . . . . . 161
6.4	Column hinging mechanism . . . . . 164
6.5	Crack definitions . . . . . 167
6.6	Short column compression strut . . . . . 169
6.7	Principal stress approaches . . . . . 170

Figure	Page
6.8 Shear-friction test specimens used by Mattock and Hawkins . . . . .	172
6.9 Deflected column . . . . .	174
6.10 Section at end of deflected column . . . . .	176
6.11 Section analysis for flexure . . . . .	178
6.12 Assumed cracking of column . . . . .	180
6.13 ACI Code shear-friction applied to column . . . . .	181
6.14 Kent and Park's concrete stress-strain curve . . . . .	186
6.15 Longitudinal bar stresses . . . . .	189
6.16 Buckled longitudinal bar . . . . .	191
6.17 Definition of pseudo-rotation . . . . .	194
6.18 Load-deflection curves and crack patterns, Specimen LS1AB . . . . .	195
6.19 Load-deflection curves and crack patterns, Specimen LS0BB . . . . .	196
6.20 Load-deflection curves and crack patterns, Specimen LM27B . . . . .	197
6.21 Load-deflection curves and crack patterns, Specimen LM28A . . . . .	198
6.22 Load-deflection curves and crack patterns, Specimen LM28B . . . . .	199
6.23 Load-deflection curves and crack patterns, Specimen FC7B . . . . .	200
6.24 Load-deflection curves and crack patterns, Specimen WS7B . . . . .	201
6.25 Cover restraint of longitudinal bars . . . . .	206
6.26 Test conditions masking cover restraint . . . . .	208
6.27 Expanded predictive guide . . . . .	210
6.28 Guide criteria . . . . .	211
6.29 Load-deflection curves and crack patterns, Specimen WS6B . . . . .	214

Figure		Page
6.30	Load-deflection curves and crack patterns, Specimen LE23BCL . . . . .	215
6.31	Load-deflection curves and crack patterns, Specimen LM25A . . . . .	216
6.32	Load-deflection curves and crack patterns, Specimen LS1BA . . . . .	217
6.33	Load-deflection curves and crack patterns, Specimen AF42CB . . . . .	218
6.34	Load-deflection curves and crack patterns, Specimen FC7A . . . . .	219
6.35	Load-deflection curves and crack patterns, Specimen LS2AA . . . . .	220
6.36	Load-deflection curves and crack patterns, Specimen LS3BB . . . . .	221
6.37	Path to flexural behavior . . . . .	231
A.1	Indirect beam loading method used by Ferguson . . .	249
A.2	Knee beam and center stub beam . . . . .	250
A.3	R/C beam truss analogy . . . . .	253
A.4	Contributing actions to beam shear resistance . . .	256
A.5	Test setup of Ohno, et al. . . . .	261
A.6	Test specimen used by Higashi and Ohkubo . . . . .	261
A.7	Effect of longitudinal reinforcement ratio (Kokusho and Ogura) . . . . .	262
A.8	Effect of transverse reinforcement ratio (Kokusho and Ogura) . . . . .	264
A.9	Effect of axial load (Kokusho and Ogura) . . . . .	265
A.10	Test used by Minami and Wakabayashi . . . . .	266
A.11	B.R.I. loading system and test specimen . . . . .	268
A.12	Specimen used by Maruyama and Ramirez . . . . .	269
A.13	Loading system used by Maruyama and Ramirez . . . .	270
A.14	Deformation paths used by Maruyama . . . . .	272
A.15	Typical loading history (Maruyama and Ramirez) . . .	273

Figure		Page
A.16	Shear-friction concept . . . . .	276
A.17	Shear-friction test specimens used by Hofbeck, et al. . . . .	277
A.18	Shear-friction test specimens used by Mattock and Hawkins . . . . .	278
A.19	Test setup used by Laible, et al. . . . .	280
A.20	Shear stress versus slip across crack . . . . .	281
A.21	Takeda's test specimens . . . . .	283
A.22	Example hysteresis curve using Takeda's model . . .	283
A.23	Flexural hysteresis loops . . . . .	284
A.24	Effect of strain rate on load-deflection relation .	284
A.25	Effect of axial load (Penzien, et al.) . . . . .	286
A.26	Effect of shear span ratio (Penzien, et al.) . . .	287
A.27	Degrading hysteresis model, Atalay and Penzien . .	288
A.28	Tie arrangement . . . . .	290
A.29	Kent and Park's concrete stress-strain curve . . .	291
A.30	Sheikh's concrete stress-strain curve . . . . .	293
A.31	Bond splitting . . . . .	295
A.32	Bond failure patterns . . . . .	297
A.33	Test setup of Hassan and Hawkins . . . . .	299
B.1	Kent and Park's concrete stress-strain relation . .	303
C.1	Column hinging mechanism . . . . .	305
C.2	Loading orientations . . . . .	307
C.3	Bilateral shear reinforcement action . . . . .	308
D.1	Stress-strain curves for #6 and #4 bars . . . . .	316
D.2	Stress-strain curves for 6 mm bars . . . . .	317
E.1	Coordinate system . . . . .	320
E.2	Load components . . . . .	321
E.3	Equations for load components . . . . .	322
E.4	Effect of geometry correction . . . . .	323

## N O T A T I O N

$a$	shear span, in.
$A_c$	area of concrete core, out-to-out of ties, sq. in.
$A_s$	area of nonprestressed tension reinforcement, sq in.
$A_v$	area of shear reinforcement within a distance $s_h$ , sq. in.
$b$	total section width, in.
$b_w$	web width, in.
$c$	distance from extreme compression fiber to the neutral axis
$C_F$	normal force on only the concrete in the compression zone
$d$	distance from extreme compression fiber to the centroid of the tension reinforcement, in.
$d_b$	nominal diameter of column longitudinal bar, in.
$f'_c$	concrete compressive strength, psi
$f_y$	yield strength of column longitudinal reinforcement, psi
$f_{yv}$	yield strength of column transverse reinforcement, psi
$h$	total section depth, in.
$j$	ratio of the internal moment arm to $d$
$l_d$	development length of bar in tension, in.
$L_c$	clear height of column, in.
$M$	moment at a section
$M_u$	ultimate moment capacity of a section
$N$	applied axial load, positive if compressive
$P_b$	axial load capacity at balanced strain conditions

$P_o$	concentric axial load capacity
$R$	pseudo-rotation (drift angle) of column
$s_h$	column tie spacing, center-to-center, in.
$V$	shear force at a section
$V_{acc}$	after cracking shear capacity of column
$V_{BS}$	lateral load capacity of column based on the bond capacity of longitudinal reinforcing bars
$V_c$	nominal shear strength provided by concrete (ACI318-77)
$V_{csc}$	concrete shear capacity
$V_{rf}$	lateral load capacity of column based on flexural capacity
$V_{rs}$	lateral load capacity of column based on shear capacity
$V_{rt}$	maximum lateral load observed in a column test
$V_{rtn}$	normalized value of $V_{rt}$
$V_s$	nominal shear strength provided by shear reinforcement (ACI318-77)
$Z_n$	core confinement criteria
$\Delta$	deflection, in.
$\rho$	ratio of nonprestressed tension reinforcement, $A_s/bd$
$\rho_s$	ratio of transverse reinforcement, $A_v/hs_h$
$\rho_w$	$A_s/b_w d$
$\sigma_x$	stress in x direction
$\sigma_y$	stress in y direction
$\sigma_{1,2}$	principal stresses
$\tau_{xy}$	shear stress

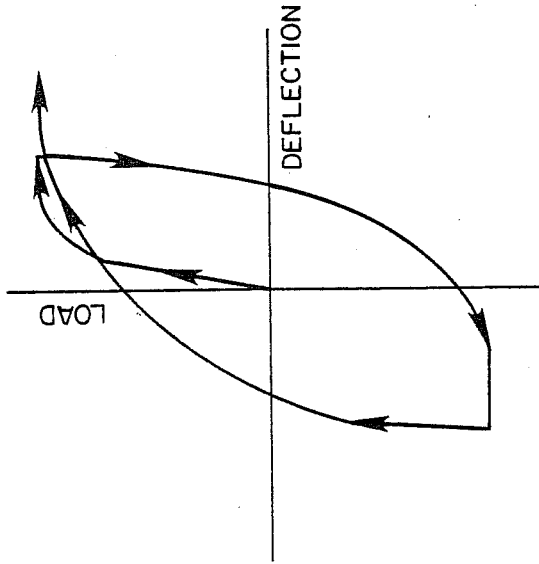
# C H A P T E R 1

## INTRODUCTION

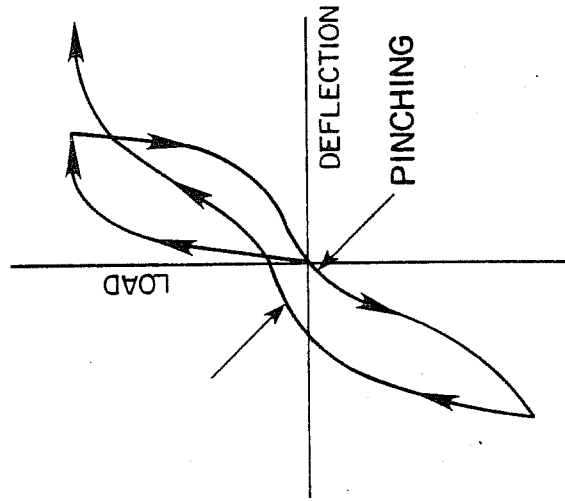
### 1.1 Overview

The purpose of the investigation is to develop guidelines for describing and predicting the behavior of short reinforced concrete columns subjected to cyclic reversed deformations. The guidelines are presented in the form of a flowchart. The flowchart encompasses a broad range of behavior and the factors which influence the behavior. The end result is a unified approach to classifying and describing the hysteretic behavior of short reinforced concrete columns.

Eleven short columns were tested in the investigation. The majority of the columns were subjected to cyclic deformations applied along two orthogonal axes (bidirectional). A constant compressive axial load was also applied to the majority of the columns. The columns were intended to exhibit either a flexure or shear dominated hysteretic behavior. Flexural behavior in its best form is characterized by load-deflection loops which are open and show little loss of load with cycling at peak deflections, Fig. 1.1a. Shear behavior is characterized by load-deflection hysteresis loops which exhibit a narrowing near zero load (pinching) and show a degradation of load with cycling at peak deflections, Fig. 1.1b. Flexural behavior is the more desirable type of behavior in earthquake design. It has an almost constant post-yield load capacity and a larger energy dissipation capacity compared to shear behavior. The transition from a flexural



Flexural Behavior  
(a)



Shear Behavior  
(b)

Fig. 1.1 Load-deflection behaviors



behavior to a shear behavior in short columns has not been previously studied, but it is assumed that the transition is gradual rather than abrupt.

The ratio of the column flexural to shear capacity was initially used to provide guidance as to the relative dominance of one type of behavior over another. The capacities were computed using the provisions of the 1977 ACI Building Code [17], but the capacities were taken as reflections of probable dominance and not as direct determinants of behavior. Behavioral characteristics observed in the eleven column tests could not be categorized easily using the computed shear or flexural capacity. As a result, short column tests reported by Japanese investigators were reviewed to develop quantitative guidelines for determining the behavioral characteristics of short columns.

## 1.2 Background

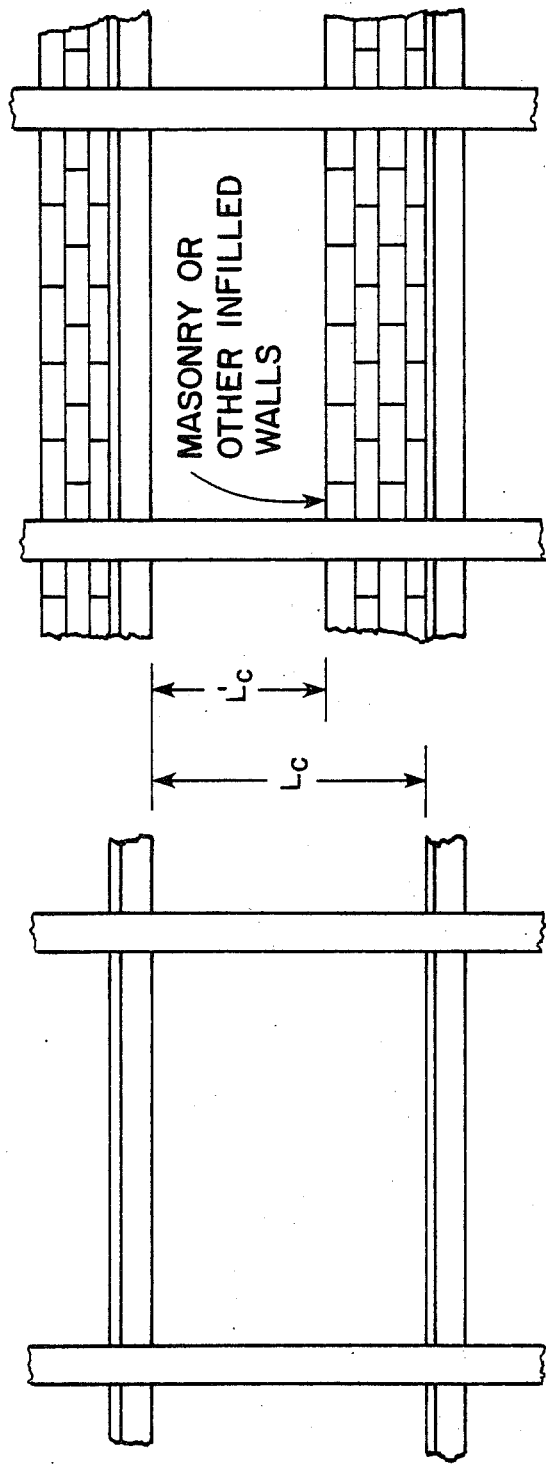
Columns governed by shear behavior should be avoided in seismic design because of their poor load-deflection characteristics. However, short columns are sometimes incorporated into structural systems either purposely or as the result of structural changes not considered in the original design. Post-earthquake damage reports from several earthquakes have mentioned shear failures in columns with small clear height-to-gross depth ratios ( $L_c/h$ ). A small ratio (less than 4) defines the column as short for the purposes of this report.

The short columns in the first three levels of the Macuto-Sheraton Hotel in Caracas, Venezuela, were an example of purposely short columns. The columns had a clear height-to gross depth ratio of about 4, and large framing members at each end. Several of the columns suffered shear failure in the 1967 Caracas earthquake [97].

"Captive" columns are the usual type of unintentional short column and may occur more frequently than purposely designed short columns. The term "captive" column is applied to columns where the bare frame clear height is reduced by structural elements that are stiff and limit the deformation of the column over a portion of its length. Figure 1.2 illustrates a "captive" column. The principal problem with "captive" columns in the past has been the tendency to design the column on the basis of bare frame dimensions and ignoring the effect of stiffening elements which are considered "nonstructural". The design of a "captive" column for a shear capacity based on bare frame dimensions can be unconservative for the case of a laterally loaded structure (seismic action). Figure 1.3 depicts a rotationally restrained member subjected to a lateral translation. The shear force required to equilibrate the system is proportional to the moment and inversely proportional to the length. Expressed in another way, the shear introduced into a fixed end elastic member by a lateral translation is

$$\frac{12EI\delta}{L^3} \quad (1.1)$$

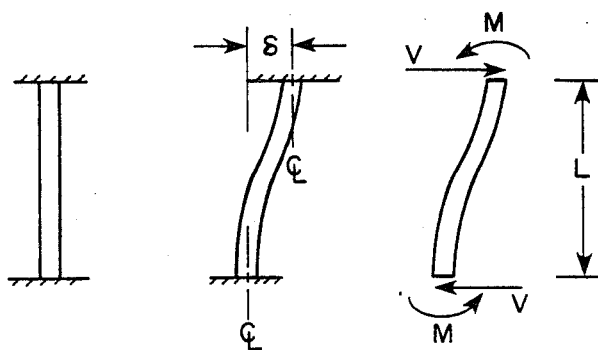
where E is the member's modulus of elasticity, I is its cross-sectional inertia,  $\delta$  is its lateral translation, and L is its length. Thus, a length reduction increases the shear stiffness of the member resulting in an increased imposed shear force. In a "captive" column, the length of the column is reduced compared to its length in the bare frame. The length reduction results in an increased imposed shear force on the column which is not accounted for in the design. Shear failures of "captive" columns were reported in both the 1968 Tokachi-Oki earthquake in Japan [10] and the 1972 Managua earthquake in Nicaragua [11].



"CAPTIVE" COLUMN

BARE FRAME

Fig. 1.2 Captive columns



$$V = \frac{2M}{L}$$

Fig. 1.3 Fixed end member

The significant aspect of short columns compared to longer columns is the high shear forces required to fully develop the flexural capacity of the member. Past investigations of members loaded cyclically with high shear forces [4,5,6] show that the hysteretic load-deflection loops exhibit deterioration of member stiffness and degradation of load capacity. The previous investigations have not developed behavioral models which describe the cyclic load-deflection relationship of members exhibiting shear dominated behavior. The study of shear dominated hysteretic behaviors [5,8,9] has emphasized detailing methods and establishing shear stress limits to preclude shear dominated behavior. A behavioral model for shear dominated behavior is necessary to properly analyze and design structures which contain members developing high shear forces.

Analytical studies using behavioral models developed from unidirectional tests have been done to determine the response of reinforced concrete frames subjected to two-dimensional ground acceleration [1,2,3]. Such studies indicate that for ductility requirements greater than about 2 the effect of bidirectional excitation was to increase the response displacement of structures compared to the response from combining the displacement obtained from unidirectional analyses for each plane. These results point to the need for behavioral models which account for the effect of bidirectional deformations. Such models would permit more realistic analyses of reinforced concrete structures.

### 1.3 Outline of Investigation

The current study is part of a larger project investigating the behavior of reinforced concrete frame elements subjected to cyclic bidirectional deformations. The emphasis is on the behavior of frame elements under conditions of high shear stress. Beam-column joints and short columns are the frame elements under study.

The investigation reported herein is devoted exclusively to short columns.

The unique aspect of the project is the inclusion of bidirectional deformations. Unidirectional deformations have been used in most past studies. The reversed cyclic deformations reflect the general nature of seismic action, but the deformations are applied slowly to obtain a clear picture of member behavior without introducing the additional complexity of dynamic loading effects. Ground accelerations are three-dimensional in nature and their action on a frame member are better represented using bidirectional rather than unidirectional deformations.

The first investigation on short columns in The University of Texas at Austin program was reported by Maruyama [14]. The principal objective was the development of a behavioral model which accounted for the effects of deformation path on the response of the column. Deformation paths included in the study ranged from unidirectional deformations along only one axis to complex paths involving movement along the diagonals of the column. No axial load was applied to the columns. The information provided an initial step in the development of the analytical tools necessary to properly represent the effects of multidimensional loadings on short column response.

Additional tests were conducted to study the effect of axial load, especially tensile load, and were reported by Ramirez [15]. Both unidirectional and bidirectional loadings were included. The results of the investigation provided insight into the behavior of short columns subjected to varying axial load. The applied axial loads ranged from constant tension or compression to reversals of axial load as the column was deformed laterally.

The columns reported by Maruyama and Ramirez were identical and purposely underdesigned in shear according to the provisions

of the 1971 ACI Building Code [16]. The Code was used as a guide to the design of the specimens. The load-deflection curves for the test columns revealed a degrading hysteretic behavior. The load and the stiffness were severely reduced with cycling. For this reason, the behavior was considered to have been controlled by shear.

One of the desired objectives of the overall study of short columns is to develop a behavioral model which encompasses the range of behavioral modes exhibited by short columns. However, before a complete behavioral model can be developed, the characteristics of the different types of behavior must be defined. In addition, the parameters which affect behavior and how they affect the behavior of short columns must be determined. Using the results of the previous studies in which shear behavior was predominant, the next step was to expand the study by including other types of behavior.

The current investigation was initially aimed at obtaining a response controlled by flexure. Flexural response is produced if plastic hinges form at each end of the column and the hinges do not exhibit deterioration with increased deformations and cyclic reversals. The resulting behavior is represented by hysteretic loops which exhibit little load loss with post-yield deformations and cycling (stable hysteretic loops). Such stable hysteretic behavior is the basis for the current design of columns subjected to seismic actions. The provisions of design codes such as ACI 318-77 [17] and the 1976 Uniform Building Code (1976 UBC) [18] state, explicitly or implicitly, that the underlying design assumption for columns is a stable plastic mechanism with high deformational capacity.

Eleven short column specimens were designed and tested to better define the parameters which determine the boundary between

flexural and shear dominated behavior. The loading history was kept constant and the reinforcing details were changed. Shear and flexural capacity were altered by varying the amount of either the longitudinal or transverse reinforcement in the columns.

The results of the eleven tests revealed a much wider range of behavior than expected. The performance of the columns was influenced by many parameters. Some of the parameters had been identified in other investigations, but had not been fully explored in a unified approach. In other investigations, only one variable was studied and others were ignored. The observations, conclusions, and recommendations of such programs are limited to the effect of isolated parameters and, for columns especially, no systematic categorization of behavior has been reported. The need for a general approach to the classification of behavior for short columns was realized after attempting to identify the behavior observed in the columns of the current series.

Diagonal-tension, bond degradation, flexural distress, and longitudinal bar buckling were observed in the current investigation. No unified approach based on the characteristics of the columns was available which adequately determined the factors influencing behavior or the relative importance of the factors to the observed column behavior.

#### 1.4 Past Research

A review of previous research is presented in Appendix A. The review emphasizes research related to the parameters influencing short column behavior. The parameters are the shear and flexural resistance of the column, bond along the reinforcement, confinement, bar buckling, and loading history. The review emphasizes the need for a unified method for determining column behavior. The past research is fragmented into essentially single variable studies with little or no consideration of the interaction



of different variables. Pertinent aspects of the previous research will be discussed in more detail in subsequent chapters.

### 1.5 Scope and Objective

The purpose of the investigation is to develop guidelines for describing and predicting the behavior of short reinforced concrete columns subjected to cyclic deformations.

A series of eleven short columns were tested to explore the behavioral changes as a result of altering the amounts of longitudinal and transverse reinforcement. The variation of reinforcement was undertaken to change the relative dominance of the flexural resistance characteristic to the shear resistance characteristic of the column. The results of the tests showed a wider range of behavioral characteristics than was expected. Additional short column test data were obtained from Japanese investigators and used to more fully define the behaviors exhibited in the current tests.

### 1.6 Organization

In Chapter 2, the design of the test specimens used in the current investigation is discussed. The load history and deformation path are presented. A discussion of nomenclature for specimen identification is presented.

In Chapter 3, the load system, test equipment (instrumentation), computerized load control system, and data acquisition system developed in the previous investigations and used in the current investigation are reviewed. The methods of data reduction are also discussed.

In Chapter 4, a detailed description of the performance of each specimen during testing is presented. Pictures of the

specimens at various stages during the tests are presented. Load-deflection curves for each specimen are also provided.

Comparisons of the results from the tests of the current investigation are described in Chapter 5.

The predictive guide is presented in Chapter 6. The guide is quantitative and is based on tests conducted elsewhere in addition to the tests of the current investigation.

In Chapter 7, a summary of the important aspects of the preceding chapters is presented. The significant conclusions and a discussion of needed future research is included.

## CHAPTER 2

### LOADING HISTORY AND TEST SPECIMEN

#### 2.1 Introduction

The general configuration of the test specimen was identical to that used in the previous two investigations (Maruyama [14] and Ramirez [15]). Identical configurations maintained the continuity between the investigations in the project. Similarly, the choice of loading history and deformation path was limited to those which had been previously used in the project. Continuity between investigations provided an enlarged data base and one in which parameters were carefully varied.

The specimen designs for the current investigation are presented. The loading history and deformation path used in the current investigation are discussed. A system for identifying the test specimens is presented to aid in the discussion of the test results. Fabrication details are not presented herein because they have been fully documented by the previous investigators [14,15] and have not been altered for the current investigation.

#### 2.2 Loading History and Deformation Path

The current investigation is the third in a series of studies on short columns. The results obtained from the investigation expands the data base created by the previous two investigations. In the first investigation [14], the effect of deformation path was studied. No axial load was applied to the specimens.

In the second investigation [15], the effect of axial load on the hysteretic behavior of the column was studied. Two of the deformation paths explored in the first investigation were utilized. The selection of loading history, deformation path, and axial load in the current investigation was limited to cases which had been explored in the first two investigations.

Loading History--In the investigations conducted by Maruyama and Ramirez, the deformations were cyclically reversed between incrementally increasing deflection limits. Within each deflection limit the specimen was cycled three times. The first deflection limit was based on the load-deflection response of a unilaterally loaded specimen tested by Maruyama. The first deflection limit was the observed deflection at the point of yielding in the column longitudinal reinforcement. This deflection was then used in all subsequent tests in the previous investigations. Higher deflection limits were multiples of the deflection established at yielding in the unilateral test. The deflection limits and number of cycles at each level were not changed between investigations for reasons of continuity and comparison.

Deformation Path--The principal deformation paths used by Maruyama are shown in Fig. 2.1. Deformation path d in Fig. 2.1 (diagonal bidirectional) was selected for the current investigation. Maruyama reported that degradation of the load-deflection response for the diagonal bidirectional deformation path was greater than that for deformation path c in Fig. 2.1, but much less than for the excessively severe square path (Case e, Fig. 2.1). The square deformation path caused such rapid degradation of the column response that it would be difficult to observe behavioral changes as a result of other variables.

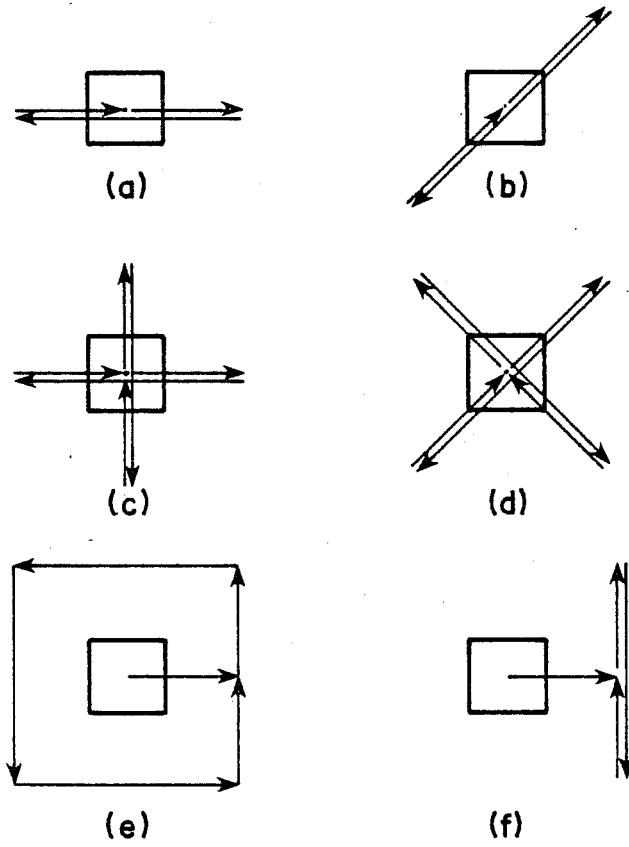
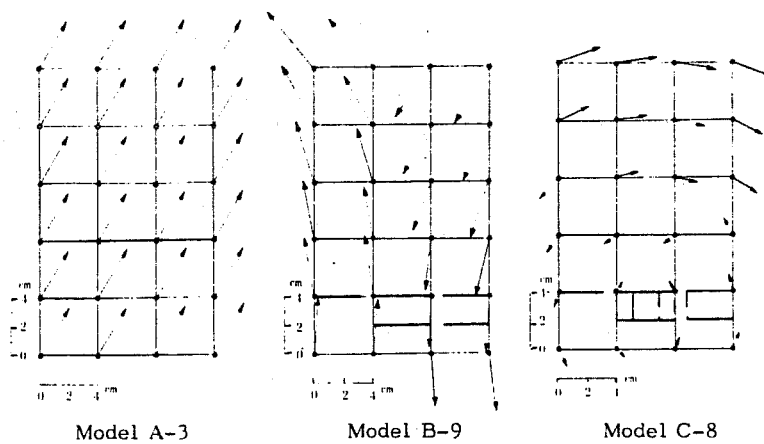


Fig. 2.1 Deformation paths used by Maruyama

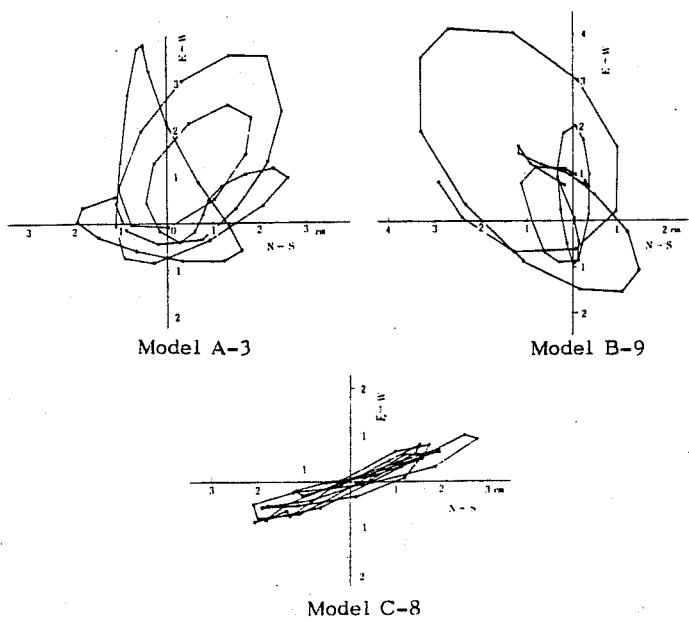
It seemed that the diagonal bidirectional deformation path was a moderate path, not the least severe but also not the most severe with regard to degradation of strength and stiffness. In addition, the diagonal deformation path would cause simultaneous bending about two axes (bilateral bending) of the column. Bilateral bending was considered to be a better representation of the effect seismic action produces on the columns in a frame structure. Figure 2.2b shows the deformation paths of a corner column in various structures (Fig. 2.2a) subjected to a two-dimensional ground acceleration [12]. The paths were determined analytically. The arrows in Fig. 2.2a show the general direction of the column movements. It is clear that the movement of the columns does generally involve bilateral effects. A schematic of the diagonal bidirectional loading history is shown in Fig. 2.3.

Axial Load--Ramirez [15] examined the effect of constant tensile or compressive axial load and alternating tensile and compressive axial load. Only one compressive axial load (120 kips) was used. A loading of 120 kips (830 psi on the gross area of the column) was based on the results of a survey done in Japan on the mean axial stress in columns of existing buildings [89]. The mean stress was about 400 psi with a maximum stress of about 1000 psi. Ramirez reported that the effect of compressive axial load was to accelerate degradation of the load-deflection curve after the maximum load was achieved. The presence of a compressive axial load would appear to be more representative of the loads generally present on a column in a structure. For these two reasons the specimens were tested with an applied compressive axial load of 120 kips.

Variations--Three of the short columns were tested



(a) Structure movement



(b) Column movement

Fig. 2.2 Column movement in earthquake [12]

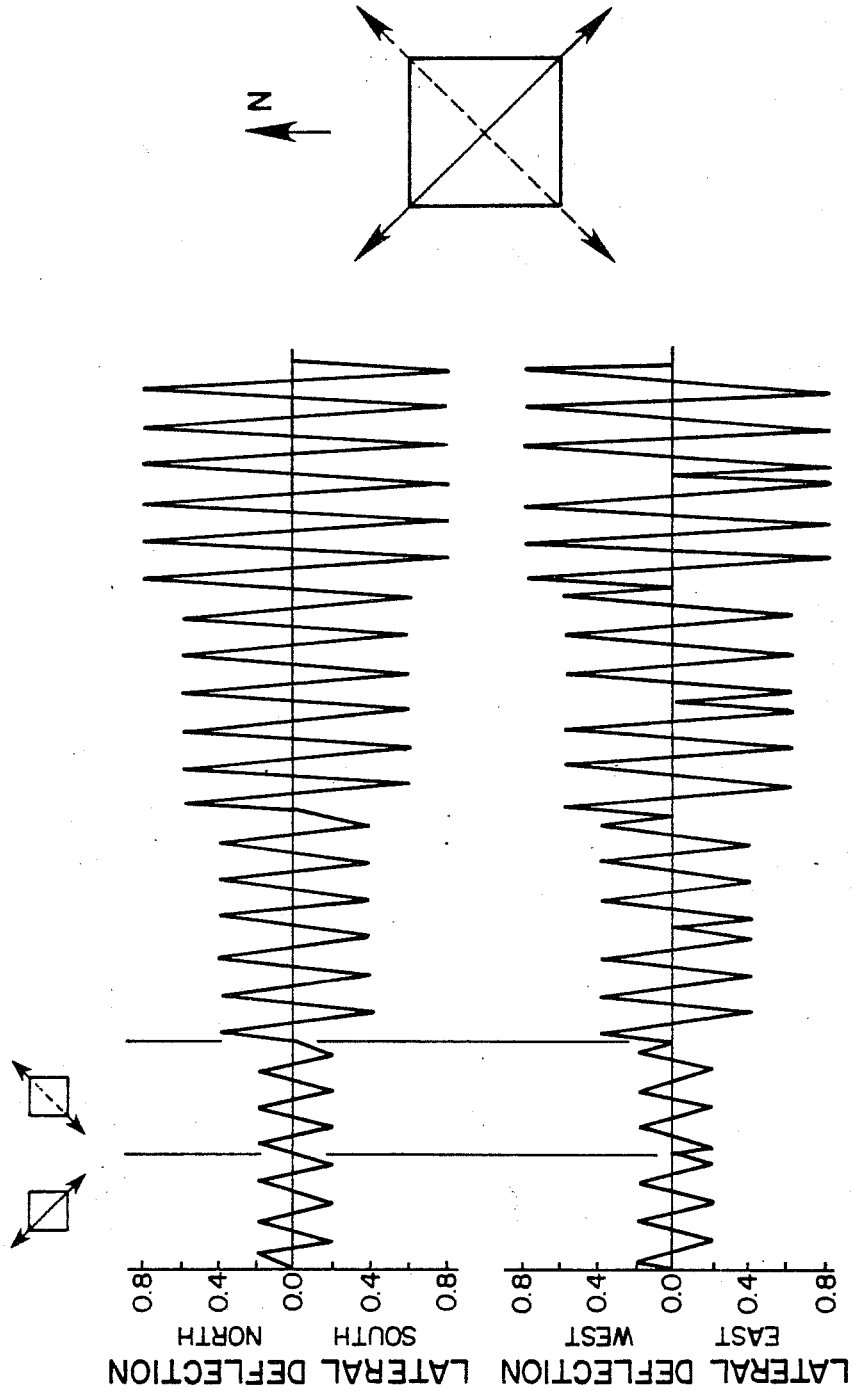


Fig. 2.3 Diagonal bidirectional loading history, current investigation



differently than previously described. In one test, the only difference was that no axial load was applied to the column. Another test had no applied axial load and was deformed along a diagonal to a large lateral deflection. It was then returned to its original position. The test was essentially a half cycle test with no applied axial load. The third test had an applied axial load and was cyclically deformed. The cycling, however, was done between only one very large lateral peak deflection. These three tests provided useful comparisons to the rest of the short column tests.

### 2.3 Series Design

2.3.1 Overview. The overall objective of the investigation (Sec. 1.5) was to develop a guide to describe and classify short column hysteretic behavior. A broad range of behaviors was desired in the test series to make the classification guide as general as possible. The column behaviors were expected to range from a nearly flexural behavior (stable, open load-deflection loops) to an extremely brittle diagonal tension failure. Shear dominated behavior (pinched, unstable load-deflection loops) would occur between the flexural behavior and the diagonal tension failure.

Prior to the investigation it was hypothesized that the behavioral mode exhibited by a short column was primarily a function of the ratio of flexural resistance to shear resistance. If the shear resistance was very much greater than the flexural resistance then shear effects would be minimal and a predominately flexural behavior would result. Conversely, if the flexural resistance was very much greater than the shear resistance then a predominately shear behavior would result, the extreme being a

diagonal tension failure. The design of the test series was based on altering the ratio of the flexural to shear resistance of the column.

Shear Resistance--The mechanism of shear resistance in a reinforced concrete member is not well understood. However, based on past research, it is generally agreed that the ultimate shear resistance is greatly enhanced by the inclusion of web (transverse) reinforcement. The shear provisions of the 1977 ACI Building Code [17] suggest that the increase in ultimate shear resistance between a beam with and a beam without web reinforcement is proportional to the area and yield strength of the reinforcement crossing the shear cracks. This observation is based on the results of a large number of monotonic tests on beams. The beams were largely simply supported and loaded on the compression face. By varying the spacing of the web reinforcement, the area of web reinforcement crossing a shear crack is varied.

Flexural Resistance--The flexural resistance of a reinforced concrete member is reasonably well defined. The techniques for its computation are available and produce results which agree quite well with test results. The ultimate flexural resistance of an underreinforced member is primarily a function of the amount and strength of the longitudinal tension reinforcement. An underreinforced member is one in which the tension steel yields before the concrete crushes. The variation of flexural resistance can be accomplished by altering the amount of longitudinal reinforcement.

2.3.2 Specimen Design. Two approaches were used to vary the ratio of shear resistance to flexural resistance. The first was to vary the amount (spacing) of transverse reinforcement while keeping the amount of longitudinal reinforcement constant. The second approach was to vary the amount (bar size) of

longitudinal reinforcement while keeping the amount of transverse reinforcement constant. The test specimens were designed in two series. The amount of transverse reinforcement in each series varied, while the amount of longitudinal reinforcement was kept constant. The two series, however, had a different amount of longitudinal reinforcement. In one series, the column section contained eight #6 bars (three in each face) uniformly arranged around the section (86 series). The other series had eight #4 bars (84 series) rather than #6 bars.

General Specimen Configuration--The geometry of the specimens tested by Maruyama and Ramirez is shown in Fig. 2.4. The column was bounded at each end by large blocks (heads) cast monolithically with the column. The heads served two functions: (1) a means of adequately anchoring the column longitudinal bars, and (2) enabling the column to be attached to the loading system so that the column could be loaded in three axes simultaneously.

The dimensions of the column represent a 2/3-scale model of a prototype column. The prototype column had an 18 in. x 18 in. cross section, eight #9 bars as longitudinal reinforcement, #3 bars for ties and a cover of 1-1/2 in. A 2/3-scale model, thus, gives a cross section of 12 in. x 12 in., eight #6 bars as longitudinal reinforcement, #2 bars for ties, and a cover of 1 in. Because it is a model, the 1 in. cover on the specimen satisfies the cover requirements of the ACI Building Code. The capacity computations for the column were based on the actual dimensions of the column specimen and not the prototype column. The columns tested by Maruyama and Ramirez had a length of 36 in. and a 12 in. x 12 in. cross section. The longitudinal reinforcement consisted of eight #6 bars uniformly spaced around the column section. The ties were 6 mm bars spaced at 2.57 in. along the column length.

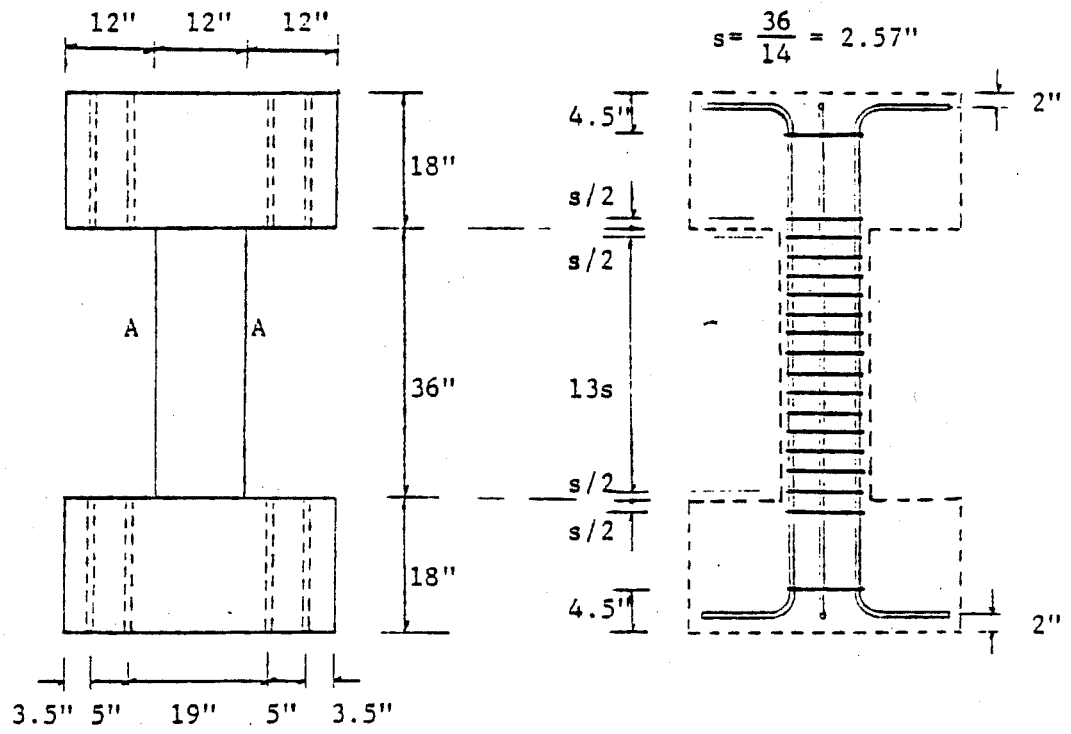


Fig. 2.4 Maruyama and Ramirez test specimen [15]

86 Series Specimens--The series of specimens with eight #6 longitudinal bars (86 series) is the basic series and includes a larger number of specimens than the 84 series, because it is more directly comparable to the specimens of the previous investigation. The prime variable is the spacing of the ties in the column. The principal effect of varying the spacing is to vary the shear resistance of the specimen. The tie spacing of 2.57 in. used in the previous investigations is taken as the reference spacing because the results of tests with such a spacing showed that the column had degrading hysteretic behavior (shear dominated). Thus, it is necessary to use a smaller spacing to achieve a flexural or stable behavior and a larger spacing to produce rapid degradation as in a diagonal tension failure.

One specimen in the 86 series was deformed through only a half cycle and had no applied axial load. It was deflected to a high peak deflection and then returned to its original position. Another 86 series specimen was cyclically deflected between a high peak deflection with no cycling at intermediate deflections. A 120 kip constant compressive axial load was applied to the column. Both were deflected along a diagonal of the column and both specimens had a tie spacing of 2.57 in. The two tests provided useful information for comparing the effect of cycling at intermediate peak deflections versus cycling at very high peak deflections. The test with no axial load was directly comparable to Maruyama's test series, while the specimen with axial load was directly comparable to the current series. The two tests were also directly comparable for the effect of axial load.

The tie spacings were selected to obtain as wide a range of expected behavior with as few tests as possible. Five tie spacings were considered sufficient to bound the behavior range of the specimen. Two spacings larger and two spacings smaller

than the 2.57 in. spacing used previously appeared to provide sufficient variation. The small tie spacings (less than 2.57 in.) were selected with the objective of ensuring a flexural failure of the column. The provisions of Appendix A of the 1977 ACI Building Code [17] were used as a guide to designing the transverse reinforcement.

Most of the columns in the current investigation were subjected to a constant compressive axial load of 120 kips. The columns were deflected along their diagonals which introduced bilateral bending to the columns. A computer program was developed to obtain the axial load versus moment diagram of the bilaterally loaded column. The program is described in Appendix B. The results from the program agreed quite well with results obtained from other published methods. The interaction curves for bending about two different axes are shown in Fig. 2.5. The curves are for an 86 series column because it is used as the basis for designing the transverse reinforcement. One axis is perpendicular to the side faces (unilateral) and the other axis is oriented 45 degrees to the side faces (bilateral). The axial loads and moments on the curve do not include capacity reduction factors.

Two sections of the 1977 ACI Building Code Appendix A (seismic design provisions) were used as a guide to the design of the transverse reinforcement. One section (A.5.9) requires that the shear (transverse) reinforcement must be designed to resist a condition of "plastic hinges at ends of members produced by lateral displacement." The other section (A.6.5) requires that confinement reinforcement be provided if the ratio of the applied axial load to the axial load at balanced strain conditions exceeds 0.4. The application of these two provision to the diagonally loaded

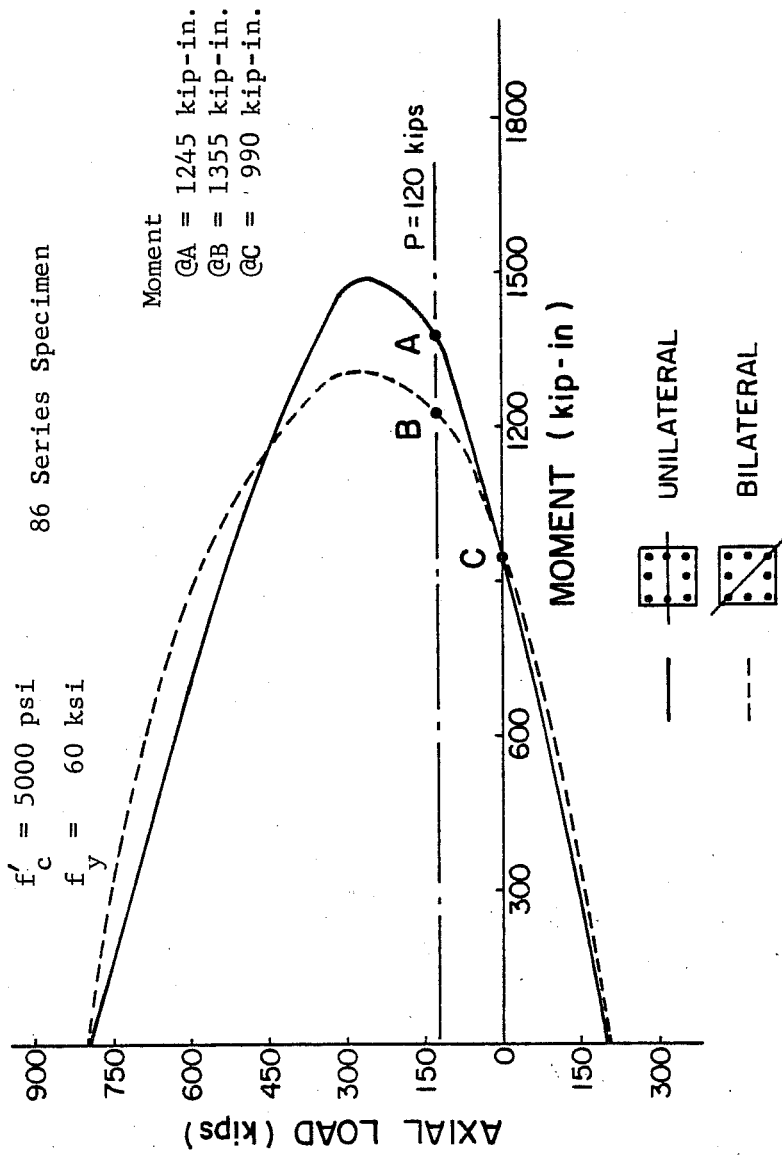


Fig. 2.5 Axial load vs. moment interaction curve

column is described in Appendix C. The tie spacing to meet each of the two provisions of Appendix A (ACI Code) was about 0.5 in.

A tie spacing of 0.5 in. was impractical for the fabrication of reinforcement and placement of concrete. A 1-1/8 in. spacing was selected as the lower limit on tie spacing. Two specimens with eight #6 longitudinal bars and a tie spacing of 1-1/8 in. were tested. One had a 120 kip constant compressive axial load applied to it and the other did not. By comparing the behavior of the two specimens it was anticipated that some indication of the applicability of the Appendix A (ACI Code) provisions would be obtained.

The upper limit on tie spacing was chosen to be 12 in. A 12 in. spacing provided negligible shear capacity due to transverse reinforcement. As a result, the behavior was expected to be much more brittle than the specimens with the 2.57 in. tie spacing. The 12 in. spacing met the ACI Building Code provisions for lateral reinforcement for compression members (ACI Sec. 7.10) and provided enough ties to fabricate a reinforcing cage which would hold its shape during construction and casting.

One specimen was fabricated with a 2.57 in. tie spacing which was based on the previous investigations. Specimens with a tie spacing of 2.57 in. exhibited a hysteretic behavior which degraded fairly rapidly. The behavior was taken to represent a condition between diagonal tension failure and stable hysteretic behavior. Two additional tie spacings were selected. In one specimen, a 1-3/4 in. spacing was used to provide a value between 1-1/8 in. and 2.57 in. and another specimen had ties at 4 in. to provide a value between 2.57 in. and 12 in.

One additional specimen was tested which contained #6 bars.



It was a spirally reinforced column with ten rather than eight #6 bars. The reinforcement of this specimen excluded it from consideration in the current investigation. A description of its design, fabrication, testing, and results can be found in Ref. 91.

84 Series Specimens--The specimens of the 84 series contained eight #4 bars as longitudinal reinforcement rather than eight #6 bars as in the 86 series. No. 4 bars were used because they were an even 2/3-scale of a #6 bar in the prototype and bars larger than a #6 bar provided too large a flexural capacity. Individual specimens in the 84 series had similar tie spacings to specimens in the 86 series in order to make direct comparisons of the effect of flexural capacity on member behavior. Three specimens were tested in the 84 series to examine the influence of reduced flexural capacity. Of most interest was the change in behavior from degrading to nondegrading hysteretic load-deflection loops. the transition was expected to occur between the specimens with tie spacings of 2.57 in. and 1-1/8 in. Therefore, the three 84 series specimens were fabricated using the small tie spacings of the 86 series in order to explore the expected transition region.

#### 2.4 Description of Test Specimens

Eleven specimens are included in the current investigation; eight specimens in the 86 series (#6 longitudinal bars) and three in the 84 series (#4 longitudinal bars). The tie spacings in the 86 series range from a low of 1-1/8 in. to a high of 12 in., as shown in Fig. 2.6. The specimen with the 12 in. spacing was expected to exhibit an extremely brittle diagonal tension failure, while the specimen with no axial load and

a tie spacing of 1-1/8 in. was expected to exhibit much more stable load-deflection curves than the specimens tested in the previous investigations.

The tie spacings of the specimens in the 84 series ranged from 1-1/8 in. to 2.57 in. The three specimens of the 84 series had the same tie spacing as three of the specimens in the 86 series, so that comparisons for the effect of longitudinal steel could be made. Details of the 84 series specimens are shown in Fig. 2.7 and Table 2.1.

A description of the concrete and reinforcing steel properties is given in Appendix D.

## 2.5 Notation

To simplify discussion of the test specimens, a notation consisting of a four group code was established. The general form of the notation is:

T - UV - W - X

T = level of axial load.

O = no axial load

C = 120 axial compression

U = number of longitudinal bars in the section

8 - eight longitudinal bars, or

10 - ten longitudinal bars (only used for the spiral)

V = longitudinal bar size

6 - #6 longitudinal bars

4 - #4 longitudinal bars

TABLE 2.1 TEST SPECIMENS

Specimen Identifier	Longitudinal Reinforcement	Tie Spacing* (in.)	Axial Load (kips)	Loading History**
0-86-14-DM	8- #6 Bars	2.57	0	Cyclic***
C-86-14-DM	8- #6 Bars	2.57	120	Cyclic***
0-86-32-D	8- #6 Bars	1.125	0	Cyclic
C-86-32-D	8- #6 Bars	1.125	120	Cyclic
C-86-21-D	8- #6 Bars	1.75	120	Cyclic
C-86-14-D	8- #6 Bars	2.57	120	Cyclic
C-86-09-D	8- #6 Bars	4.0	120	Cyclic
C-86-03-D	8- #6 Bars	12.0	120	Cyclic
C-84-32-D	8- #4 Bars	1.125	120	Cyclic
C-84-21-D	8- #4 Bars	1.75	120	Cyclic
C-84-14-D	8- #4 Bars	2.57	120	Cyclic

\* Ties were 6mm bars.

\*\* Deformation path was diagonal bidirectional.

\*\*\* Between large peak deflections only

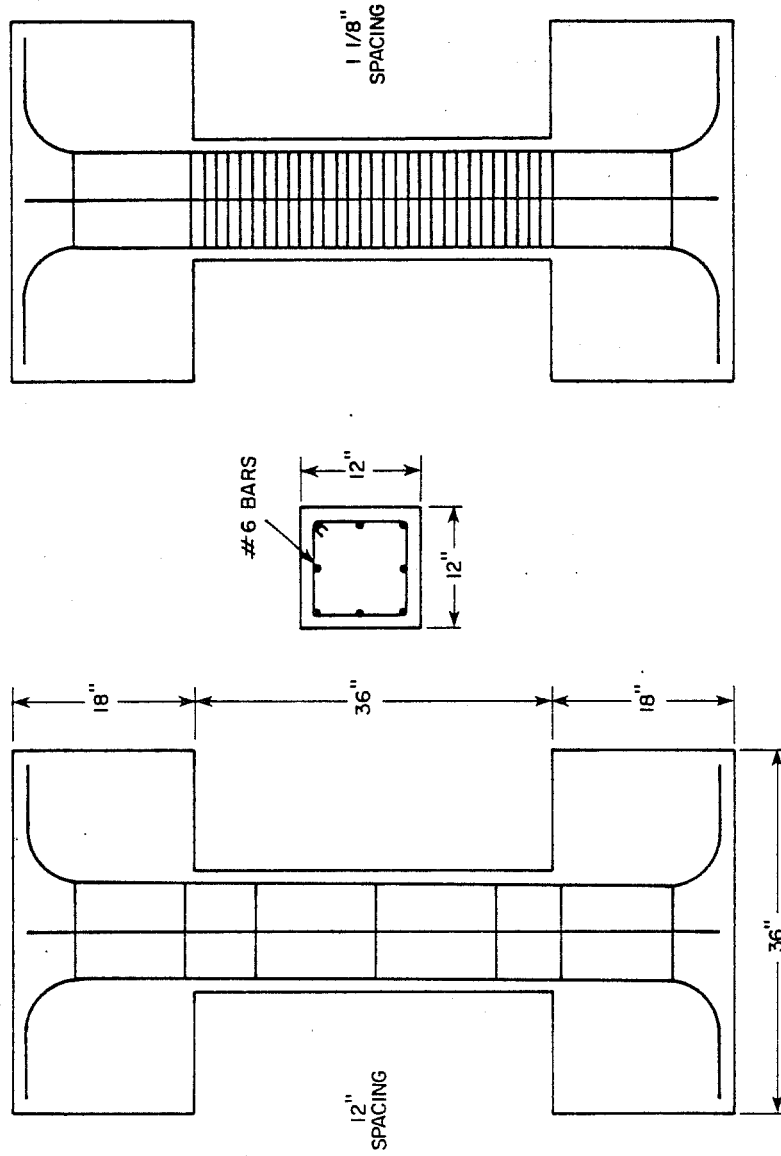


Fig. 2.6 86 series tie spacings

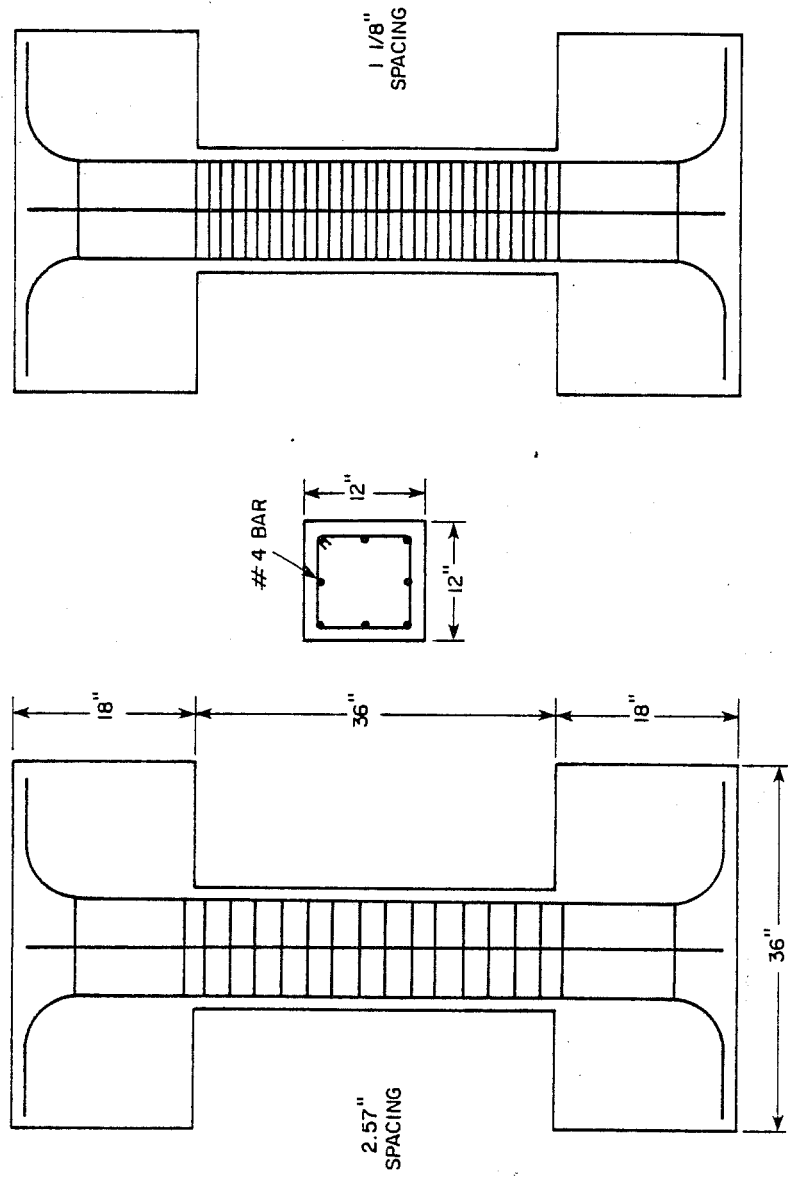


Fig. 2.7 84 series tie spacings

W = number of ties within the 36 in. column

3 - 12 in. spacing

9 - 4 in. spacing

14 - 2.57 in. spacing

21 - 1.75 in. spacing

32 - 1.125 in. spacing

X = loading history

D - cyclic along the diagonal, incrementally increasing peak deflection limits

DM - cyclic along the diagonal, one large peak deflection limit only

Example:

The specimen with ties at 2.57 in. and eight #6 longitudinal bars, subjected to the cyclic incrementally increasing deflections, and a 120 kip compressive axial load is

C - 86 - 14 - D

The specimens listed in Table 2.1 are identified using this notation.

## CHAPTER 3

### LOADING SYSTEM, INSTRUMENTATION, AND DATA REDUCTION

#### 3.1 Introduction

A description of the load frame and hydraulic system used to load the specimens is presented in this chapter. The instrumentation used to monitor the displacements, loads, and strains is described. The computer-based load-control and data acquisition systems is described. The manner in which data were processed and presented are explained.

Additional discussion of the loading system and instrumentation is presented in Refs. 14, 15, 92, and 93, which reported on the earlier investigations. Much of the design and fabrication of the loading system and instrumentation used in the current investigation was developed in the previous two investigations.

#### 3.2 Loading System

Reaction Frame--The deformation path imposed on the specimen required the simultaneous action of loading rams acting in three orthogonal directions (Fig. 3.1). The complexity and capacity of the loading system necessitated the construction of a permanent test facility--the reinforced concrete floor-wall reaction system (reaction wall) shown in Fig. 3.2 and fully described in Ref. 94. As can be seen, the reaction system consists of a structural tie-down floor and two orthogonal buttressed walls. The walls provide the reaction to rams loading the specimen horizontally in two directions while the floor provides a means of anchoring the

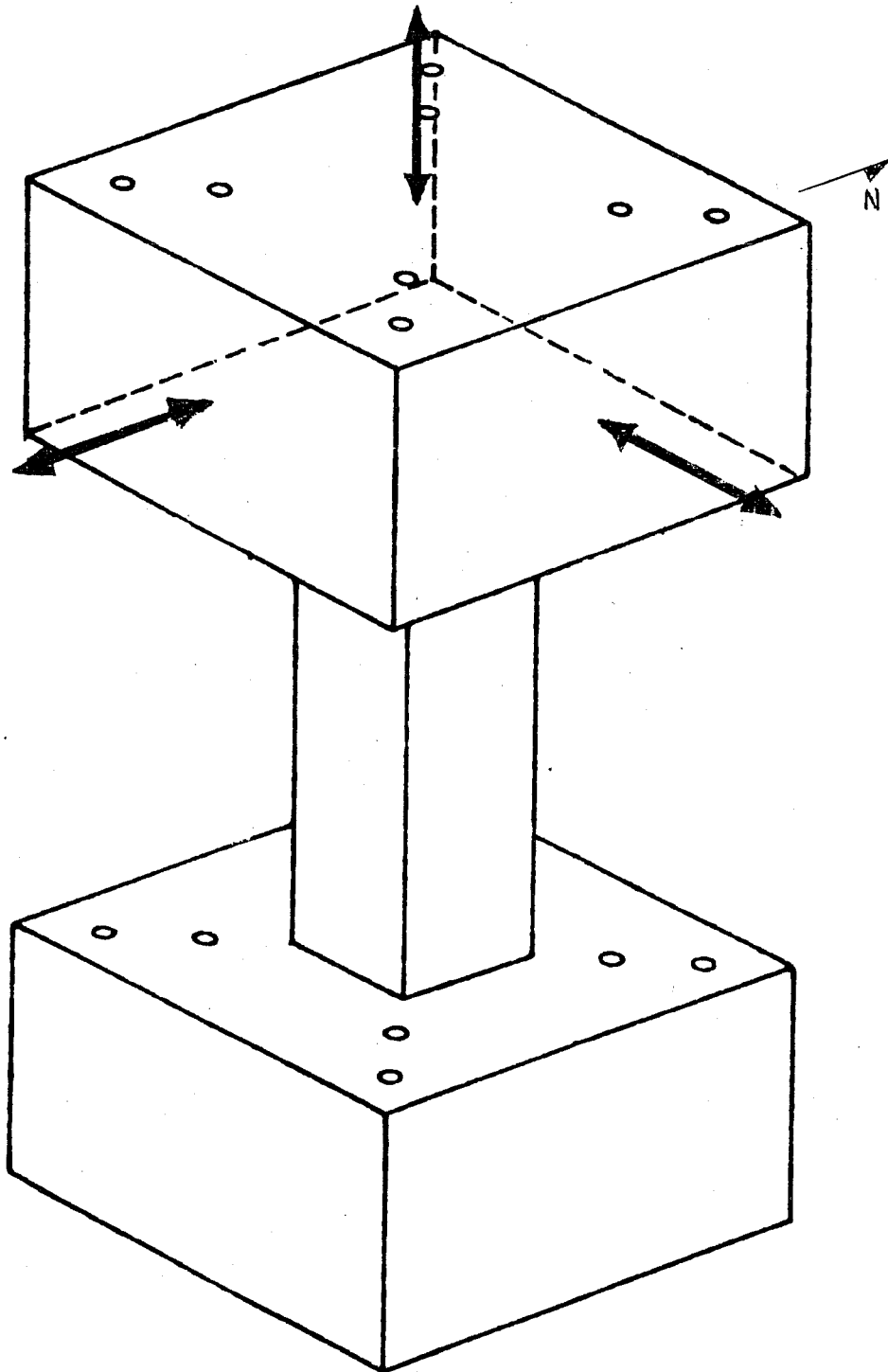


Fig. 3.1 Principal loading directions



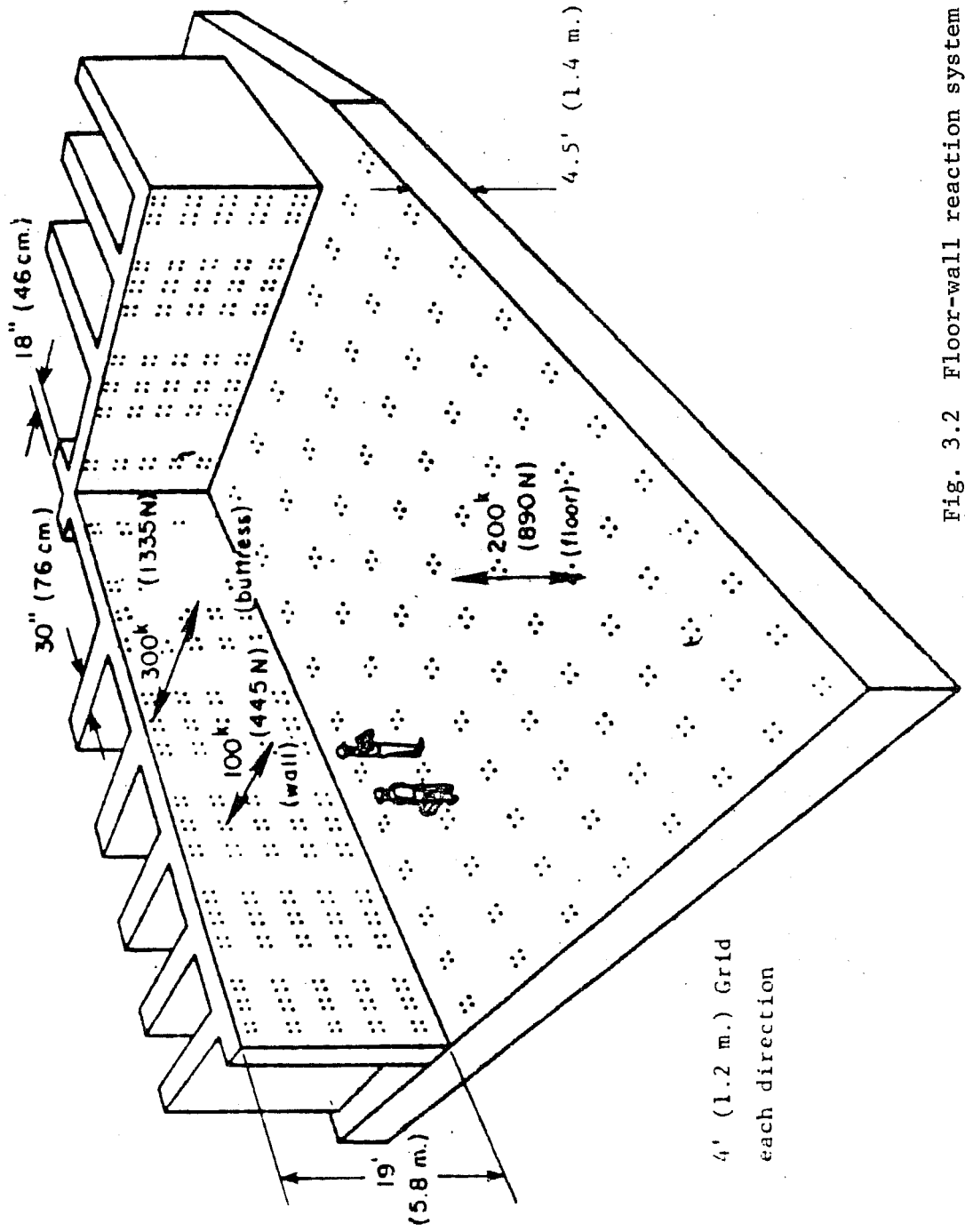


Fig. 3.2 Floor-wall reaction system [15]

reaction frame for the axial or vertical load applied to the specimen.

A picture of the actual test frame and hydraulic rams is shown in Fig. 3.3. The key elements of the loading system in the picture are the reaction wall, the test frame anchored to the floor to resist the axial load, and the hydraulic rams.

Hydraulic System--The hydraulic system is made up of two separate components. The first subsystem is the closed-loop hydraulic system which controls the three active load components. The second subsystem is separate from the first and is composed of interconnected hydraulic rams whose only function is to restrain the specimen ends from rotating during loading.

The closed-loop hydraulic system has three rams, three accumulators, and a central hydraulic pump. The rams--one for axial loading, the other two for lateral loading--are servo-controlled. The feedback to the servo controller is the output of either a load cell or a deformation transducer. One accumulator was used for each ram to control oil pressure and reduce oil volume surges in the hydraulic lines. The three loading rams and their relation to the specimen are shown in Fig. 3.4. The axial ram has a static load capacity of 300 kips and a piston stroke of 6 in. It was attached to the vertical reaction frame and the upper loading head on the specimen. The two lateral rams each have a static load capacity of 150 kips and a piston stroke of 12 in. The lateral rams were attached to the reaction wall and the upper loading head of the specimen.

In Fig. 3.4 the specimen is shown to be bounded at each end by a loading head which is a welded assembly of structural wide flange members. The specimen was attached to the loading head and base by passing eight high-strength threaded rods through both

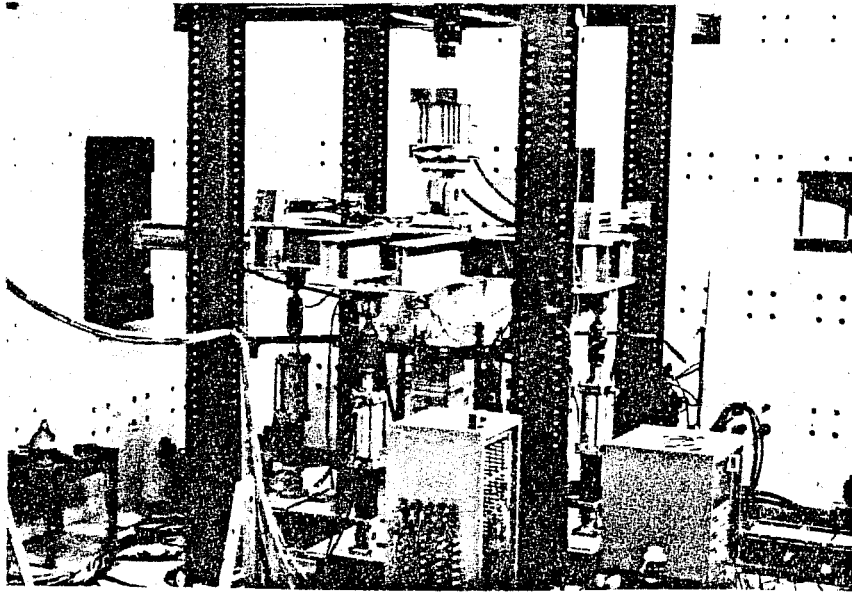


Fig. 3.3 Test setup

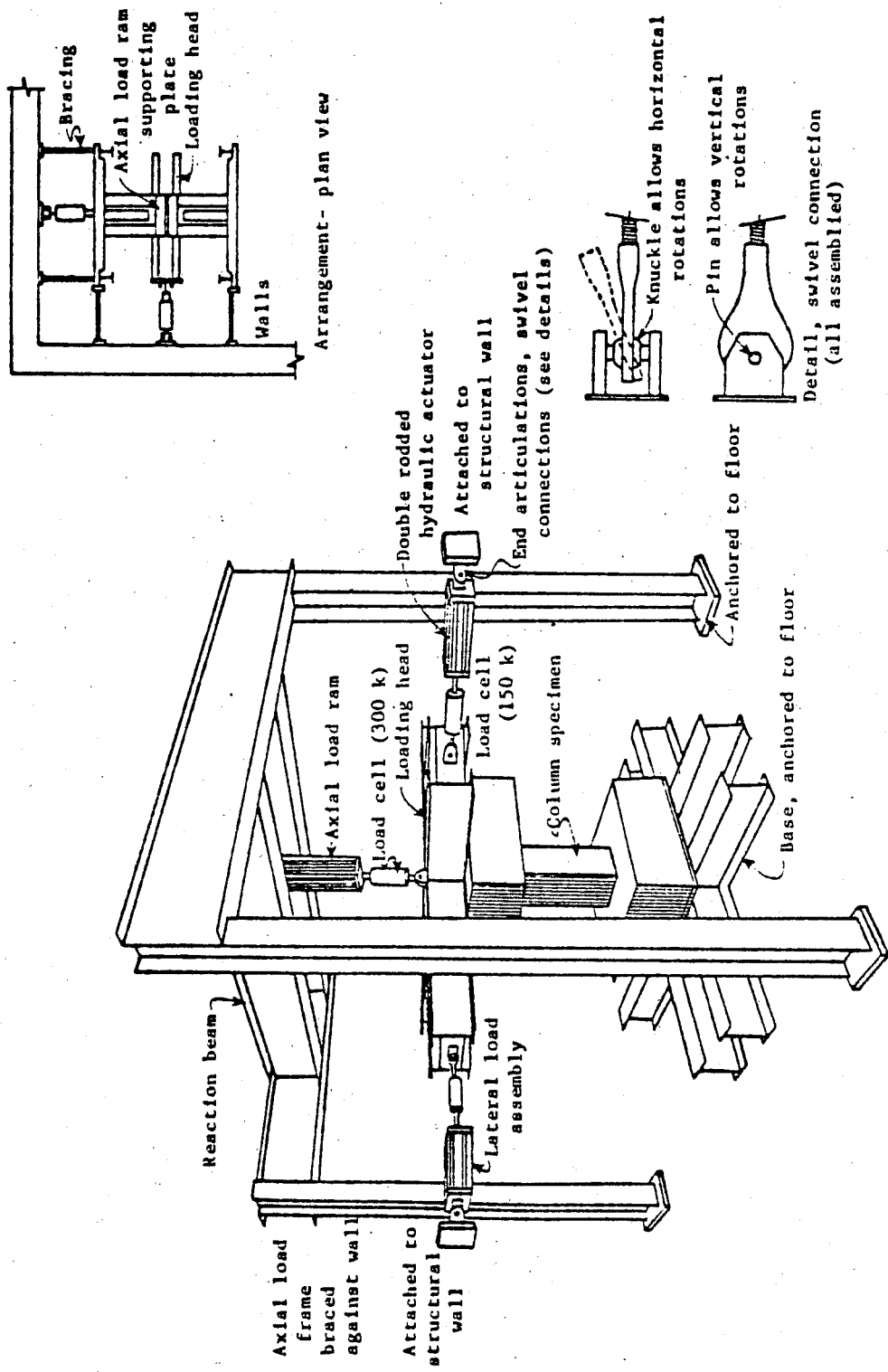


Fig. 3.4 Loading rams

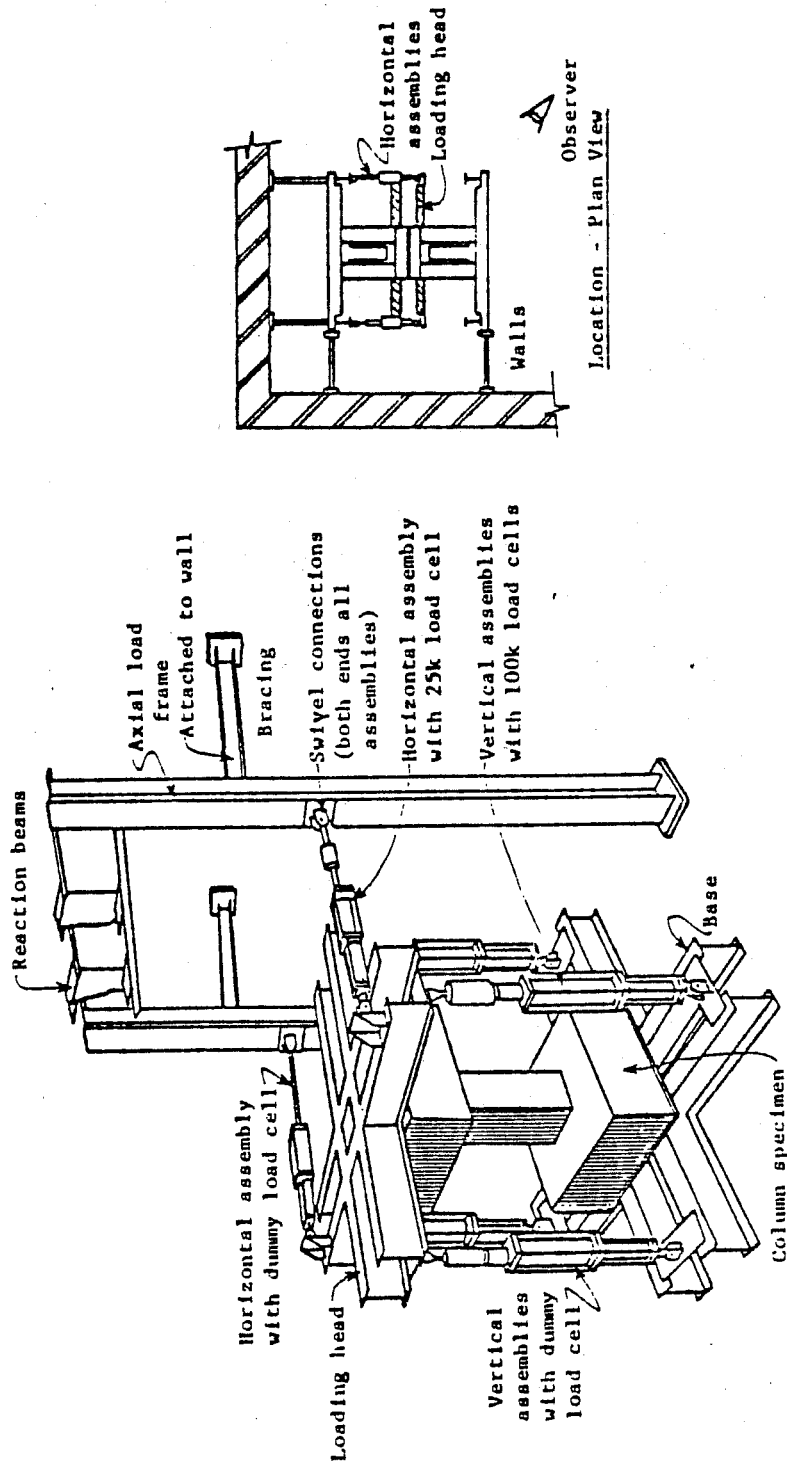
the loading head and the concrete end block. Nuts are threaded on each end of the rod and tightened, clamping the head to the end block. A gypsum cement was placed between the loading head and end block prior to tightening to ensure a smooth bearing surface. The base head is bolted to the test slab while the upper crosshead is free to translate in any direction.

The test column represents a column bounded by very stiff framing elements. It is desired that the column ends only translate to better model the condition of a fixed end member. Rotation of the ends of the member is restrained by a system of cross-coupled hydraulic rams shown in Fig. 3.5. The base very effectively restrains rotations of the lower end block of the specimen because it is anchored to the test slab. The upper block, however, requires the positioning rams to restrain its rotation during loading. The upper loading head acts as a lever to decrease the load required in the rams to resist the rotation of the upper end block.

The restraining system is composed of three pairs of rams. There are two pairs of vertical rams to resist rotation in the vertical plane and one pair of horizontal rams to resist any tendency to twist (Fig. 3.5). Each pair is cross-coupled, as shown in Fig. 3.6. The coupling of opposing cells in the rams forces the rams to undergo identical movements. Both rams may extend or retract equally, as in the case of a vertical translation of the upper loading head. However, because of cross-coupling one ram in a pair cannot retract while the other ram extends. The resistance to differential displacement restrains rotation of the upper head. The three pairs of restraining rams restrain rotation in any direction.

### 3.3 Instrumentation

Three types of measuring devices were used to monitor the performance of the specimen during testing--load cells, linear



Positioning System - Schematic

Fig. 3.5 Restraining rams

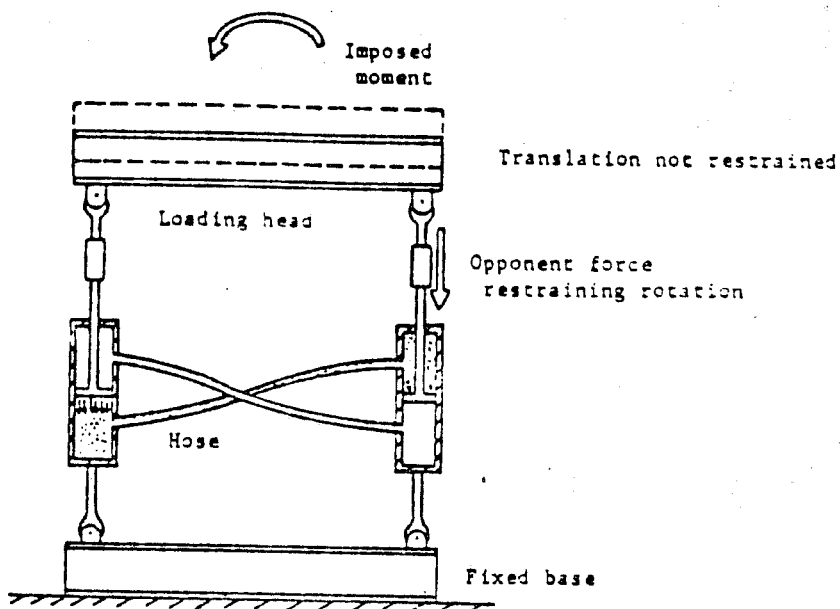


Fig. 3.6 Coupled restraining rams

potentiometers (pots), and strain gages.

Load Cells--Load cells were mounted on each of the loading rams and on one ram in each pair of restraining rams. The load cells on the loading rams contained double bridges. One bridge was used for data acquisition and the other was used as feedback to the servo controller. Separate bridges were used to eliminate the possibility of having the data acquisition system interfere with the servo controller feedback signals. The signals from the lateral loading rams were also plotted on x-y recorders.

Linear Potentiometers--In a potentiometer the output voltage varies directly with the position of the slide rod. Twelve potentiometers were used to monitor the deflection and rotation of the specimen end blocks at the locations shown in Fig. 3.7. The lateral deflections of the lower block were not monitored because they were found to be negligible. The method of mounting the potentiometers is shown in Fig. 3.8. A bolted frame was built around the specimen and cemented to the test slab and braced against the axial load reaction frame to prevent movement. Welded pipes on the frame members provide a means of clamping the potentiometers to the frame and ensure proper placement of the pots. The slide rods on the pots were spring-loaded and the rods rested on metal plates glued to the specimen to allow for specimen movement.

The signals of two lateral potentiometers were used in conjunction with the load cell signals from the lateral loading rams to drive two x-y recorders and to produce the load-deflection curves along each of the two loading axes.

Strain Gages--Strain gages were attached to both tie and longitudinal reinforcement to provide an indication of the effect of external loading on the performance of the reinforcement.



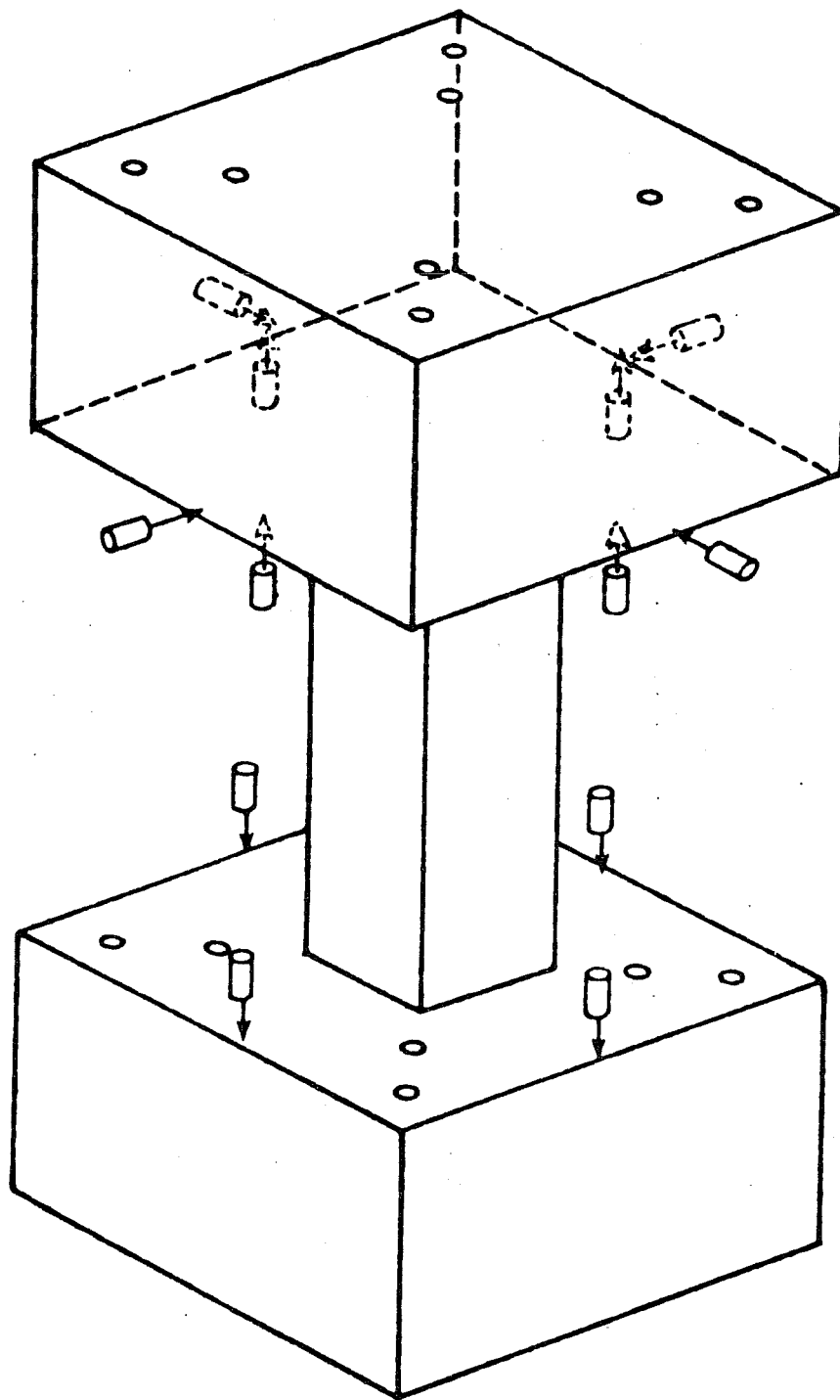
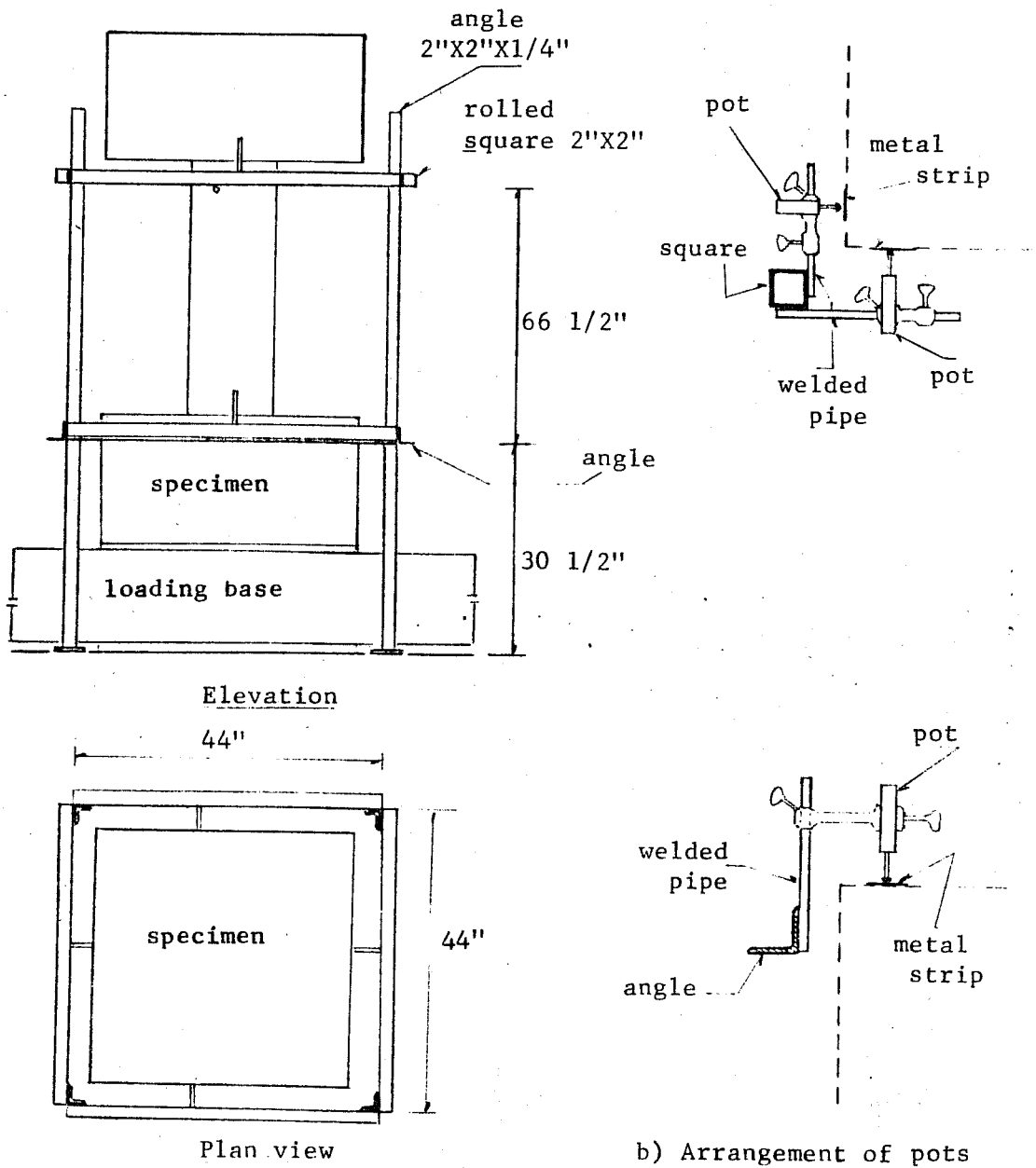


Fig. 3.7 Linear potentiometer locations [14]



a) Supporting Frame

b) Arrangement of pots

Fig. 3.8 Linear potentiometer mounting frame [15]

Strain gage locations are shown in Fig. 3.9 for a specimen with a tie spacing of 2.57 in. Gages were placed on all four faces of six ties and on the corner longitudinal bars at the intersection of the column and the end blocks. As the tie spacing varied, the ties were not at the same location in the column, so the gages were attached to the ties closest to the locations described in Fig. 3.9. The gages on the longitudinal bars were unaffected by tie spacing and were in the same location for all specimens.

#### 3.4 Computer-based Load Control System

The loading of the specimen and data acquisition are both controlled through the use of a minicomputer. The operator issues commands to the computer from a console at the test site. The computer interprets the user commands and issues the proper instructions to the servo-controllers and a VIDAR data scanner. A schematic of the system is shown in Fig. 3.10.

The minicomputer acts as the manager of the system in that it accepts commands, interprets the commands, operates the equipment necessary to fulfill the commands, monitors the condition of the system, and records any data obtained from the VIDAR data scanner.

The servo-controller acts on command from the minicomputer, but carries out the command independently of the minicomputer. A servo-controller directs the ram piston to extend or retract until the command signal is matched by a feedback signal from the ram. The feedback may either be load or deformation. As an example, if a command signal is issued to a deformation controlled ram then the servo controller will move the ram piston until the feedback signal from the deformation transducer is equal to the command signal. The servo controller will then keep the piston

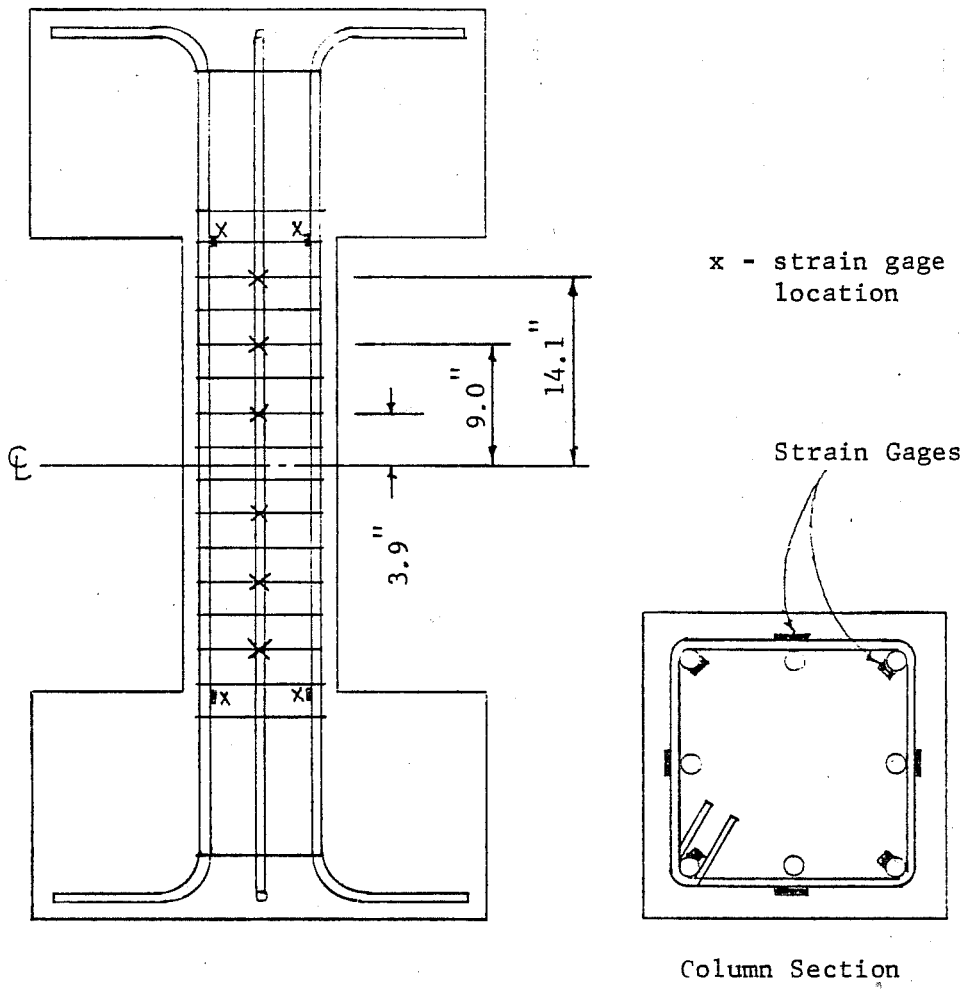


Fig. 3.9 Strain gage locations

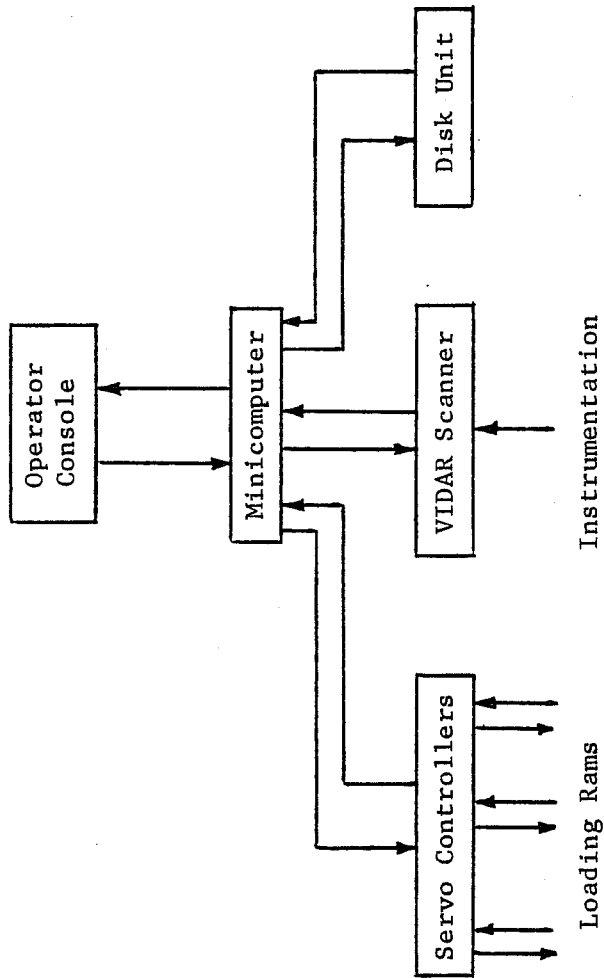


Fig. 3.10 Load control system

at that deformation until the command signal is changed. The same concept is true for the case of load controlled rams. In the current investigation the axial ram was load controlled because a constant 120 kip load was to be maintained. The lateral rams were deformation controlled because deflections and not loads were applied to the column.

The VIDAR data scanner reads the analog signal from each measuring device and converts it to digital voltage. The digital voltage is transmitted to the minicomputer which then stores it on a disk unit for later use. The VIDAR data scanner is started on command of the minicomputer.

The advantage of the load control system was that precision control of the ram movements and automatic data acquisition were possible with very little direct intervention by the operator.

### 3.5 Data Reduction

Data reduction encompasses the entire process from the raw digital voltages to finished plots or tables of the data in the usual engineering units. The number of steps in the process varies with the complexity of the data and the manipulations required to arrive at the desired form of the data. In the current investigation, an average of 24,000 pieces of data were obtained in each test. In one test alone, over 34,000 pieces of data were recorded. The manipulation and study of such a vast amount of data required computer-based data reduction techniques. The nature of the tests prompted an extensive use of plotted data rather than tabulated data, because trends and characteristics are much easier to see in plots.

The preliminary step in reducing the data is the conversion of the digital voltages to more common engineering units such as

kip and inches. Following this, the load cell readings for the loading rams are adjusted to account for changes in loading geometry during movement of the specimen. The rationale for the adjustment is described in Appendix E. Particular data are then isolated for additional manipulation and plotting. The most common and informative plot from a cyclic test is the load versus deflection relationships. In the current investigation, the direction of deflection (loading) is not coincident with the direction of data measurement because the specimen is deflected along the diagonals. As a result, the measured data (load and deflection) are vectorially summed to obtain a load-deflection relationship along the actual axes of deflection.

Once all the manipulations were done, the data were plotted using a digital plotter. The load-deflection curves in Chapter 5 are such plots. It should be noted, however, that the load-deflection curves are smoothed curves in the regions of low load. The low level signals of the load cells were disturbed by interference, making it necessary to smooth the plotted curves using the load-deflection curves obtained from the x-y recorder plots. The smoothing was done manually using load values taken from the x-y recorder curves. The x-y recorder plots were not affected by the signal interference.

## C H A P T E R 4

### DESCRIPTION OF SPECIMEN PERFORMANCE

#### 4.1 Introduction

Chapter 4 contains a description of the load-deflection curves and crack patterns for each of the tests in the current investigation. The description avoids any comparisons between tests or explanations for the observed condition of the specimens. The comparative studies and explanations are presented in Chap. 5.

For each test in the current investigation, load-deflection curves are described and the observed condition of the test specimen at certain times during the test is described using pictures of the crack patterns. The strain gage data is not presented in the descriptions of the column tests. The strain gage data generally provided information confirming observations made from crack patterns and load-deflection curves. Particularly useful strain gage data is presented during comparisons in the subsequent chapters. In many columns, the gages performed satisfactorily only during the first part of the loading history. Abrasion of the gages by concrete moving across them and bar yielding led to the loss of information from many gages. The values of strain from the ties and longitudinal bar gages are highly questionable. Bending of the ties due to core expansion could produce very high strain readings which are not indicative of the axial strains. Similarly, the longitudinal bar gages may give readings which are significantly influenced by high shear transfer forces across the ends of the column.

The measurements of lateral load and lateral deflection



were taken along axes perpendicular to the faces of the column. However, as shown in Fig. 4.1, the specimens were deflected along axes parallel with the diagonals of the specimens. In order to present load-deflection curves that represent the action of the specimen along its deformation path, it is necessary to transform the measurements obtained on one set of axes to equivalent values on the diagonal axes. The required change in axes orientation was shown in Fig. 4.2. Resultant loads or deflections are determined by taking the square root of the sum of the squares of the measurements, as shown in Fig. 4.3. The end result of the transformation is load-deflection curves that represent the action along the lines of movement. Cycles in the first and third quadrants are considered to act along the first diagonal and cycles in the second and fourth quadrants are along the second or orthogonal diagonal, as illustrated in Fig. 4.4.

The lateral loads used in the load-deflection curves of the 86 series specimens were normalized to reduce the effect of differing concrete compressive strength between the tests. The normalization was done by multiplying the lateral loads by the factor

$$\sqrt{\frac{5000}{f'_c}} \quad (4.1)$$

where  $f'_c$  was the concrete compressive strength of the test being normalized. The relation  $\sqrt{f'_c}$  was used because the 86 series specimens were dominated by shear effects and bond effects. Both of which are generally considered to be functions of  $\sqrt{f'_c}$  by the 1977 ACI Building Code [17], the ACI-ASCE Committee 426 report [49], and the ACI Committee 408 recommendations for development length [84]. The factor (Eq. 4.1) was nondimensional and was intended to normalize the lateral loads to represent a specimen with a concrete compressive strength of

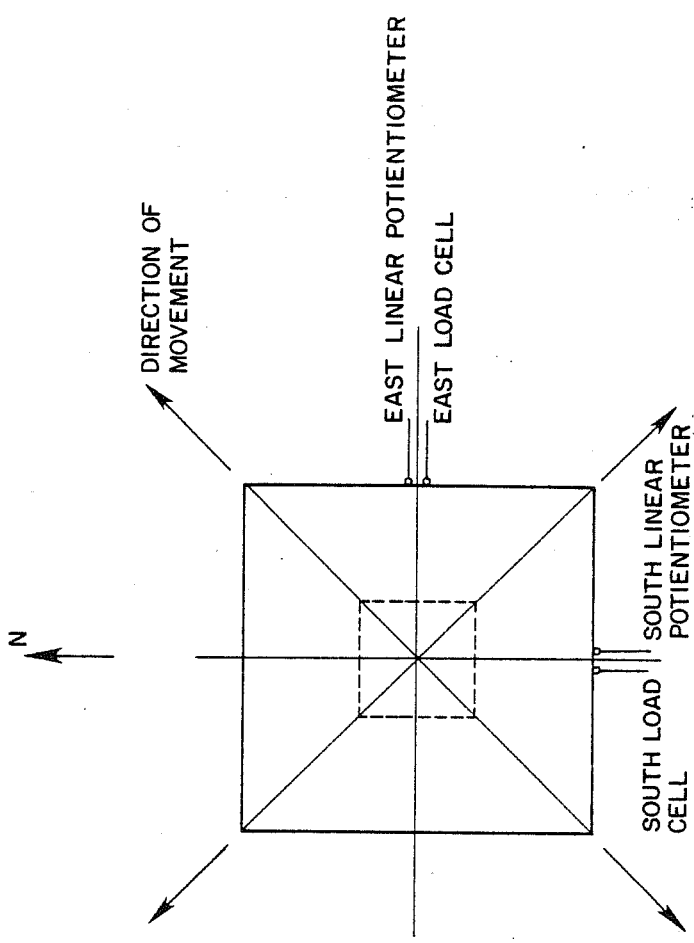
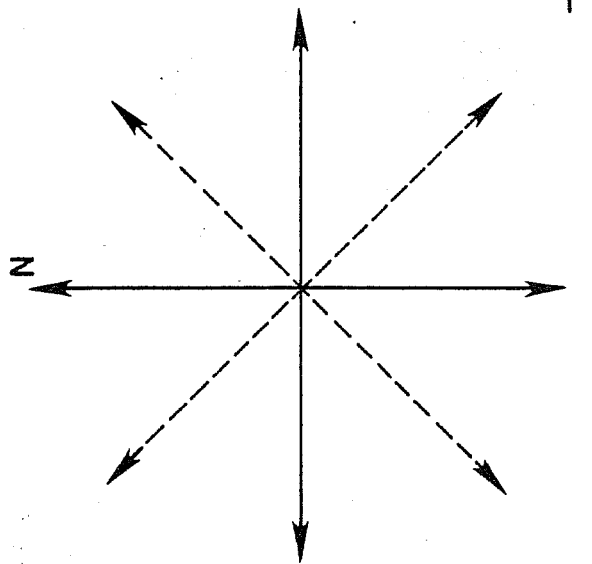


Fig. 4.1 Deformation path



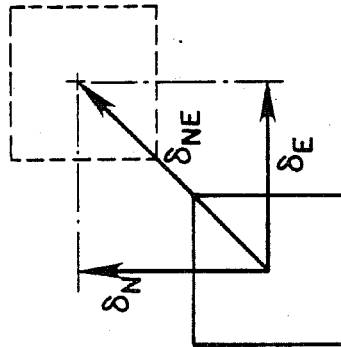
+

AXES OF MEASUREMENT

X

AXES OF MOVEMENT AND  
RESULTANT MEASUREMENTS

Fig. 4.2 Axes of measurement and deformation



$$\delta_{NE} = \sqrt{\delta_E^2 + \delta_N^2}$$

WHERE  $\delta$  REPRESENTS BOTH THE LATERAL  
LOAD AND DEFLECTION

Fig. 4.3 Computation of resultant measurements

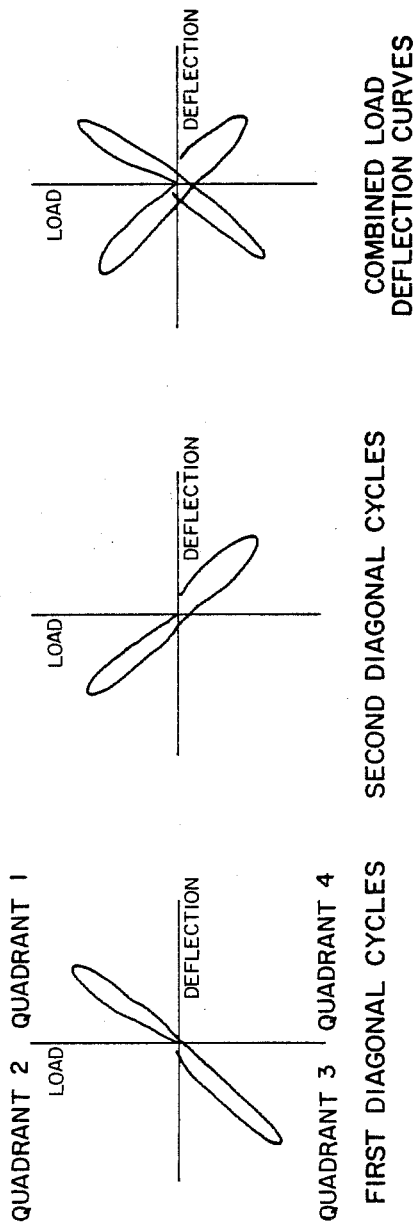


Fig. 4.4 First and second diagonals

5000 psi, which was approximately the average strength of the tests in the current investigation.

The specimens were cycled between the deflection levels of 0.28, 0.57, 0.84, and 1.13 in. in practically every test. For some specimens the test was continued to higher deflections. To denote the four principal deflection levels used during the test,  $1\Delta$ ,  $2\Delta$ ,  $3\Delta$ , and  $4\Delta$  were used. The symbol  $\Delta$  represents the initial deflection level of 0.28 in. and other deflection levels are multiples of  $\Delta$ . As discussed in Sec. 2.2, the initial deflection level comes from the investigation conducted by Maruyama [14]. It is the deflection at which first longitudinal bar yielding occurred in a unidirectionally deflected column. For clarity, on each load-deflection curve the locations of the four  $\Delta$  levels are labeled.

For a given specimen, the pictures of crack patterns are denoted by a letter from A to E as part of the figure number, such as Fig. 4.6A. The letters also appear on the corresponding load-deflection curve to pinpoint the stage at which the picture of the crack pattern was taken.

#### 4.2 Specimen 0-86-14-DM

The specimen had no applied axial load, ties spaced at 2.57 in., and was deformed along the northwest-southeast diagonal to a peak deflection of 1.4 in., as shown in Fig. 4.5. The peak lateral load was reached at a resultant deflection of approximately 0.5 in. The lateral load carried by the specimen dropped as deflection increased past 0.5 in. The lateral load decreased rapidly between 0.5 and 0.75 in., but then more gradually with increased displacements to the limits of the test. When the direction of deformation was reversed to return the specimen to

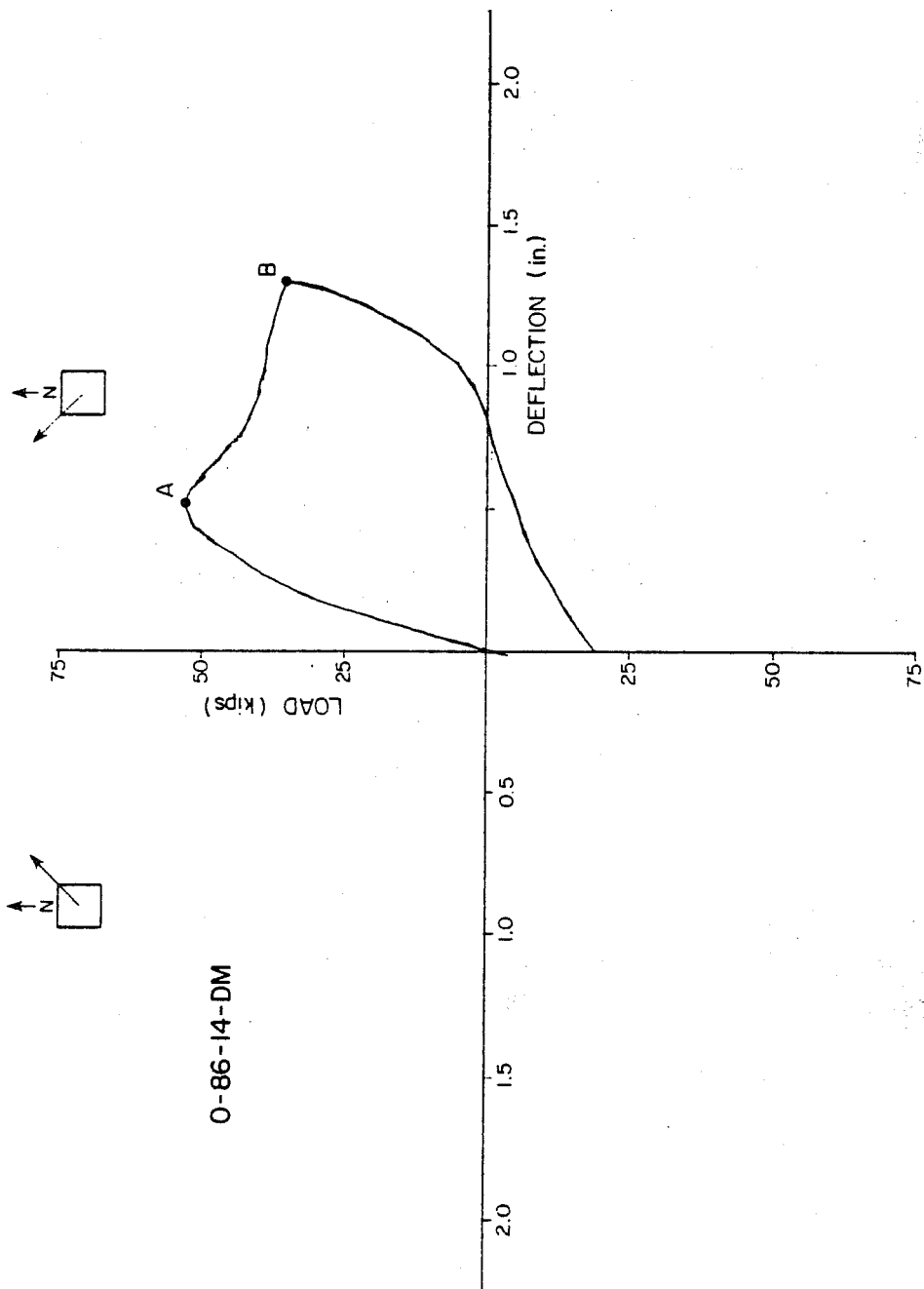
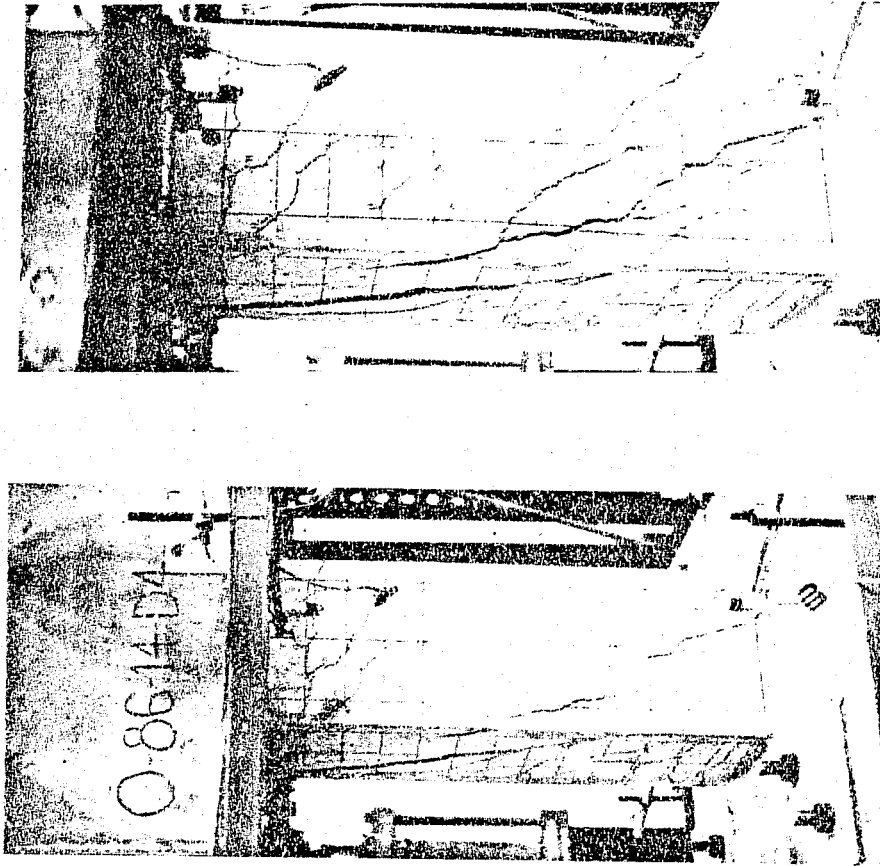


Fig. 4.5 Specimen O-86-14-DM load-deflection curve (half cycle)



(A) Peak load (B) Peak deflection

Fig. 4.6 Specimen 0-86-14-DM crack patterns



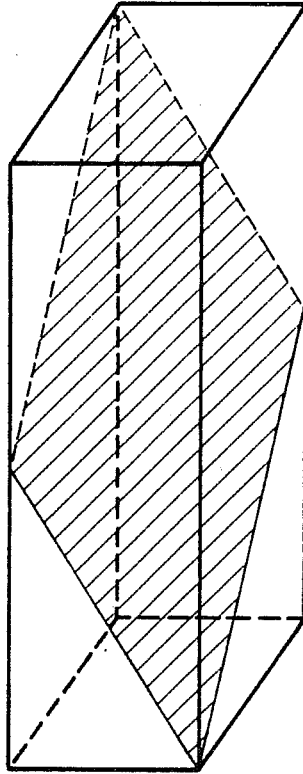


Fig. 4.7 Crack wrap around effect

its initial position, the specimen exhibited an initially very stiff unloading curve with a change to a moderate stiffness near zero lateral load.

The physical condition of the specimen at the point of peak lateral load and at the peak displacement is shown in Figs. 4.6A and 4.6B, respectively. The crack patterns consist of large diagonal cracks throughout the length of the column. The major cracks wrap around a corner and continue on the adjacent face. A major crack plane oriented along the diagonal can be seen emerging on all faces of the specimen, as shown in Fig. 4.7, by cutting a box with an inclined plane.

#### 4.3 Specimen C-86-14-DM

The specimen had ties spaced at 2.57 in. and an applied compressive axial load. It was deformed along the northwest-southeast diagonal to a deflection of 1.4 in. The specimen was then returned to its original position along the same path. To investigate the effect of one cycle at such a high peak deflection the specimen was deformed along the same diagonal, but in the opposite direction to the same value of deflection as reached in the initial direction. The specimen was returned to its original position and a similar procedure was followed for loading along the orthogonal diagonal. In effect, the specimen was subjected to cyclic deformations between very large peak deflection limits.

The initial loading applied to the specimen is shown in Fig. 4.8. The peak lateral load was reached at about 0.5 in. The peak lateral load was maintained only up to a deflection of 0.6 in. when a sharp drop in lateral load occurred. After the sharp drop, the rate of loss of lateral load remained fairly constant with increased deflection. When the deflection of the

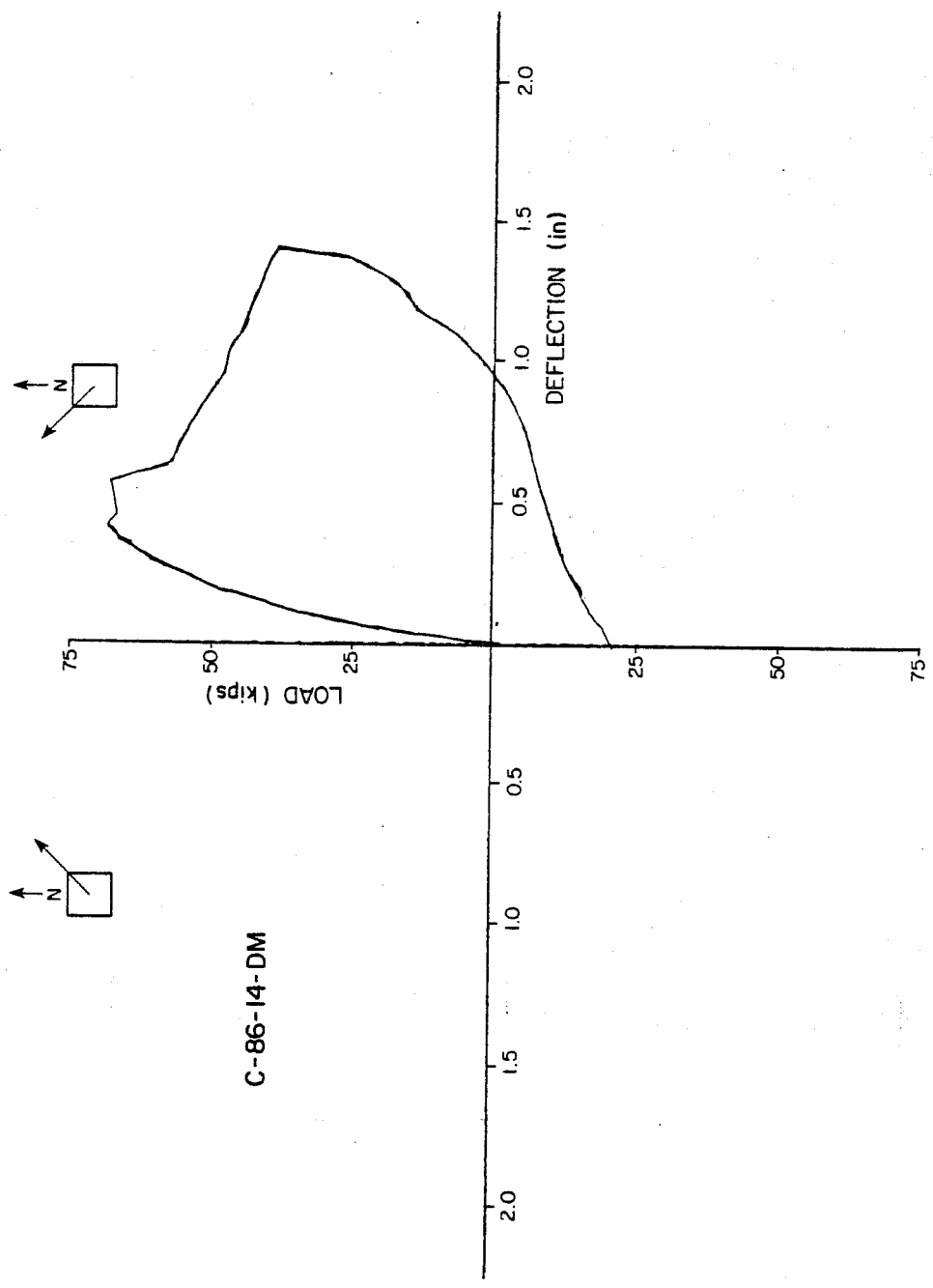


Fig. 4.8 Specimen C-86-14-DM load-deflection curve (half cycle)

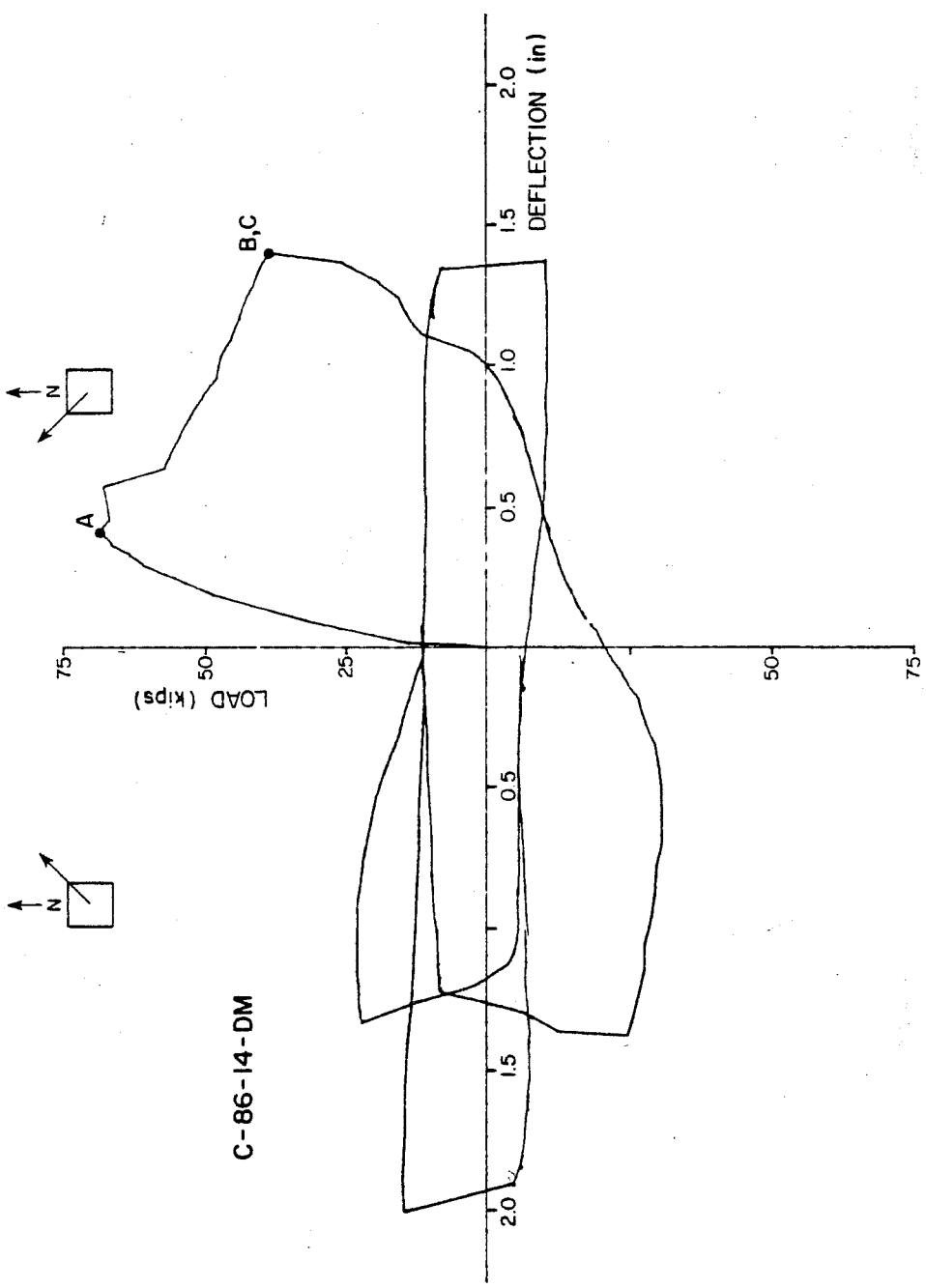
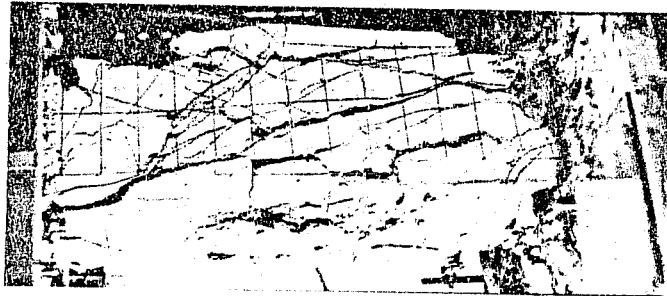
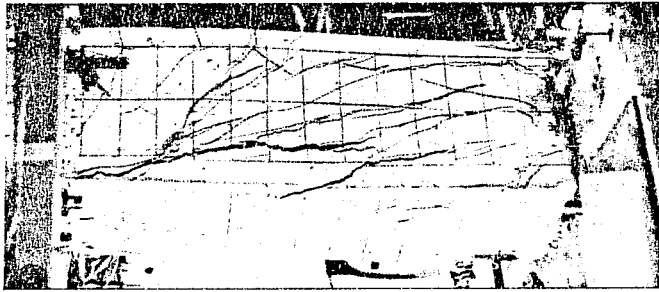


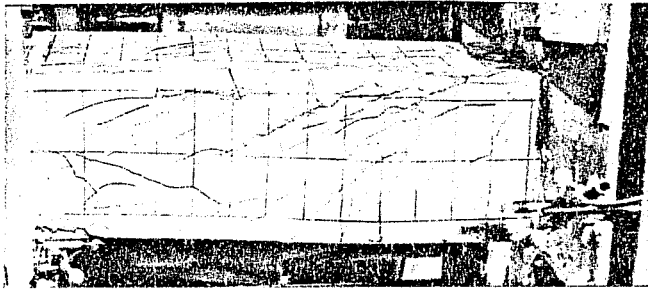
Fig. 4.9 Specimen C-86-14-DM load-deflection curves



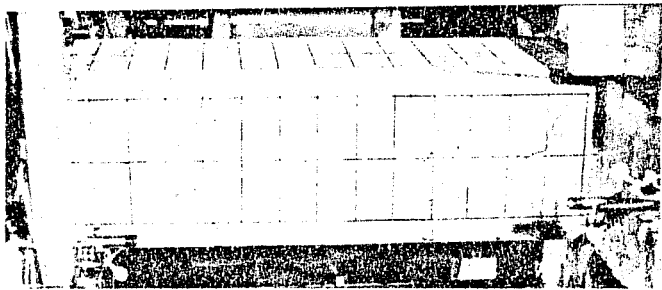
(D) EOT



(C) 5Δ



(B) 5Δ



(A) 1Δ

Fig. 4.10 Specimen C-86-14-DM crack patterns

specimen was reduced as it returned to its initial position, the load-deflection curve showed a very stiff unloading curve, but near zero lateral load, the stiffness rapidly approached zero before increasing again as the specimen neared zero deflection.

The complete load-deflection curve for the specimen, Fig. 4.9, showed quite clearly that the specimen deteriorated very rapidly after completing the first cycle to high peak deflection limits. In the orthogonal direction very low peak lateral loads were reached as a consequence of the severe damage to the specimen during the first cycle.

The crack patterns mirrored the damage indicated by the load-deflection curves. Figures 4.10A through 4.10D show the specimen at various stages of the test. Figure 4.10A shows the east face of the specimen at a deflection of 0.29 in. during the initial loading towards the northwest. Only a few flexure and flexure-shear cracks are visible. Figure 4.10B shows the same face of the specimen at the peak NW deflection. A number of diagonal cracks were present, with the major ones being quite wide and extending the length of the specimen. Figure 4.10C clearly shows the tendency of the cracks to wrap around corners of the specimen. Figure 4.10D shows the northeast corner of the specimen at the end of the test when the specimen had suffered severe damage as the result of cycling between high displacement levels.

#### 4.4 Specimen 0-86-32-D

The specimen had ties at the minimum spacing, 1-1/8 in., used in the current investigation and no applied axial load.

The load-deflection curves, Fig. 4.11, revealed that the behavior of the specimen was not stable. The peak lateral load occurred at a deflection of about  $3\Delta$ . Cycling between deflection

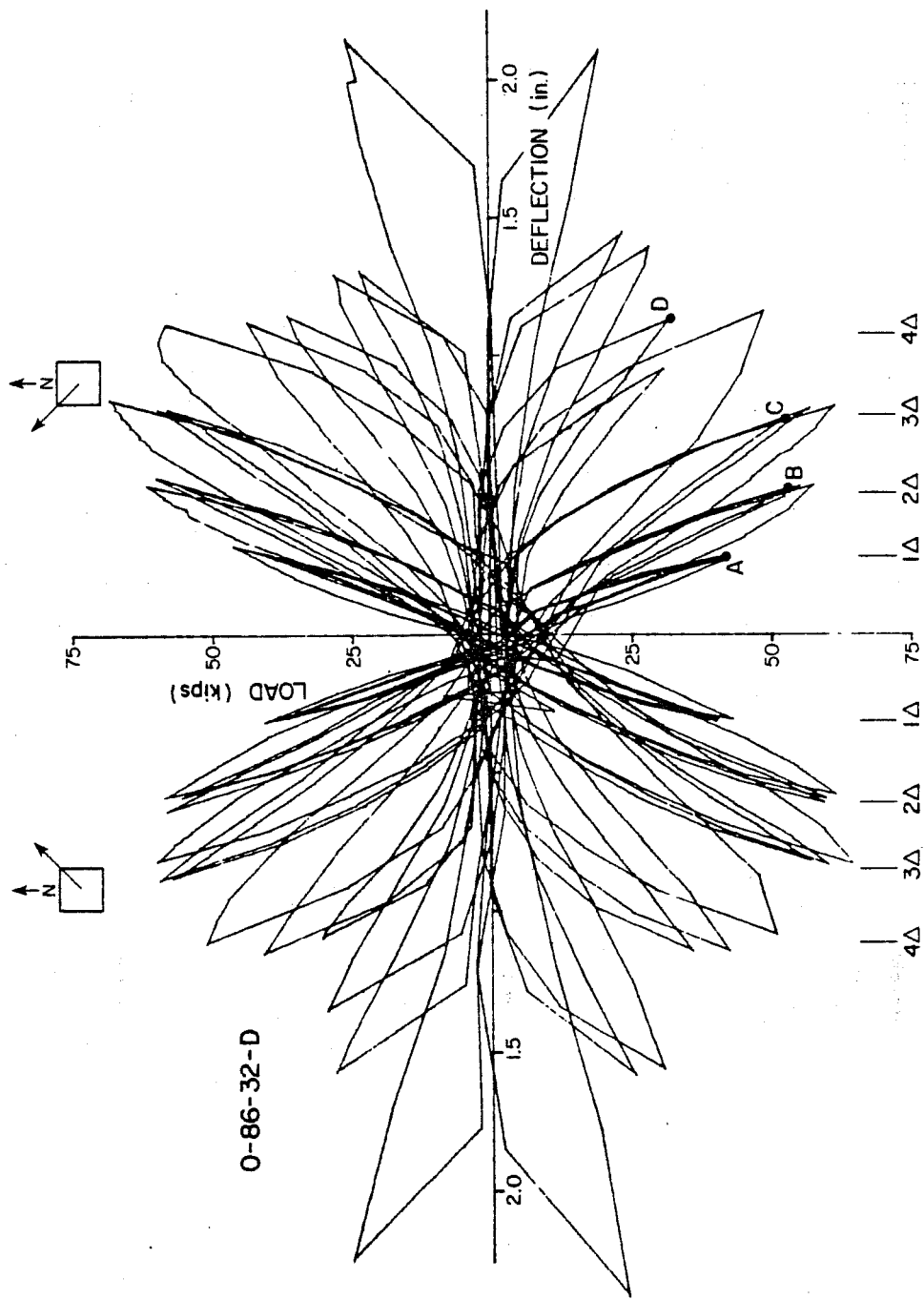
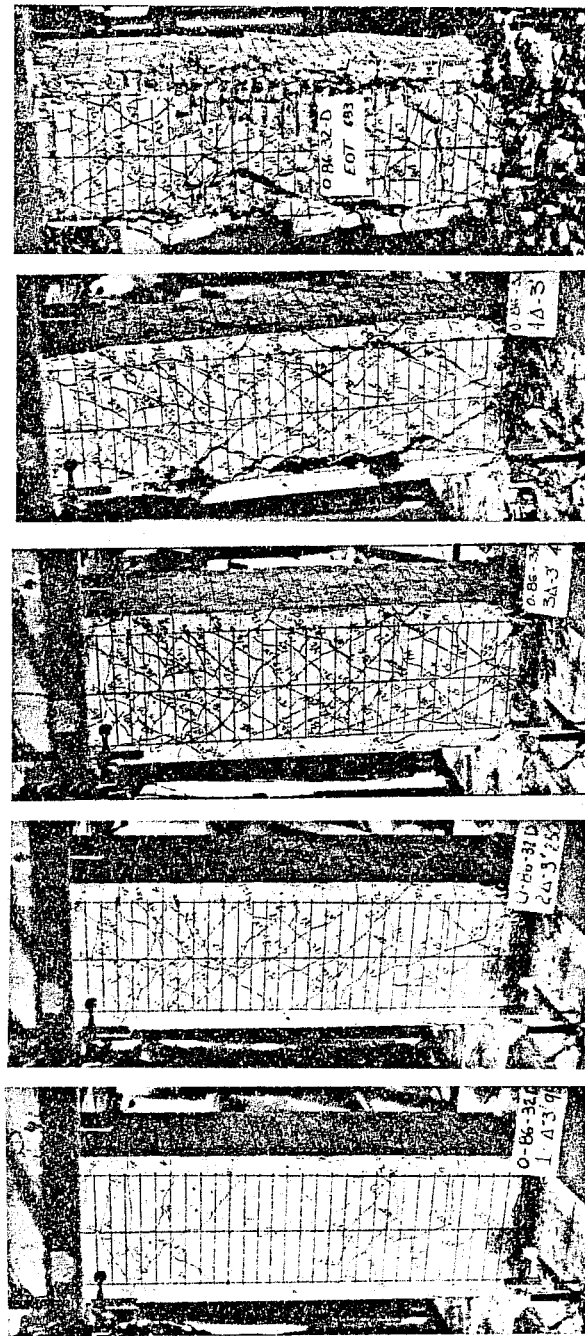


Fig. 4.11 Specimen O-86-32-D load-deflection curves



(A) 1Δ                      (B) 2Δ                      (C) 3Δ                      (D) 4Δ                      (E) EOT

Fig. 4.12 Specimen 0-86-32-D crack patterns



limits of  $3\Delta$  produced a noticeable drop in lateral load between the first and second cycles, but not between the second and third cycles. The peak lateral load was not achieved again even with increased deflection, as indicated by the first cycle at the next higher deflection increment of  $4\Delta$ . In fact, the load was decreasing as deflection approached  $4\Delta$ . Cycling between the deflection limit of  $4\Delta$  produced significant drops in lateral load with each cycle. The trend of reduced lateral load with cycling continued at higher deflection levels. It was noticed, however, that increased deflection brought a limited increase in the lateral load compared to the last cycle at a lower deflection.

The overall shape of the hysteretic loops changed during the test, especially upon reaching the peak lateral load. After the peak was reached, the curves exhibited increasing "pinching" toward the origin where the stiffness of the specimen was very low.

Figures 4.12A through 4.12D show the south face at the end of cycling between deflection limits of  $1\Delta$ ,  $2\Delta$ ,  $3\Delta$ , and  $4\Delta$ , respectively. Cycling at  $1\Delta$ , which did not yield the longitudinal reinforcement, did little to the specimen except produce flexural cracks and some flexure-shear cracks. As would be expected, the cracking was nearer the ends than the center. By the end of cycling at  $2\Delta$ , well distributed inclined cracks had formed all along the specimen. The cracks were quite narrow and closed readily. At the end of cycling at  $3\Delta$  the cover of the specimen was severely cracked and spalling of the cover concrete at the bottom of the column was observed. The cycles at  $4\Delta$  caused a large percentage of the cover to spall off, especially at the corners. The specimen showed no sign of a major diagonal crack as had been observed in the previously described tests. Instead, the cracks penetrated only through the cover. The condition of

the specimen at the conclusion of the test, Fig. 4.12E, clearly showed three major features. The first was the nearly complete loss of cover. Cover visible in the photo remained only because it was attached to instrumentation wires and wires tying the reinforcement together. The second feature was the relatively intact core of the column. The third and most interesting feature was the complete loss of concrete around the longitudinal bars in the middle region of the column.

#### 4.5 Specimen C-86-32-D

Specimen C-86-32-D had ties at the minimum spacing used in the current investigation, 1-1/8 in., and an applied compressive load.

The load-deflection curves, Fig. 4.13, show a rapidly deteriorating specimen. The peak lateral load occurred at a deflection of  $2\Delta$  during the first cycle at that deflection level. Subsequent cycles at the same deflection exhibited unstable characteristics. Of more interest was the first cycle at the next higher deflection level,  $3\Delta$ . There was a sharp drop in both stiffness and lateral load after the imposed deflection exceeded  $2\Delta$ . The second cycle showed a marked change in the shape of the curve and all following cycles at that and higher deflection levels exhibited similar characteristics--long regions of very low stiffness. Only near the deflection limits of each cycle did the lateral load increase significantly.

Figures 4.14A through 4.14D show the west face of the specimen at the end of cycling at the deflection levels of  $1\Delta$ ,  $2\Delta$ , and  $3\Delta$  and at the end of the test, respectively. Very little cracking occurred during cycling at  $1\Delta$ . Primarily, it was flexural cracking with a few flexure-shear cracks. The cycling

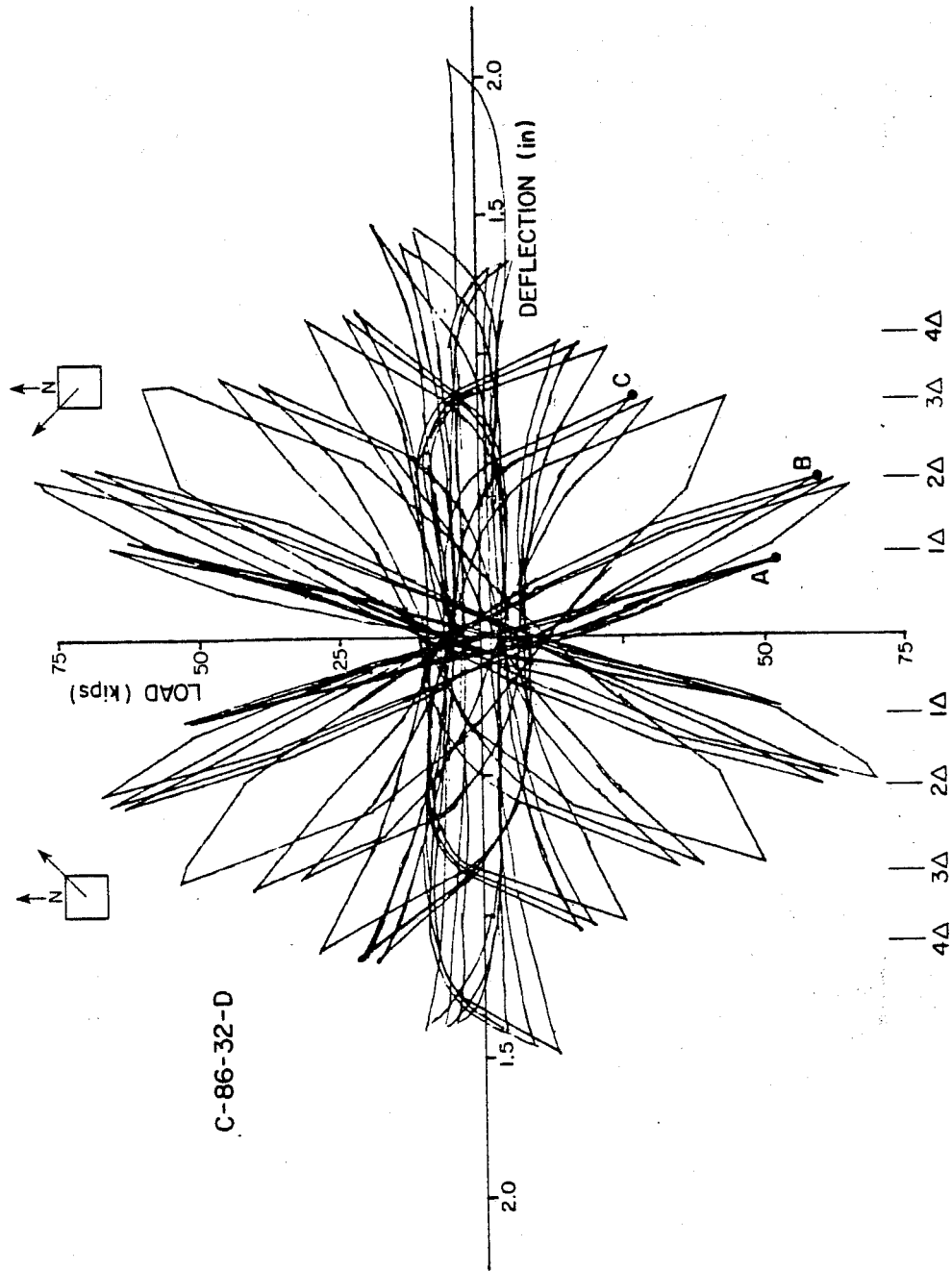
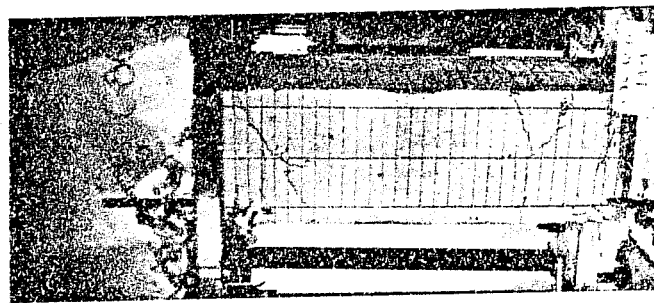
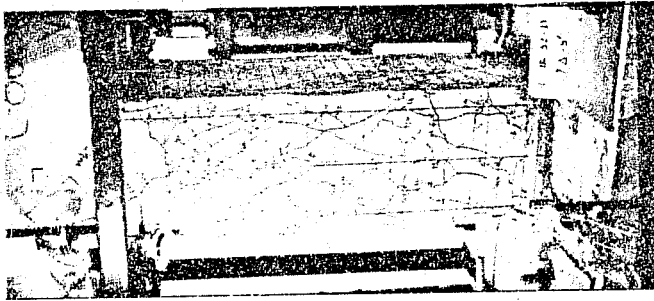
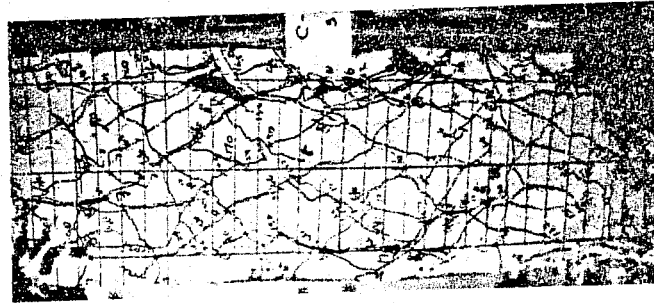


Fig. 4.13 Specimen C-86-32-D load-deflection curves



(A) 1Δ

(B) 2Δ

(C) 3Δ

(D) EOT

Fig. 4.14 Specimen C-86-32-D crack patterns

between deflection limits of  $2\Delta$  produced a large amount of cracking, most of which was inclined and not connected to flexure cracks. Of interest was the cracking along the corner longitudinal bars. These cracks started corner cover spalling which became prominent during the cycling at  $3\Delta$ . Also, during cycling at  $3\Delta$  the cover at the bottom end of the column spalled off. By the end of the test, nearly all of the cover had become ineffective and a great deal had fallen off. The concrete core was partially fragmented, but the majority of it seemed relatively intact. The concrete around the longitudinal bars was gone in the midheight region of the column. There was little evidence of significant concrete crushing in the core at the ends of the specimen.

#### 4.6 Specimen C-86-21-D

The specimen had ties spaced at 1-3/4 in. spacings and an applied compressive axial load.

The load-deflection curves for this specimen, Fig. 4.15, illustrated the very rapid deterioration in stiffness and lateral load after the specimen reached peak lateral load. The peak lateral load occurred at the deflection of about  $2\Delta$  during the first excursion to that deflection. The second and third cycles within the deflection limit of  $2\Delta$  caused a significant drop in the lateral load at that deflection. The effect of cycling at  $2\Delta$  was severe enough to cause the lateral load capacity at the next higher deflection limit to fall below that obtained during the third cycle at the lower deflection limit. The degradation was so rapid that forcing the specimen to a bigger deflection produced no increase in lateral load.

Figures 4.16A through 4.16D show the west face at the end

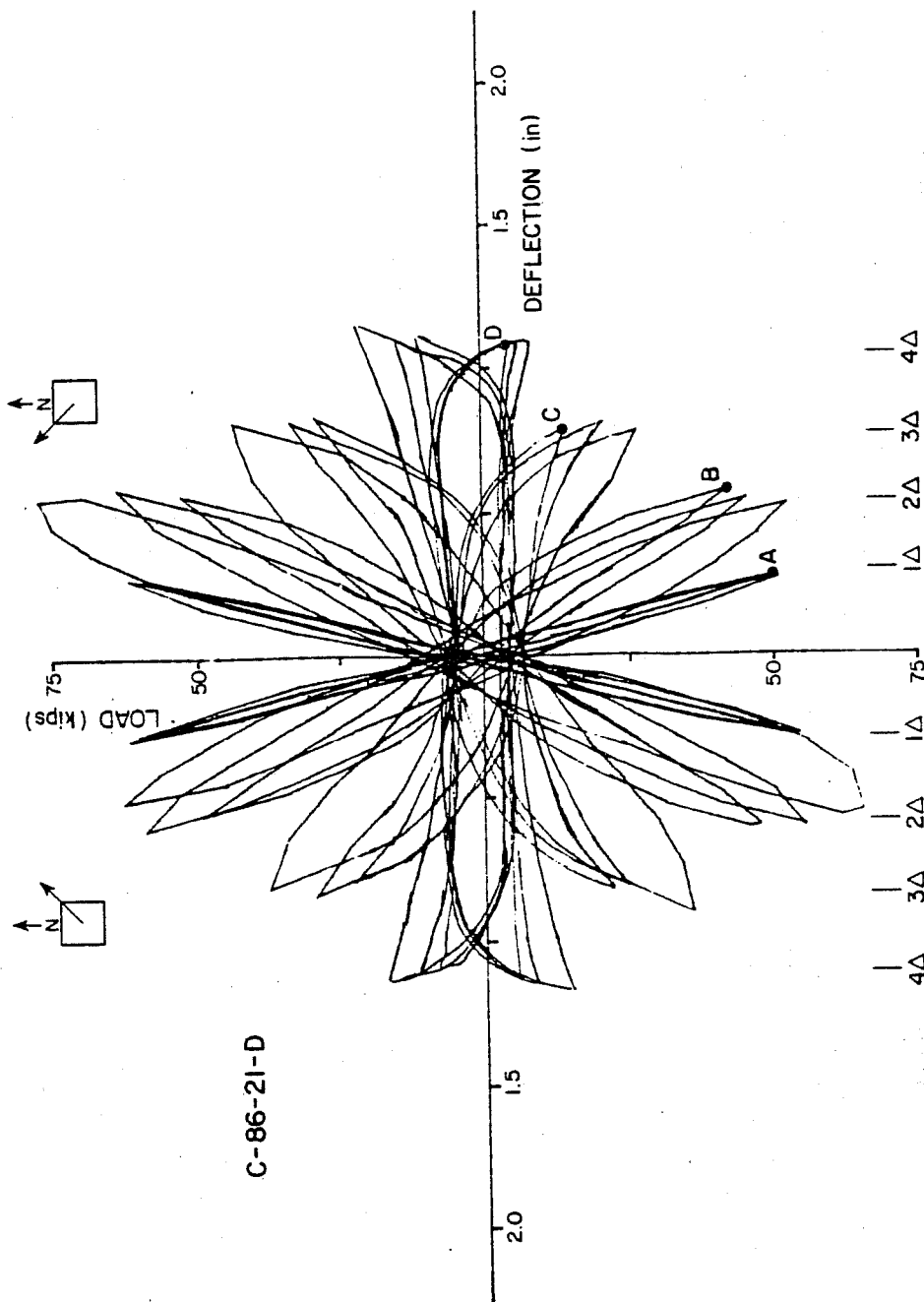
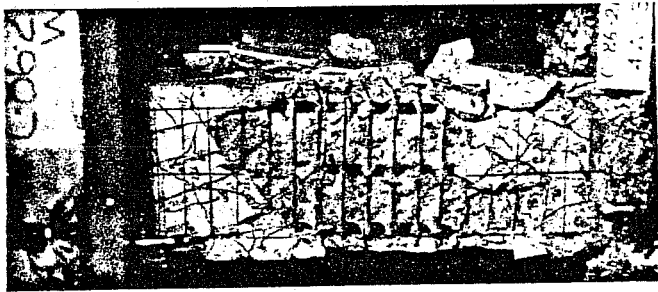
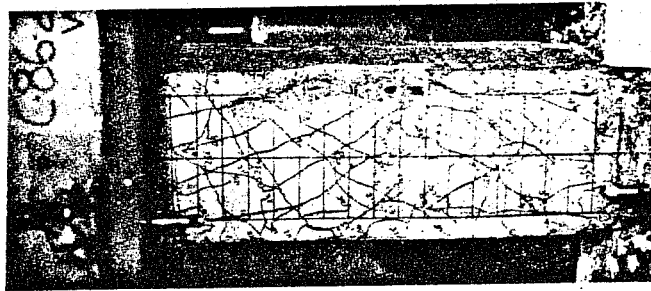


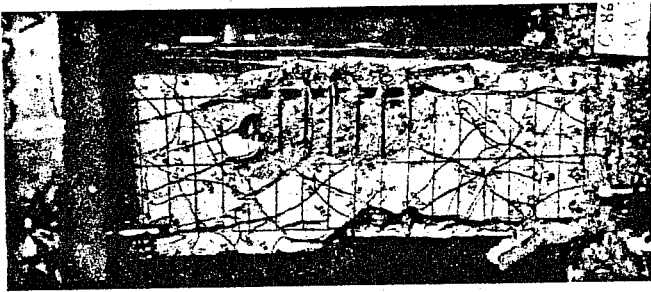
Fig. 4.15 Specimen C-86-21-D load-deflection curves



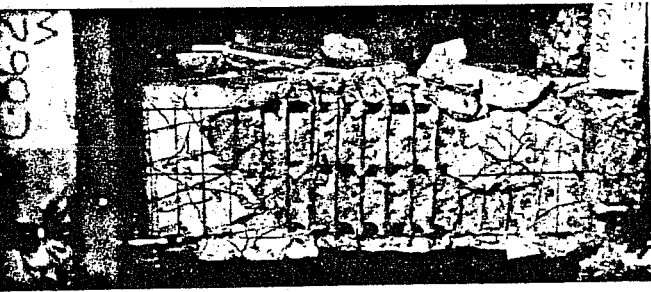
(A) 1Δ



(B) 2Δ



(C) 3Δ



(D) 4Δ

Fig. 4.16 Specimen C-86-21-D crack patterns

of cycling at each of the four deflection limits,  $1\Delta$ ,  $2\Delta$ ,  $3\Delta$ , and  $4\Delta$ . There was a limited amount of cracking at the end of cycling at  $1\Delta$ . Generally it was flexure cracking, but there were a few flexure-shear cracks. The specimen showed considerable cracking by the end of cycling at  $2\Delta$ . Long inclined cracks formed all along the length of the column. In addition, the cover at the bottom corners of the column spalled off, but not the sides. The cycling at  $3\Delta$  caused extensive spalling of the cover at the midheight of the specimen and cycling at  $4\Delta$  merely continued the process started in the previous cycles. It was clear that the midheight of the column was the most severely damaged part of the specimen. The ends of the column were relatively intact with only minor cracking, spalling, and damage to the core section. In the middle of the column, however, long lengths of the longitudinal bars did not have even mechanical bond to the concrete core, as the concrete around the bars had been ground away.

#### 4.7 Specimen 0-86-14-D

This specimen was tested by Maruyama [14] as part of an investigation into the effect of deformation path on member behavior. The loading path is the same as that used in the current series and is included in this discussion. It had no applied axial load and had ties spaced at 2.57 in.

Figure 4.17 shows the load-deflection curves for the specimen. The first cycles at a deflection of  $1\Delta$  were nearly elastic. The first excursion to a deflection of  $2\Delta$  reached the point of peak lateral load capacity for this specimen. The second and third cycles at the same deflection both had lower lateral load capacities than the cycle which preceded it. Of more interest was the reduction in lateral load of the first cycle at  $2\Delta$  along the second diagonal compared to the capacity along the first diagonal.



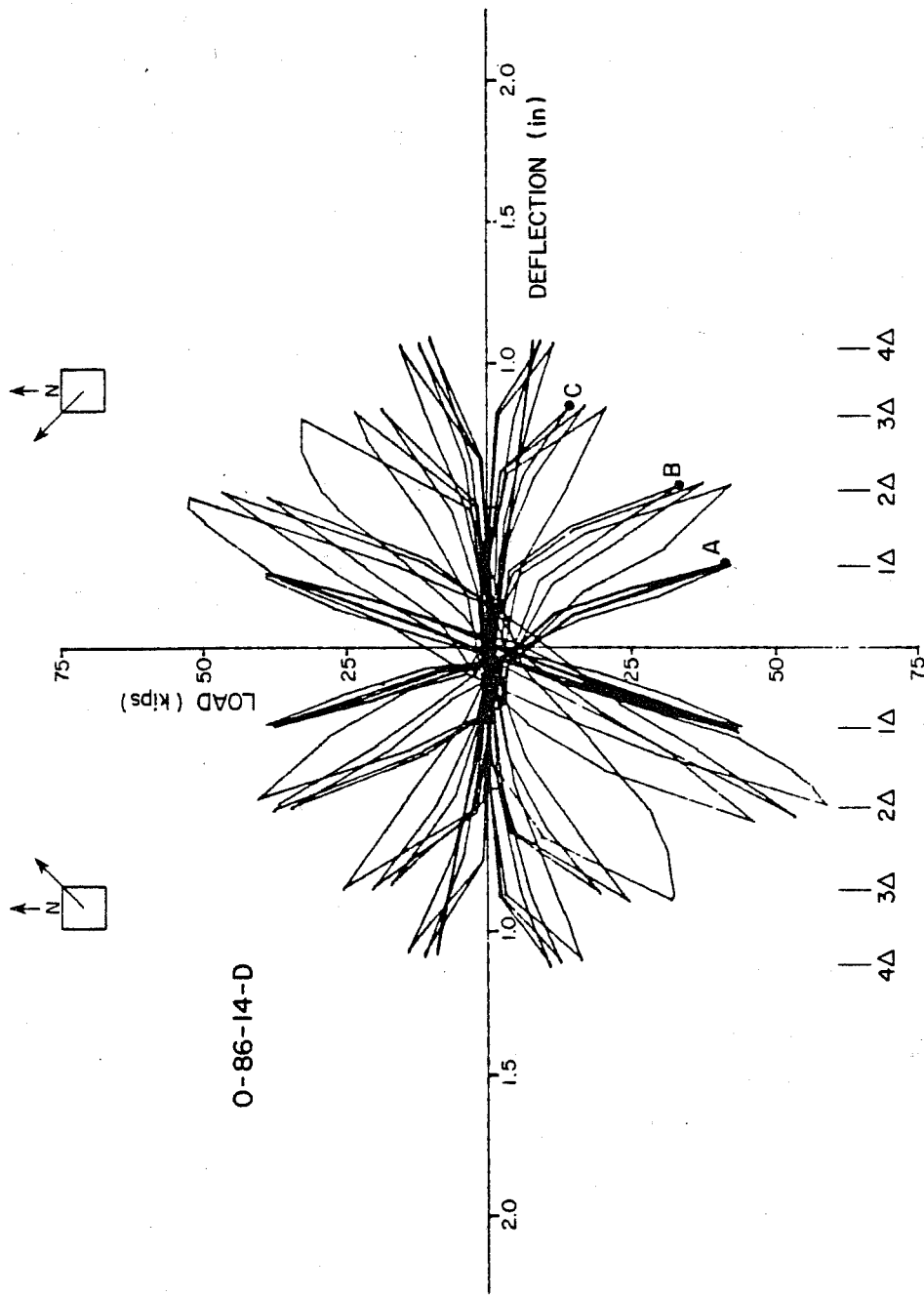


Fig. 4.17 Specimen O-86-14-D load-deflection curves

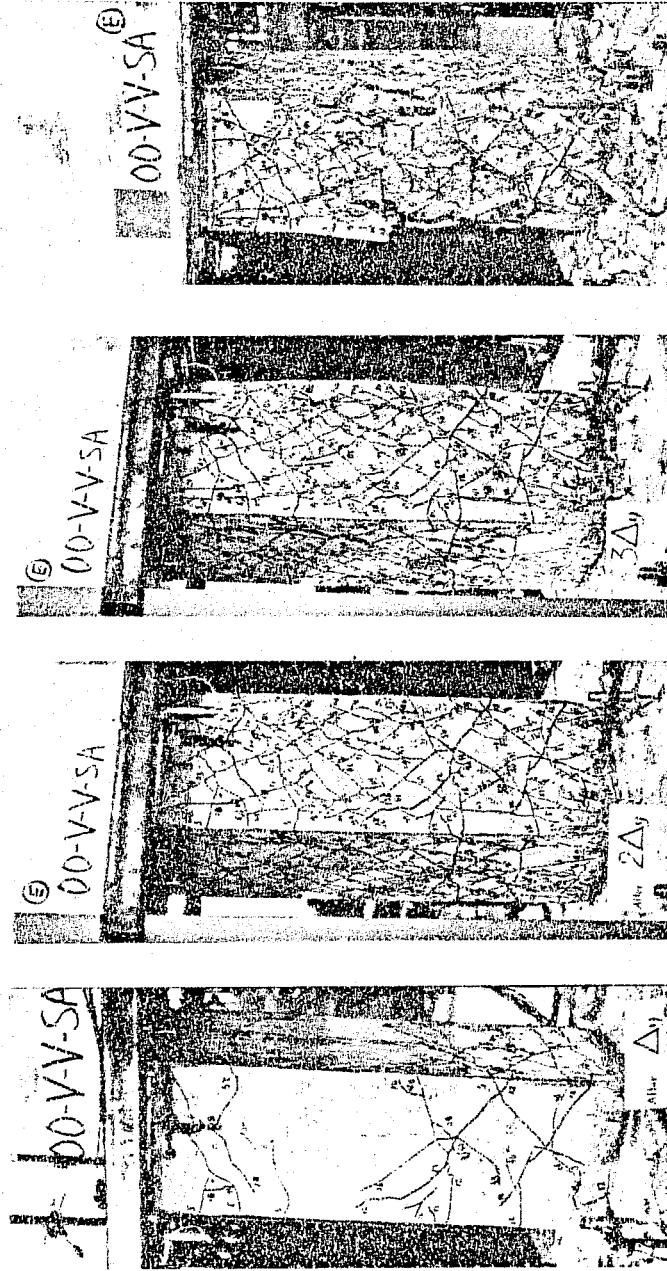


Fig. 4.18 Specimen 0-86-14-D crack patterns

Also, the three cycles along the second diagonal showed more stable behavior than the three cycles in the first direction at  $2\Delta$ . The first excursion to the next higher deflection level,  $3\Delta$ , definitely showed the reduced peak lateral load as the curve bent over before reaching the deflection of  $3\Delta$ . There was a distinct change in the shape of the hysteretic loops between the first cycle at  $3\Delta$  and the subsequent cycles which were quite narrow compared to the first cycle at  $3\Delta$ . Also, there were long regions of very low stiffness with some lateral load capacity increase at large deflections in the subsequent cycles.

Figures 4.18A through 4.18D show the east face at the end of cycling at each of the four deflection levels. Cycling at the first deflection level produced flexure and flexure-shear cracks with the cracking mainly at the ends, but the cracking at the bottom end extended to the midheight of the column. Cycling at the second deflection level caused a fairly large number of inclined cracks to form along the length of the column. None was very wide. Cycling at the third deflection level did not seem to cause many new cracks to form, but some of the existing cracks became wider. There was some spalling of the cover at the bottom corners. Cycling at the last and highest deflection limit caused a significant amount of cover loss concentrated primarily around the midheight of the column. The concrete around the longitudinal bars in this region of spalling was ground away and the core showed signs of fragmentation but not much crushing. The ends of the column were relatively intact.

#### 4.8 Specimen C-86-14-D

The tie spacing of 2.57 in. used in this specimen was identical to that used in the previous investigations and except for the presence of a compressive axial load this test duplicated

the test done by Maruyama, described in the previous section.

The load-deflection curves, Fig. 4.19, showed a rapid degradation of both stiffness and lateral load after the peak lateral load was reached. The cycles at  $1\Delta$  exhibited essentially elastic behavior with little loss of stiffness or lateral load with cycling. The peak lateral load was achieved at the first cycle to  $2\Delta$ . The loss in lateral load was significant when the deflection reached  $2\Delta$  in the opposite direction. The loss in lateral load continued with cycling at  $2\Delta$ . The lateral load at the next higher deflection level,  $3\Delta$ , was lower than it was in the last cycle at the previous deflection level. The loss of lateral load continued as a result of both cycling and increased imposed deflections. The final attempt to reach a point where the lateral load increased showed that the stiffness and lateral were virtually zero.

Figures 4.20A through 4.20D show the south face of the specimen at the end of cycling at each of the four deflection levels. There was a modest amount of cracking of the specimen as a result of cycling at  $1\Delta$ . Most of the cracking was in the lower half of the specimen, indicating the higher stiffness of the lower end of the specimen relative to the upper end. The cracks were primarily flexure and flexure-shear. The damage caused by cycling at a deflection of  $2\Delta$  was quite extensive, with a large number of inclined cracks along the length of the specimen. Some of the cracks were quite wide. The corner cover had spalled off, but little cover spalled off near the ends. Cycling at  $3\Delta$  widened the existing inclined cracks and furthered cover spalling. The condition of the specimen by the end of cycling at  $4\Delta$  indicated the inability of the specimen to undergo the deflections imposed on it. Practically all the cover had spalled off revealing fragmentation

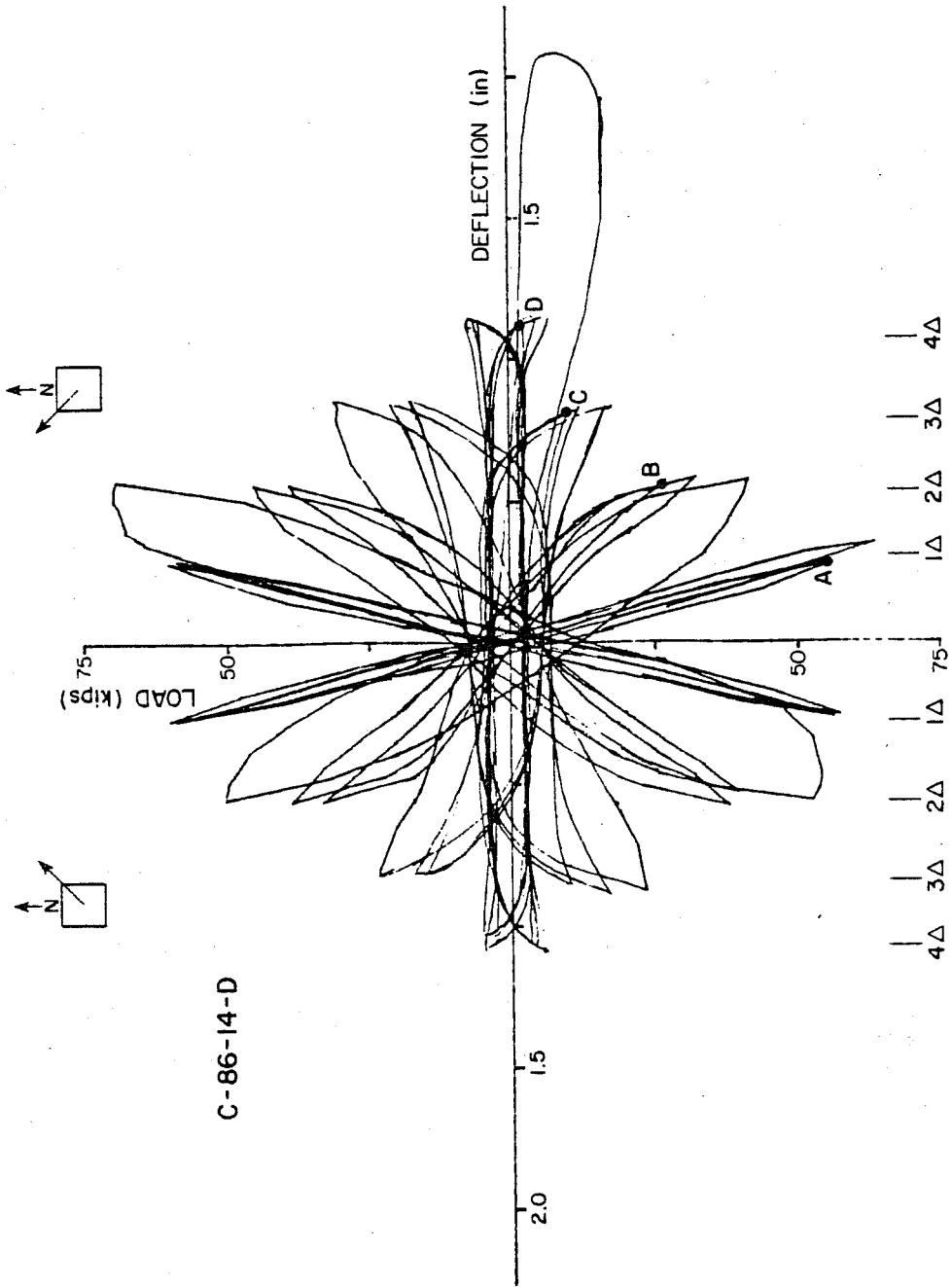


Fig. 4.19 Specimen C-86-14-D load-deflection curves

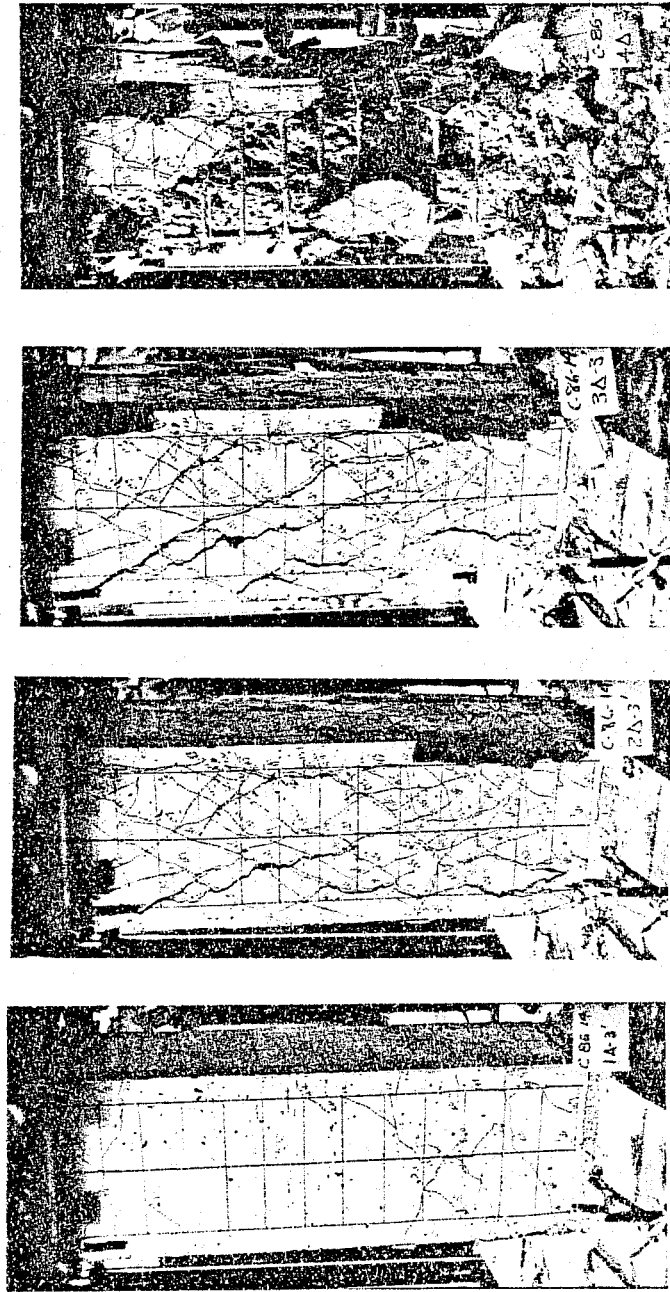


Fig. 4.20 Specimen C-86-14-D crack patterns

of the core in the midheight region of the specimen. No concrete was in contact with the corner longitudinal bars in the midheight region of the specimen. The core concrete near the ends of the column was relatively intact, showing no signs of crushing or fragmentation.

#### 4.9 Specimen C-86-09-D

Specimen C-86-09-D had a tie spacing of 4 in. and an applied compressive axial load.

The load-deflection curves, Fig. 4.21, exhibited a rapid deterioration of stiffness and lateral load after the specimen had reached its peak lateral load. The cycles at  $1\Delta$  did not measurably affect the mechanical characteristics of the specimen. The first cycle at  $2\Delta$ , the next deflection level after  $1\Delta$ , followed the shape of the curves already produced by the previous cycles until the lateral load reached its peak. The specimen held the peak lateral load during the first excursion to  $2\Delta$ , which was a monotonic loading to that deflection level, but on reversing the deflection the lateral load was sharply reduced at  $2\Delta$  in the opposite direction. Also, the second cycle showed a large decrease in both the stiffness and lateral load of the specimen. The damage caused by the three cycles along the first diagonal of the specimen clearly affected the behavior of the specimen when it was cycled along the second diagonal between the same deflection levels. The rapid degradation of both stiffness and lateral load continued at the  $3\Delta$  deflection level. The specimen had essentially zero stiffness and zero lateral load by the end of cycling at  $3\Delta$ . An attempt to increase the lateral load by forcing the specimen through large deflections failed to produce more than 10 percent of the peak lateral load of the specimen.

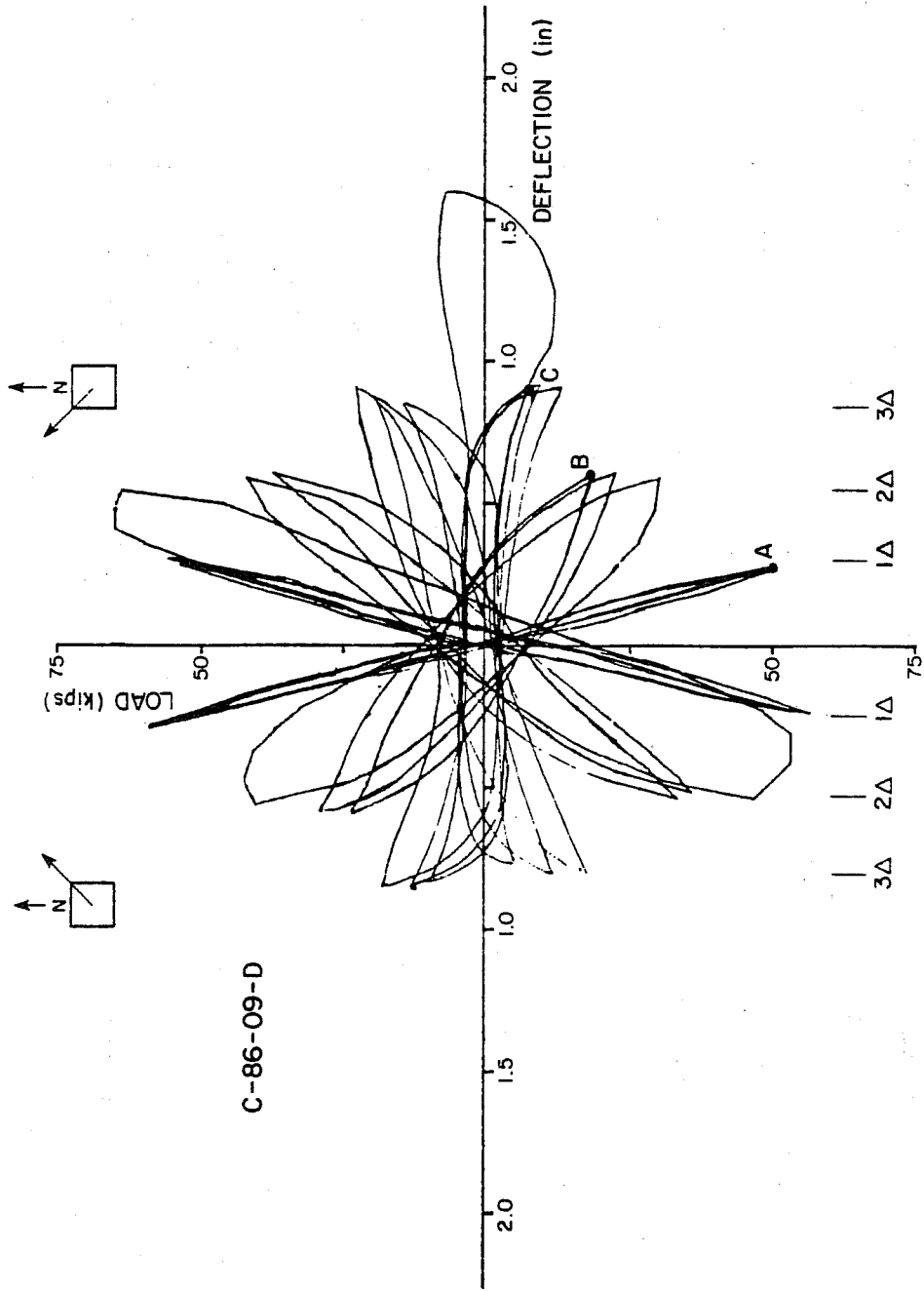
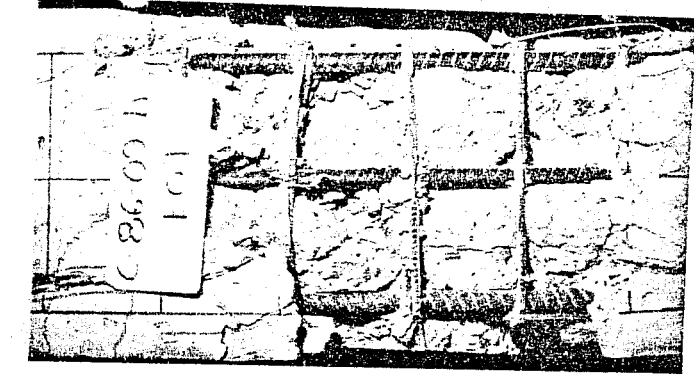
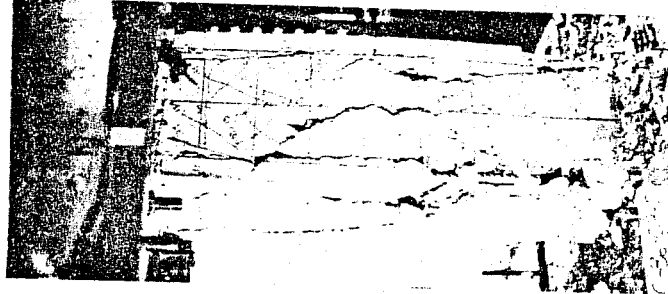


Fig. 4.21 Specimen C-86-09-D load-deflection curves

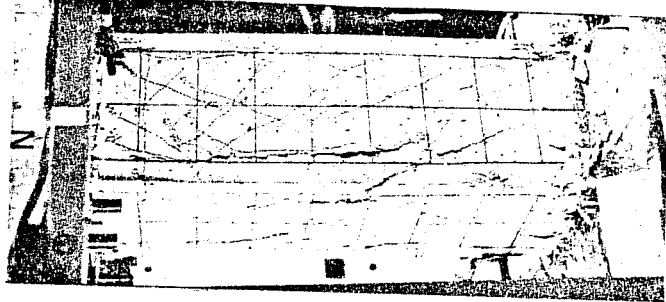




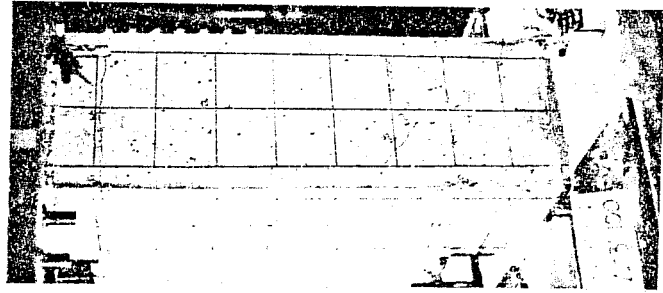
(D) EOT



(C) 3Δ



(B) 2Δ



(A) 1Δ

Fig. 4.22 Specimen C-86-09-D crack patterns

Figures 4.22A, B, and C showed the northeast corner at the end of cycling at the deflection limits  $1\Delta$ ,  $2\Delta$ , and  $3\Delta$ , respectively. The condition of the specimen at the end of the test was typified by Fig. 4.22D. There were few cracks at the end of cycling at  $1\Delta$ . The cracks were primarily flexure with some flexure-shear cracks. The cracks were more prevalent at the bottom end of the column. At the end of cycling at  $2\Delta$ , inclined cracks were present along the length of the column. Some of the inclined cracks were quite wide. The corner cover at some points of the specimen was spalling or had spalled off. There was little spalling at the ends of the specimens except for the corners. Cycling at a deflection of  $3\Delta$  caused large portions of the corner cover to spall off exposing the longitudinal corner bars. The large inclined cracks seemed to be indicators of cover spalling and the crack width at the cover was not directly indicative of the crack width in the core. This was observed by visually comparing the crack width before the cover spalled to the crack width after the cover had spalled. There was considerable damage to the midheight region of the specimen, but little damage to the ends at the end of testing. The core concrete in the damaged region was fragmented into large blocks and inclined cracks penetrated into the core. The concrete around the longitudinal bars had been ground away leaving the bars essentially unbonded to the concrete core.

#### 4.10 Specimen C-86-03-D

The specimen had ties at a 12 in. spacing and an applied compressive axial load. It was expected to fail in a brittle manner. The load-deflection curves, Fig. 4.23, showed that the specimen did indeed fail very rapidly. The cycles at  $1\Delta$  did not seem to affect the behavior as the loops were relatively stable. The specimen failed suddenly during the first attempt to reach a

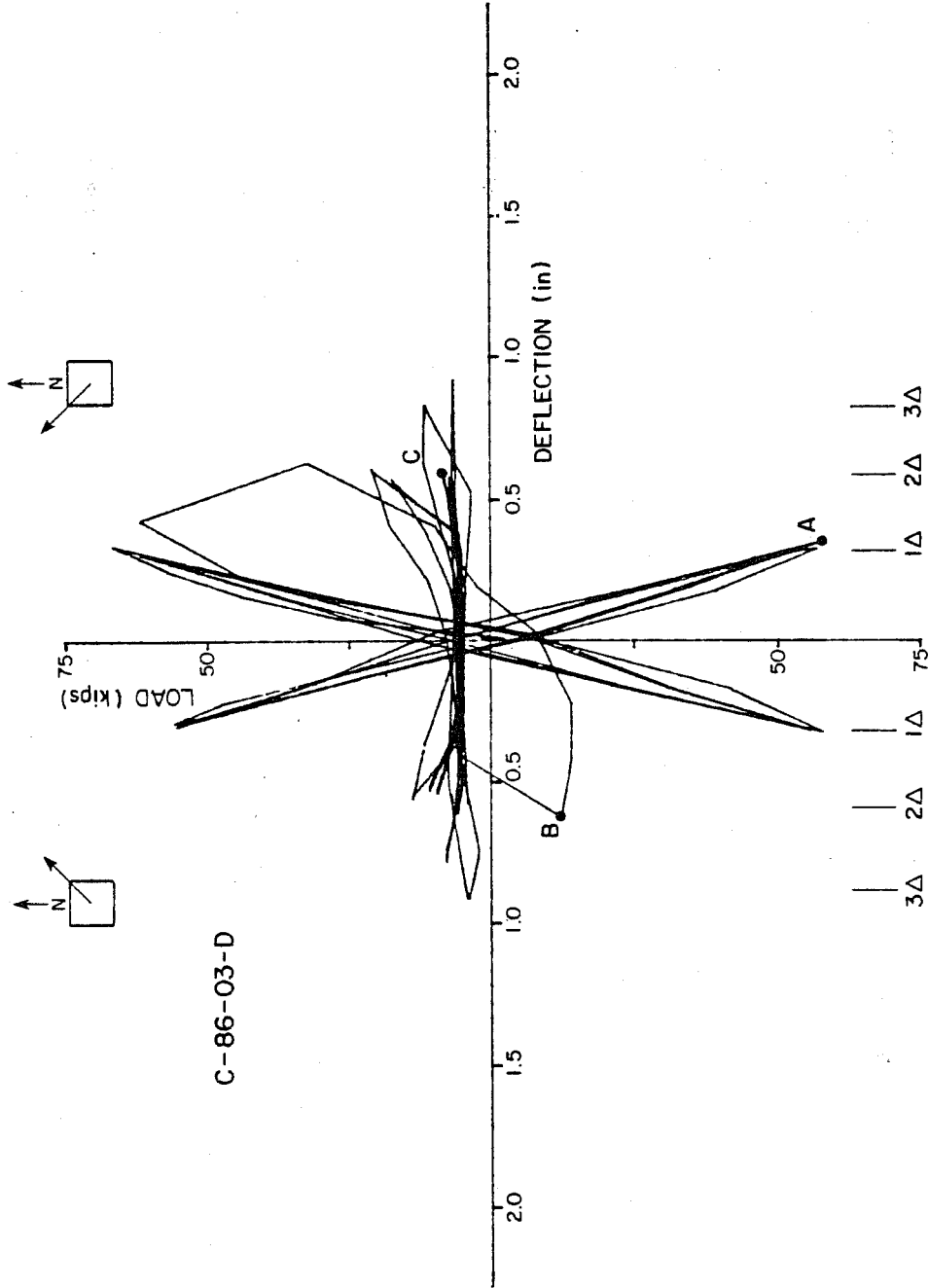


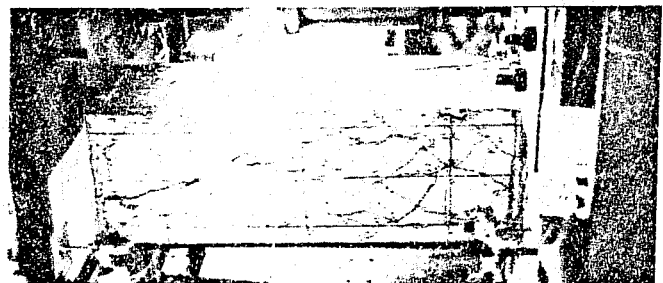
Fig. 4.23 Specimen C-86-03-D Load-deflection curves



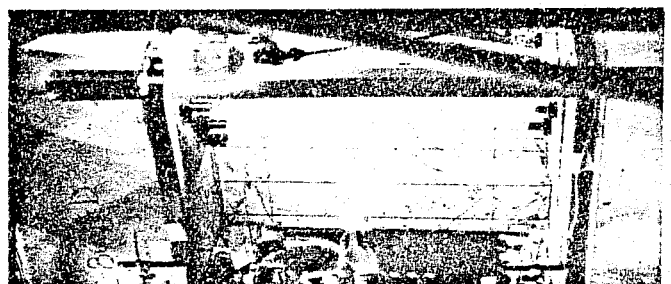
(D) EOT



(C) 2Δ



(B) 2Δ-1



(A) 1Δ

Fig. 4.24 Specimen C-86-03-D crack patterns

deflection of  $2\Delta$ . At no time did the specimen reach the peak lateral load achieved in the first cycle at  $1\Delta$ . Cycling at the deflection of  $2\Delta$  completely destroyed remaining lateral load and stiffness. Cycling between deflection limits of  $3\Delta$  was continued, but there was no resistance to the imposed deflections.

Figure 4.24A shows the east face at the end of cycling at the first deflection level,  $1\Delta$ . The cracking was not widespread; it was mainly at the ends of the specimens. There were a few flexural cracks and some inclined cracks, but they were limited in length and width. Figure 4.24B shows the east face of the specimen after one cycle at the critical deflection level of  $2\Delta$ . There were large inclined cracks on all four faces which seemed to wrap around the corners, similar to the pattern shown in Fig. 4.7. There were not many inclined cracks; instead, a few wide cracks grew wider as the test continued. Figure 4.24C of the east face after cycling at  $2\Delta$  shows the loss of large pieces of cover and, generally, disintegration of the specimen. Figure 4.24D, taken at the end of the test, shows the severe damage to the concrete core caused by the test. The core was fragmented into large blocks with the major cracks observed on the cover penetrating into the core. The concrete around the longitudinal bars was no longer intact in the midheight region of the specimen. There was little sign of concrete compressive crushing near the ends or in the damaged core region.

#### 4.11 Specimen C-84-32-D

The specimen C-84-32-D and the remaining specimens had #4 bars for the longitudinal reinforcement and an applied compressive axial load. Specimen C-84-32-D had ties at the minimum spacing used in the current investigation, 1-1/8 in.

The load-deflection curves for this specimen, Fig. 4.25, show that until the specimen reached a deflection level of  $4\Delta$  the hysteretic loops were quite stable. At the deflection level of  $4\Delta$  the longitudinal bars began to buckle. However, the transverse reinforcement was sufficient to prevent a sudden loss of lateral load capacity and axial load capacity. The hysteretic loops were open and full throughout the test with only a minor amount of pinching of the loops near the origin. The peak lateral load was reached at  $2\Delta$  and was maintained through the cycling at  $2\Delta$  and  $3\Delta$ .

Figures 4.26A through 4.26D show the west face at the end of cycling at the first four deflection levels,  $1\Delta$ ,  $2\Delta$ ,  $3\Delta$ , and  $4\Delta$ . Cycling at  $1\Delta$  produced few cracks on the specimen. The cracks that appeared were mainly flexural cracks, with a few flexure-shear cracks principally at the bottom end of the column. Cycling at the next deflection level,  $2\Delta$ , caused cracking at the top end of the column similar to that at the bottom end. Few new cracks appeared at the bottom end of the specimen, but considerable compressive crushing and spalling of the cover at the bottom corners occurred. Cycling at a deflection level of  $3\Delta$  caused some vertical cracks to appear along the center longitudinal bars. In addition, spalling began at the top end of the column especially at the corners. Cycling at  $4\Delta$  continued the process of spalling at the ends of the column exposing the core on all four sides at the bottom and top of the specimen. Vertical cracks formed along some of the corner longitudinal bars.

Figure 4.26E shows the southwest corner of the specimen after conclusion of the test. The buckled longitudinal bars can be seen at the bottom end of the specimen. Most of the damage occurred at the ends of the specimen. The core was relatively

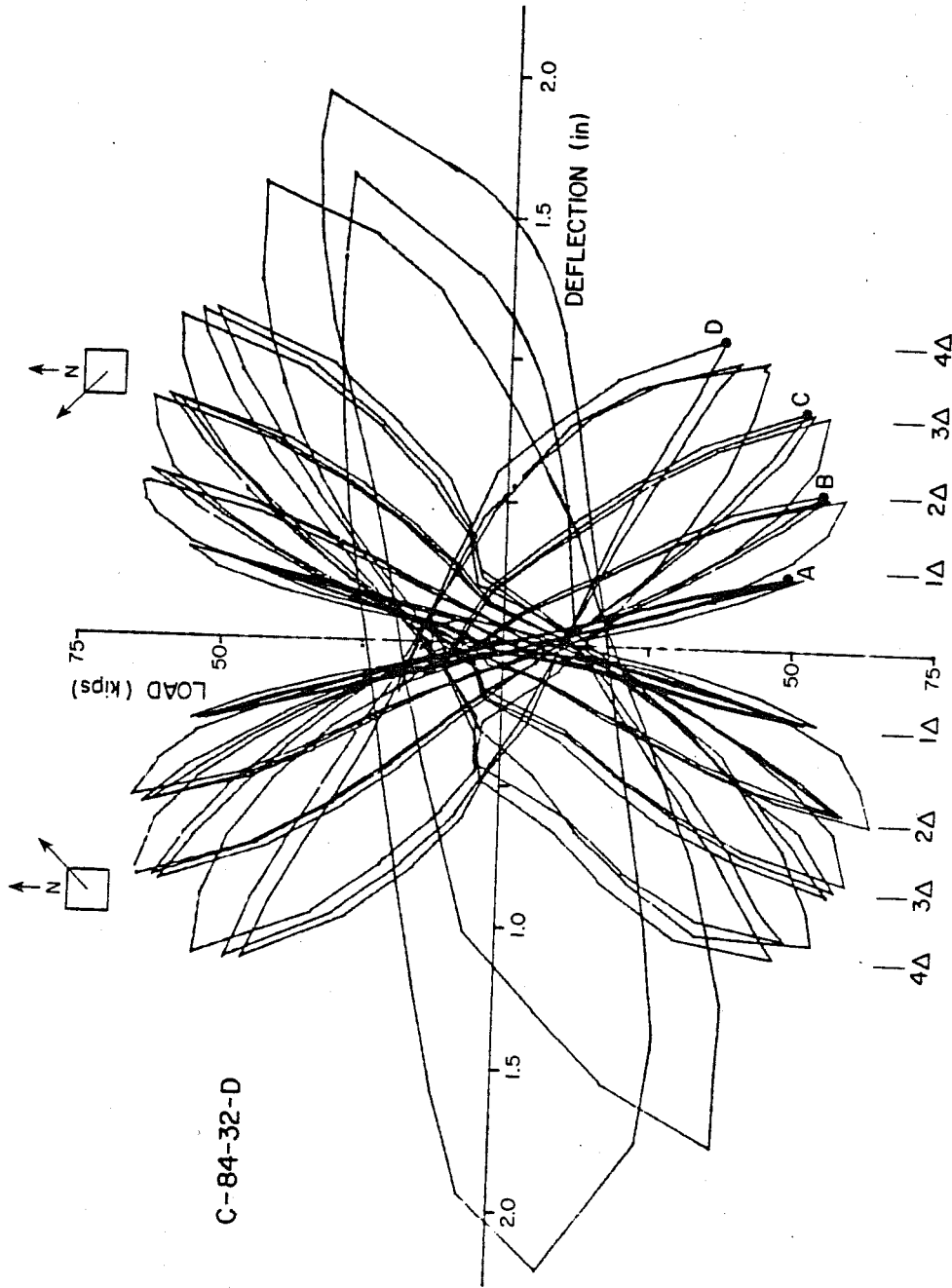
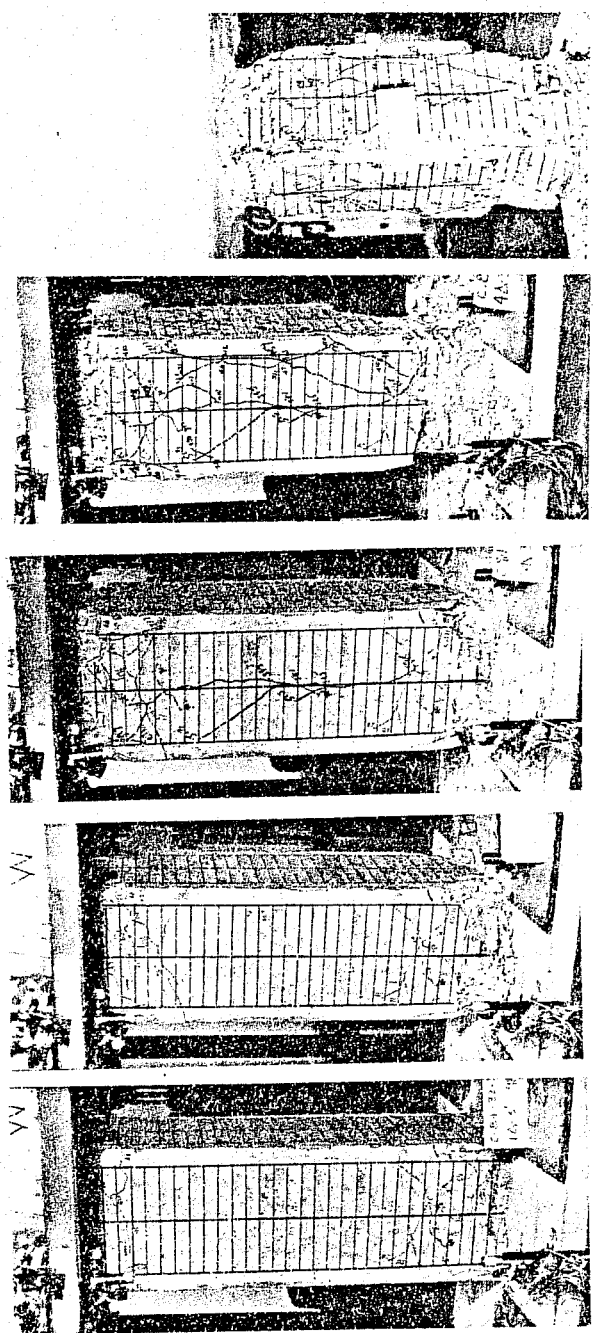


Fig. 4.25 Specimen C-84-32-D load-deflection curves



(A) 1Δ (B) 2Δ (C) 3Δ (D) 4Δ (E) EOT

Fig. 4.26 Specimen C-84-32-D crack patterns



intact and did not show signs of fragmentation. The longitudinal bars, except for those that buckled, were solidly encased in concrete which appeared to be sound and not pulverized.

#### 4.12 Specimen C-84-21-D

The specimen had ties at 1-3/4 in. spacings.

The load-deflection curves, Fig. 4.27, showed that the hysteretic behavior was stable through the cycling at the  $2\Delta$  deflection level. The peak lateral load was reached during the first excursion to a deflection of  $2\Delta$ . The behavior of the specimen began to degrade with the first attempt to reach a deflection of  $3\Delta$ . The lateral load at  $3\Delta$  was less than that at  $2\Delta$ , but more importantly, the lateral load at  $3\Delta$  decreased with each cycle. Both longitudinal bar buckling and inclined cracking occurred during cycling at  $3\Delta$ . The hysteretic behavior of the specimen deteriorated with cycling at  $4\Delta$  to the point where little stiffness or lateral load remained. Buckling of the longitudinal bars caused the test to be halted and cycles at  $4\Delta$  along the second diagonal were omitted to protect the instrumentation attached to the specimen from damage.

Figures 4.28A, B, and C show the west face at the end of cycling at  $1\Delta$ ,  $2\Delta$ , and  $3\Delta$ . Cycling at  $1\Delta$  produced flexure and flexure-shear cracks in the end regions of the column. There was more cracking at the lower end of the column than the upper end. Cycling at  $2\Delta$  caused some extension of the existing flexure-shear cracks at the lower end of the specimen and caused new cracks at the upper end. There was some spalling of the corners at the bottom end of the specimen. Cycling at  $3\Delta$  caused a large number of inclined cracks to form along the column length. In addition, vertical cracks formed along the center longitudinal bars and some

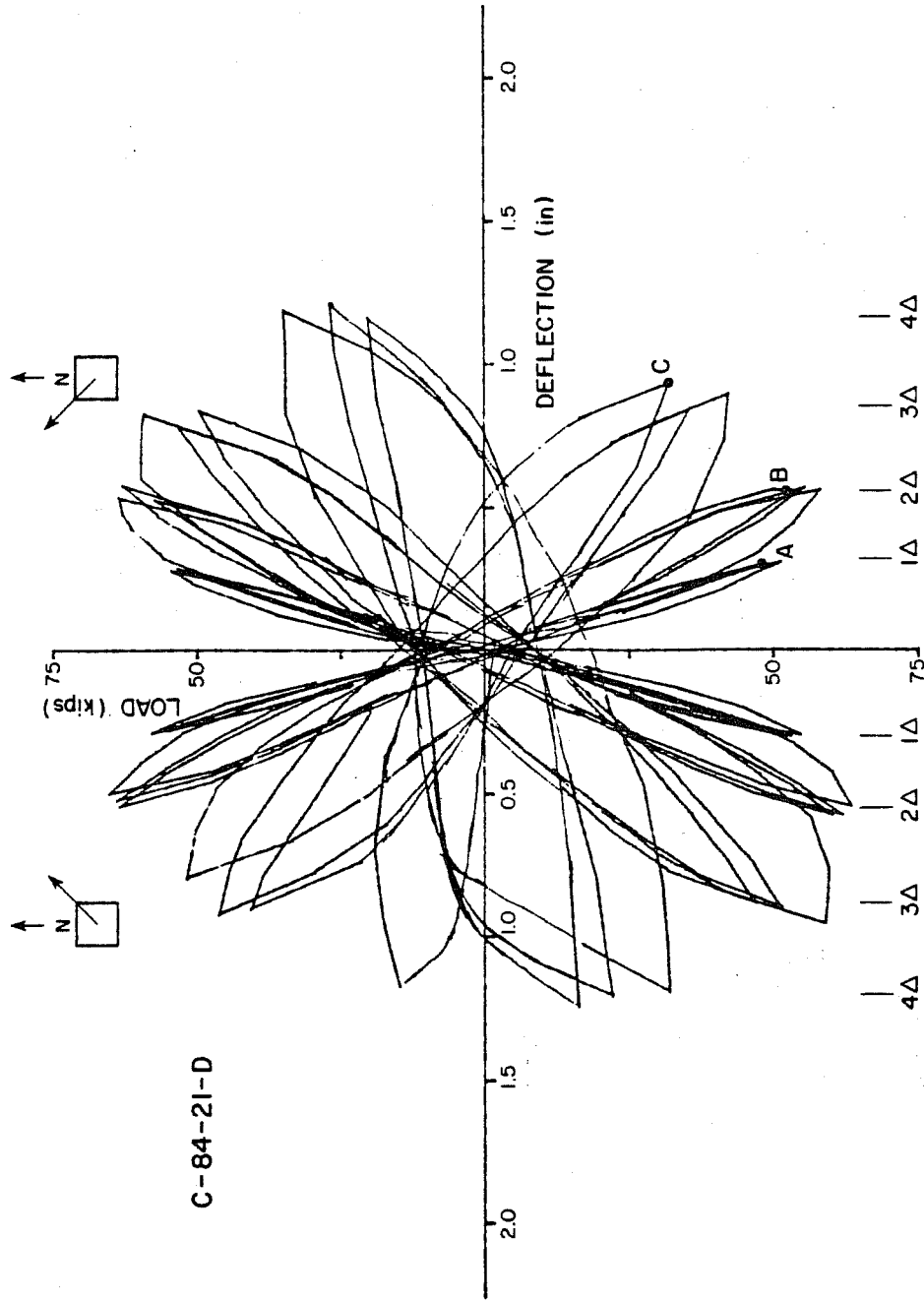
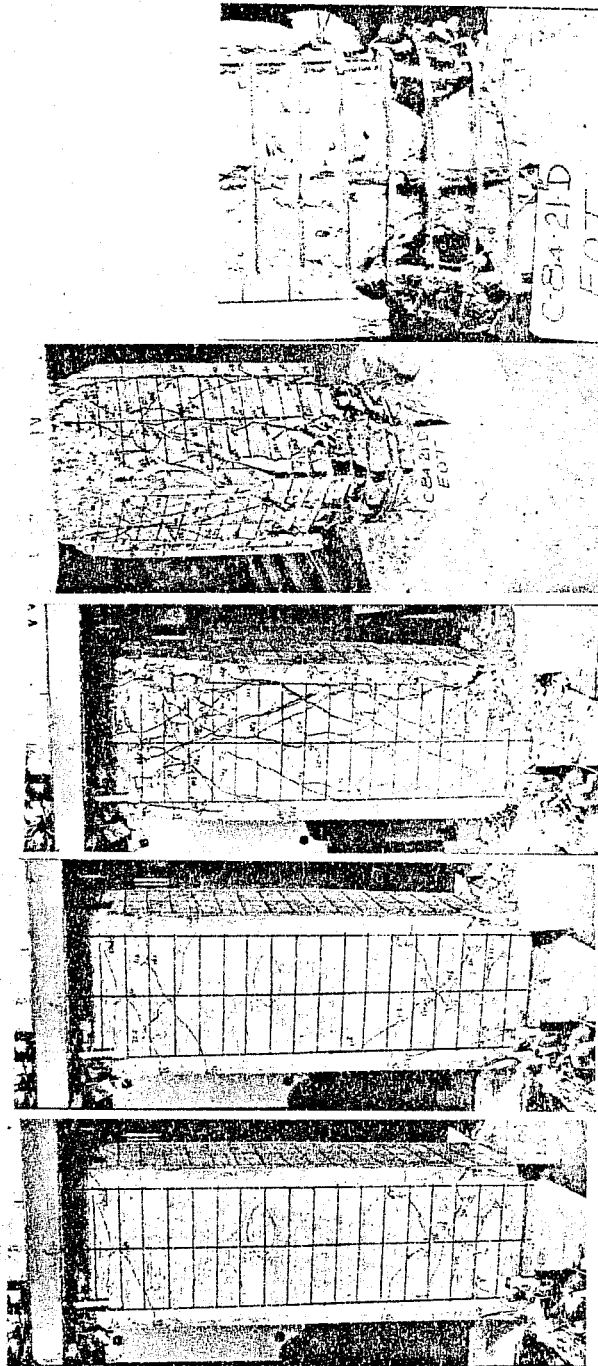


Fig. 4.27 Specimen C-84-21-D load-deflection curves



(A) 1Δ (B) 2Δ (C) 3Δ (D) EOT (E) EOT

Fig. 4.28 Specimen C-84-21-D crack patterns

of the corner bars. Spalling of the corner cover was pronounced at the lower end of the specimen. Figure 4.28D shows the condition at the end of the test. Of most interest is the loss of core at a section just above the bottom end of the specimen. A close-up of this region, Fig. 4.28E, shows the buckled longitudinal bars and the small amount of core concrete remaining intact. The rest of the core had been crushed and the concrete was brushed away to reveal the remaining core. The remainder of the column appeared to be relatively sound.

#### 4.13 Specimen C-84-14-D

The specimen had ties spaced at 2.57 in. along its length.

The load-deflection curves, Fig. 4.29, indicate relatively stable hysteretic behavior through cycling at the  $2\Delta$  deflection limit. The peak lateral load was achieved at  $2\Delta$  during the first cycle to that deflection limit. There was a small drop in lateral load between the first and second cycles at  $2\Delta$ , but the second and third cycles at  $2\Delta$  had nearly the same lateral load. The attempt to achieve a deflection of  $3\Delta$  caused the specimen to degrade quite rapidly. The influence of the longitudinal bar buckling on the degradation was difficult to evaluate. The lateral load and stiffness dropped with each cycle at  $3\Delta$  and especially with the cycles along the second diagonal. The failure of the specimen was an explosive failure caused by the inability of the column to carry the axial compressive load. The failure did not occur at the peak displacement of  $4\Delta$ , but rather when the specimen was near zero deflection after the first cycle at  $4\Delta$ .

Figures 4.30A, B, and C show the west face at the end of cycling  $1\Delta$ ,  $2\Delta$ , and  $3\Delta$ . The cracking after cycling at  $1\Delta$  was mainly flexural, but there were a number of noticeable flexure-

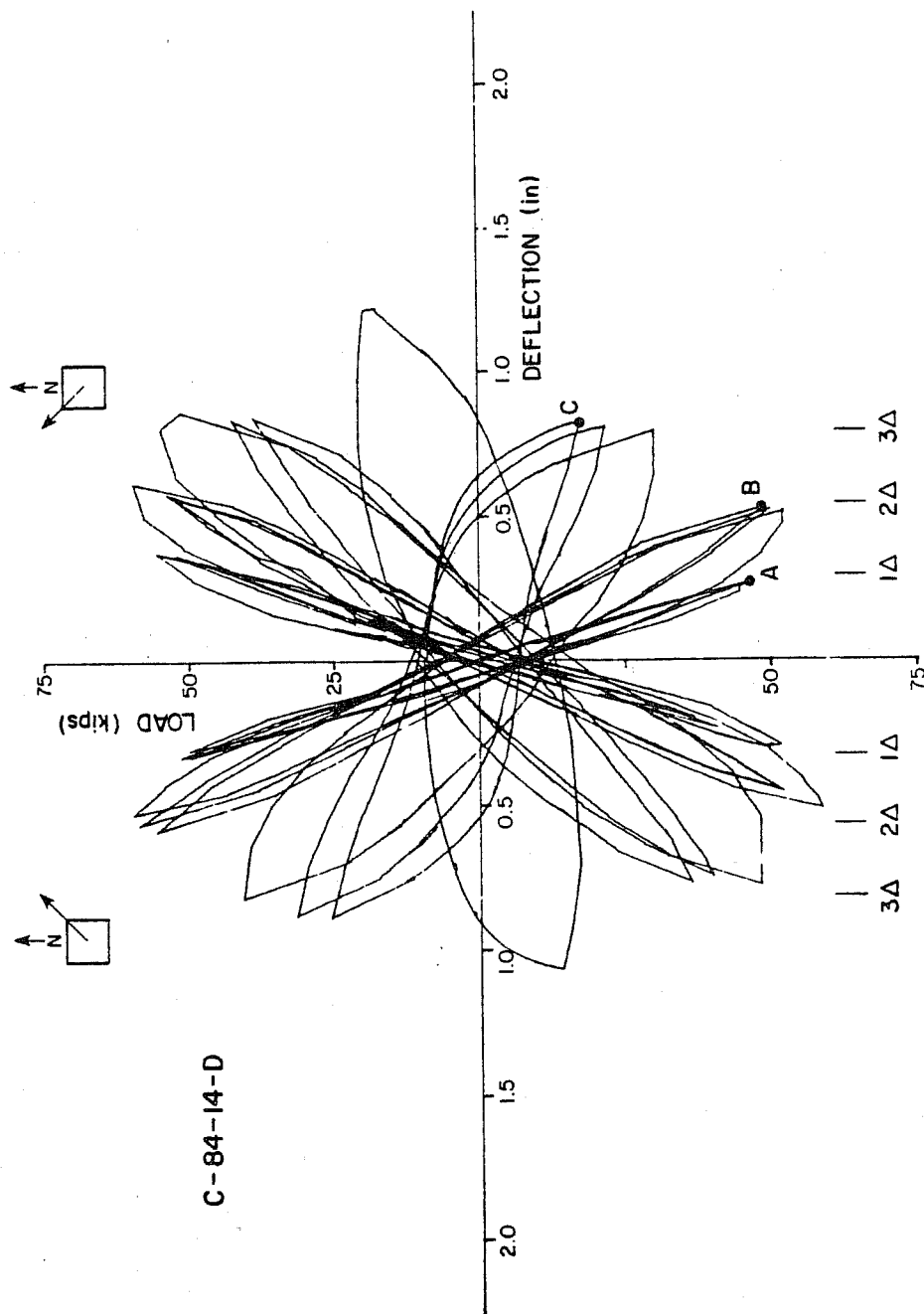
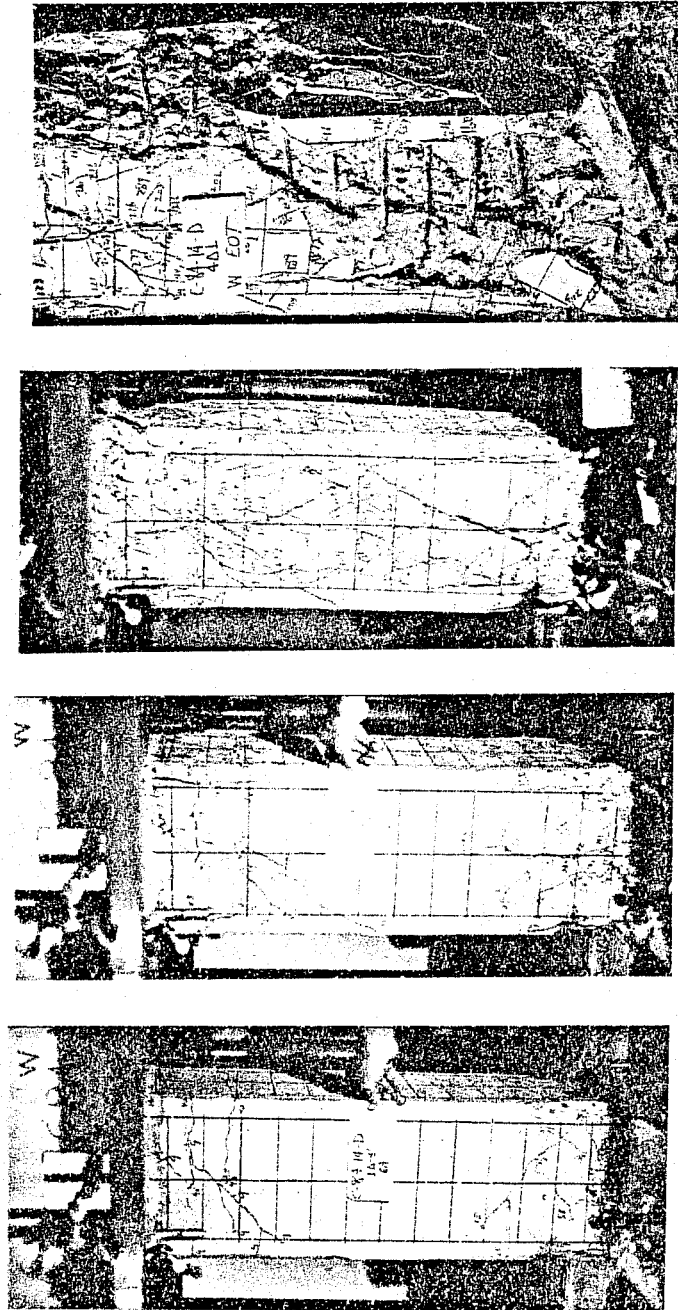


Fig. 4.29 Specimen C-84-14-D load-deflection curves



(A) 1Δ

(B) 2Δ

(C) 3Δ

(D) 4Δ

Fig. 4.30 Specimen C-84-14-D crack patterns

shear cracks. Cycling at  $2\Delta$  caused some spalling at the bottom corners of the column and extended some of the existing flexure-shear cracks. In addition, several inclined cracks appeared in the end regions and a vertical crack was noticed along the center bars at the lower end of the column. Cycling at  $3\Delta$  caused spalling at both the top and bottom end of the specimen. The cover spalled in the areas around the longitudinal bars which buckled. Significantly more inclined cracking occurred throughout the specimen. Figure 4.30D shows the west face of the specimen after the failure. The specimen shortened over an inch vertically, which was the limit of the axial ram extension. The core was fragmented and the longitudinal bars were severely bent.

## C H A P T E R 5

### COMPARISON OF TEST RESULTS

#### 5.1 Introduction

In Chapter 4, the performance of the specimens during testing was described. In this chapter the results are compared and reasons for the observed behavior are discussed. In addition, a qualitative guide to classification of behavior based on the comparisons of the tests is presented. The guide is in the form of a flowchart and provides a rational approach to determining the probable behavior of a short column.

The notation and symbols used to simplify data presentation are explained. The effects of the variables studied in the current investigation are discussed. The variables include axial load, deformation history, spacing of the column ties, and diameter of the longitudinal reinforcing bars. Finally, a qualitative guide for column behavior is developed.

Chapter 5 is devoted exclusively to the study of the results of the eleven tests in the current investigation. In Chapter 6, the results of tests conducted elsewhere are combined with the results of this investigation to produce an expanded predictive guide which takes into consideration a wider range of variables and is quantitative rather than qualitative.

#### 5.2 Background and Nomenclature

The specimens, Fig. 5.1, were 36 in. long columns idealized as having fixed ends, except that the upper block of the specimen was free to translate in space. Most of the specimens



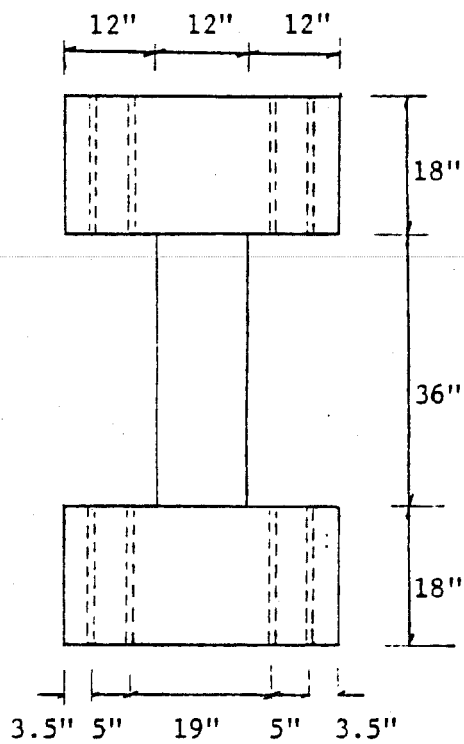


Fig. 5.1 Test specimen geometry

were subjected to constant compressive axial load throughout the test. The axial load was produced by a load control system, meaning the load was constant, but the axial deformation varied to accommodate the necessary applied load. The lateral or horizontal translations were applied by a deformation control system so that the upper block position was maintained at the desired deflection, while the load to hold it there was free to vary to accommodate the imposed deflections. After the axial load was applied, only the lateral deflection of the upper block was purposely varied.

The deflection paths were imposed on the specimen along the diagonals shown in Fig. 5.2. The northwest-southeast diagonal was defined as the first diagonal and it was the diagonal along which deflections were first applied. The northeast-southwest diagonal was defined as the second diagonal and was the other diagonal along which the specimen was deflected.

The hydraulic rams which moved the upper block laterally were oriented along the east-west and north-south axes of the specimen. Thus, to deflect the specimen along the diagonal required simultaneous action by the two rams. More importantly, the lateral loads and deflections were measured along the same axes as the rams. In order to simplify presentation of the data, all applicable data were transformed to axes coincident with the direction of deflection. As discussed in Chapter 4, the transformation was done by taking the square root of the sum of the squares of the original measurements. In most cases, this was close to  $\sqrt{2}$  times one of the lateral components. The specimen movements closely followed the diagonals of the column.

A system was adopted to identify points in the load history used in the test program. Most of the tests were cycled

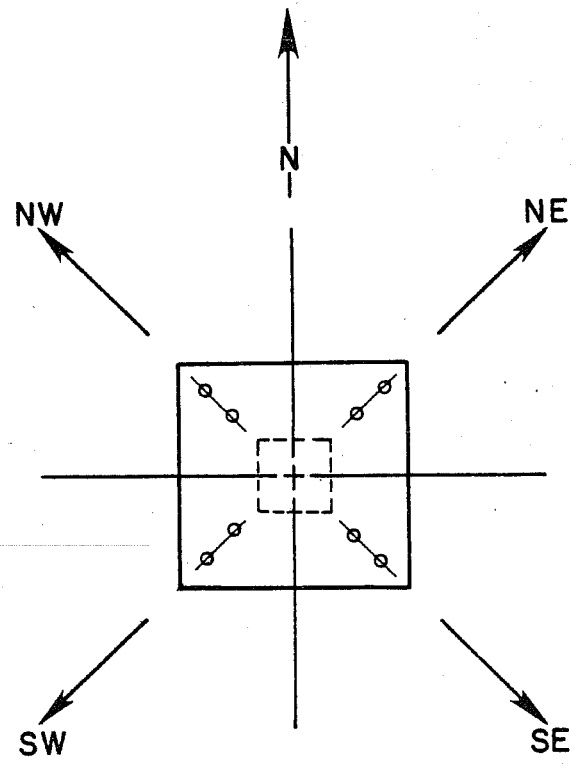


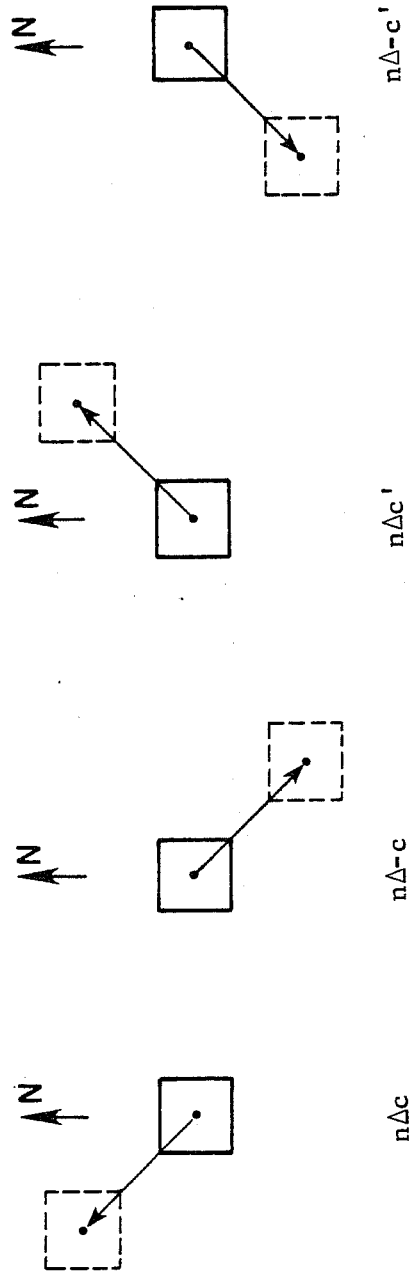
Fig. 5.2 Deformation path

three times along each diagonal between four deflection limits. The peak deflections were incrementally increased during a test, but each test used the same four deflection limits. The points of peak deflections for each cycle are assigned a unique symbol. The scheme for the symbols is shown in Fig. 5.3. Each deflection limit in the tests is an integer multiple of the first deflection limit. The nominal deflection limits were 0.28, 0.57, 0.84, and 1.13 in. Thus  $1\Delta$  was the same as 0.28 in.,  $2\Delta$  was 0.57 in., and so on. The  $n\Delta$  describes the deflection limit at which the specimen was cycled. A number is added after  $n\Delta$  to identify which of the cycles the specimen was at within the  $n\Delta$  deflection limit. The prime indicates that the deflection occurs along the northeast-southwest diagonal. The positive or negative sign of the cycle number indicates if the peak is in the original direction of a diagonal or the reversed direction. Examples of the symbol system are shown in Fig. 5.4 using a typical load-deflection curve.

### 5.3 Computed Lateral Loads.

The ratio of the shear capacity to the flexural capacity of the columns is an indication of the relative dominance of one type of behavior over the other. It is useful to compute the ratios for later comparison with the observed column behavior. Table 5.1 contains the computed lateral load capacities for each specimen based on both its flexural and shear capacity. The methods used to compute the capacities is described in the following sections.

5.3.1 Flexural Capacity. The lateral load capacity (along a diagonal) of the short column based on flexure was derived on the basis of a hinging mechanism forming at the ends



$n$  is the deflection increment number 1,2,3,...  
 $\Delta$  is the nominal deflection, 0.28 in.  
 $c$  is the cycle number 1,2,or3

Fig. 5.3 Peak deflection symbols

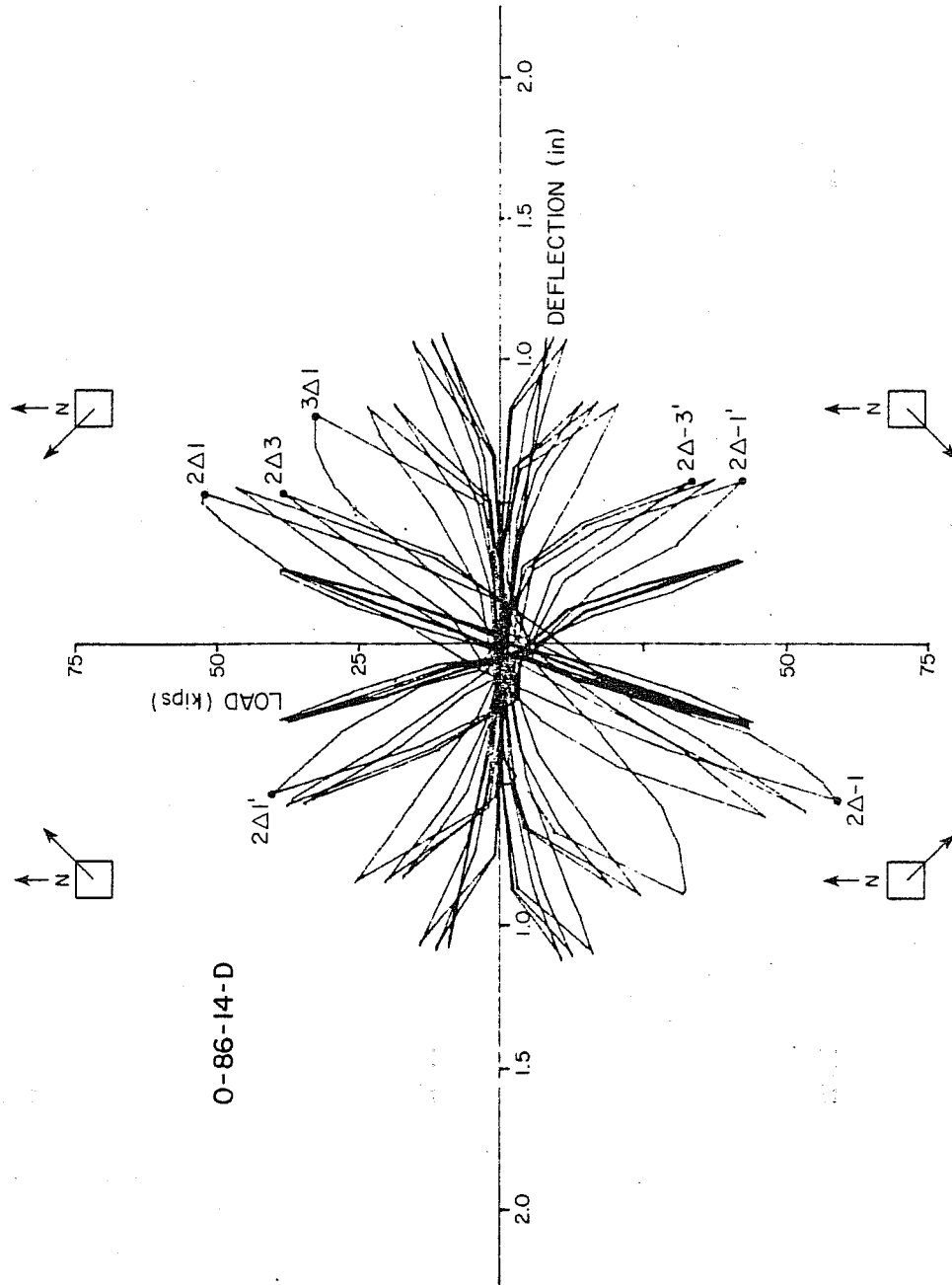


Fig. 5.4 Examples of peak deflection symbols

TABLE 5.1 COMPUTED LATERAL LOAD CAPACITIES FOR TEST SPECIMENS

Test Name	$f'_c$	N	$V_c$	$V_s$	$V_{rs}$	$M_u$	$V_{rf}$	$\frac{V_{rs}}{V_{rf}}$
0-86-14-DM	5950	0	17.8	21.6	39.4	1206	67	0.58
C-86-14-DM	5250	140	19.3	21.9	41.2	1422	79	0.52
0-86-32-D	4550	0	15.9	49.3	65.2	1152	64	0.98
C-86-32-D	5400	120	18.9	49.3	68.2	1440	80	0.85
C-86-21-D	5750	140	19.7	31.7	51.4	1494	83	0.61
0-86-14-D	5050	0	16.6	21.6	38.2	1134	63	0.60
C-86-14-D	4650	140	18.5	21.9	40.4	1422	79	0.51
C-86-09-D	5750	140	19.7	14.0	33.7	1494	83	0.41
C-86-03-D	6100	120	19.8	4.6	24.4	1440	80	0.30
C-84-32-D	4850	140	17.0	49.7	66.7	1098	61	1.10
C-84-21-D	4850	140	17.3	31.9	49.2	1044	58	0.84
C-84-14-D	5450	120	17.5	21.7	39.2	1008	56	0.70

- $f'_c$  - concrete compressive strength, psi
- N - compressive axial load, kips
- $V_c$  - concrete shear strength (ACI318-77), kips
- $V_s$  - reinforcement shear strength (ACI318-77), kips
- $V_{rs}$  - shear strength  $V_c + V_s$ , kips
- $M_u$  - ultimate bilateral moment capacity, kip-in.
- $V_{rf}$  - lateral load capacity based on  $M_u$ , kips

of the column. As shown in Appendix C the lateral load (shear) required to equilibrate the mechanism is

$$V = \frac{2M}{L} \quad (5.1)$$

where  $V$  = lateral load (shear force)  
 $M$  = ultimate moment capacity of the section  
 $L$  = length of the column.

The ultimate bilateral moment capacity for each column was computed using the computer program described in Appendix B. Measured material strengths were used to compute the moment capacities. The lateral load required to achieve the flexural capacity of the column is denoted as  $V_{rf}$  in Table 5.1. It should be noted that the actual flexural capacity of the columns may be affected by the high shear forces present in conjunction with high normal forces.

5.3.2 Shear Capacity. The 1977 ACI Building Code [17] shear capacity equations (Chap. 11) are used as the basis for computing the shear capacity of the columns. The shear capacity of a member is taken as the summation of a contribution by the concrete ( $V_c$ ) and a contribution by the shear reinforcement ( $V_s$ ). The  $V_s$  term is based on a truss analogy (described in Appendix A) and has the form

$$V_s = \frac{A_v f_y d}{s} \quad (5.2)$$

where  $A_v$  = area of shear reinforcement within a distance  $s$ ,  
 sq. in.  
 $f_y$  = yield strength of shear reinforcement, psi  
 $s$  = spacing of shear reinforcement in direction  
 parallel to longitudinal reinforcement, in.



$d$  = distance from extreme compression fiber to centroid of longitudinal tension reinforcement, in.

The  $V_c$  term represents a conservative approximation of the shear force required to produce inclined cracking. As discussed in Appendix A the  $V_c$  term is based on a principal tensile stress criterion, but was fitted to a large amount of experimental data. The  $V_c$  equation is

$$V_c = \left( 1.9\sqrt{f'_c} + 2500\rho\frac{V_u d}{M_u} \right) b_w d \quad (5.3)$$

where  $V_c$  = concrete contribution to shear capacity

$b_w$  = web width of member, in.

$d$  = as above

$V_u$  = factored shear force at section

$M_u$  = factored moment at section

$\rho$  = longitudinal tension reinforcement ratio,  $A_s/bd$

$A_s$  = area of longitudinal tension reinforcement, sq. in.

$b$  = total width of member, in.

The total shear capacity of the member is  $V_c + V_s$ . This summation is purposely made to give low estimates of shear capacity to preclude shear failure when using the ACI Building Code in design.

The applicability of the ACI Code Chap. 11 equations to the short columns tested in this investigation is uncertain for a number of reasons; 1. the relatively short length-to-depth ratio of the columns, 2. the manner in which the loads are applied to the column, 3. the cyclic reversed loading of the columns, and 4. loading along the diagonal of the columns.

Length-to-depth Ratio and Loading Condition--The ACI Code contains special provisions for deep beams. Deep beams are defined by the Code as having a length-to-effective depth ratio of less than 5 and loaded on the compression face. The effective depth is the distance from the extreme compression fiber to the centroid of the longitudinal tension reinforcement. The deep beam provisions are mainly based on tests of simply supported beams with one- or two-point loadings on the compression face. As shown in Fig. 5.5 it is possible for the applied load in such beams to be transferred to the reaction through a compression strut. However, in order for the strut to become effective the proportions of the beam must be such that the ratio of the length 'a' (Fig. 5.5) to the member effective depth 'd' is less than about 2.5. The short columns do not have an applied load on the compression face of the column. The ratio of distance between load and reaction and the effective depth is 4 (Fig. 5.6).

Loading History--The shear capacity equations in the ACI Code are based on beams loaded monotonically. The short columns were loaded cyclically. In the review of past experimental tests on beams subjected to reversed loading [49] there is no clear indication as to the effect of cycling on shear capacity. Generally, cycling at a very high shear level causes a loss of shear capacity. Cycling at lower shear loads may not significantly effect the peak shear capacity of the member. The results of the current investigation indicate that the maximum shear resistance is not affected by the loading history used herein. Figure 5.14 shows the first quadrant load-deflection curves from a cyclic test (C-86-14-D) and a load-deflection curve from a test in which no cycling was done at intermediate peak deflections. Neither specimen achieved its

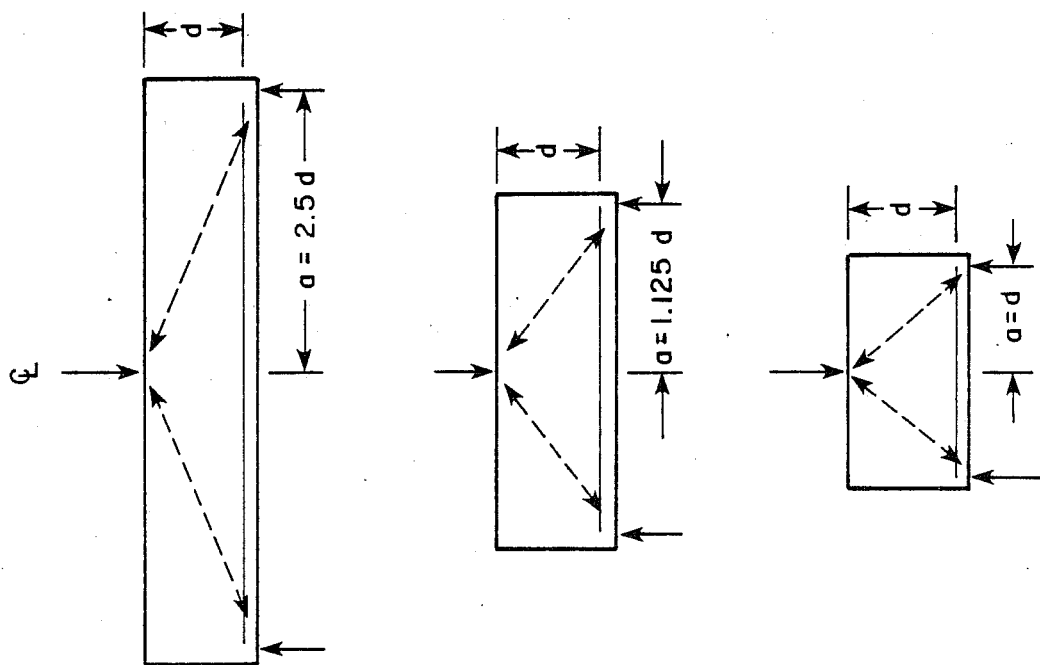
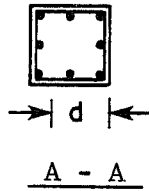
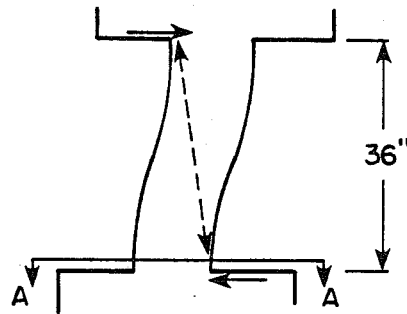


Fig. 5.5 Deep beams



$d = 8.625$  in.  
86 series column

Fig. 5.6 Compression strut  
in specimen

computed flexural capacity. It is likely that shear capacity governed the maximum lateral load achieved by the columns. It is clear that the cycles prior to achieving the maximum lateral load did not significantly affect the maximum load (peak shear force) of the member. Therefore, the ACI Code provisions though based on monotonic tests are assumed to be valid for the cyclically loaded columns in this investigation.

Diagonal Loading--The shear capacity of a diagonally loaded member is not specifically defined in the ACI Code. The tests on which the capacity equations are based were done on members oriented as shown in Fig. 5.7a (unilateral). The applicability of the provisions to a member loaded along its diagonal (bilateral), Fig. 5.7b, is uncertain. However, the results of two tests on short columns provide some guidance as to the applicability of the provisions to diagonally loaded members.

One test (120C-U) was a unilateral test reported by Ramirez [15]. The column was cyclically deflected using incrementally increasing peak deflection limits. The other test was a bilateral test from the current investigation (C-86-14-DM). The column was cyclically deflected between a single large peak deflection limit. Both columns were subjected to a 120 kip axial compression. Neither column reached its computed flexural capacity. The maximum lateral load achieved by each was assumed to be based on its shear capacity. Test 120C-U (unilateral) reached a maximum lateral load of 63 kips and had a concrete compressive strength of 4550 psi. Test C-86-14-DM (bilateral) reached a maximum lateral load of 68 kips and had a concrete compressive strength of 5250 psi. Part of the small difference between the two lateral loads was probably the result of differing concrete strengths. The results indicate that for a square symmetrical

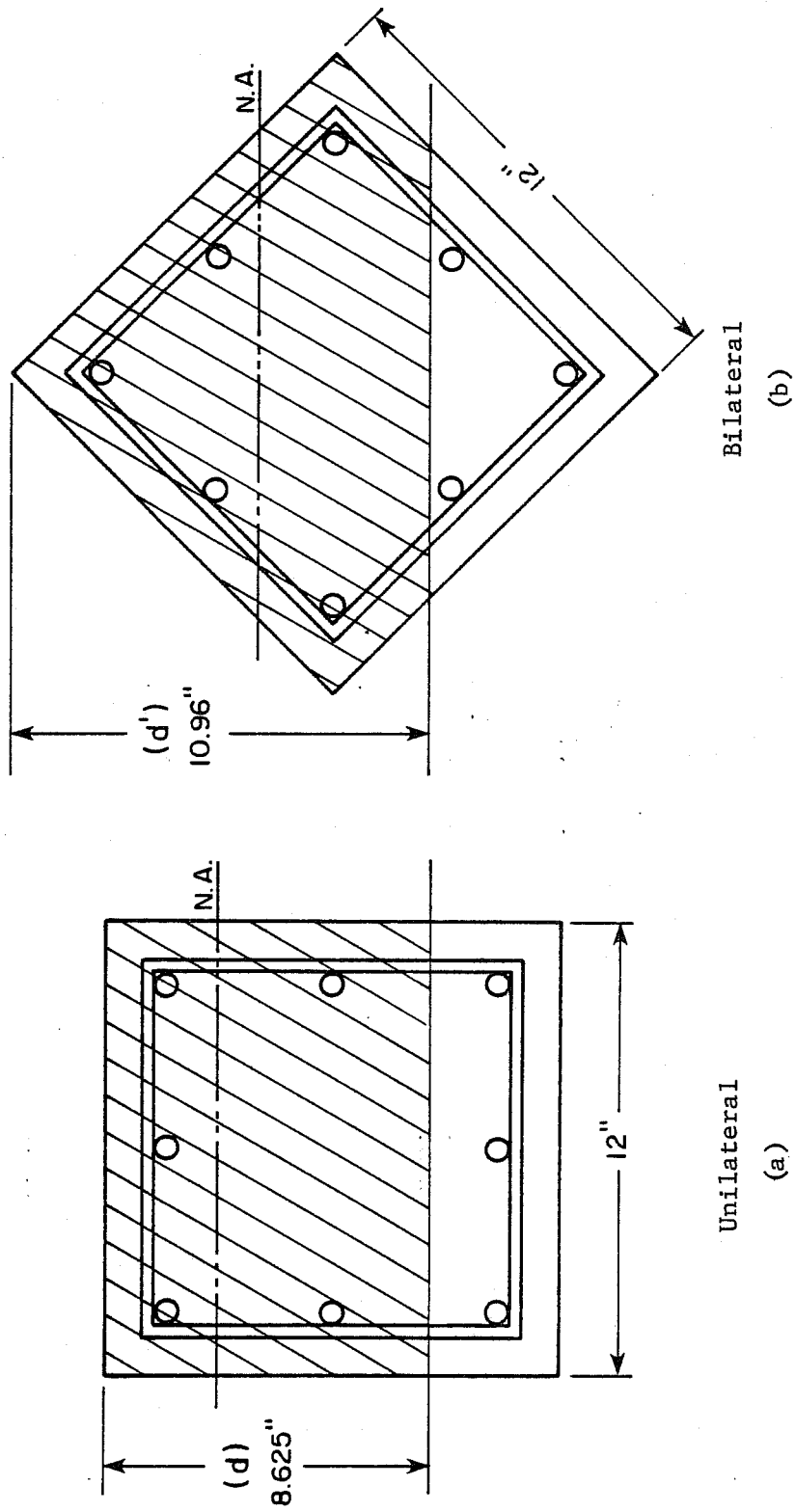


Fig. 5.7 Unilateral vs. Bilateral loading

Unilateral  
(a)

Bilateral  
(b)

section the shear capacity was relatively independent of loading orientation.

The ACI Code Chap. 11 shear provisions did not provide specific guidance to the calculation of the shear capacity of a diagonally loaded member. The provisions were applied in the manner described below. The sections shown in Fig. 5.7a and Fig. 5.7b represent an 86 series column section. The location of the neutral axis at ultimate conditions (peak compressive concrete strain of 0.003) was found using the section analysis program described in Appendix B. For the compressive axial loads considered, the location of the neutral axis caused the lower five longitudinal bars to be in tension. Using this information, the distance from the extreme compression fiber to the centroid of the longitudinal tension reinforcement was calculated. The distances are labelled  $d$  and  $d'$ , unilateral and bilateral, respectively. The term for the concrete shear capacity in the ACI Code can be taken to be

$$2\sqrt{f'_c} b_w d \quad (5.4)$$

where  $f'_c$  = concrete compressive strength, psi

$b_w$  = web width of member, in.

$d$  = distance from extreme compression fiber to centroid of longitudinal tension reinforcement, in.

The term  $b_w d$  in Eq. 5.4 is taken to represent the shaded area shown in Fig. 5.7a. The shaded area in Fig. 5.7b is taken to represent  $b_w d'$  for the diagonally loaded member. Calculation of the two shaded areas reveals that they are nearly identical (103.5 and 107.9 sq. in., respectively). The unilateral concrete shear capacity can be expected to be nearly equal to the bilateral concrete shear capacity.

The total shear capacity of a member is taken by the ACI Code (Chap. 11) to be the sum of both the concrete capacity and the capacity contributed by shear reinforcement. For the unilateral loading case, the shear reinforcement contribution was

$$V_s = \frac{A_v f_y d}{s} \quad (5.5)$$

where  $V_s$  = shear reinforcement contribution to the shear capacity  
 $A_v$  = area of shear reinforcement within a distance  $s$ , sq. in.  
 $f_y$  = yield strength of shear reinforcement, psi  
 $s$  = spacing of shear reinforcement in direction parallel to the longitudinal reinforcement, in.  
 $d$  = distance from extreme compression fiber to centroid of longitudinal tension reinforcement, in.

It was shown in Appendix C that the contribution of the shear reinforcement in a diagonally loaded member was

$$V'_s = \frac{A_v f_y d'}{s\sqrt{2}} \quad (5.6)$$

where  $V'_s$  = shear reinforcement contribution to the shear capacity (diagonally loaded member)  
 $A_v$  = as above  
 $f_y$  = as above  
 $s$  = as above  
 $d'$  = distance from extreme compression fiber to centroid of longitudinal tension reinforcement for diagonally loaded member, in.

Using the values for  $d$  and  $d'$  shown in Fig. 5.7a and Fig. 5.7b as a guide, the unilateral shear reinforcement contribution to



the shear capacity of the section was

$$V_s = \frac{A_f (8.625 \text{ in.})}{v_y s} \quad (5.7)$$

and the bilateral shear reinforcement contribution was

$$V'_s = \frac{A_f (10.96 \text{ in.})}{s\sqrt{2}} \quad (5.8)$$

or

$$V'_s = \frac{A_f (7.75 \text{ in.})}{s}$$

The ratio of the unilateral to the bilateral shear reinforcement contribution is 8.625/7.75 (=1.11). On the basis of the test results and calculations, it can be concluded that for the short columns in the current investigation the shear capacity was relatively unaffected by the direction of loading.

In summary, it was found that the ACI Code Chap. 11 shear equations could be applied to the short columns on the basis of a general approach. However, as will be discussed in subsequent sections the values obtained from the equations were very conservative compared to the observed shear resistance of the members.

An example of the calculations for determining the  $V_c$  and  $V_s$  terms of the ACI Code Chap. 11 shear equations is shown in Fig. 5.8. Because the shear capacity along the diagonal is very close to the unilateral shear capacity no modifications to the ACI Code equations were made. The capacities in the equation and the result of the equation were diagonal capacities.

Specimen C-86-32-D

$$V_c = \left( 1.9\sqrt{f'_c} + 2500\rho_w \frac{V_u d}{M_u} \right) b_w d \quad (\text{ACI318-77 Eq. 11-6})$$

$$f'_c = 5400 \text{ psi} \quad b_w = 12 \text{ in.} \quad d = 8.625 \text{ in.}$$

$$\rho_w = \frac{A_s}{b_w d} = \frac{5(0.44 \text{ sq in.})}{12 \text{ in.} (12 \text{ in.})} = 0.021$$

$$V_u = \frac{2M_u}{L_c} = \frac{2M_u}{36 \text{ in.}} = \frac{M_u}{18 \text{ in.}} \quad (\text{See Fig. 5.6})$$

$M_m$  replaces  $M_u$  according to ACI318-77 Eq. 11-7.

$$N_u = 120 \text{ kips}$$

$$h = 12 \text{ in.}$$

$$M_u = 1440 \text{ kip-in.}$$

$$M_m = M_u - N_u \frac{(4h-d)}{8}$$

$$M_m = 1440 \text{ kip-in.} - 120 \text{ kips} \frac{(4(12 \text{ in.}) - 8.625 \text{ in.})}{8}$$

$$M_m = 1440 \text{ kip-in.} - 590 \text{ kip-in.}$$

$$V_c = \left( 1.9\sqrt{5400} + 2500(0.021) \frac{1440(8.625)}{18(1440-590)} \right) (12)(8.625)$$

$$V_c = 18900 \text{ lbs. (18.9 kips)}$$

$$V_s = \frac{A_v f_y d}{s} \quad (\text{ACI318-77 Eq. 11-17})$$

$$V_s = \frac{0.088(73)(8.625)}{1.125}$$

$$A_v = 2(0.044 \text{ sq in.}) = 0.088 \text{ sq in.}$$

$$f_y = 73 \text{ ksi}$$

$$V_s = 49.3 \text{ kips}$$

$$s = 1.125 \text{ in.}$$

Fig. 5.8 Shear capacity calculation

#### 5.4 Measured Lateral Loads

The measured peak lateral loads,  $V_{rt}$ , are listed in Table 5.2. The values of  $V_{rt}$  were taken as the maximum measured lateral load achieved during each test, regardless of the point in the load history at which it occurred. Also listed in Table 5.2 are the normalized peak lateral loads,  $V_{rtn}$ , which were obtained by multiplying  $V_{rt}$  by the factor

$$\sqrt{\frac{5000}{f'_c}}$$

The justification for normalizing in this manner is discussed in Sec. 4.1. The normalization is applied only to the 86 series specimens because they were primarily dominated by shear and bond, both of which are functions of  $\sqrt{f'_c}$ .

One indication of desirable cyclic hysteretic behavior is the stability of the loops; that is, the tendency for the loops at a given deflection limit to achieve the same peak lateral load. The degree of instability is measured by the percentage loss of lateral load capacity between the first and third cycles at each deflection limit. The percentage losses are listed in Table 5.3 for each of the cyclic tests in the current investigation. The table headings use the symbols discussed earlier. As an example, the first column shows the percentage drop between the lateral loads at  $1\Delta 1$  and  $1\Delta 3$  and the second column between  $1\Delta-1$  and  $1\Delta-3$ . Dashes in the table indicated that the test was stopped prior to those deflection limits.

#### 5.5 Effect of Compressive Axial Load

There were two sets of comparative tests in which axial load was changed-- 0-86-14-DM versus C-86-14-DM, both monotonic

TABLE 5.2 COMPUTED AND OBSERVED LATERAL LOAD CAPACITIES

Test Name	$f'_c$	N	$V_{rs}$	$V_{rf}$	$V_{rt}$	$\frac{V_{rt}}{V_{rs}}$	$\frac{V_{rt}}{V_{rf}}$	$\frac{V_{rs}}{V_{rf}}$	$V_{rtn}$
O-86-14-DM	5950	0	39	67	55	1.41	0.82	0.58	50
C-86-14-DM	5250	140	41	79	68	1.66	0.86	0.52	66
O-86-32-D	4550	0	65	64	63	0.97	0.98	0.98	66
C-86-32-D	5400	120	68	80	80	1.18	1.00	0.85	77
C-86-21-D	5750	140	51	83	81	1.59	0.98	0.61	76
O-86-14-D	5050	0	38	63	60	1.58	0.95	0.60	60
C-86-14-D	4650	140	40	79	65	1.63	0.82	0.51	67
C-86-09-D	5750	140	34	83	67	1.97	0.81	0.41	62
C-86-03-D	6100	120	24	80	73	3.04	0.91	0.30	66
C-84-32-D	4850	140	67	61	63	0.94	1.03	1.10	63*
C-84-21-D	4850	140	49	58	62	1.27	1.07	0.84	62*
C-84-14-D	5450	120	39	56	61	1.56	1.09	0.70	61*

\* Not normalized

- $f'_c$  - concrete compressive strength, psi  
 N - compressive axial load, kips  
 $V_{rs}$  - lateral load capacity based on shear, kips  
 $V_{rf}$  - lateral load capacity based on flexure, kips  
 $V_{rt}$  - observed maximum lateral load, kips  
 $V_{rtn}$  - normalized values of  $V_{rt}$ , kips

TABLE 5.3 PERCENTAGE LOSS IN LATERAL LOAD BETWEEN FIRST AND THIRD CYCLES

Test Name	1Δ	1Δ-	1Δ'	1Δ-'	2Δ	2Δ-	2Δ'	2Δ-'	3Δ	3Δ-	3Δ'	3Δ-'	4Δ	4Δ-	4Δ'	4Δ-'
0-86-32-D	6	7	6	4	10	8	9	5	14	19	12	10	39	33	39	33
C-86-32-D	12	3	3	1	18	16	14	14	29	31	40	38	31	34	37	38
C-86-21-D	3	4	5	5	34	31	27	26	34	32	39	44	38	-	-	-
0-86-14-D	8	3	6	7	29	26	21	19	44	37	32	30	35	34	35	33
C-86-14-D	5	5	4	11	41	29	35	35	42	52	35	41	18	30	16	-
C-86-09-D	4	2	5	5	47	29	44	42	21	29	14	30	-	-	-	-
C-86-03-D	2	1	3	7	40	29	-	-	-	-	-	-	-	-	-	-
C-84-32-D	4	6	3	5	9	3	8	9	8	10	7	9	12	16	17	23
C-84-21-D	6	6	1	5	10	9	10	15	5	6	47	x	41	-	-	-
C-84-14-D	6	0	6	0	4	0	16	10	23	30	41	39	-	-	-	-

tests with intermediate tie spacing, and 0-86-32-D versus C-86-32-D, both cyclic with the minimum transverse reinforcement spacing used in the test program.

The load-deflection curves for 0-86-14-DM and C-86-14-DM were plotted on the same axes in Fig. 5.9. The presence of a compressive axial load increased the initial stiffness of the curve and the maximum lateral load capacity. Both of these effects were expected, since past research has shown that the presence of a compressive axial load less than that at balanced strain conditions increases both the ultimate moment capacity (and therefore  $V_{rf}$ ) and the shear capacity,  $V_{rs}$ , compared to the same section with no axial compressive load.

It seemed that the presence of a compressive axial load increased the degradation of the lateral load for imposed deflections greater than the deflection at which the maximum lateral load was achieved. This was illustrated in Fig. 5.9 by the fact that the lateral load capacity at about 0.5 in. was higher with axial load by the slope of the curve drops sharply after the peak. The capacity is maintained at a higher level in specimen 0-86-14-DM than specimen C-86-14-DM at large deflections.

The comparison between 0-86-32-D and C-86-32-D reveals the same effects as discussed for the previous two specimens. In fig. 5.10 the lateral loads for peaks  $1\Delta 1$ ,  $2\Delta 1$ ,  $3\Delta 1$ ,  $4\Delta 1$ , and 1.4 in. were plotted for both tests to provide an envelope curve which highlights the trends. As before, the initial stiffness and maximum lateral load were higher for the specimen with the compressive axial load. Also, the specimen with the compressive axial load showed a much faster degradation of stiffness and lateral load than the specimen without compressive axial load. An additional comparison was made between 0-86-32-D and C-86-32-D

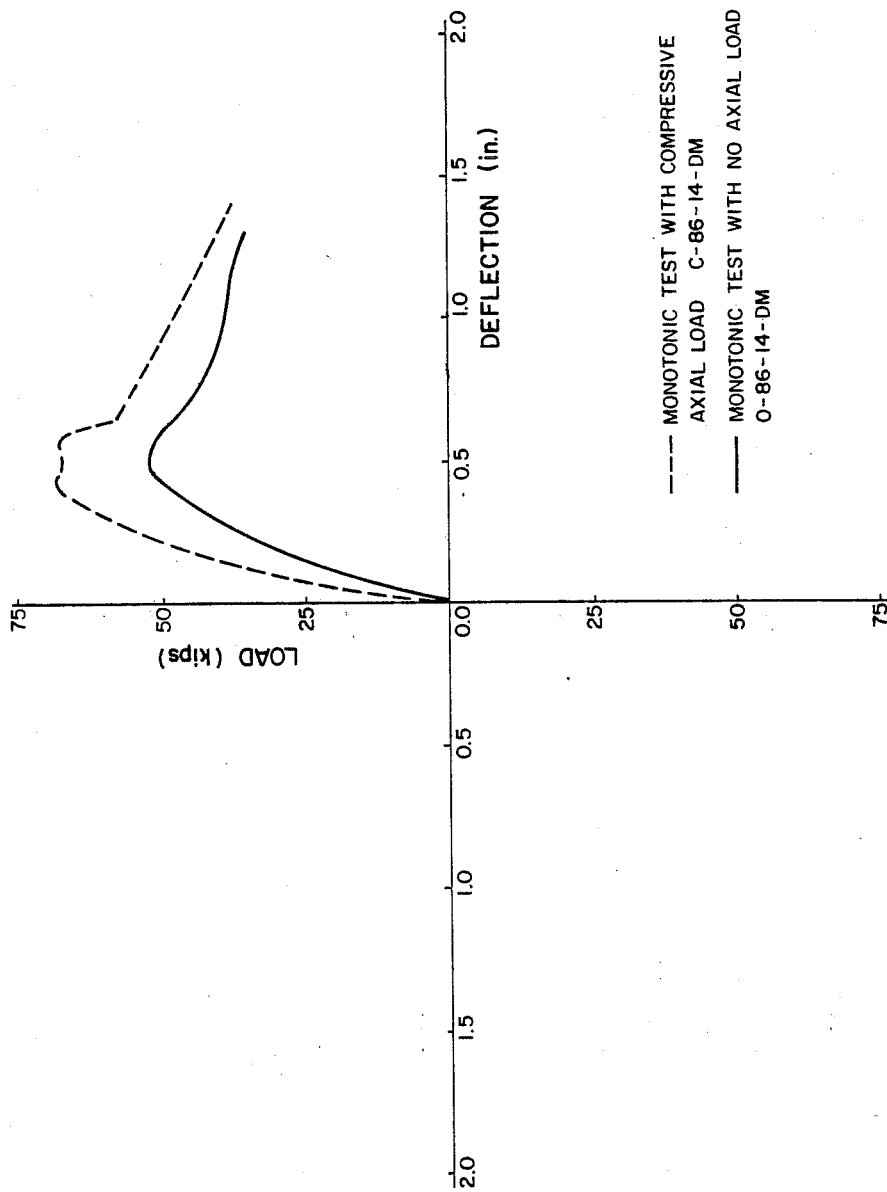


Fig. 5.9 Effect of axial load (monotonic)

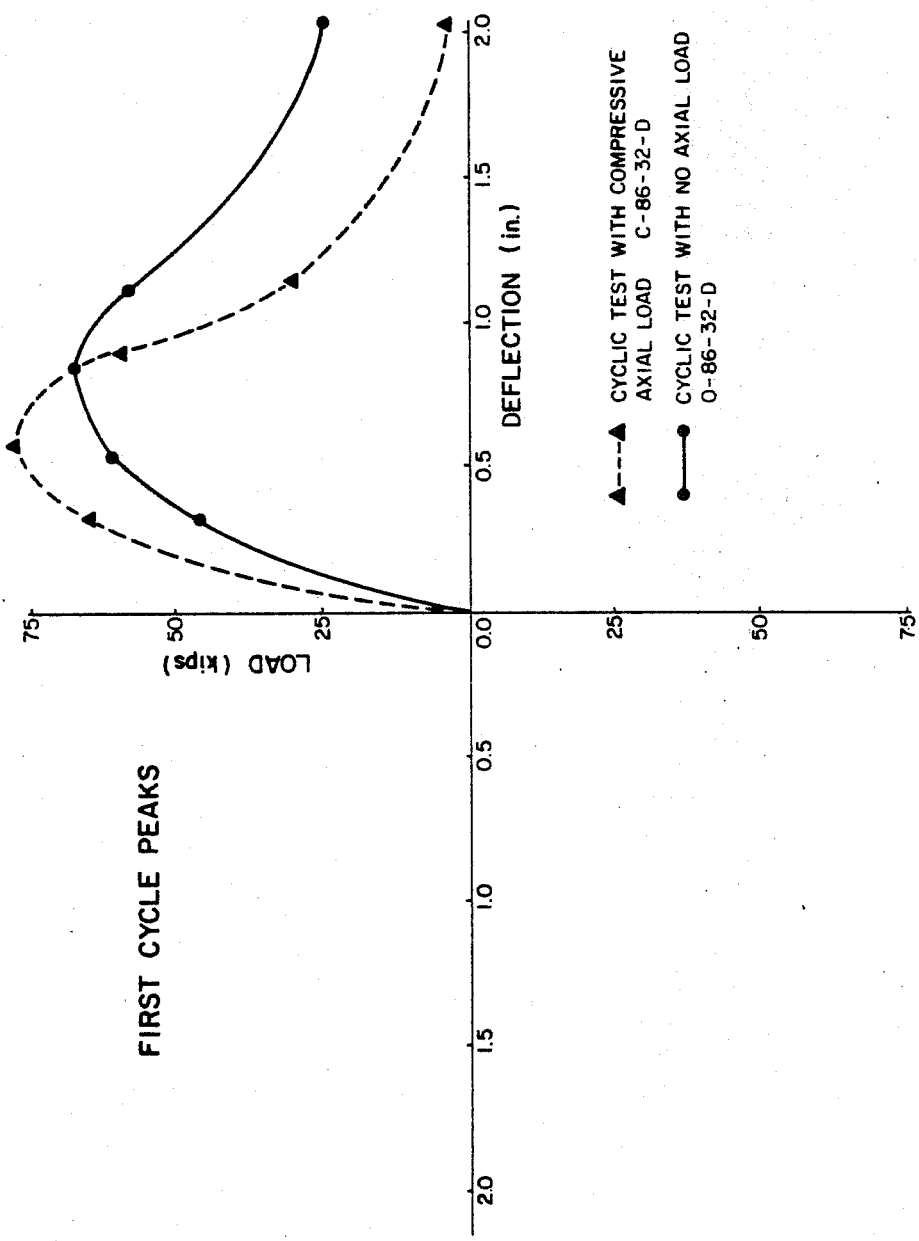


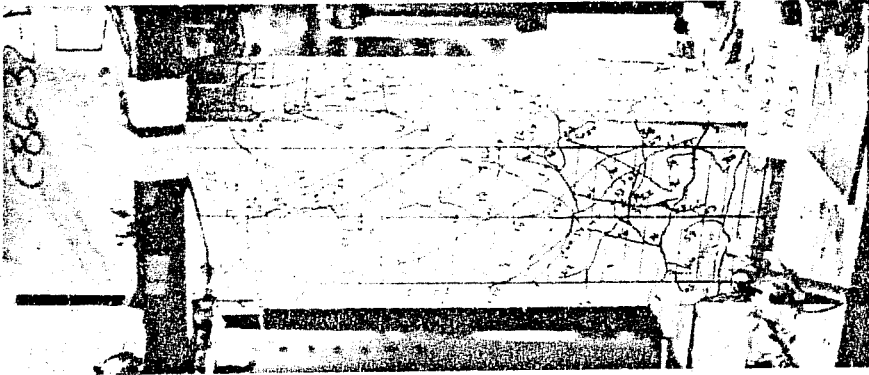
Fig. 5.10 Effect of axial load (cyclic tests)



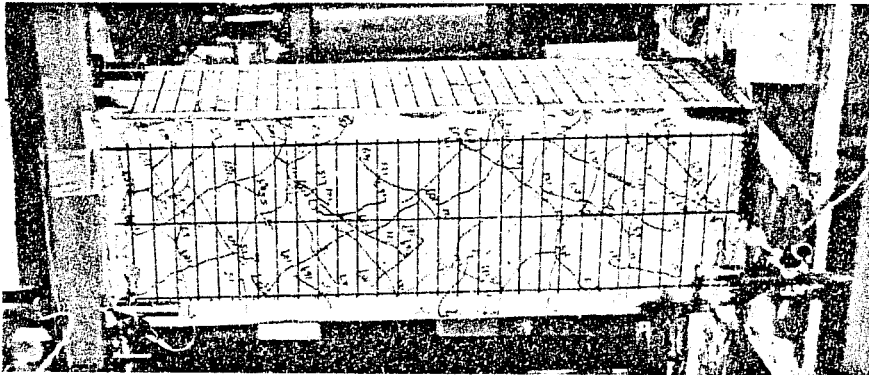
to determine the effect compressive axial load had on the angle of the inclined cracks. The crack patterns for the east faces of both specimens at peak  $2\Delta-3$  (Fig. 5.11) show no noticeable difference in the orientation of the inclined cracks.

One other indication of behavior is the percentage loss of lateral load at the cycle peaks. The percentages (Table 5.3) showed that during the early stages of loading the specimens without axial load had more stable cyclic loops than those with axial load. However, in both sets of tests a deflection level was reached where the percentage losses became about the same. The presence of axial load did not appear to cause the initiation of degradation, since the degradation also occurred in the tests with no axial load, but rather the compressive axial load caused the degradation to begin at a lower deflection.

The study of strains in the tie gages for the four tests led to an explanation for the increased degradation in the axially loaded columns. Figure 5.12 shows typical tie strains for the C-86-32-D and O-86-32-D tests at the first cycle and third cycle peaks in the northwest (first) direction. Also shown are the measured lateral loads at the same peaks. Similarly, Fig. 5.13 shows typical tie strains and lateral loads for the C-86-14-DM and O-86-14-DM tests at the deflections  $1\Delta$ ,  $2\Delta$ ,  $3\Delta$ , and  $4\Delta$  along the initial northwest direction. A feature which stands out in both figures is that the lateral load degrades only when the tie strains approach or exceed their yield strains. There is a large increase in the strain at the  $2\Delta$  deflection limit in all tests. This is expected because the specimens exhibited a significant amount of inclined cracking during loading to the  $2\Delta$  deflection level. The manner in which transverse reinforcement improves shear resistance is uncertain. The usual approach is to assume a truss action as in the ACI Building Code. However, the

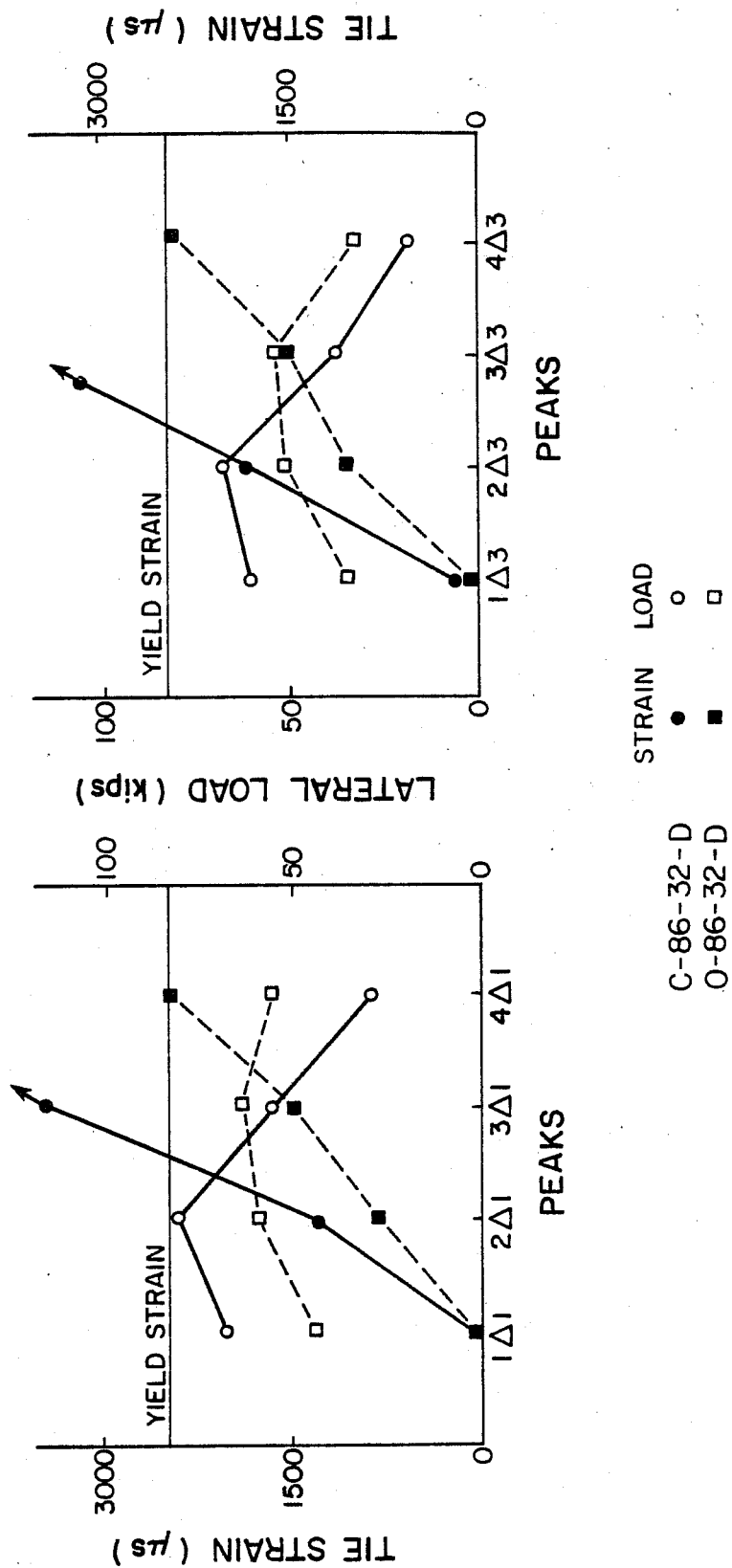


(b) With axial load



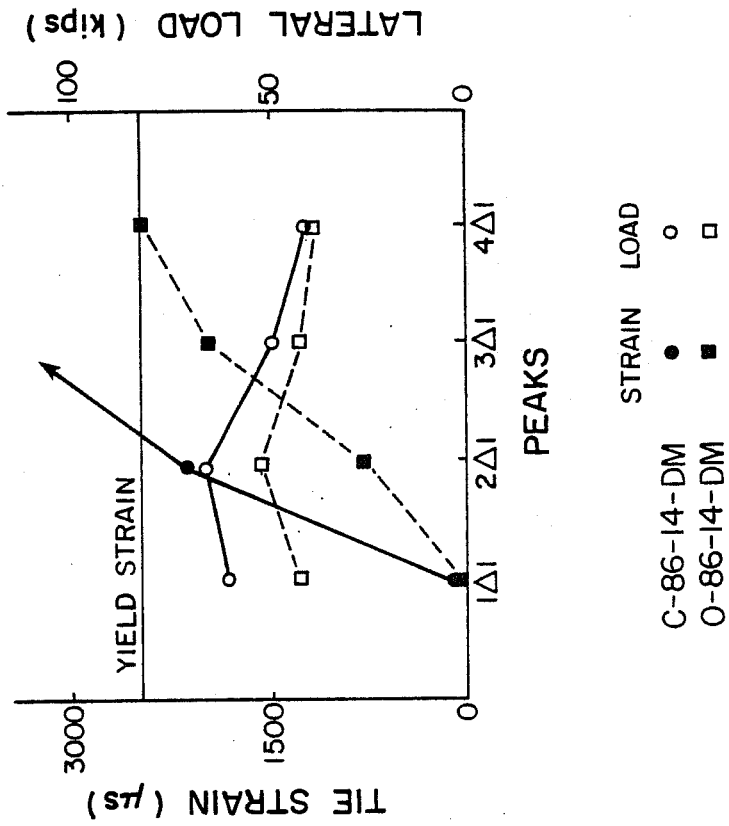
(a) Without axial load

Fig. 5.11 Effect of axial load on cracking



(Gage is 9 in. from top, east face)

Fig. 5.12 Tie strains (ties at 1-1/8 in.)



(Gage is 9 in. from top, east face)

Fig. 5.13 Tie strains (ties at 2.57 in.)

ACI-ASCE Committee 426 report [49] indicates that some investigators have concluded that the primary function of web reinforcement is the control of inclined crack width. Such control aids in maintaining aggregate interlock along the crack. Aggregate interlock is reported [40] to be a significant shear resisting mechanism in beams with no web reinforcement. Thus, the lateral load capacity after inclined cracking is most directly related to the amount of transverse reinforcement crossed by the cracks.

For the two specimens in each comparison, the amount of transverse reinforcement is equal and it can be assumed that the shear capacity after cracking is roughly the same, provided axial compression does not directly affect the transverse reinforcement effectiveness. Reported research [41] suggests that it does not. The presence of a compressive axial load increases the imposed shear on the section by increasing the flexural capacity and the concrete contribution to shear capacity. The higher amount of shear with axial load requires a larger amount of transverse reinforcement to maintain crack width control. As shown in Fig. 5.12 and Fig. 5.13 the tie strain in the specimens with axial load increase faster than in the specimens with no axial load. This suggests that the transverse reinforcement is indeed more highly stressed in the specimen with axial load causing the ties to yield sooner and thus reduce the effectiveness of the aggregate interlock mechanism and the confinement.

Based on four tests with two axial load levels, the effect of compressive axial loads less than the axial load at balanced strain conditions can be summarized as follows:

1. Axial load increased the stiffness of the load-deflection curves prior to achievement of the maximum lateral load.

2. Axial load increased the maximum lateral load attained by a column.
3. Axial load increased the rate of degradation of both the stiffness and lateral load after achievement of the maximum lateral load.
4. Axial load had negligible effect on the orientation of the inclined cracks.

These observations are similar to the conclusions presented by Ramirez [15], who conducted an earlier investigation into the effect of axial load on column behavior.

#### 5.6 Effect of Cyclic Deformations

Specimens C-86-14-DM and C-86-14-D are compared to illustrate the effect of a monotonically applied loading versus a cyclically applied loading. Load-deflection curves are plotted in Fig. 5.14. The influence of cycling is readily apparent after the specimen had achieved its maximum lateral load. Prior to that point, however, the cyclic loading curves follow the monotonic curve very closely. Cycling at or beyond the deflection at which the maximum lateral load occurred caused a significant and permanent reduction in the stiffness and lateral load capacity of the cyclically loaded specimen compared to the monotonically loaded one. It is important to note that both specimens suffered loss of lateral load following the peak. Cycling probably was severe because the specimen had a degrading type of failure even when loaded monotonically. The effect of cycling may not have been as pronounced if the specimens had a more flexurally dominated monotonic response.

#### 5.7 Effect of Transverse Reinforcement Spacing

The spacing of the ties was one of the two main variables

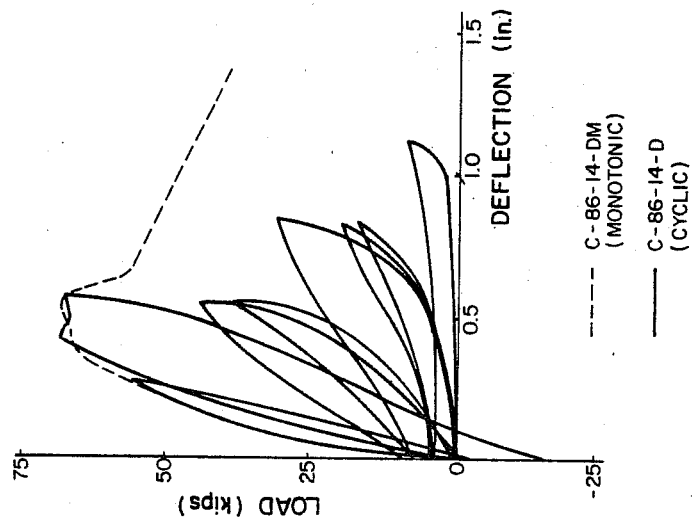


Fig. 5.14 Effect of loading history

in the current test series. The ties were expected to provide shear capacity and confinement to the core of the column. The specimens in the previous investigations of this project were assumed to have exhibited severe degradation of the load-deflection curves because of an insufficient shear capacity. The increased amounts of transverse reinforcement in several specimens of the current investigation was expected to provide enough shear capacity to cause a more flexurally dominated behavior. A possible result would be that the specimens would form the plastic mechanism and exhibit the stable load-deflection curves of a flexural hysteretic behavior.

A flexural dominated behavior is not merely defined as the ability to reach the flexural capacity of the member. The maximum load achieved must also be maintained through increasing deformations and cyclic reversals of loading. Thus, while a short column may achieve its computed flexural capacity it may not exhibit a flexure dominated behavior. The attainment of the flexural capacity may be a one time occurrence after which other effects (such as shear) cause degradation of the hysteretic behavior. However, as a first step in determining the likelihood of flexural behavior the ratio of flexural to shear capacity may be of interest. This check would quickly determine if a shear dominated behavior would occur, but it would not be sufficient to determine if a flexural behavior would occur. Other requirements may need to be satisfied in order to assure a flexural behavior.

Table 5.2 lists the computed capacities based on shear and flexure ( $V_{rs}$  and  $V_{rf}$ ) and the increased maximum lateral load ( $V_{rt}$ ) for each specimen. The ratios of  $V_{rt}$  to  $V_{rf}$  indicated that a number of specimens achieved flexural capacity. Specimens 0-86-32-D, C-86-32-D, C-86-21-D, C-84-32-D, C-84-21-D, and



C-84-14-D achieved their computed flexural capacity. However, the comparison of the ratio of  $V_{rt}$  to  $V_{rs}$  for these tests indicated that shear capacity should have controlled the maximum lateral load of the specimens. As an example specimen C-84-14-D had a  $V_{rt}$  to  $V_{rf}$  ratio of 1.09, but its  $V_{rt}$  to  $V_{rs}$  ratio was 1.56. The maximum lateral load was approximately 50 percent greater than that predicted by the 1977 ACI Building Code [17] Chap. 11 shear capacity equation. The same result was found in those specimens which did not achieve their flexural capacity. The ratios of  $V_{rt}$  to  $V_{rs}$  were significantly greater than 1. Specimen C-86-03-D had a  $V_{rt}$  to  $V_{rs}$  ratio of 3.04.

Figures 5.15 and 5.16 illustrate the relationship between the computed flexure and shear capacities and the measured maximum lateral loads. The general form of the plots is maximum lateral load versus tie spacing. The average values for the ACI Building Code terms  $V_c$  and  $V_c + V_s$  for the axially loaded specimens of each series are plotted. Also plotted is the average computed flexural capacity of the columns in each series. Figure 5.15 shows the data points for the 86 series specimens and Fig. 5.16 shows the data points for the 84 series. It is quite clear that the ACI Code shear capacity equations are conservative for the short columns. In addition, the trend of the shear equations is not reflected in the data. The data from the 86 series indicates that the shear capacity of the short column does not continuously vary with the amount of transverse reinforcement provided. Instead, there is a basic strength which is independent of the transverse reinforcement until the amount of transverse reinforcement is sufficient to allow the column to reach its flexural capacity. A possible explanation of this phenomenon is presented in Chap. 6.

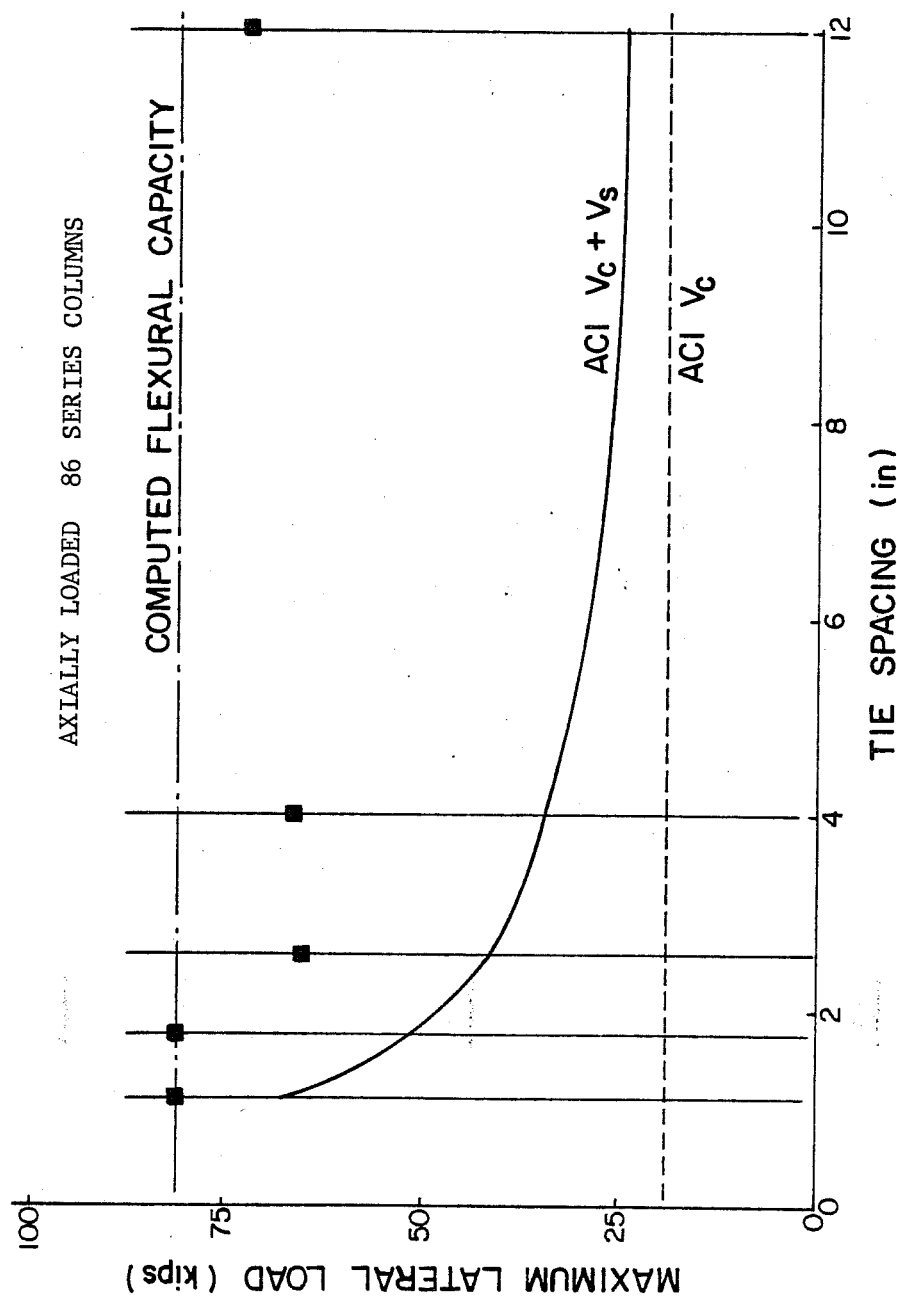


Fig. 5.15 Measured vs. computed lateral load capacities (86 series)

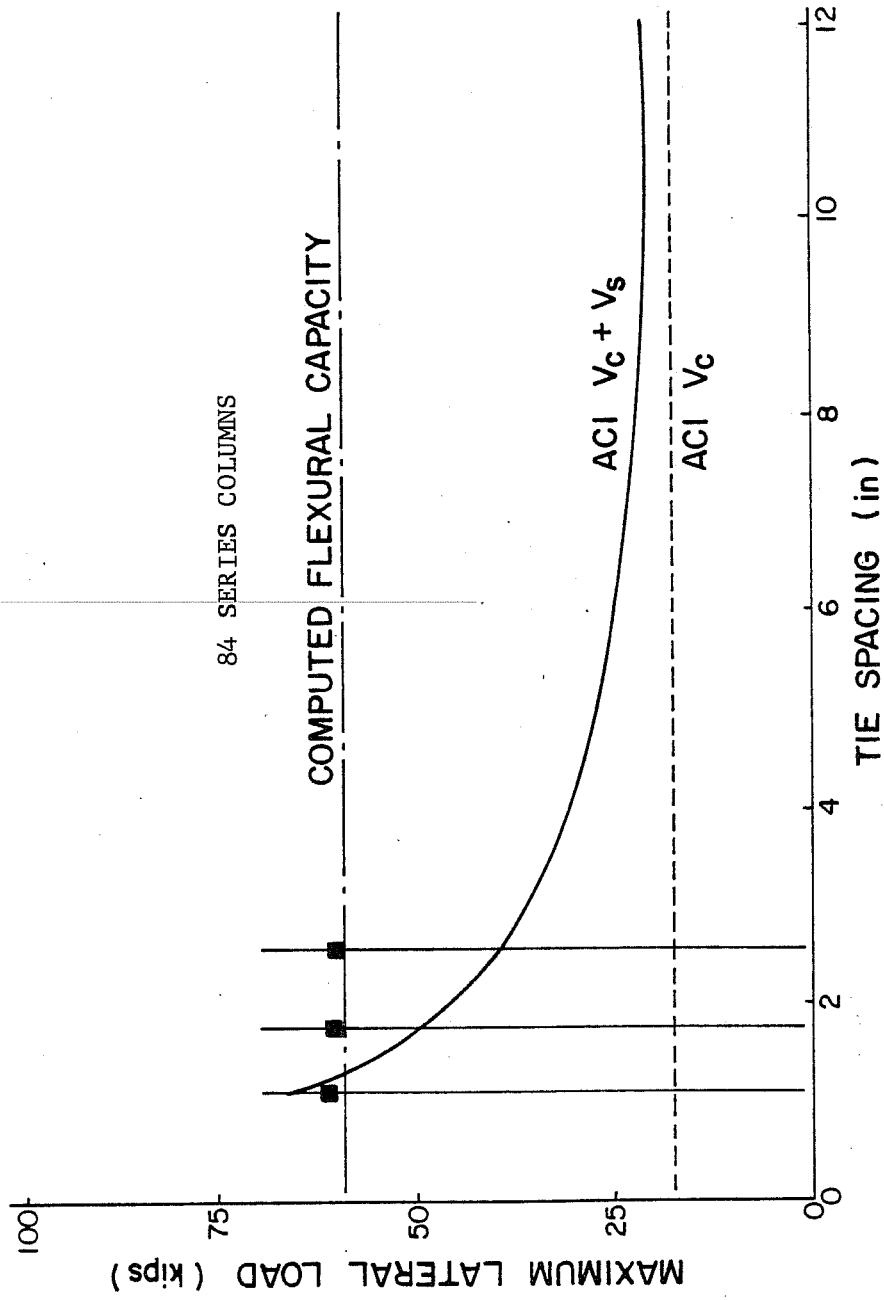


Fig. 5.16 Measured vs. computed lateral load capacities (84 series)

The attainment of flexural capacity is a necessary, but not sufficient condition of flexure dominated behavior. If the column can not maintain the maximum lateral load (degrading hysteretic behavior) it is not considered to be a flexure dominated behavior. A measure of the columns ability to sustain its maximum lateral load during cycling at a peak deflection is the percentage loss in lateral load between the first and third cycles. The percentage losses are shown in Table 5.3. Specimens C-86-14-D, C-86-09-D, and C-86-03-D all had large losses beginning at the  $2\Delta$  deflection level. These specimens also had very similar maximum normalized maximum lateral loads. Specimen C-86-21-D had the next largest losses at the  $2\Delta$  level, while specimen C-86-32-D had the lowest losses among the five axially loaded 86 series cyclic tests. Comparison of the actual load-deflection curves for the five specimens showed a distinct decrease in the rate of overall degradation with decreased tie spacing. Figure 5.17 shows envelopes of the peaks at  $1\Delta$ ,  $2\Delta$ ,  $3\Delta$ , and  $4\Delta$  for each specimen and illustrates that increased amounts of transverse reinforcement does cause a more flexurally dominated behavior.

There was an improvement in hysteretic behavior with decreased tie spacing, but in none of the 86 series specimens was stable hysteretic behavior (flexure dominated) observed. Specimen 0-86-32-D exhibited the most satisfactory behavior and yet, as the losses in Table 5.3 and the envelope of peaks in Fig. 5.10 showed, it did not exhibit stable behavior after the  $3\Delta$  deflection level was reached. The deflection level  $3\Delta$  was where the maximum lateral load was reached. Specimen 0-86-32-D did not maintain its flexural capacity after achieving it. By comparison, specimen C-84-32-D showed stable loops through the  $3\Delta$  deflection limit and even though its longitudinal

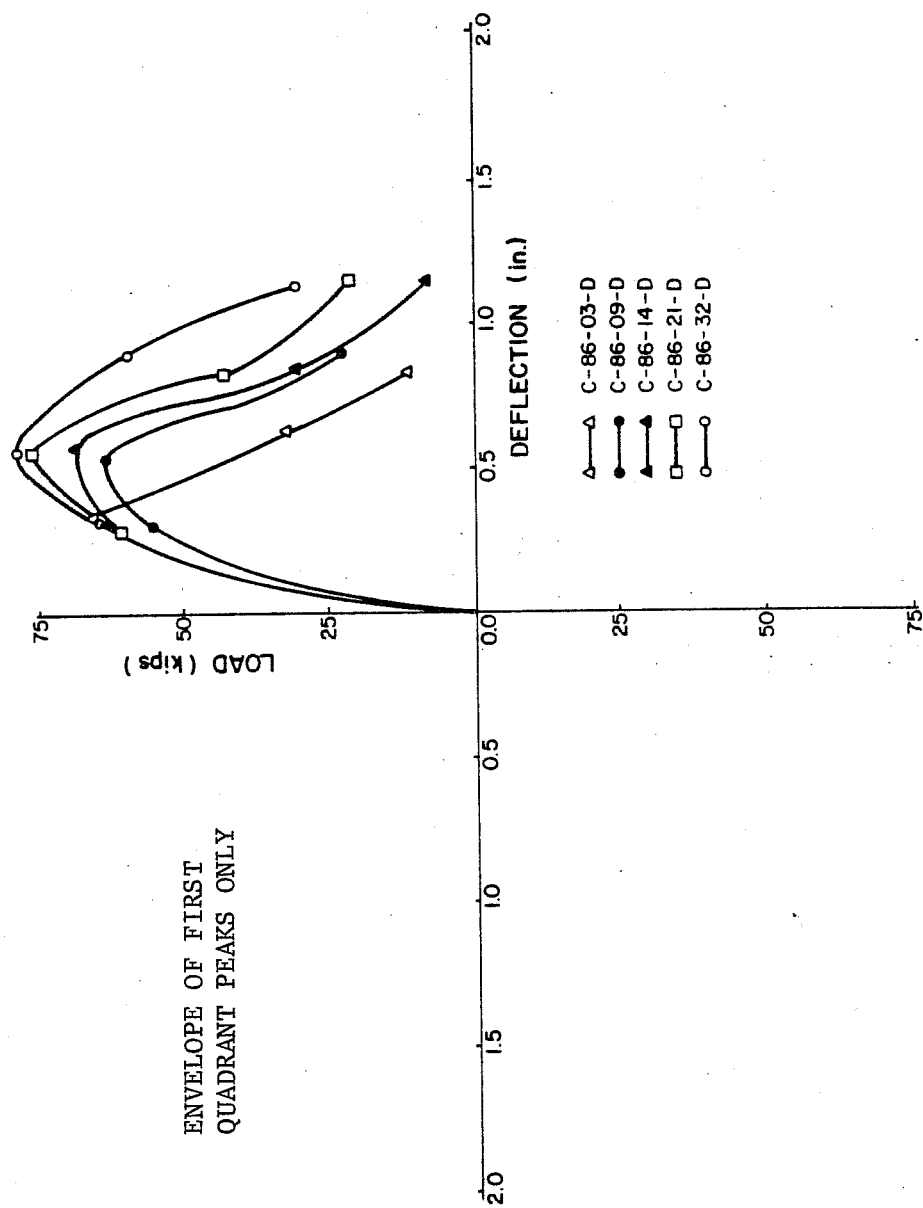


Fig. 5.17 Effect of tie spacing on hysteresis degradation

bars were buckling showed less percentage load loss at the  $4\Delta$  deflection limit than 0-86-32-D. More importantly, C-84-32-D maintained its flexural capacity from the  $2\Delta$  deflection limit to the  $4\Delta$  deflection limit at which point longitudinal bar buckling reduced its lateral load capacity. The computed flexural and shear capacities (Table 5.2) were about the same for the C-84-32-D and 0-86-32-D specimens, but the load-deflection curves for C-84-32-D were more open and stable than those for 0-86-32-D.

The differences between the behavior of specimens 0-86-32-D and C-84-32-D raised questions as to the cause of degradation in the specimens of the 86 series. It did not seem to be solely a function of the amount of transverse reinforcement. There was a noticeable difference in behavior between 0-86-32-D and C-84-32-D and even more so between C-86-32-D and C-84-32-D. The parameter which seemed to most directly relate to the discrepancy was the other principal variable in the test series--the size of the longitudinal bars.

#### 5.8 Effect of Longitudinal Bar Diameter

There was a significant difference in observed behavior between the 86 and 84 series other than the differences related to longitudinal bar buckling in the 84 series. From the rather poor hysteretic behavior exhibited by all of the specimens in the 86 series, it was concluded that the size of the longitudinal bars influenced the flexural capacity and the development length required for bond.

At the beginning of the current investigation it was hypothesized that the ratio of shear capacity to flexural capacity determined the probable mode of failure. The ratio

of computed shear to flexural capacity for each specimen is listed in Table 5.1. The ratio for 0-86-32-D was 0.98. A flexural dominated behavior was expected. However, as illustrated by the load-deflection curves (Fig. 4.11), the specimen did not exhibit stable hysteretic behavior. There was a degradation of load even at the deflection level where the maximum lateral load was achieved. The specimen could not maintain its maximum load, even if the deflection was not increased. The degradation of load and stiffness with increased deflection was pronounced and it would seem that the specimen did not exhibit the characteristics of a flexurally dominated behavior. Thus, it is likely that the ratio of shear to flexural capacity is only one criterion for determining the failure mode and that some other factor is also responsible for the degrading hysteresis load-deflection loops of specimen 0-86-32-D and the other 86 series columns.

Based on the results of earlier Japanese investigations, bond degradation was a possible reason for the poor performance of the 86 series specimens compared to the specimens in the 84 series. There were several features about the observed behavior of the specimens which suggested bond degradation. The first was the location of maximum damage to the specimen. Each of the 86 series specimens exhibited more damage to the core and cover loss in the middle third of the column, while the specimens of the 84 series, especially C-84-21-D, showed more damage at the ends of the column. It was observed that the concrete surrounding the longitudinal bars in the 86 series was ground away in the damaged area destroying the composite action. The #4 longitudinal bars were embedded in sound concrete in the middle region of the specimen throughout the test.

Another factor which suggested bond degradation was the

change in shape (pinching) of the hysteretic loops in the 86 series specimens during the tests, as illustrated in Fig. 5.18 for specimen 0-86-32-D. The load-deflection curves show a change at the  $3\Delta$  deflection limit at which the maximum lateral load was achieved. The deflection at which the maximum lateral load was achieved was the critical point where the characteristics of the load-deflection curve changed in all the 86 series tests. Cycling to deflections less than the critical deflections caused minor, if any, lateral load degradation, but some stiffness degradation. By contrast, cycling at or beyond the critical deflection caused significant losses in lateral load and stiffness. In addition, the shape of the curve changed. Shown in Fig. 5.19 is a typical example of the observed change. The shape of the curve prior to cycling at the critical deflection limit is indicated by line AB, which had a constantly negative curvature with a zero slope as the peak is reached. In the next cycle, the shape is changed, as shown by the curve between C and D, which had a negative curvature during loading from C and tended toward a zero slope or low stiffness near zero deflection. After passing zero deflection, the stiffness increased with a positive curvature rather than the negative curvature of line AB. At approximately point D, the curvature changed from positive to negative and the slope tended towards zero as the lateral load peaked. Point E was drawn as being below point B. This was generally true of the 86 series tests, since point B in the tests was the maximum lateral load reached by the specimens.

Pinching is not only caused by bond degradation along the longitudinal bars. Sliding shear at the ends of the member can also contribute to the pinching. Sliding shear is the relative movement between a member and a joint caused by a flexural crack which penetrates the total depth of the member.



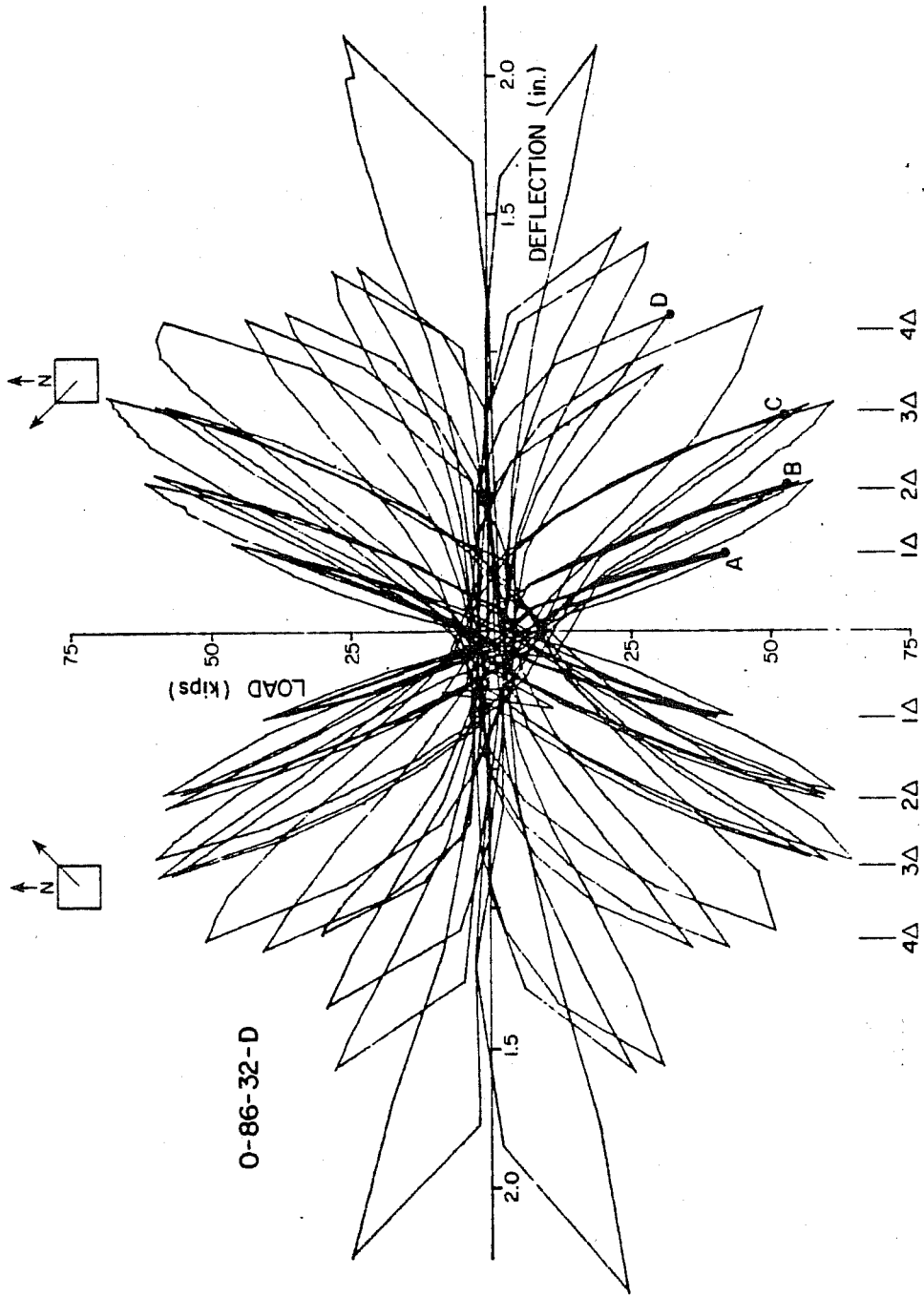


Fig. 5.18 Specimen 0-86-32-D load-deflection curves

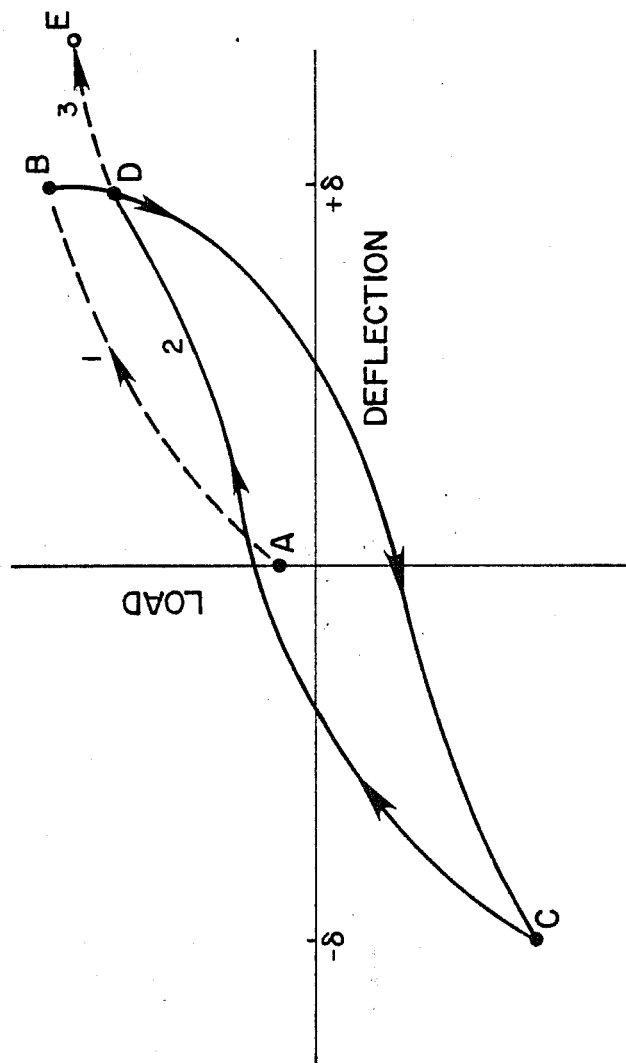


Fig. 5.19 Shape change observed in hysteresis loops

Shear is transferred across such a crack (Fig. 5.20) by doweling action of the longitudinal bars and aggregate interlock along the crack surfaces. Another possible contributor to pinching is the effect of flexural cracks formed by tension steel yielding which do not close until compression yielding when the load is reversed. Until the crack closes to permit the concrete to act in compression only the tension and compression steel act to resist the moment. The stiffness of the steel couple is much less than the combined concrete and steel couple. The reduced stiffness is the pinched portion of the hysteresis loops.

The relationship between bond degradation and loss of load capacity and stiffness was suggested by Hassan and Hawkins [90], who observed rapid degradation of bond in specimens where the reinforcement was subjected to load reversals which caused the bar to have alternating compressive and tensile yielding. In the current series the longitudinal steel reached its peak stress when the specimen achieved its maximum lateral load capacity. According to an analysis of the section the majority of the longitudinal bars were yielded at ultimate conditions. Because of the loading condition, the longitudinal bars, especially at the corners, were subjected to reversed yielding as the deflections were cycled. Cycling between deflections corresponding to maximum load would produce the same kind of rapid degradation observed by Hassan and Hawkins.

The development length in tension for the column longitudinal bars using the ACI Building Code provisions and the proposed recommendations of ACI Committee 408 [84] are listed in Table 5.4. The two approaches gave similar results and an average development length (tension) for the #6 bar was taken to be 20 in. and 13 in. for the #4 bar. If the inflection point of the specimen was approximately the midheight of the column, the

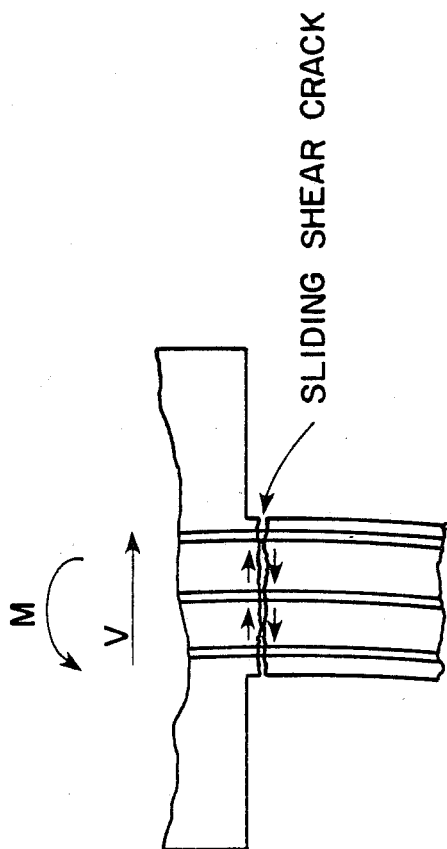


Fig. 5.20 Sliding shear

TABLE 5.4 COMPUTED LONGITUDINAL BAR  
DEVELOPMENT LENGTHS (Tension)

Test Name	$l_{d1}$ in.	$l_{d2}$ in.
0-86-32-D	20.6	18.6
C-86-32-D	20.6	17.1
C-86-21-D	20.6	16.5
0-86-14-D	19.6	16.4
C-86-14-D	20.6	18.4
C-86-09-D	20.6	22.9
C-86-03-D	20.6	22.3
C-84-32-D	13.7	12.3
C-84-21-D	13.7	12.3
C-84-14-D	13.7	11.6

$l_{d1}$  - based on ACI318-77

$l_{d2}$  - based on Committee 408  
recommendations [84]

maximum length available for development was 18 in. The actual point of inflection could not be determined because strains (stresses) along the longitudinal bars were not measured. The nature of the loading on the columns caused every corner bar to be highly stressed in tension repeatedly during the loading history. A shift of the inflection point from midheight would cause a more severe development length requirement as the shift would shorten the development length available for at least one bar (Fig. 5.21). It is clear that bond degradation is an important reason for the observed differences in hysteretic behavior between the 86 series and the 84 series specimens when the available development lengths are compared to that required. It should be noted that development length recommendations are based on monotonic tests, further aggravating anchorage problems for the #6 bar.

### 5.9 Summary of Observations

From the results of the test program, several interesting observations on the behavior of short reinforced concrete columns can be made. The observations are based on twelve tests. All were deformed along the diagonals of the specimen and the cyclic deformation histories were identical. The main variables in the test program were the spacing of the column ties and the size of the longitudinal reinforcing bars. Secondary variables were axial load and deformation history.

The presence of a compressive axial load less than the load at balanced strain conditions increased the initial stiffness of the specimen and increased the maximum lateral load carried by the specimen. However, the compressive axial load increased the rate of degradation of both the lateral load and stiffness after the specimen reached its maximum lateral load.

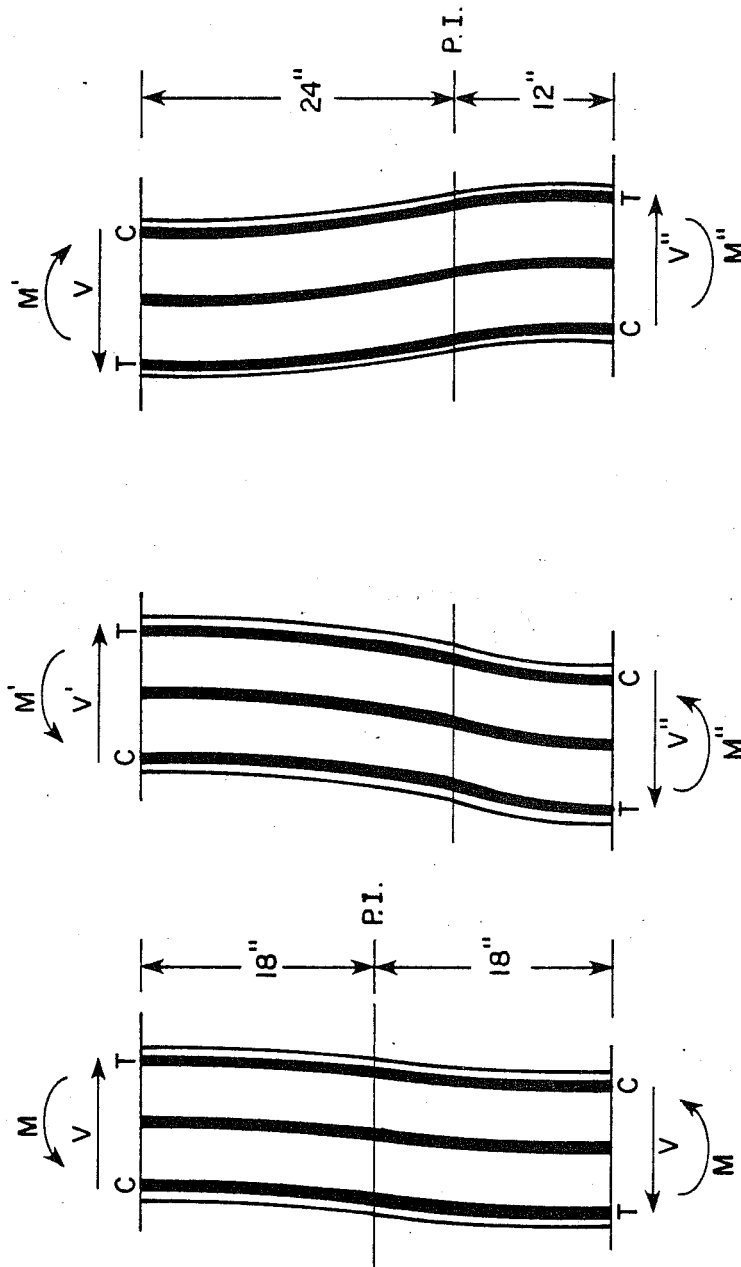


Fig. 5.21 Available development lengths

Cyclic reversed deflections caused the specimen to degrade faster than if the specimen had been monotonically deflected. The effect of cycling was most significant if the specimen was cycled at deflections equal to or greater than the deflection at which the maximum lateral load was achieved.

The spacing of the column ties varied from 12 in. to 1-1/8 in., but it did not significantly affect the maximum lateral loads applied to the test specimens. If the tie spacing was small, there was sufficient transverse reinforcement to allow the specimen to reach its flexural capacity. If there was not enough transverse reinforcement, the tie spacing did not affect the maximum lateral load achieved by the specimen. The spacing of the column ties did affect the rate of degradation of lateral load following the achievement of the maximum lateral load. Decreased tie spacing decreased the rate of degradation.

In the current test series, the longitudinal bar diameter was the parameter which most affected the characteristics of the load-deflection curves, such as pinching. The bars were required to undergo cycles at high stress reversal. At best, the bars had only one-half of the column length for anchorage, because the column was bent in double curvature with a point of inflection near midheight.

## 5.10 Classification Guide

5.10.1 Overview. The points listed in the summary provide the basis for formulating a qualitative decision tree to guide the designer to the kind of behavior a column would exhibit if subjected to cyclic lateral deflections. The decision tree was developed in the form of a flowchart with branches



dependent on the characteristics of the column. The criteria for branch selection were qualitative because the data from the one test series were inadequate to give quantitative criteria. Thus, the predictive guide was developed to give indications of the effect and significance of various parameters on column behavior subjected to conditions similar to those used in this investigation. An approach is presented in Chap. 6 which incorporates the concepts presented herein with quantitative guidance based on Japanese test data.

5.10.2 Principal Criteria. The framework of the decision tree, Fig. 5.22, incorporates four principal capacities or criteria related to the section shear capacity, the section flexural capacity, the capacity to transfer shear between the longitudinal steel and the concrete, and the efficiency of transverse reinforcement for inclined crack width control. The shear capacity,  $V_{csc}$ , is probably affected by the same variables used in the ACI Building Code provisions for the  $V_c$  term but not in the proportions or significance indicated in those provisions. The flexural capacity, as computed in this chapter (Sec. 5.2) gives a good indication of the maximum lateral load capacity of the column and is used to calculate the  $V_{rf}$  term in the decision tree. The current test series did not provide enough data to even suggest the form of the term for bond capacity. The qualitative criterion,  $V_{BS}$ , was included to emphasize the need to consider development length in column design. For the purpose of the flowchart, the bond criterion is expressed as a lateral load capacity.

The fourth capacity is a measure of the effectiveness of the transverse reinforcement in permitting the column to maintain the lateral load at inclined cracking and, if necessary, to achieve the flexural capacity of the column. The transverse reinforcement

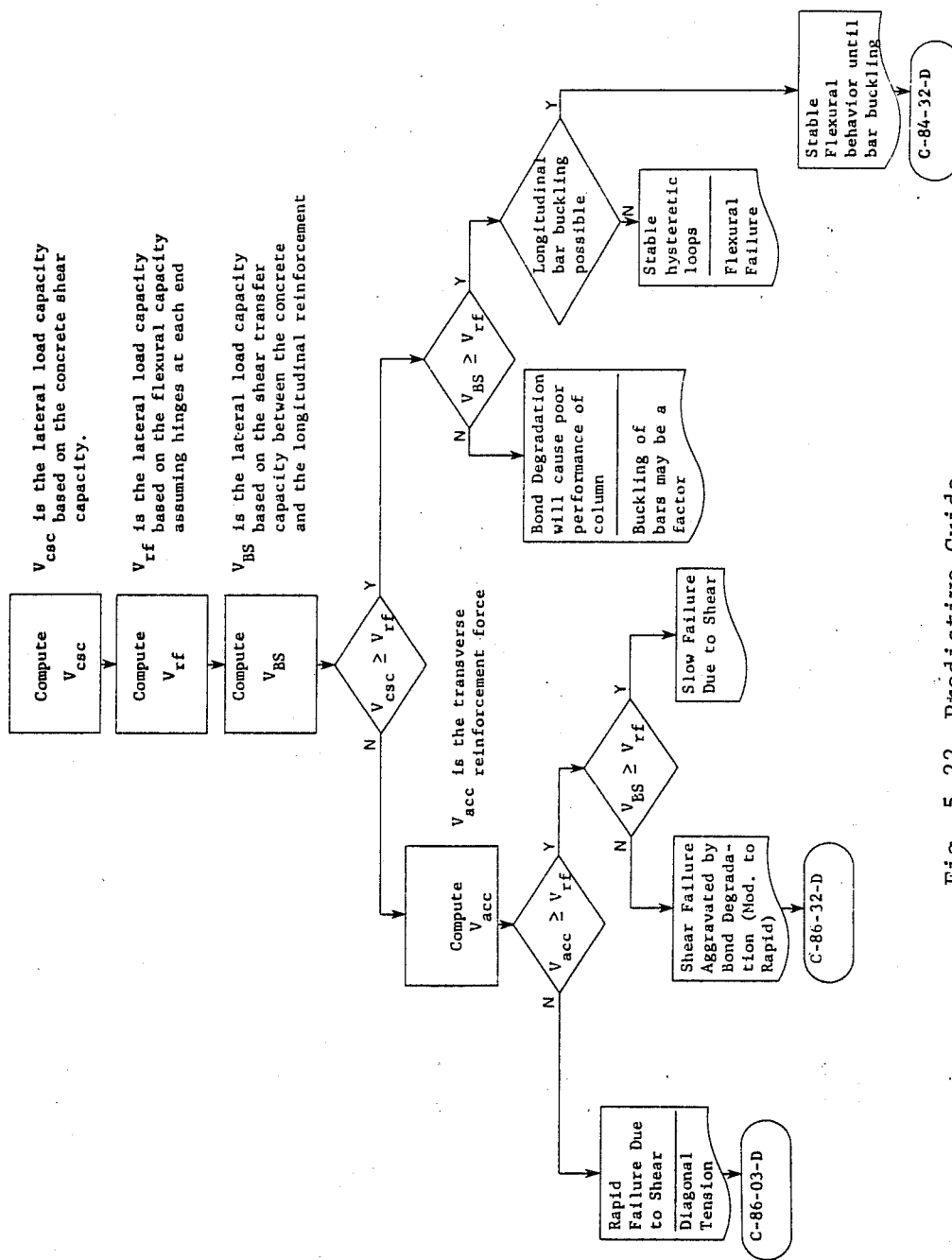


Fig. 5.22 Predictive Guide

criterion is  $V_{acc}$  in the flowchart.  $V_{acc}$  initially represented the force that the transverse reinforcement was expected to carry if crossed by cracks. In its simplest form this action of the transverse reinforcement is idealized, as shown in Fig. 5.23, where a specimen split from corner to corner relies on the transverse reinforcement to carry the lateral load. Ideally, the amount of lateral load the reinforcement carries is the total area of transverse steel crossed by the crack times the yield strength of the steel. If the transverse reinforcement capacity to carry shear is less than the shear corresponding to the flexural capacity, then at some point the transverse reinforcement will yield and limit the maximum lateral load capacity. The load-deflection relations for specimens C-86-03-D and C-86-09-D (Figs. 4.23 and 4.21, respectively) show large drops in lateral load capacity and an inability to maintain a lateral load capacity at least roughly equal to the yield force of the ties. Both of these observations led to the conclusion that it is not the force in the ties which equilibrates the applied shear, but the shear transferred through the section by aggregate interlock. Aggregate interlock is most effective when the crack widths are small. If the transverse reinforcement yields at the onset of inclined cracking, then the cracks open unrestrained, which drastically reduces the effectiveness of the aggregate interlock and as a result the lateral load capacity also decreases. The  $V_{acc}$  term still holds significance as a criterion which determines whether or not there is sufficient transverse reinforcement to prevent its yielding at the onset of cracking. If the reinforcement does not yield, then the aggregate interlock remains effective. If enough transverse reinforcement is provided to keep the crack widths sufficiently narrow, then the aggregate interlock mechanism may be capable of permitting the column to reach its flexural capacity.  $V_{acc}$  is taken to represent the required transverse reinforcement force necessary for

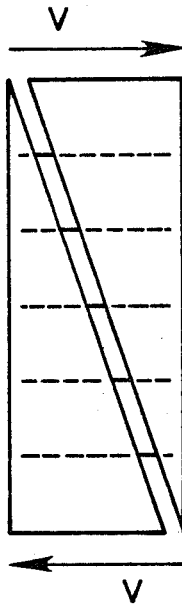


Fig. 5.23 Action of ties

the column to reach its flexural capacity.

5.10.3 Initial Steps. The initial steps of the flowchart, Fig. 5.22, are the computation of the criteria  $V_{csc}$ ,  $V_{rf}$ , and  $V_{BS}$ . The bond criterion,  $V_{BS}$ , is computed at the outset because it can be a factor in either shear dominated or flexure dominated behaviors. Except for  $V_{rf}$ , the criteria represent concepts. Quantification is done in Chap. 6.

The first branch of the flowchart compares the lateral load capacity based on shear and flexure. The comparison of the two capacities divides the behaviors into two broad categories--shear dominated and flexure dominated. The terms do not define the actual cause of degradation, but point to the initial characteristics of behavior. Thus, for a shear dominated behavior the shear capacity is less than the flexural capacity and inclined cracks form in the section. The extreme case of shear dominated behavior is a diagonal tension failure, but less rapid degradation could occur and still be a shear dominated behavior. The same idea applies to flexure dominated behavior. The flexural capacity is less than the shear capacity and few, if any, inclined cracks form. The extreme case of flexure dominated behavior is the formation of two hinges in the column and very stable load-deflection curves. The comparison generally separates the columns into two groups, those in which inclined cracking exclusive of flexure-shear cracks occur (shear dominated) and those in which inclined cracking does not occur (flexure dominated).

5.10.4 Shear Dominated Behavior. If the lateral load capacity based on shear is less than the lateral load capacity based on flexure, then the behavior is shear dominated and follows the NO branch of the  $V_{csc}$  to  $V_{rf}$  comparison in

the flowchart, Fig. 5.22. A shear dominated behavior is characterized by the formation of inclined cracks along the column length. These inclined cracks separate the column into multiple sections and, in order to transfer shear through the column, it is necessary to rely on aggregate interlock along the cracks. The term  $V_{acc}$  is a measure of the transverse reinforcement's effectiveness in providing restraint against crack width opening. If  $V_{acc}$  is insufficient, which is taken to be less than  $V_{rf}$ , then the reinforcement is unable to restrain crack width growth at initial crack formation and the column suffers a rapid failure similar to a diagonal tension failure. An example of such a failure is specimen C-86-03-D whose load-deflection curves are shown in Fig. 4.23 and Fig. 5.24a.

If  $V_{acc}$  is sufficient to at least initially restrain the crack widths, then the hysteretic behavior will show some stability. The number of cycles or deflection levels for which the column will remain stable is uncertain, but if the bond criterion is inadequate ( $V_{BS} < V_{rf}$ ), then the hysteretic loops will show instability sooner than if the bond criterion was adequate. An example of a moderate shear behavior made worse by bond degradation is specimen C-86-32-D, whose load-deflection curves are shown in Figs. 4.13 and 5.24b. The rate of hysteretic degradation is determined by the amount of transverse reinforcement provided and the presence of bond degradation. If large amounts of transverse reinforcement are provided and little or no bond degradation occurs, then the hysteretic load-deflection curves can be quite stable.

5.10.5 Flexure Dominated Behavior. If the maximum lateral load based on shear is greater than that based on flexure, then the column failure is a flexure dominated behavior and the

flowchart follows the YES branch at the  $V_{csc} \geq V_{rf}$  comparison. It is assumed that because the lateral load will not exceed that which would cause inclined cracking, transverse reinforcement for additional capacity is unnecessary. The comparison of  $V_{BS}$  to  $V_{rf}$  serves as the indicator to the possibility of bond degradation. If  $V_{BS} < V_{rf}$ , then bond degradation will occur and cause the hysteretic load-deflection loops to become unstable with both the load and stiffness degrading with cycling and increased deflections. If the bond capacity is greater than the flexure capacity ( $V_{BS} \geq V_{rf}$ ), then the hysteretic loops will exhibit stable characteristics unless longitudinal bar buckling should occur during the loading history. An example of a column exhibiting stable hysteretic behavior until bar buckling causes behavior deterioration is specimen C-84-32-D. Its load-deflection curves are shown in both Figs. 4.25 and 5.24c.

5.10.6 Summary. Section 5.10 described the classification guide for short column behavior. It was qualitative and based solely on the results and observations of the tests conducted in the current investigation. Chapter 6 presents an expanded guide based on additional data from tests conducted elsewhere. The guide in Chapter 6 includes a wider class of columns and uses quantitative rather than qualitative classification criteria.

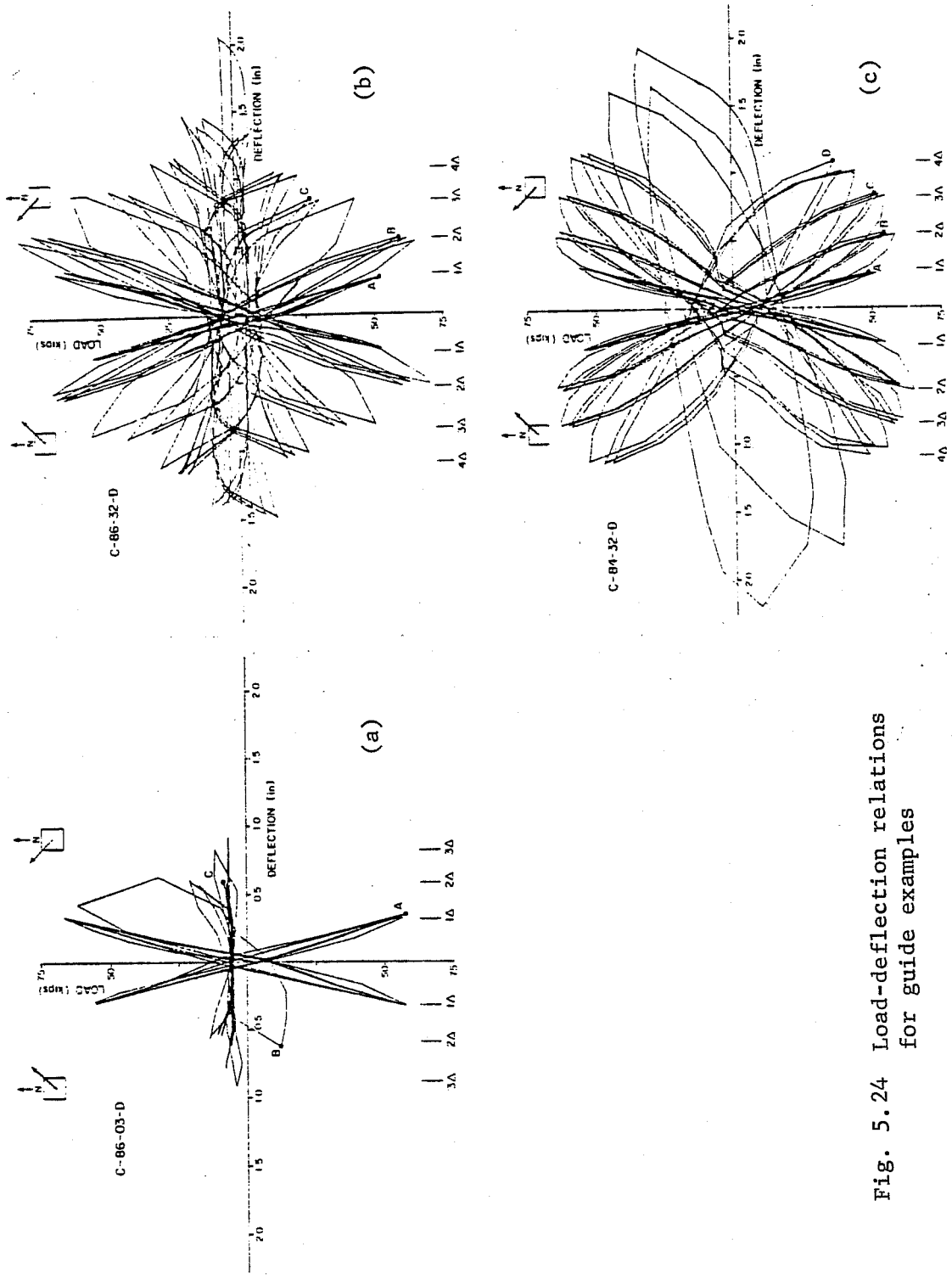


Fig. 5.24 Load-deflection relations for guide examples



## CHAPTER 6

### EXPANDED GUIDE TO BEHAVIOR CLASSIFICATION

#### 6.1 Introduction

The predictive guide presented in Chapter 5 was based only on the results of tests in the current investigation. Because of the limited amount of data (12 tests) the guide was qualitative in nature. The present chapter continues the development of a guide to behavior by using test data from several Japanese investigations to expand the scope of the guide. The expansion includes a broadening of the class of columns considered in the guide and the inclusion of quantitative criteria to replace the qualitative concepts presented in Chapter 5.

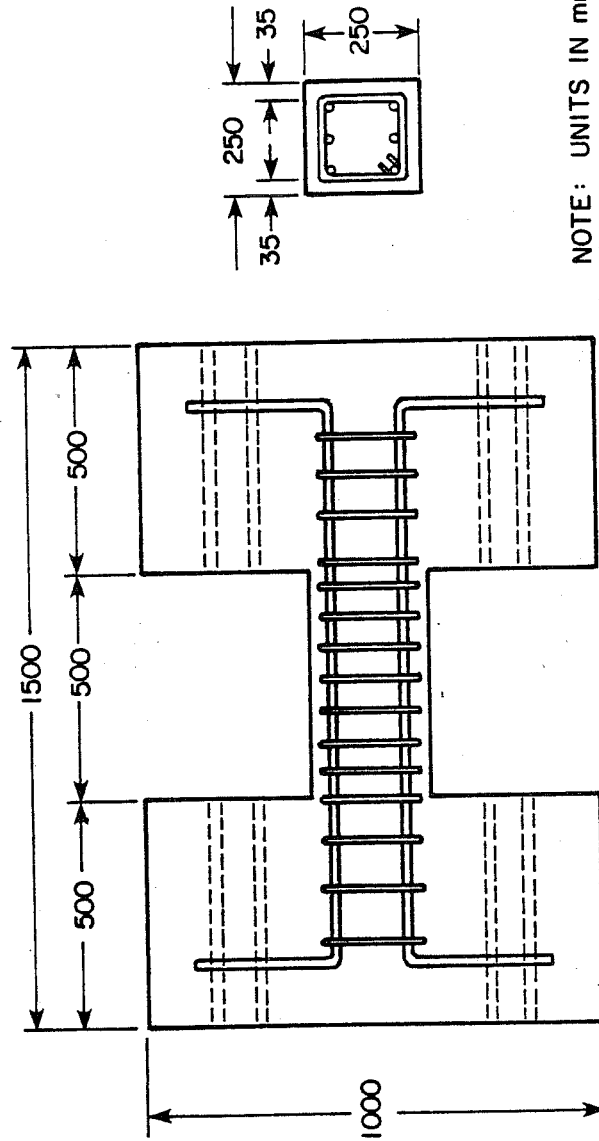
The Japanese tests used as supplemental data in the chapter are discussed. The specimen characteristics, loading conditions, and major parameters for the tests are presented with the emphasis being on the relation of the Japanese tests to the tests of the current investigation. An overview of the expanded predictive guide is presented. The criteria used in the predictive guide are discussed individually. For each criterion the development of the quantitative expressions is presented. A description and discussion of the predictive guide is included and examples of the various kinds of predicted behavior are presented including load-deflection curves and crack patterns. A brief discussion of the application of the predictive guide to the tests of the current investigation and the guide's implication to design concludes the chapter.

## 6.2 Japanese Investigations

The 1968 Tokachi-Oki earthquake in Japan caused numerous column failures and as a result an extensive research program was undertaken to study the behavior of columns, especially short columns, subjected to cyclic reversed deformations. The additional test data used to expand the predictive guide came from several of the Japanese investigations in this program [58,60]. The load-deflection curves and crack patterns for the Japanese specimens used as illustrative examples in this chapter were also taken directly from Refs. 58 and 60.

One of the prime reasons for using the Japanese investigations was the completeness of the presented data. The material properties of the specimen, load-deflection curves, crack patterns, and description of failures were needed in order to use the results for a quantitative study of behavior. The typical Japanese test specimen, Fig. 6.1, was very similar in overall shape to the specimens used in the current investigation. The major differences were that the column cross section was smaller, 9.8 in. versus 12 in. square, and the Japanese specimens used six rather than eight longitudinal bars. The loading system was similar to that used in the current investigation. In fact, the loading system developed by the Building Research Institute in Japan, shown in Fig. 6.2, provided the model for the system constructed for the current investigation. There were no major differences in the action of the two loading systems on the test specimen, except that the Japanese system could only apply unilateral deformations.

The concern for the similarity of specimen geometry and loading system was prompted by the importance of bond degradation on the observed behavior of the tests in the current investigation (Sec. 5.8). Bond was known to be affected by many variables and it was considered necessary that as few variables as possible be



NOTE: UNITS IN mm

Fig. 6.1 Typical Japanese test specimen

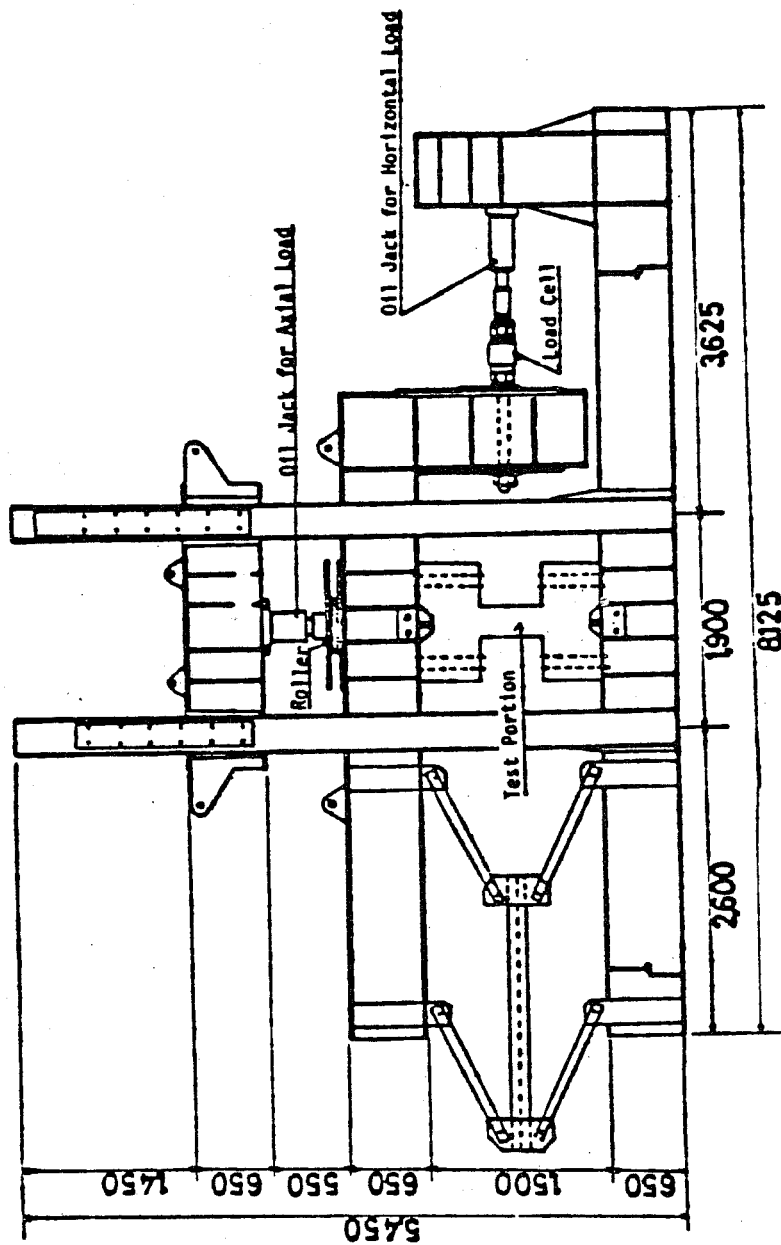


Fig. 6.2 B.R.I. loading system [58]

introduced into the comparisons. The test specimen configuration and loading system in the current investigation were considered to better model an actual column subjected to cyclic reversed deformations than other types of specimen, such as cantilever beams, especially with regard to the bond requirements of the longitudinal reinforcing bars.

The Japanese test program included variations in concrete compressive strength, clear height of the column, diameter of the longitudinal bars, diameter and spacing of the column ties, and axial load. The loading history was not varied and consisted of unilateral reversed cyclic deformation of the column using incrementally increased deflection limits with ten cycles at each limit. The size of the column cross section and number of longitudinal bars were also kept constant.

The variation of parameters in the Japanese tests was not as systematic as expected. Generally, the parameters were altered in an attempt to obtain desirable behavior (flexure dominated) rather than a wide range of behavior, both brittle and ductile. The emphasis on achieving acceptable performance resulted in more of the tests exhibiting satisfactory rather than unsatisfactory behavior. However, there were a sufficient number of tests which exhibited less satisfactory behavior and could be used to expand the predictive guide. Over ninety tests were studied in which concrete strength, column clear height, longitudinal bar diameter, tie diameter and spacing, and axial load were varied. The Japanese data available for study consisted of load-deflection curves and crack patterns at selected points during the loading history.

### 6.3 Outline of Predictive Guide

Figure 6.3 is a schematic of the expanded predictive guide. It is brief and provides an outline of the guide which will serve as a framework on which the discussion of the criteria governing behavior will be based.

The skeletal guide is composed of two primary stems: one for shear-dominated behaviors and the other for flexure-dominated behaviors. It must be remembered that these terms do not necessarily identify the mechanism responsible for the final behavior, but delineate the two stems according to the general behavioral characteristics of the member. The branches (junctions) in the skeletal guide are identified with letters. Note that the branches for bond, core loss, and bar buckling are labeled the same for both the shear and flexure-dominated behaviors. The common labeling emphasizes the observation that the phenomena mentioned are dependent on the same parameters regardless of the final behavioral modes.

The key junction is at A, which divides the behavior of columns into two groups, those in which degradation is inevitable, i.e., shear-dominated, and those in which stable flexural behavior is a possibility, i.e., flexure-dominated. From the study in Chapter 5, the criteria that decide the stems are the concrete shear capacity,  $V_{csc}$ , and the flexural capacity,  $V_{rf}$  (Sec. 5.10.2).

Junction B divides the shear-dominated behavior into essentially rapidly failing or gradually degrading mechanisms. The division is strictly a function of the amount of transverse reinforcement provided. The quickly failing columns do not have sufficient reinforcement to restrain the inclined cracks from widening after initial formation. The criteria governing junction B are the after cracking capacity,  $V_{acc}$ , and the flexural

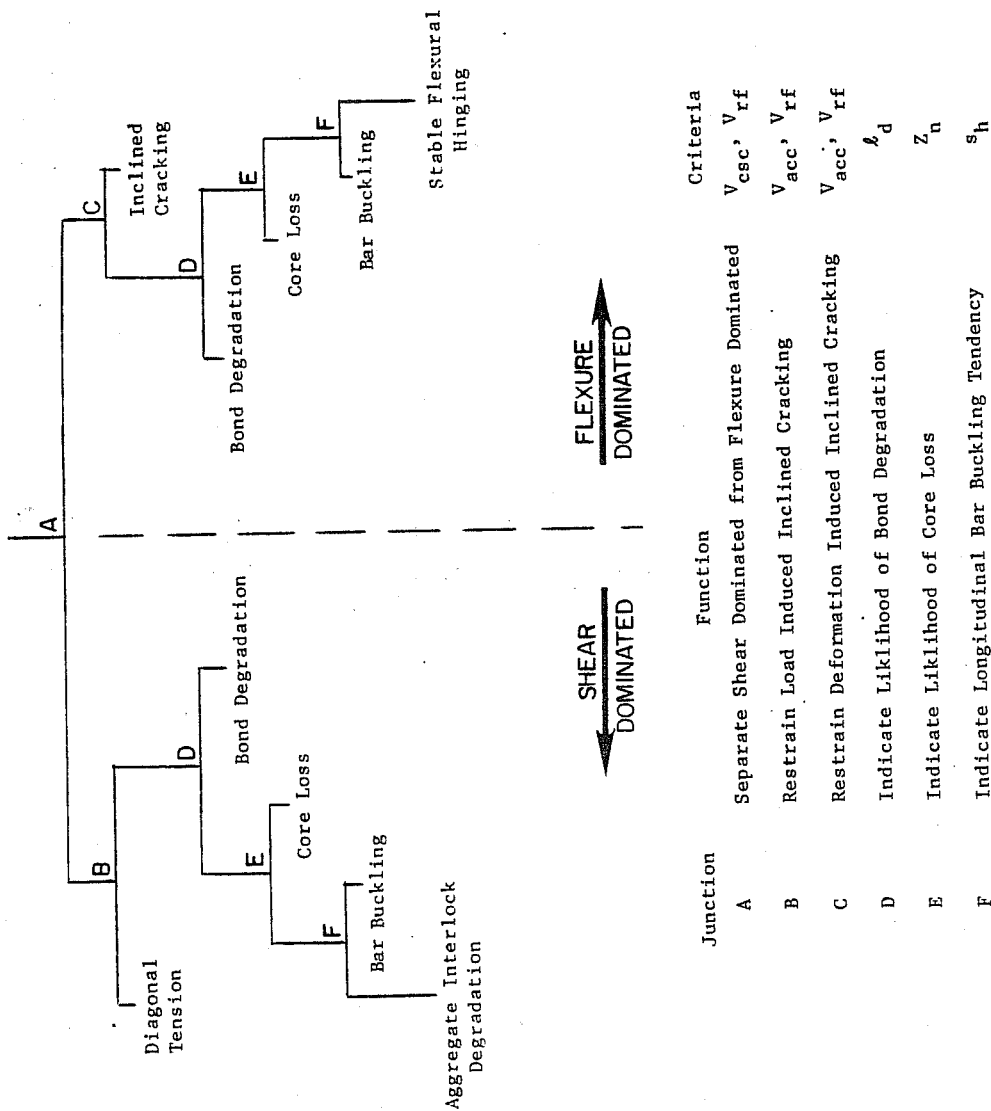


Fig. 6.3 Schematic of expanded predictive guide

capacity,  $V_{rf}$  (Sec. 5.10.2).

Junction C provides an indication of the need for a minimum amount of transverse reinforcement in a column which is subjected to severe loading conditions, especially cyclic reversed loadings. In deformation controlled loadings, it is possible to open cracks not merely as a function of the applied loads, but also as a function of strain level. Cyclic loadings at high deflection levels open cracks which then propagate through the column. A certain amount of transverse reinforcement is necessary to control these cracks. The branch criteria for junction C are the after cracking capacity,  $V_{acc}$ , because it is a direct function of transverse reinforcement and the flexural capacity,  $V_{rf}$ .

Junctions D, E, and F are related to detailing requirements rather than load capacities. The bond criterion is a function of development length (in tension),  $l_d$ . The core loss criterion is a function of the effectiveness of the transverse reinforcement to confine the core and the criterion is given the label,  $Z_n$ . The buckling criterion is a function of the tie spacing,  $s_h$ , in the column.

The table in Fig. 6.3 summarizes the criteria associated with each junction and branch. In the following section the development of the quantitative expressions for each criterion is presented. Finally, the expanded predictive guide is presented and discussed.

#### 6.4 Predictive Guide Criteria

The six criteria governing behavioral modes in the expanded predictive guide are:

- $V_{rf}$  - lateral load capacity based on flexure
- $V_{csc}$  - lateral load capacity based on shear



- $V_{acc}$  - after cracking lateral load capacity
- $l_d$  - longitudinal bar development length (tension)
- $Z_n$  - confinement of the core
- $s_h$  - column tie spacing

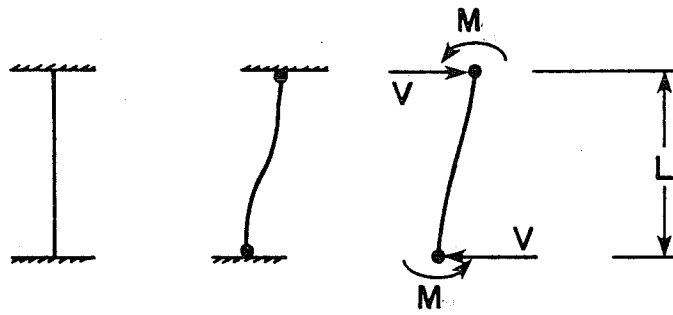
Comparisons of these criteria at the junction determine which branch to follow in the predictive guide. The development of the criteria was empirical and the comparisons were selected to best represent observed behavior. Therefore, the criteria best represent the behavior of the columns tested by the Japanese.

Each criterion is discussed individually in the subsections which follow. The expanded guide and the applicability of the guide to the tests of the current investigations will be discussed afterwards.

6.4.1 Flexural Capacity -  $V_{rf}$ . The flexural capacity of the section is expressed as a lateral load. The derivation of the flexural capacity was discussed in Chapter 5 but will be reviewed briefly here. As shown in Fig. 6.4, the column is assumed to be fixed at each end. One end is translated relative to the other and hinges form at both ends of the column. The hinge capacity is the ultimate moment capacity of the section. The lateral load to equilibrate the system is:

$$V_{rf} = \frac{2M}{L} \quad (6.1)$$

The flexural capacity is taken to be the design capacity of the column. Following normal design recommendations, the flexural capacity is generally established as the limiting capacity. The concept of flexure dominating behavior is the basis for the seismic provisions of most design codes. The ultimate moment capacity and thus the flexural capacity is the most easily defined capacity for a reinforced concrete flexural member. The



$$V = \frac{2M}{L}$$

Fig. 6.4 Column hinging mechanism

computation is well-documented and reliable methods are widely available. With proper detailing, the ultimate moment capacity is also stable under cyclic conditions. Therefore, it is not surprising that the flexural capacity is taken to be the limiting capacity with all other capacities purposely oversized to force a flexural hinging mechanism.

A comparison of the computed flexural capacities ( $V_{rf}$ ) using the standard ACI Building Code [17] approach and the maximum lateral loads ( $V_{rt}$ ) attained in the Japanese tests showed a very high degree of agreement (average ratio of  $V_{rf}$  to  $V_{rt}$  was 0.97). Based on this, it is suggested that  $V_{rf}$  be computed by Eq. 6.1 and that  $M$  be computed using any experimentally verified method. Strain hardening of the longitudinal reinforcement and any other effects which tend to increase the flexural capacity should be included in the computation of  $M$ .

6.4.2 Concrete Shear Capacity -  $V_{csc}$ . The concrete shear capacity is perhaps the most important value used in the predictive guide. If it is less than the flexural capacity, the column will follow in the shear-dominated branch which inevitably leads to a degrading behavior.

The concrete shear capacity is solely dependent on the capacity of the concrete section to transfer shear and is unaffected by the amount of transverse reinforcement in the column. The idea of a basic concrete capacity is not new. The early investigations into shear strength of simply supported beams revealed that the load at which the first diagonal tension crack occurred was independent of the amount of shear reinforcement in the beam. Formation of the diagonal tension crack in beams with medium to long shear spans and no shear reinforcement was a failure condition. The concept of a basic concrete capacity is

incorporated in the ACI Building Code Chapter 11 provisions for shear strength. The  $V_c$  term in the ACI Code is based on the concept that there is a concrete capacity which is independent of shear reinforcement, as shown by the form of the equation

$$V_c = \left( 1.9 \sqrt{f'_c} + 2500 \rho_w \frac{V_u d}{M_u} \right) b_w d \quad (6.2)$$

where  $V_c$  = shear strength provided by concrete  
 $f'_c$  = concrete compressive strength, psi  
 $V_u$  = shear force at section  
 $M_u$  = moment at section  
 $\rho_w = A_s / b_w d$   
 $A_s$  = area of nonprestressed tension reinforcement, sq. in.  
 $b_w$  = web width, in.  
 $d$  = distance from extreme compression fiber to centroid of longitudinal tension reinforcement, in.

The  $V_{csc}$  term is very similar in concept to the ACI Building Code term. A lateral load applied to the column which exceeds  $V_{csc}$  causes inclined cracks to form in the column. Inclined cracking, as used in the current investigation, defines cracks which are inclined to the transverse axis of the member and form independently of flexure-shear cracks. An illustration of the difference between flexure-shear and inclined cracks is shown in Fig. 6.5.

The difficulty arises not in the concept of  $V_{csc}$ , but in finding a suitable equation for estimating the concrete shear capacity of a column. It was pointed out in Chapter 5 that the term  $V_c$  as used by the ACI Code gave consistently low estimates of shear capacity. It was not expected that the ACI equations would agree well with the current specimens because they were based on monotonic tests of specimens with significantly different loading conditions. In addition, the ACI Code  $V_c$  term was purposely

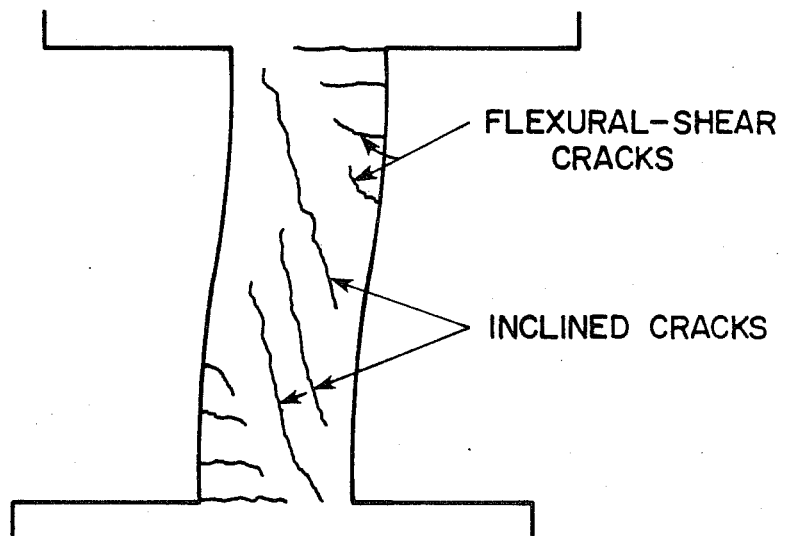


Fig. 6.5 Crack definitions

formulated to be conservative. As a result, an equation for  $V_{csc}$  was developed. Two approaches were taken to developing an equation. The first approach was based on a principal stress criterion. The second approach was based on a modified shear-friction concept.

Principal Stress Concept--The possibility of a compression strut forming between the upper and lower corners of the column (Fig. 6.6) was explored. A principal stress criterion was used as the basis for a capacity equation. The general form of the principal stress equation was

$$\sigma_{1,2} = \frac{\sigma_x + \sigma_y}{2} \pm \sqrt{\left(\frac{\sigma_x - \sigma_y}{2}\right)^2 + \tau_{xy}^2} \quad (6.3)$$

where  $\sigma_{1,2}$  = the principal stresses  
 $\sigma_x$  = x axis normal stress  
 $\sigma_y$  = y axis normal stress  
 $\tau_{xy}$  = shear stress

Two approaches were considered. One approach assumed that the shear and compression forces could be combined to represent a uniaxial thrust on the strut. The other approach looked at the stress state in the concrete compression zone near the end of the column.

Figure 6.7a shows an idealized short column. At each end of the column there is a shear force (V), a compressive force through the concrete compression zone (C), and a tension force from the longitudinal reinforcement (T). The resultant of the shear and compression forces are taken as a uniaxial thrust on the compression strut. The angle of the resultant force is assumed to coincide with the angle of the strut for simplicity. The area of the strut is taken to be the area of the compression zone in the absence of better information. The attempt to adjust

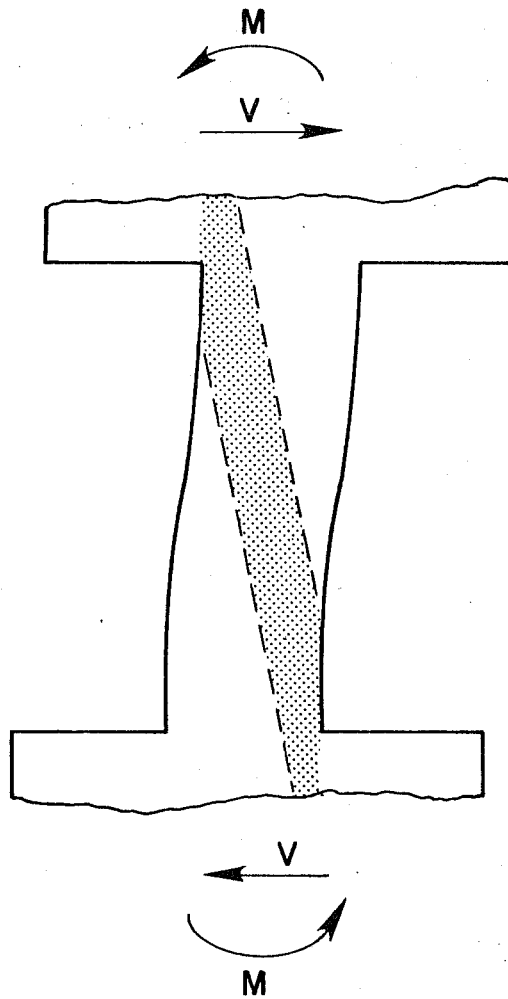


Fig. 6.6 Short column compression strut

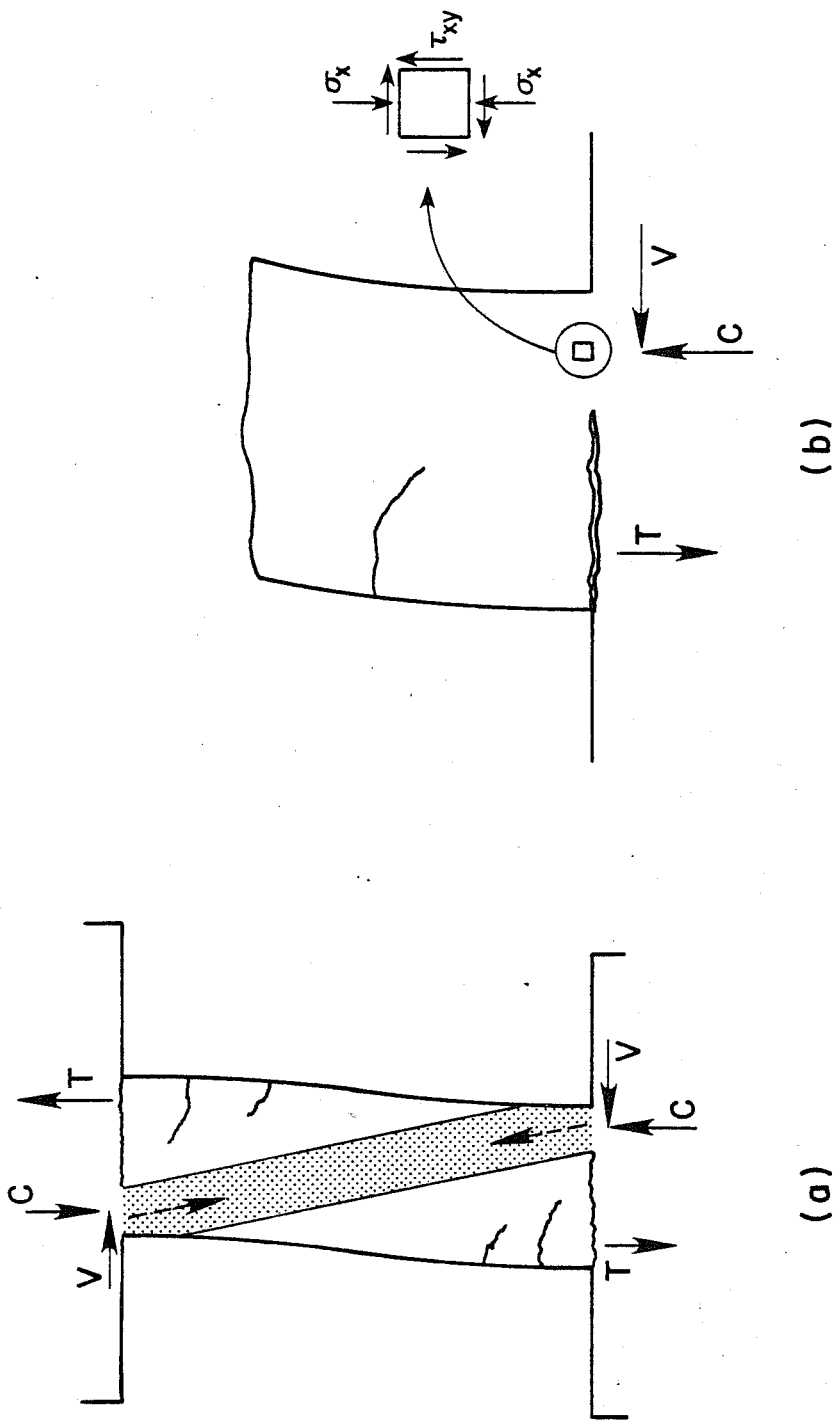


Fig. 6.7 Principal stress approaches



the equation to fit the available data revealed that there is at present an insufficient amount of data on which to develop an equation which properly represents the case of a short column. The lack of data can be directly attributable to the avoidance of diagonal-tension (brittle) failures in past research programs on short columns.

The other approach (Fig. 6.7b) substitutes the concrete compression zone normal stress for the  $\sigma_x$  term and the shear stress on the concrete compression zone for the  $\tau_{xy}$  term in Eq. 6.3. The shear stress is taken to be  $V$  divided by the compression zone area. However, as with the other approach there is an insufficient amount of data on which a suitable equation can be based.

Shear-Friction Concept--The modified shear-friction approach was motivated by the results of experimental tests reported by Mattock and Hawkins [63]. The thrust of their investigation was a study of the shear transfer capacity across a crack in concrete. Most of the specimens had preformed cracks, but some tests were conducted on uncracked sections. Three different specimen configurations were tested, Fig. 6.8, and each had a well-defined plane of shear weakness with transverse reinforcement across the crack. The most interesting result of their work for the current investigation was the fact that the maximum shear transfer capacity across the shear plane was the same for both initially cracked and uncracked sections. This result suggested that it was possible to use a shear-friction equation for concrete shear capacity. Based on the experimental evidence, the proposed equation by Mattock and Hawkins was considered suitable. The equation was an expression for the shear stress which can be transferred across a crack

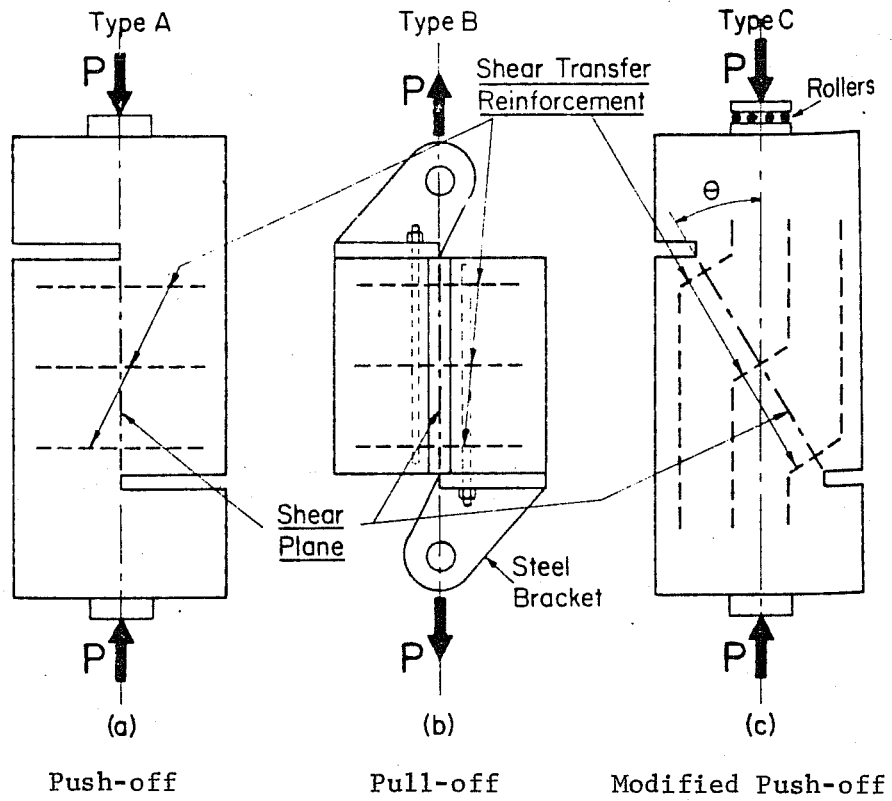


Fig. 6.8 Shear-friction test specimens used by Mattock and Hawkins [63]

$$v_u = 200 \text{ psi} + 0.8(\rho f_y + \sigma_{nx}) \quad (6.4)$$

where  $v_u$  = shear stress, psi  
 $\rho$  = total area of transverse reinforcement divided by area of the cracked plane  
 $f_y$  = yield strength of transverse reinforcement, psi  
 $\sigma_{nx}$  = externally applied normal stress on the cracked area, positive if compressive, psi

The limits on the shear stress were

$$v_u \leq 0.3f'_c \quad \text{and}$$

$$v_u \geq 360 \text{ psi}$$

Equation 6.4 was modified to account for differences between the columns and the simple specimens tested by Mattock and Hawkins.

Modified Shear-Friction Concept--The motivation for considering a shear-friction approach came from the observation that the Japanese tests could be grouped according to the amount of significant inclined cracking exhibited by the columns. The division was important because it suggested that the external shear was resisted initially by shear stresses acting on a plane parallel with the shear force. Inclined cracks formed after the external shear force exceeded the capacity of the shear-friction mechanism. The inclined cracks caused a change in the manner in which the shear was transferred in the column. The shear force was transferred across the inclined cracks by aggregate interlock rather than parallel to the applied lateral load. It was first necessary to determine the area of the section initially resisting shear parallel to the applied load.

Figure 6.9 shows an idealized column cracked in flexure due to monotonic loading. Sections which had no flexural cracking would have low concrete shear stresses compared to the shear

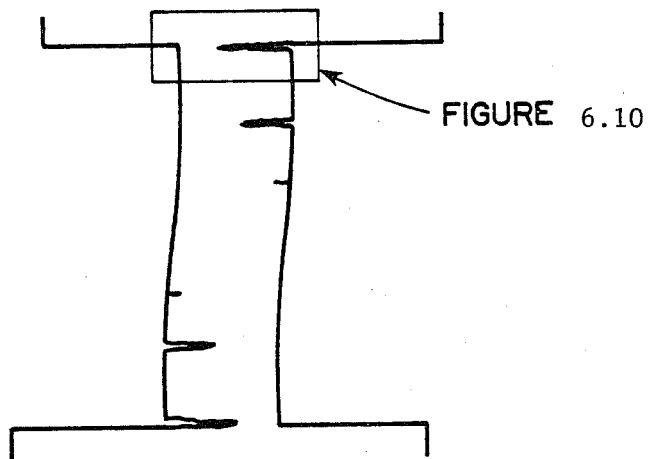


Fig. 6.9 Deflected column.

stresses in the compression zone concrete at the cracked sections. The concrete in the compression zone of the cracked section would be expected to carry most of the shear acting at the cracked section. It can be visualized that the uncracked compressive zone, Fig. 6.10, is similar to the uncracked specimens tested by Mattock and Hawkins. Under cyclic loading reversals, the plane at the end of the column would be fully cracked by reversals of moment. Instead of the shear transferring across an uncracked section, the shear must be transferred across a precracked section. However, as noted earlier, Mattock and Hawkins showed that if the normal stress was high the shear transfer capacity across the crack would be similar to the shear transfer capacity across an uncracked section. The normal stress in the compressive zone was the stress required for equilibrium of the section and near ultimate conditions might be quite high. Using the Whitney stress block as a guide, the average stress on the compressive block would be about 85 percent of the concrete compressive strength. Therefore, if the section was cracked, the normal stress was high enough to ensure that a portion of the cracked surface was in contact and that the shear transfer capacity would be mobilized.

Mattock and Hawkins' equation was changed very little in applying it to the column tests. The term for transverse reinforcement was dropped because the effect of a large longitudinal steel area on a small concrete compression zone carrying shear was unknown and it was, therefore, conservative to eliminate  $\rho$  from the equation. The suggested equation for  $V_{csc}$  is

$$V_{csc} = 200bc + 0.8C_F \quad (6.5)$$

but  $360bc < V_{csc} < 0.3bc f'_c$

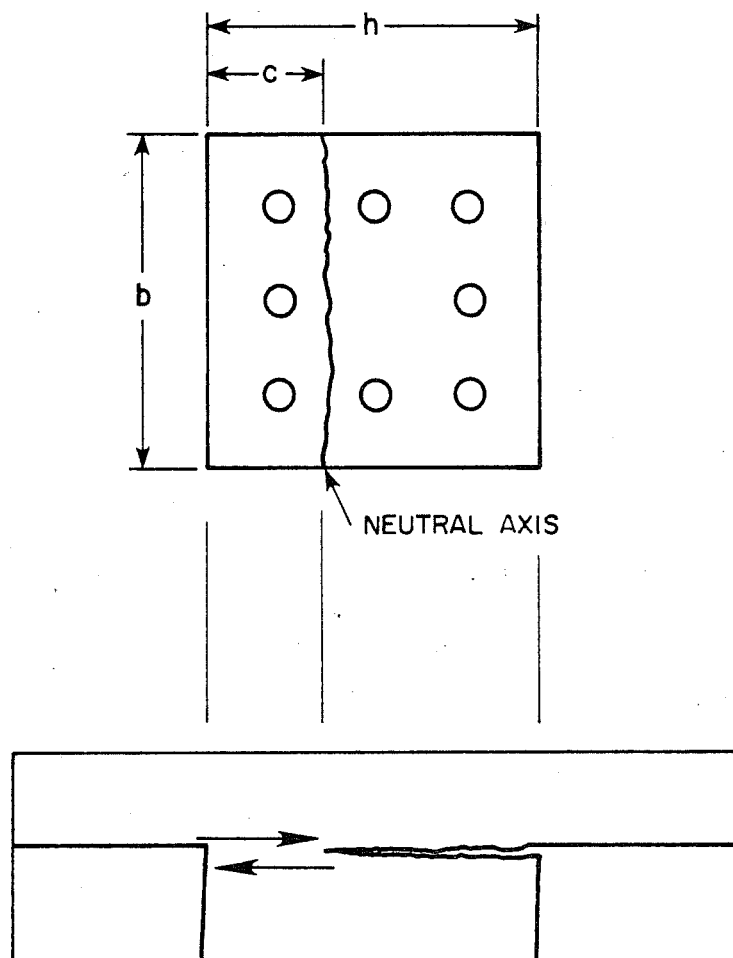


Fig. 6.10 Section at end of deflected column

where  $V_{csc}$  = concrete shear capacity  
 $b$  = width of column, in.  
 $c$  = distance from extreme compression fiber to the neutral axis, in.  
 $C_F$  = normal force on only the concrete in the compressive block

The limits on  $V_{csc}$  were taken to be the same as proposed by Mattock and Hawkins. The term  $C_F$  was defined as the force on the concrete. Any force in the compression steel would not be effective as a normal stress acting on the concrete. The computation of  $C_F$  is straightforward and comes directly from the usual flexural analysis of a section, as shown in Fig. 6.11.

6.4.3 After Cracking Capacity -  $V_{acc}$ . It was noted in Sec. 6.4.2 that there was a drastic change in the shear resisting mechanism if the concrete shear capacity was exceeded. The change was the result of the formation of inclined cracks that destroyed the integrity of the concrete section. The shear could no longer be carried across a section parallel to the applied shear force and had to be transferred from one end of the column to the other across the inclined cracks that developed. The key differences between transferring shear across inclined cracks and across flexure cracks is that the flexure crack affected only a short length along the column and, in addition, the crack in the compression zone had a significant amount of normal stress to keep the crack width small. Increased deformation of the column widened the inclined cracks and there was little normal external stress across the crack length. Instead, the restraint to inclined crack widening was almost exclusively a function of the amount of transverse reinforcement crossing the cracks.

Shear Transfer Across Inclined Crack--The nature of the shear transfer suggested a shear-friction approach. The use

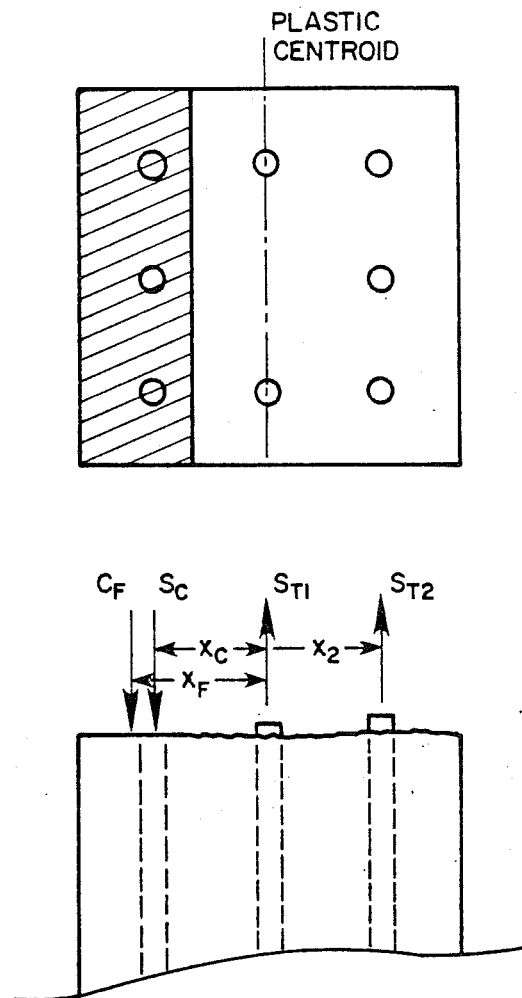


Fig. 6.11 Section analysis for flexure



of Mattock and Hawkins' Eq 6.4 was considered. However, its application to the inclined cracks was felt to be unconservative. Equation 6.4 was based on monotonic loading and test specimen conditions which did not adequately reflect the conditions in the columns. Although the ACI Code provisions for shear-friction were also based on monotonic tests, the results were more conservative than the values given by Mattock and Hawkins' equation. A conservative approach was selected and therefore the ACI Code provisions were used as the basis for the equation for  $V_{acc}$ .

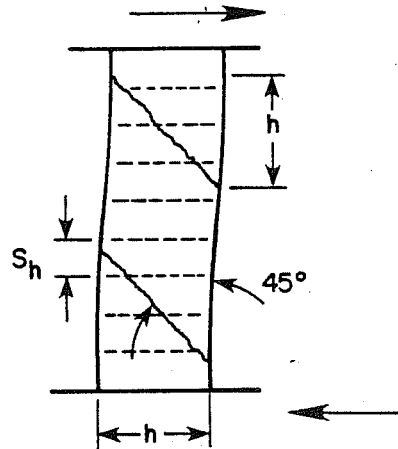
The ACI Building Code provisions for shear-friction consist of a coefficient of friction times the force normal to the crack. The equation is

$$V_n = A_{vf} f_y \mu \quad (6.6)$$

where  $V_n$  = shear force transferable across the crack  
 $A_{vf}$  = area of shear-friction reinforcement, sq. in.  
 $f_y$  = yield strength of shear-friction reinforcement, psi  
 $\mu$  = coefficient of friction (taken as 1.4)

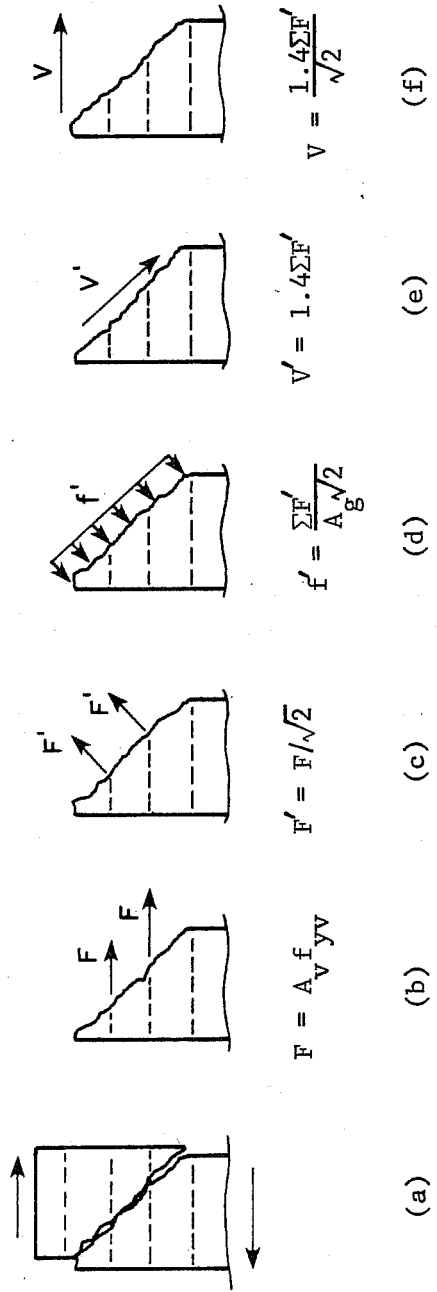
The application of Eq. 6.6 to the column tests is described in Figs. 6.12 and 6.13.

Derivation of  $V_{acc}$  --Figure 6.12 shows the basic assumptions made about the column and the inclined cracks. The column has a total depth of  $h$ . The column ties are spaced along the column at  $s_h$  intervals. A crack is assumed to form at an angle of  $45^\circ$  across the entire column. The crack orientation is roughly the angle observed in the current investigation of short columns. Figure 6.13 describes the application of the ACI Code shear-friction equation to the column with inclined cracks. Figure 6.13 is not a freebody of the column. The tension longitudinal steel is not considered as shear reinforcement because it may already



$S_h$  = SPACING OF TIES  
 $h$  = DEPTH OF SECTION

Fig. 6.12 Assumed cracking  
of column



(g)

$$\Sigma F' = \frac{\Sigma F}{\sqrt{2}} = \frac{f_{yv}}{\sqrt{2}} \Sigma A_v = \frac{f_{yv}}{\sqrt{2}} \frac{h}{s_h} A_v$$

$$V_{acc} = \frac{1.4}{\sqrt{2}} \frac{f_{yv}}{\sqrt{2}} \frac{h}{s_h} A_v = \frac{0.7 h f_{yv} A_v}{s_h}$$

Fig. 6.13 ACI Code shear-friction applied to column

be yielded in tension as a result of bending. The compression longitudinal steel is not considered as shear reinforcement because it is at the periphery of the section and it is not known how effective it would be to the interior area resisting shear. Similarly, a compressive axial load is transferred through the concrete compression zone and how its effect could be averaged over the area is not well defined. The effect of longitudinal bar dowel action is neglected because the amount of shear resistance it provides is uncertain. Thus, the effect of longitudinal steel and axial load are omitted and it is conservative to do so.

Step a shows a portion of the column which includes an inclined crack. As the two sections of the column override each other, the ties yield exerting a tensile force of  $F$ , as shown in step b.

The ACI Code equation uses only the normal force, so  $F$  for each tie is divided by  $\sqrt{2}$  to obtain the component of force acting normal to the crack,  $F'$  (step c). The action of the tie forces is to keep the two surfaces in contact so that a compressive stress is applied to each section as illustrated in step d. The shear force that can be transferred parallel to the crack is the coefficient of friction (1.4) times the restraining force normal to the crack as given by  $V'$  in step e. The component of  $V'$  parallel to the applied lateral load is  $V$  and obtained by dividing  $V'$  by  $\sqrt{2}$  (step f). Step g describes the replacement of the summation of tie forces by its geometric equivalent based on the assumed orientation of the crack to arrive at the final form of  $V_{acc}$  ( $V$ ) which is

$$V_{acc} = \frac{0.7hf_y A_v}{s_h} \quad (6.7)$$

where  $V_{acc}$  = after cracking shear capacity  
 $h$  = gross section depth, in.  
 $s_h$  = tie spacing, in.  
 $f_{yv}$  = yield strength of tie bars, psi  
 $A_v$  = twice the area of one tie bar, sq. in.

The upper limit on  $V_{acc}$  was taken to be

$$V_{acc} \leq 0.2A_c f'_c$$

where  $A_c$  = core area of column, out-to-out of ties, sq. in.  
 $f'_c$  = concrete compressive strength, psi

Mattock and Hawkins suggested a limit of  $0.3f'_c$  for the shear stress parallel to the crack. The value of  $0.3f'_c$  is divided by  $\sqrt{2}$  to obtain the horizontal component of the limit,  $0.2f'_c$ , similar to obtaining  $V$  from  $V'$  in steps c and f of Fig. 6.13. The stress of  $0.2f'_c$  is multiplied by the core area to obtain the horizontal force limit. The core area was adopted to recognize the likelihood of cover spalling in specimens with a large number of ties. The limit of  $0.2A_c f'_c$  cannot be verified by experimental evidence because none of the reported specimens had enough transverse reinforcement to approach the limit.

In reality,  $V_{acc}$  is a measure of the effectiveness of the transverse reinforcement in restraining cracks from widening thus reducing aggregate interlock along the inclined cracks. Because the aggregate interlock provides the principal shear resistance, it is imperative that the inclined crack widths remain as narrow as possible, which implies that the transverse reinforcement should not yield because the restraint to crack opening would be negligible following yielding. It is also true that the more transverse reinforcement crossing a crack, the greater the restraint to crack widening. Thus,  $V_{acc}$  represents the trend

observed in the test programs because  $V_{acc}$  is directly proportional to the amount of transverse reinforcement crossing a crack.

6.4.4 Core Confinement -  $Z_n$ . Confinement of the core is necessary to maintain the flexural capacity of column hinging regions. In the columns under consideration, confinement is provided by ties spaced along the length of the column. The principal objective of the criterion for confinement is the determination of the amount of transverse reinforcement (diameter of tie and spacing) to adequately confine the core.

The first attempt at developing a criterion for confinement was based on the confinement specified for spirally reinforced columns by the ACI Building Code. The amount of spiral reinforcement is given as a volume of reinforcement per volume of concrete confined. The ACI equation is

$$\rho_s = 0.45 \left( \frac{A_g}{A_c} - 1 \right) \frac{f'_c}{f_y} \quad (6.8)$$

where  $\rho_s$  = ratio of volume of spiral reinforcement to volume of core (out-to-out of spirals) of a spirally reinforced compression member

$A_g$  = gross area of section (sq in.)

$A_c$  = area of core of spirally reinforced compression member measured to outside diameter of spiral (sq in.)

$f_y$  = yield strength of spiral reinforcement (psi)

The values of  $\rho_s$  computed for the tests conducted here and in Japan did not provide a clear indication of the value for  $\rho_s$  needed for adequate confinement. While the Japanese specimens were not spirally reinforced, it was hoped that the values of  $\rho_s$  would provide a useful indicator of confinement effectiveness. Therefore, other approaches which offered a more realistic assessment of confinement were considered.

It was concluded that the equation for  $\rho_s$  was not suitable for the conditions imposed on the test columns. Equation 6.8 is based on the condition that the core of a spirally reinforced column have the same concentric axial load capacity as the gross section before the cover spalls. The loading condition imposed on the hinging regions of a column is not similar to the conditions assumed for Eq. 6.8. The hinging regions are subjected to cyclic conditions of high shear forces, and large strain gradients along both the depth and the length of the column.

The function of confining reinforcement in the columns was to prevent the compressive concrete block from losing load capacity at high deformation levels. The idea of limiting the loss of capacity led to an examination of the descending branch of the concrete stress-strain curve. The slope of the descending branch is an indicator of the effectiveness of the confinement. The better confined a section, the more gradual is the slope of the descending branch. Kent and Park [77] proposed a concrete stress-strain curve for concrete sections confined by rectangular ties. The curve, shown in Fig. 6.14, is composed of three segments. The segment of interest is the descending branch idealized as a straight line. The slope of the straight line descending branch is denoted by  $Z$  and given by the equations

$$Z = \frac{0.5}{\epsilon_{50c} - 0.002} \quad (6.9)$$

$$\epsilon_{50c} = \frac{3 + 0.002f'_c}{f'_c - 1000} + \frac{3}{4} \rho_s \sqrt{\frac{b''}{s_h}}$$

where  $\rho_s$  = volume of transverse reinforcement divided by volume of concrete core measured to outside of hoops  
 $b''$  = confined core width measured to outside of hoop (in.)  
 $s_h$  = tie spacing (in.)

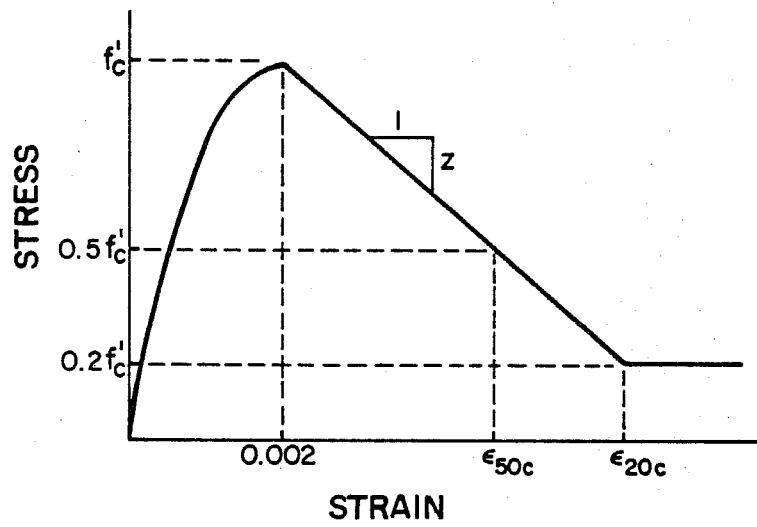


Fig. 6.14 Kent and Park's concrete stress-strain curve



As the confinement became more effective, Z approached zero. The Z values for the reported tests reflected the broad trend of the test results. The effect of compressive axial load, however, was not adequately represented by the Z term. The Z term was modified to incorporate some effect of axial load. The modification was straightforward and was intended only to reflect the trend of the observed influence of axial load on short column hysteretic behavior. The presence of an axial load required a larger amount of confinement steel and so the Z term was multiplied by the factor

$$\frac{1}{1 - \frac{N}{P_o}} \quad (6.10)$$

where N = the applied compressive axial load, considered positive

P<sub>o</sub> = the concentric compressive axial load capacity of the section

The modified Z term was denoted as Z<sub>n</sub> and was expressed as

$$Z_n = \frac{Z}{1 - \frac{N}{P_o}} \quad (6.11)$$

6.4.5 Longitudinal Bar Buckling. Buckling of the longitudinal bars was common in the Japanese tests which had bar diameters less than about 0.5 in. In the current investigation, all three of the specimens with #4 bars, 0.5 in. diameter, exhibited longitudinal bar buckling. Small diameter bars are more likely to buckle than large diameter bars and it does not seem possible to prevent such buckling using practical reinforcing details.

However, the number of times the bar is subjected to reversals of deformation which cause yielding may be as significant a parameter as the diameter of the bar. At or beyond yielding a reinforcing bar has very low stiffness and is very likely to buckle. The premise that the number of cycles producing yielding is a major parameter in bar buckling is supported by the test results. Small diameter bars exhibited a greater tendency to buckle than larger diameter bars. A column with small longitudinal bars is much more likely to achieve flexural hinging because its flexural capacity is lower than the same section with larger bars. With flexural hinging and cyclic reversed loadings, the longitudinal bars will undergo cyclic reversed yielding. On the other hand, if flexural hinging can not be maintained because of degradation due to some other effect such as bond or shear, the bar will not be subjected to the same number of reversed cyclic yieldings, thus making it less susceptible to buckling. An example of the above idea is illustrated by the results of specimens C-84-32-D and C-86-32-D of the current investigation. Shown in Fig. 6.15 are plots of the stresses in the northeast corner longitudinal bar at the intersection of the column and lower block. The stresses were obtained from the measured strains using a computer program developed by Longwell [95]. The bar stress is plotted against the lateral deflection of the column for cycles along only the northeast-southwest diagonal of the column. It is quite obvious that the longitudinal bar in specimen C-84-32-D was subjected to repeated reversed yieldings while the longitudinal bar in C-86-32-D only had three cycles at yielding before degradation reduced the need for the bars to develop high stresses. In C-84-32-D the longitudinal bars buckled while in C-86-32-D they did not.

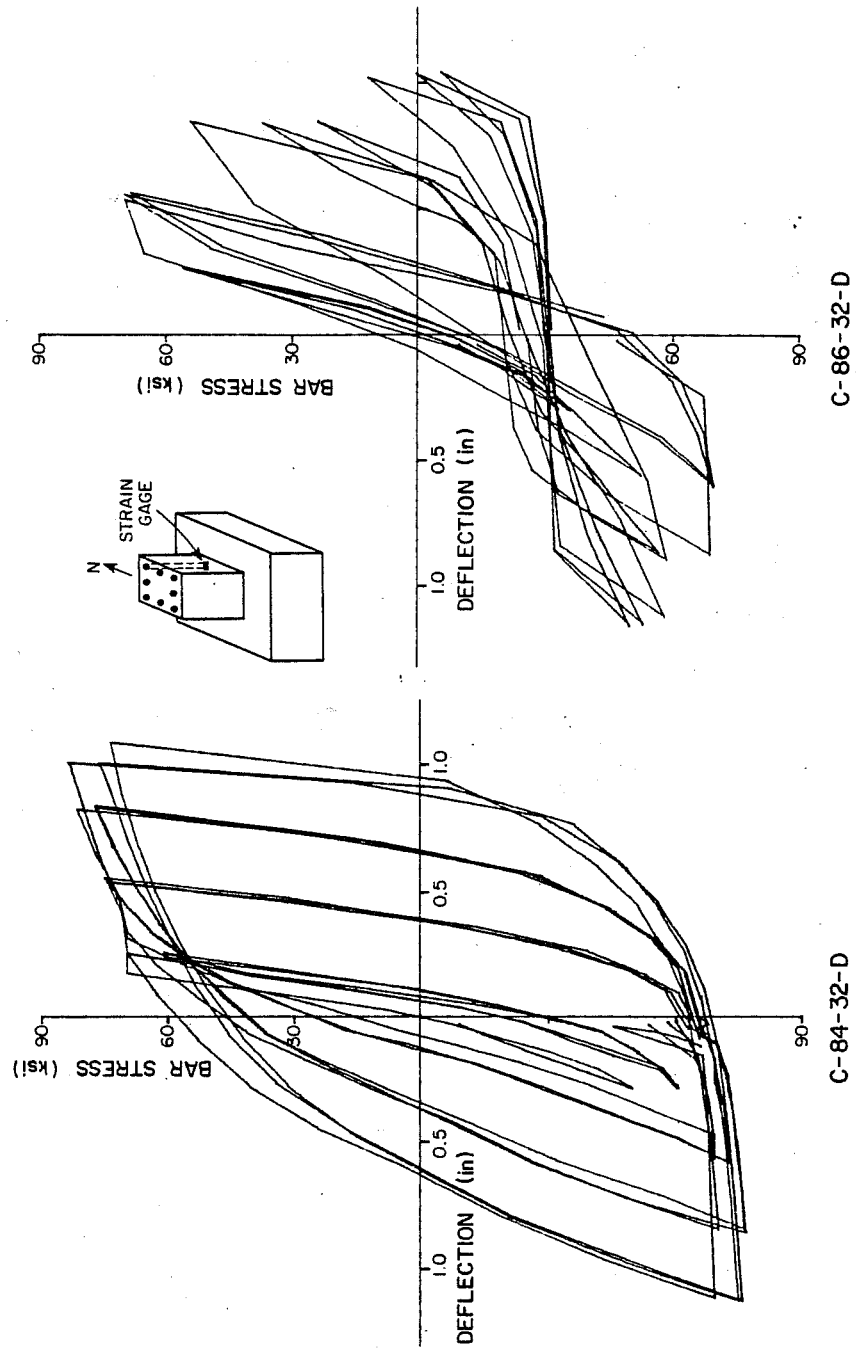


Fig. 6.15 Longitudinal bar stresses

The cases of buckling observed in the current investigation illustrates the practical impossibility of preventing bar buckling. In specimen C-84-32-D the ties were spaced at about twice the longitudinal bar diameter and still the bars buckled. It can be said, however, that decreased tie spacings can and do restrain the bars more effectively, delaying the onset of buckling. The interesting feature of buckling in the columns is that the bars not only buckled outwards, but inwards and sideways as well. It is very difficult to conceive of a realistic reinforcing detail which would prevent the bar from buckling sideways along the face of the column. An example of the bar buckling sideways is the corner bar of specimen C-84-14-D (Fig. 6.16), which buckled along the face of the specimen.

Buckling probably cannot be prevented, but it can be restrained so that under moderate cyclic loading it will not be a factor. Based on the results of specimen C-84-32-D, it is suggested that, within the hinging regions of the column, the tie spacing be no greater than twice the longitudinal bar diameter, and outside the hinging region no greater than four times the longitudinal bar diameter. These recommendations should be considered as guides to illustrate the severity of the requirements needed to restrain longitudinal bar buckling.

6.4.6 Bond Degradation. Bond degradation is the most difficult aspect of the column behavior to understand. It is not possible to develop a quantitative criterion for bond degradation which accounts for the effect of the important parameters because of the limited amount of data and the complexity of the phenomena. However, a broad discussion of the observed effects of various parameters on bond degradation is presented. The discussion is primarily based on the results of the Japanese tests, but some additional insight to the problems of bond were obtained from the



Fig. 6.16 Buckled longitudinal bar

current investigation. In addition to discussing the effect of parameters on bond, a criterion is presented to determine if bond degradation can occur or not. An explanation of the reasons that the midheight region of the column was the most damaged region in the 86 series of the current investigation will be given.

Test Results--Twenty-four of the tests in the Japanese program exhibited bond distress. These tests constitute the data base for examining the effects of various parameter changes. Seven tests provide illustrative examples of the observed trends and are listed in Table 6.1 along with specimen characteristics. The load-deflection curves and selected crack patterns for each test are given in Figs. 6.18 through 6.24. Each crack pattern for a given test is labeled with a letter. Those letters appear on the load-deflection curves at the deflection level at which the crack patterns were drawn. The crack patterns were drawn at the end of cycling at the denoted deflection level.

Test Parameters--The parameters varied in the Japanese tests were concrete strength, longitudinal bar diameter, percentage of transverse reinforcement, and axial compressive load. Table 6.1 lists the above parameters for each test as well as several others, including the percentage that the applied axial compressive load was of the axial load at balance, the diameter and spacing of the column ties, the ratio of clear height to gross depth of the column, the pseudo-rotation of the column, and the figure number of the load-deflection curve. The pseudo-rotation of the column (drift angle), labeled R, was defined as the lateral deflection of the column divided by its clear height as shown in Fig. 6.17. The use of drift angles avoided the confusion of differing lateral deflection levels because of different column clear heights. For example, a lateral deflection of 0.4 in. for a 36 in. column represents a more severe condition than the

TABLE 6.1 SPECIMEN CHARACTERISTICS FOR BOND COMPARISON

Test Name	$f'_c$	$d_b$	N - % bal	$\phi - s$	$\rho_w$ %	$\frac{L_c}{h}$	R	Load-Deflection Figure No.
LS1AB	2750	13	66 - 64	9 - 47	1.08	3	0.024	6.18
LS0BB	2750	16	33 - 32	9 - 47	1.08	3	0.011	6.19
LM27B	3500	16	66 - 51	9 - 42	1.22	4	0.010	6.20
LM28A	3500	16	33 - 26	9 - 40	1.27	4	0.028	6.21
LM28B	3500	16	33 - 26	6 - 37	0.61	4	0.016	6.22
FC7B	6400	16	66 - 33	9 - 67	0.76	4	0.039	6.23
WS7B	3900	16	66 - 46	10 - 67	0.83	4	0.019	6.24

$f'_c$  - concrete compressive strength, psi

$d_b$  - diameter of longitudinal bar, mm

N - compressive axial load, kips

% bal - (N/balance axial load) x 100%

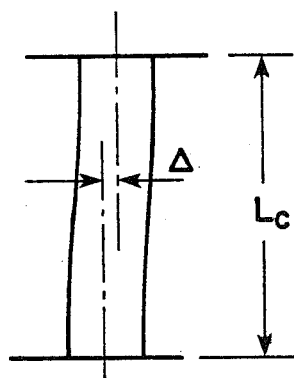
$\phi - s$  - diameter and spacing of transverse reinforcement, mm

$\rho_w$  % - percentage of transverse reinforcement ( $A_v/s_h$ )

$L_c/h$  - column length / column depth

R - psuedo-rotation of column ( $\Delta/L_c$ ) at first bond cracking

$\Delta$  - lateral deflection of column end



$$R = \frac{\Delta}{L_c}$$

Fig. 6.17 Definition of pseudo-rotation



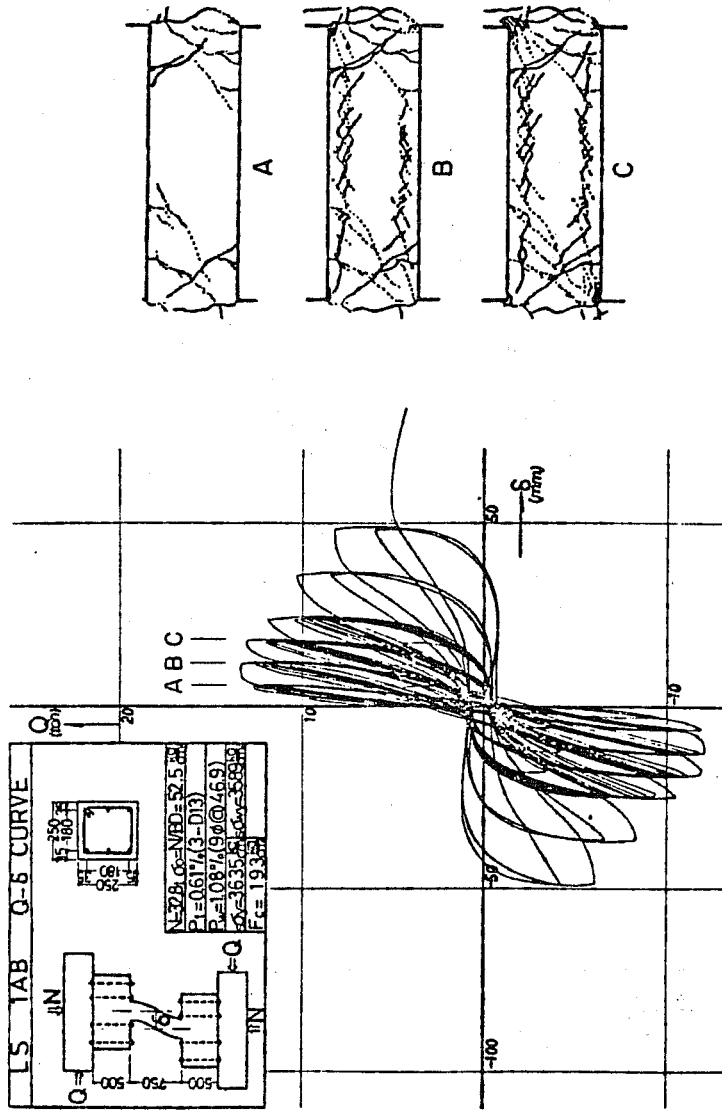


Fig. 6.18 Load-deflection curves and crack patterns, Specimen LS1AB [60]

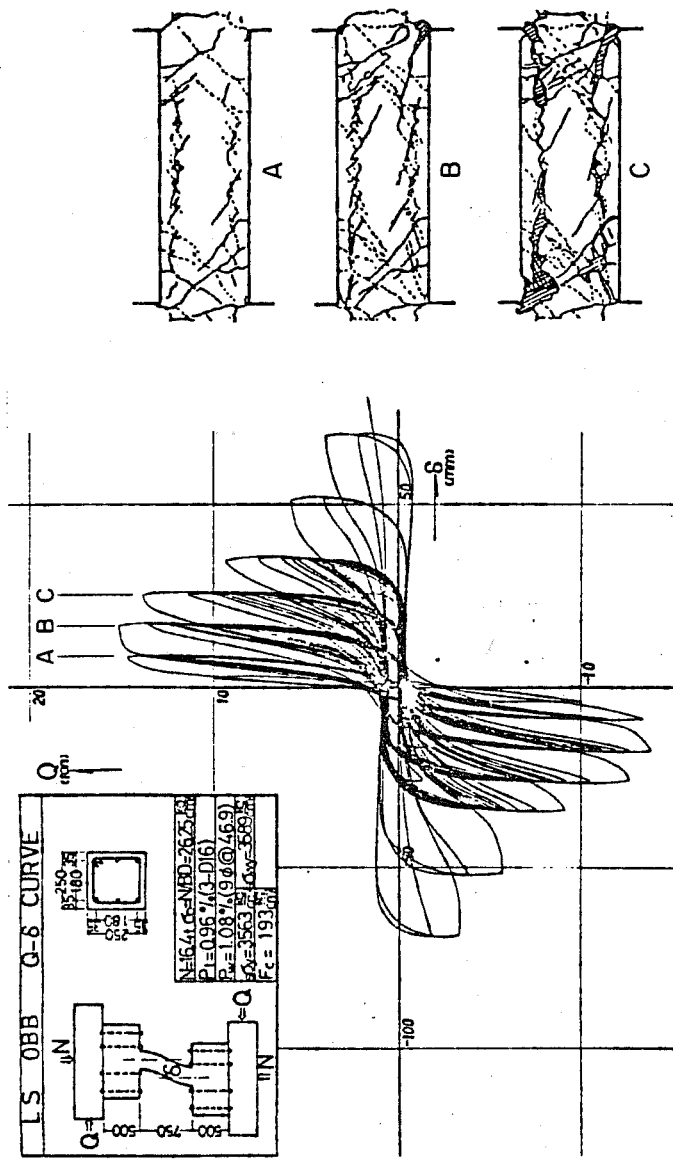


Fig. 6.19 Load-deflection curves and crack patterns, Specimen LS0BB [60]

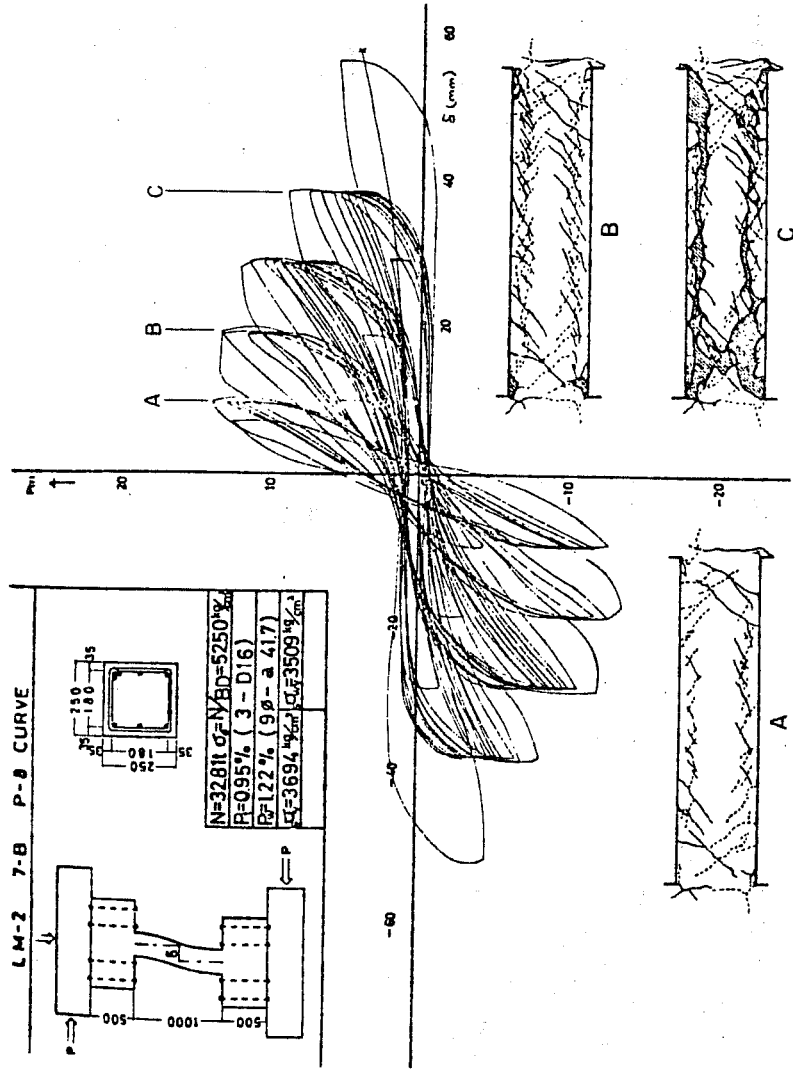


Fig. 6.20 Load-deflection curves and crack patterns, Specimen LM27B [58]

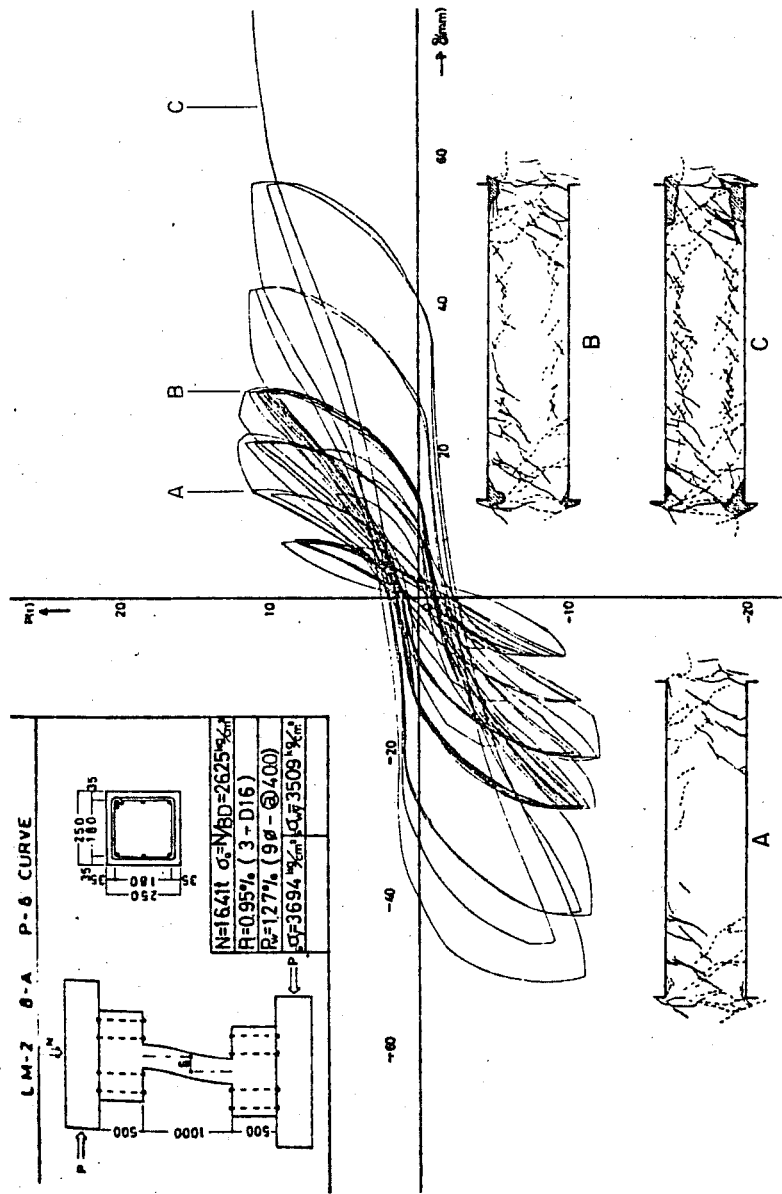


Fig. 6.21 Load-deflection curves and crack patterns, Specimen LM28A [58]

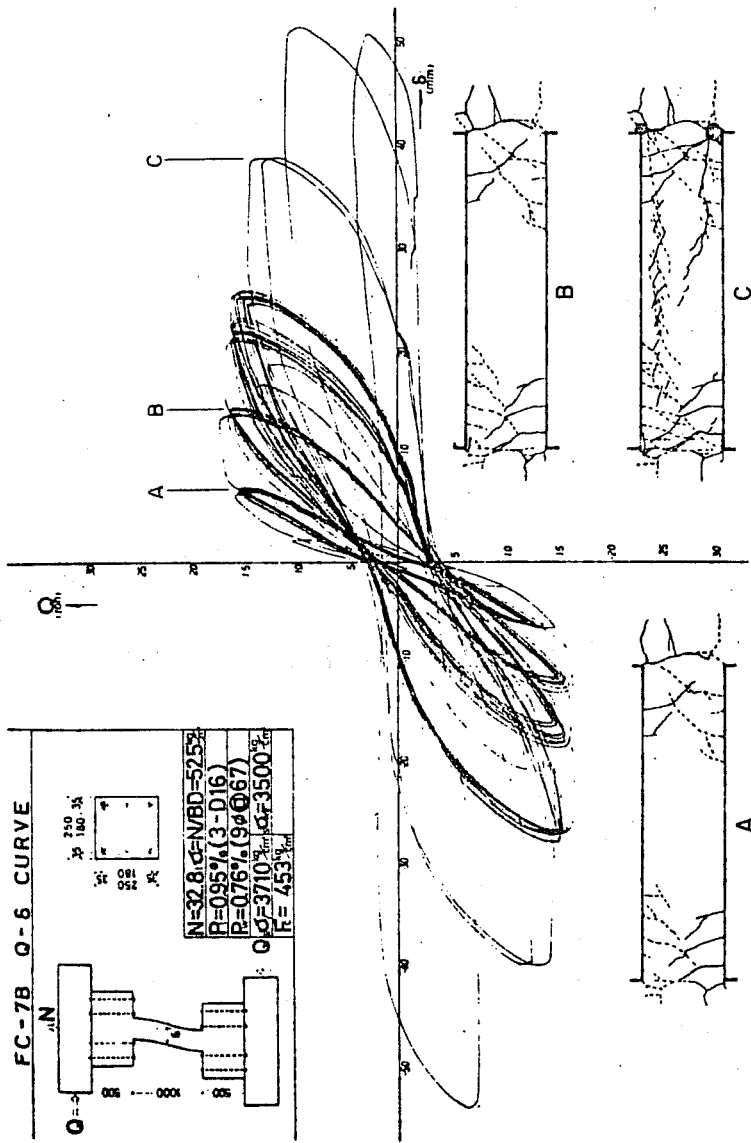


Fig. 6.23 Load-deflection curves and crack patterns, Specimen FC7B [58]

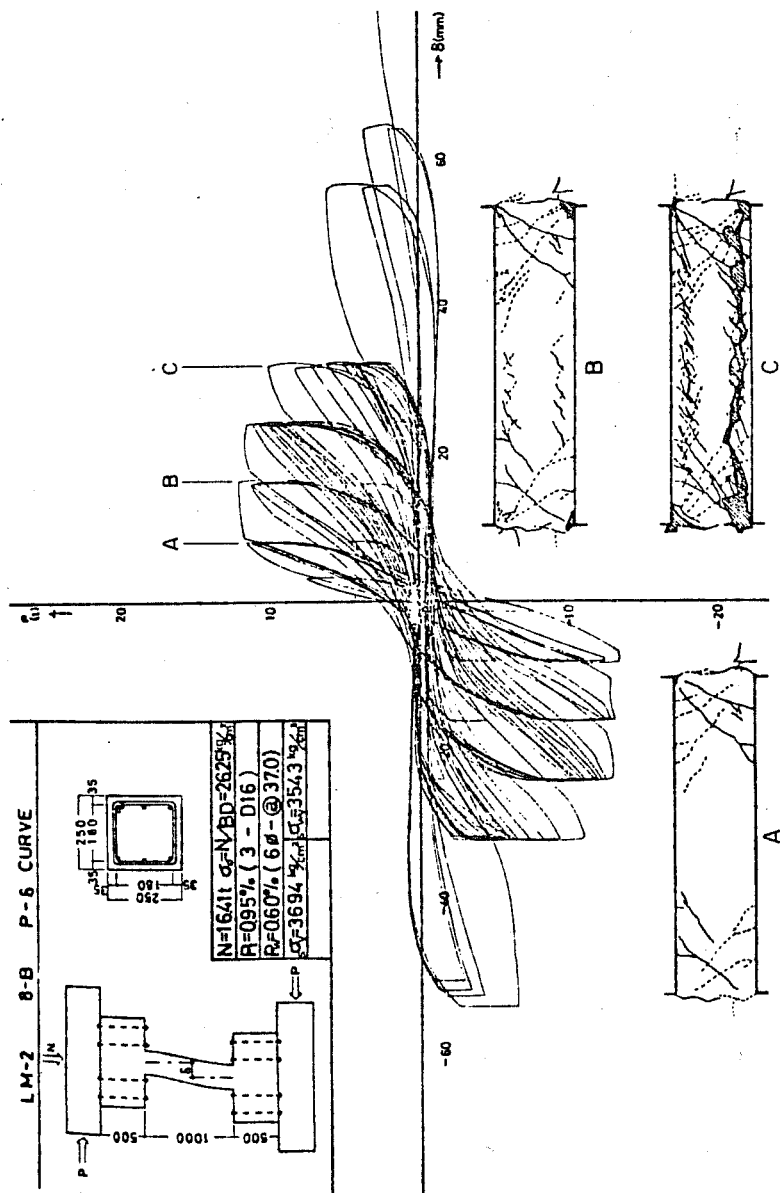


Fig. 6.22 Load-deflection curves and crack patterns, Specimen LM28B [58]

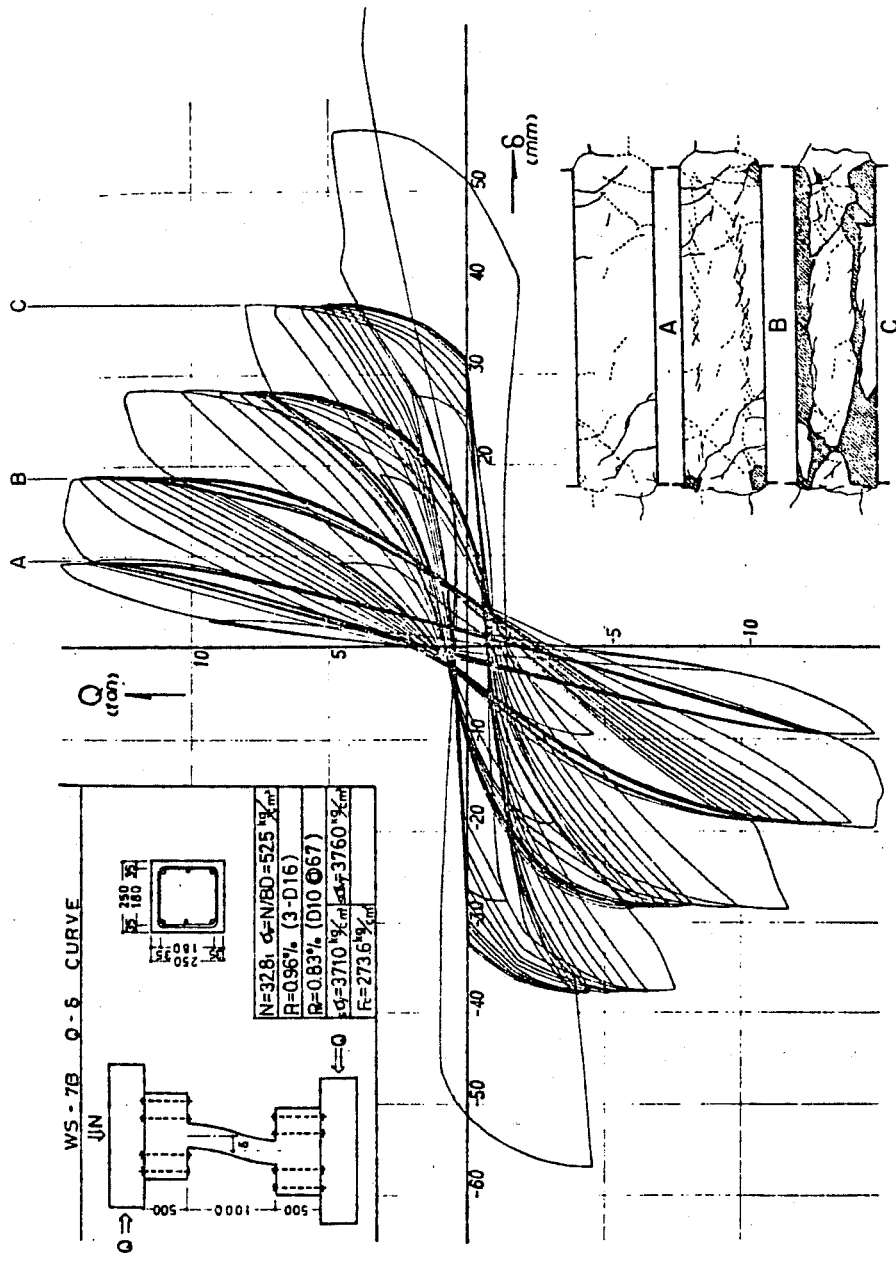


Fig. 6.24 Load-deflection curves and crack patterns, Specimen WS7B [58]

same lateral deflection for a 108 in. column. The severity is reflected in the drift angles, 0.011 and 0.004, respectively. The R values listed in Table 6.1 represent the drift angles at which bond cracking along the longitudinal bars was first observed.

Concrete Strength--Increased concrete compressive strength increased the drift angle at which bond distress occurred. Such an effect was expected since research into required development lengths showed a tendency for the required development length to decrease with increased concrete strength. Specimens FC7B (Fig. 6.23) and WS7B (Fig. 6.24) illustrate the impact of concrete strength. FC7B with a concrete strength of 6400 psi reached an R of 0.039 while WS7B with a concrete strength of 3900 psi reached an R of 0.019 before significant degradation of capacity due to bond occurred.

Axial Load--Increased compressive axial load caused a decrease in the pseudo-rotation at first bond cracking. The effect of increased axial compression was shown by specimens LM27B (Fig. 6.20) and LM28B (Fig. 6.22). LM27B had twice the axial load of LM28B, though both axial loads were less than balance. LM27B reached a pseudo-rotation of 0.010 before first bond cracking, while LM28B with half the axial load reached a pseudo-rotation of 0.028 before first bond cracking appeared along the longitudinal bars.

Bar Diameter--Based on the equations for development length, it was expected that the diameter of the longitudinal bars was an important parameter in the bond cracking mechanism. Specimens LS1AB and LSOBB in Table 6.1 demonstrate how significantly bar diameter affects bond distress. Specimen LS1AB had a smaller bar diameter, 13 mm (0.51 in.), than specimen LSOBB, 16 mm (0.63 in.), but LS1AB had twice the axial load of LSOBB. The effect of increased axial load was to decrease the pseudo-rotation at first



bond cracking, but the decreased bar diameter was expected to compensate for the effect of axial load. However, comparison of the values of pseudo-rotation pointed out the major significance of bar diameter on bond characteristics. Specimen LSlAB (Fig. 6.18) reached a pseudo-rotation of 0.024, while LSOBB (Fig. 6.19) reached a pseudo-rotation of 0.011 at the first sign of bond cracking. Obviously, the smaller bar diameter of LSlAB was a much more important parameter determining bond distress than the amount of axial load.

Transverse Reinforcement-- The effect of increased percentages of transverse reinforcement was to increase the value of pseudo-rotation at which the first bond cracking appeared. Specimens LM28A and LM28B illustrated the effect of transverse reinforcement. Specimen LM28A (Fig. 6.21) had double the percentage of transverse reinforcement of specimen LM28B (Fig. 6.22), 1.27 percent to 0.61 percent, and reached approximately double the pseudo-rotation of LM28B, 0.028 to 0.016.

The load-deflection curves and crack patterns for the specimens listed in Table 6.1 illustrate the degrading effect of bond distress on the member hysteretic behavior. In addition, the load-deflection relationships point out the difficulty in isolating the influence of individual factors causing hysteretic degradation, since several factors or combinations of factors cause the same general effect.

Minimum Development Length-Bond Degradation--It was not possible in the current investigation to develop an equation to predict or describe bond degradation. Because of the number of parameters influencing bond degradation, a large amount of experimental data are needed to define quantitatively the mechanism of bond or stress transfer under cyclic loading. Such a volume of data is not available. However, a criterion suggested by

Japanese investigators [96] is examined. The criterion is based on the required development length of the reinforcing bar,  $l_d$ , and is as follows:

$$l_d \leq h \quad (6.12a)$$

$$\text{and } l_d \leq L_c/2 \quad (6.12b)$$

where  $h$  = gross section depth  
 $L_c$  = clear height of column

This criterion is based on the observed performance of the tests and is not a descriptive criterion which models the effect of various parameters on bond degradation. It is a conservative guide which gives reasonable assurance that bond distress will not occur. The criterion expressed in Eq. 6.12 does not offer any indication of the likelihood of bond distress if the criterion is not satisfied.

The results of the tests of the current investigation, especially the 86 series, suggest an explanation for the reasons the criterion given by Eq. 6.12 gives a bound on bond degradation. Consider first the observed condition of the specimens at the end of testing. It was noted in Chapter 5 that the damage to the specimens in the 86 series consisted of severe cracking and cover loss, which was concentrated in the middle third of the column length with the end regions exhibiting much less cracking by comparison. Also, specimen C-84-21-D suffered an almost complete loss of the core concrete about 8 in. from the end of the column, not at the end as might be expected. In all probability the large blocks at each end of the column restrained the concrete near the blocks in a manner very similar to the effect observed in concrete compressive cylinder tests using solid steel platens at the ends. How far along the column length the restraint was effective is

open to question, but based on the observed specimen condition it is reasonable to assume that the restraint extended about a distance equal to the column total depth,  $h$ . Within a distance  $h$  from the ends, the concrete remained relatively intact and able to develop bond stresses and to limit bond degradation. Thus, the criterion  $l_d \leq h$  provides that the bar will be embedded in concrete expected to remain intact.

The criterion  $l_d \leq L_c/2$  was based on the loading imposed on the column. A longitudinal bar in a column experiences compression yielding at one end of the column and tension yielding at the other. The stresses in the bar are zero near midheight, because a point of inflection occurs near midheight. With load reversal the upper and lower halves of the bar transfer tensile stress to the concrete over a distance of one-half the clear height of the column.

The criterion for bond given in Eq. 6.12 is intended to prevent the occurrence of bond distress and its validity was observed in many Japanese tests and in the current investigation.

Failure Patterns--The physical condition of the 86 series specimens suggests that bond degradation was not only a function of development requirements. In many of the 86 series specimens, no concrete remained around the longitudinal bars near the midheight of the columns. The concrete was ground away in a region in which low bar stresses were expected. Such distress was expected to occur at the ends. However, the Japanese tests also showed the same tendency for bond cracks to first appear away from the ends of the column. Bond degradation occurs with the loss of composite action between the reinforcing steel and the concrete surrounding it. Shown in Fig. 6.25 is an idealization of the effect of bending the longitudinal bar. Fig. 6.25a shows a simple cantilever reinforced concrete beam with no transverse reinforcement. A pure moment is applied to the free end of the

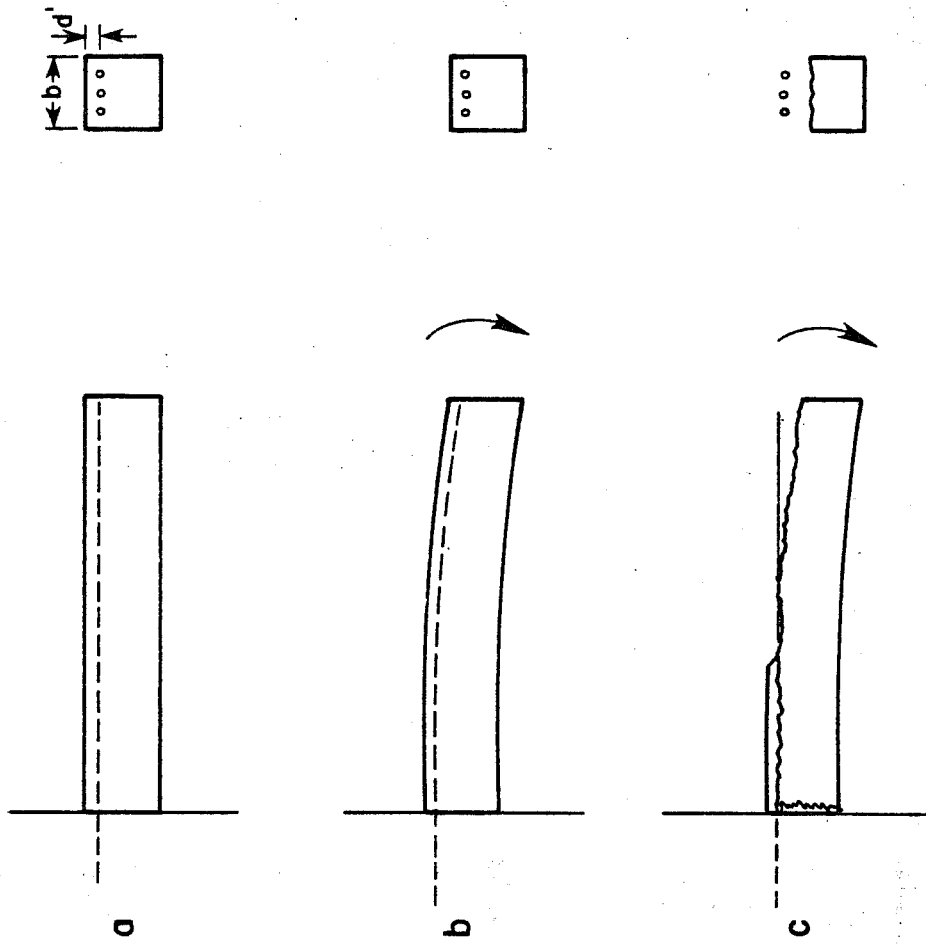
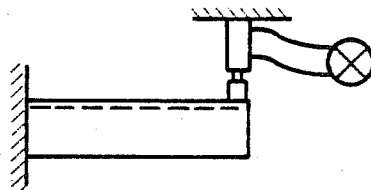


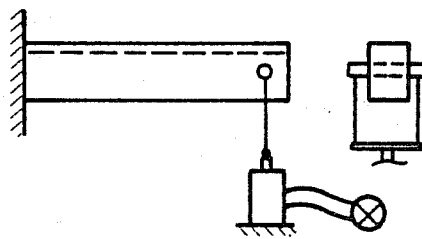
Fig. 6.25 Cover restraint of longitudinal bars

beam (Fig. 6.25b) producing the usual deflected shape. Figure 6.25c shows a possible failure mechanism. The cover is insufficient to force the bars to deflect in the same manner as the beam. As a result, the section splits across the line of bars, releasing the bars, splitting the cover, and totally destroying composite action. The beam would then fail since the concrete section alone could not carry the applied force. This phenomenon has not been reported in previous research reports. The loading conditions and test specimens precluded a failure of the type. In monotonic tests, the load is applied directly on the tension face of the beam, as shown in Fig. 6.26a. Obviously, the presence of the loaded bearing plate precludes the possibility of the cover spalling and destroying composite action between the concrete core and the tension steel. In cyclic tests, a load may be applied through a pin passing through the beam, as shown in Fig. 6.26b. However, to reduce shear problems at the point of load application, reinforcement is provided near the end of the beam. The transverse reinforcement may effectively restrain the tendency of the bars to split away from the concrete.

In the columns used in the current investigation and in the Japanese tests there were no external restraints to the bar prying the concrete cover off near the midheight of the column. In the column the only restraint to the bars is the ties. The ties hold the bar against the core concrete so that even as the cover spalls away, the bars cannot separate from the core. However, if the only means left to transfer stress is on the surface between the core and the bar, it will not require many cycles to crush the concrete ahead of the lugs of the bar. In addition, as the ties yield the bar separates from the core, making it easier for the concrete to be ground away by the lugs. It becomes clear that increased amounts of transverse reinforcement



(a)



(b)

Fig. 6.26 Test conditions masking cover restraint

are beneficial to bond because they provide greater restraint to maintain the bar against the core.

It is interesting to note that the cover was not pried off in specimen C-84-32-D as it was in specimen C-86-32-D, even though both tests had the same number of ties. Referring again to the cantilever beam in Fig. 6.25, the reason for the different behavior may be traced to the diameter of the bar. The larger the diameter of the tension bar, the stiffer it is in bending. The stiffer the bar, the more restraint the cover must develop to prevent spalling due to prying of the bar. With a given cover and amount of transverse reinforcement, it is more likely that spalling will occur with larger bar diameters.

#### 6.5 Expanded Predictive Guide

The final form of the predictive guide for behavior classification is shown in Fig. 6.27. The general outline of the guide is based on the results of the current investigation discussed in Chapter 5. The quantitative criteria in the expanded guide are based primarily on the data from the Japanese tests. The criteria that determine branch selection in the flowchart are empirical in nature and reflect the trends observed in the tests. The principal objective of the predictive guide is to present a unified, rational approach for behavior classification and an indication of the effect of key parameters on column hysteretic behavior.

Primary Branches--The flowchart in Fig. 6.27 is shown in two parts; however, the part on the right is the continuation of the part on the left. The first five steps in the flowchart indicate criteria-- $V_{rf}$ ,  $V_{csc}$ ,  $V_{acc}$ ,  $Z_n$ , and  $l_d$ --which must be computed. The equations for the criteria are listed in Fig. 6.28.

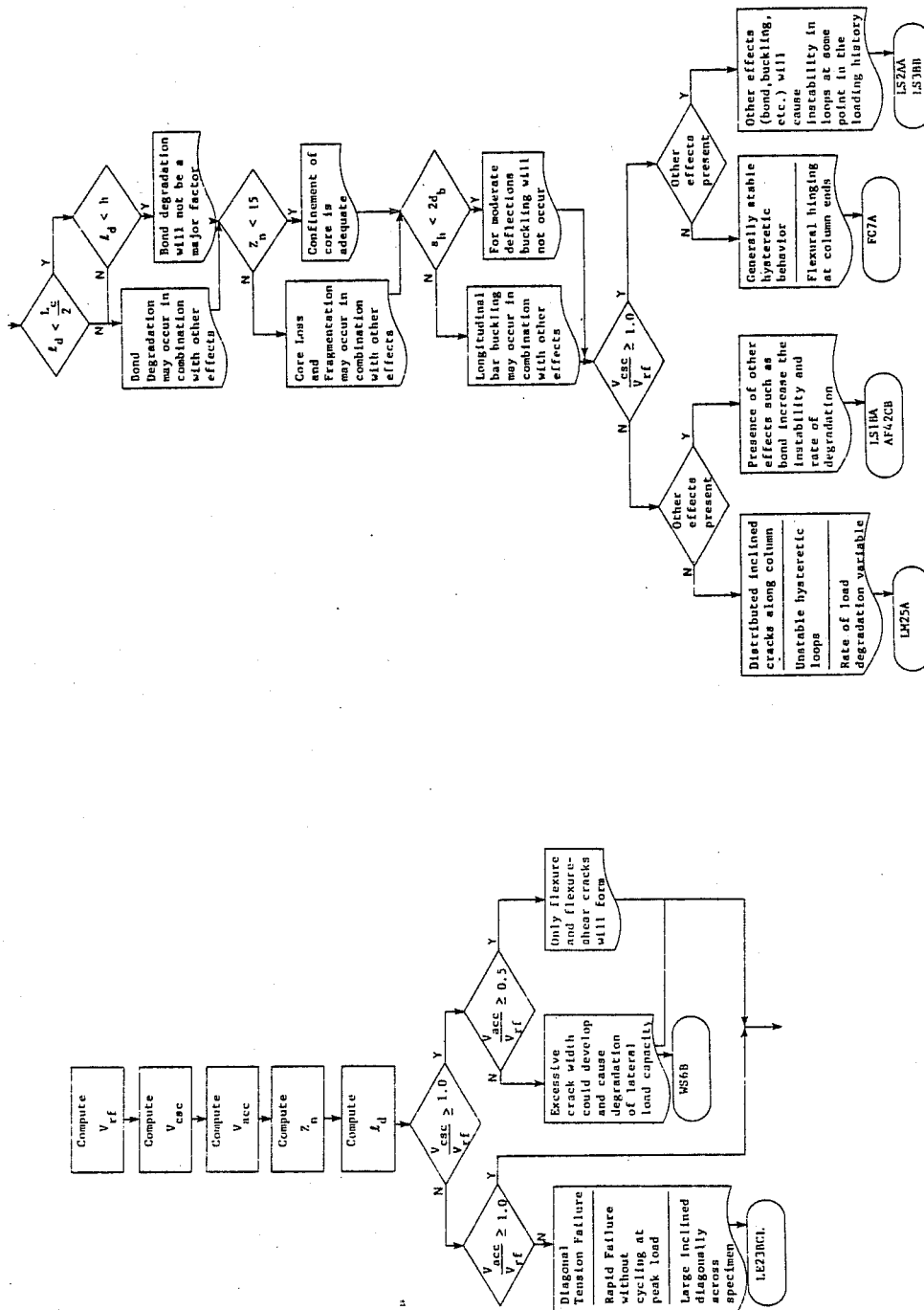


Fig. 6.27 Expanded predictive guide



FLEXURAL CAPACITY

$$V_{rf} = \frac{2M_u}{L_c}$$

CONCRETE SHEAR CAPACITY

$$V_{csc} = 200bc + 0.8C_F$$

$$V_{csc} \leq 0.3bcf'_c$$

$$V_{csc} \geq 360bc$$

AFTER CRACKING CAPACITY

$$V_{acc} = 0.7 \frac{h}{s_h} A_v f_{yv}$$

$$V_{acc} \leq 0.2A_c f'_c$$

CONFINEMENT CRITERION

$$Z_n = \frac{1}{(1 - \frac{N}{P_0})} \left( \frac{0.5}{\epsilon_{50c} - 0.002} \right)$$

$$\epsilon_{50c} = \frac{3 + 0.002f'_c}{f'_c - 1000} + \frac{3}{4} \rho_s \sqrt{\frac{b'}{b}} s_h$$

BOND CRITERION

$l_d$  = computed by provisions of the ACI Building Code for bars in tension

BAR BUCKLING CRITERION

$s_h < 2d_b$  for large deformation cycling

$s_h < 4$  to  $6d_b$  for moderate cycling

Fig. 6.28 Guide criteria

After computing the criteria, a comparison is made of the ratio of lateral load capacity based on shear to lateral load capacity based on flexure ( $V_{csc}$  to  $V_{rf}$ ). The value of 1.0 for the ratio  $V_{csc}/V_{rf}$  is taken to be the dividing line between shear-dominated and flexure-dominated behaviors. The ratio of  $V_{csc}$  to  $V_{rf}$  provides a good indication of the likelihood of inclined cracking, the condition necessary for a shear-dominated behavior.

Diagonal Tension Failure--If the ratio of  $V_{csc}$  to  $V_{rf}$  is less than 1.0, the behavior is termed shear-dominated and the column will exhibit inclined cracking. At inclined cracking the shear-resisting mechanism relies on aggregate interlock along the cracks to transfer shear. It is natural to expect that the effectiveness of the aggregate interlock mechanism is dependent on the amount of transverse reinforcement and the ratio of  $V_{acc}$  (after cracking capacity) to  $V_{rf}$  gives an indication of the effectiveness of aggregate interlock. If the ratio  $V_{acc}/V_{rf}$  is less than 1.0, the transverse reinforcement is inadequate and the column will fail in a brittle manner following the formation of one or two large inclined cracks. A test specimen which exhibited such a failure is LE23BCL. The specimen is noted below the description of behavior in the flowchart. Examples illustrating different kinds of behavior are noted at other points in the flowchart. The information required to compute the criteria and the values of the criteria are listed in Table 6.2 for each example. In addition, the load-deflection curves and selected crack patterns for each example specimen are shown in Figs. 6.29 through 6.36. The load-deflection curves for LE23BCL are shown in Fig. 6.29. Note that the crack patterns are labeled and that the labels appear on the load-deflection curves to denote the deflection level at which the crack patterns were drawn. The crack patterns were drawn following completion of all cycles at the denoted deflection level.

TABLE 6.2 EXAMPLE SPECIMENS IN EXPANDED GUIDE

Test	$L_c$	$c$	$f'_c$	$s_h$	$A_v$	$\rho_s\%$	$f_{yv}$	$d_b$	$A_b$	$f_y$	$M_u$	$P_0$	$N$	$C_F$
LE23BCL	19.7	2.6	2100	1.97	0.09	0.45	56700	0.39	0.12	58700	265950	212300	32800	38000
WS6B	39.4	2.0	3900	3.94	0.09	0.26	49600	0.51	0.20	60900	394000	389000	32800	53000
LM25A	19.7	2.0	3500	1.81	0.41	2.23	47100	0.51	0.20	56200	394000	353700	32800	51000
LS1BA	29.5	2.3	2750	2.28	0.20	0.61	51000	0.51	0.20	51700	354000	287500	32800	43000
AF42CB	39.4	4.3	2700	1.73	0.41	2.35	45300	0.75	0.44	50400	709200	349200	79200	79000
FC7A	39.4	2.3	6400	1.30	0.20	1.53	49800	0.63	0.31	52800	630400	615300	65600	82000
LS2AA	29.5	3.4	2750	1.65	0.20	1.22	51000	0.39	0.12	54300	368750	264800	65600	67000
LS3BB	59.1	2.4	2750	1.57	0.04	0.25	55200	0.63	0.31	50700	472800	316300	32800	46000

Test	$V_{If}$	$V_{csc}$	$V_{acc}$	$Z_n$	$l_d$	$\frac{V_{csc}}{V_{If}}$	$\frac{V_{acc}}{V_{If}}$
LE23BCL	27000	16000*	8000	51	9.2	0.59	0.67
WS6B	20000	23000*	8000	119	12.4	1.15	0.40
LM25A	40000	21000*	73000	14	11.5	0.53	1.83
LS1BA	24000	19000*	31000	47	10.6	0.79	1.29
AF42CB	36000	34000*	74000	15	17.1	0.94	2.06
FC7A	32000	43000*	53000	19	13.5	1.34	1.66
LS2AA	25000	28000*	43000	28	8.5	1.12	1.72
LS3BB	16000	19000*	10000	77	12.8	1.19	0.63

For each test :  
 $b = 9.84$  in.  
 $h = 9.84$  in.  
 $b' = 8.46$  in.  
 $A_c = 71.57$  sq in.

Units are inches and pounds

\* Upper bound on  $V_{csc}$  controlled.

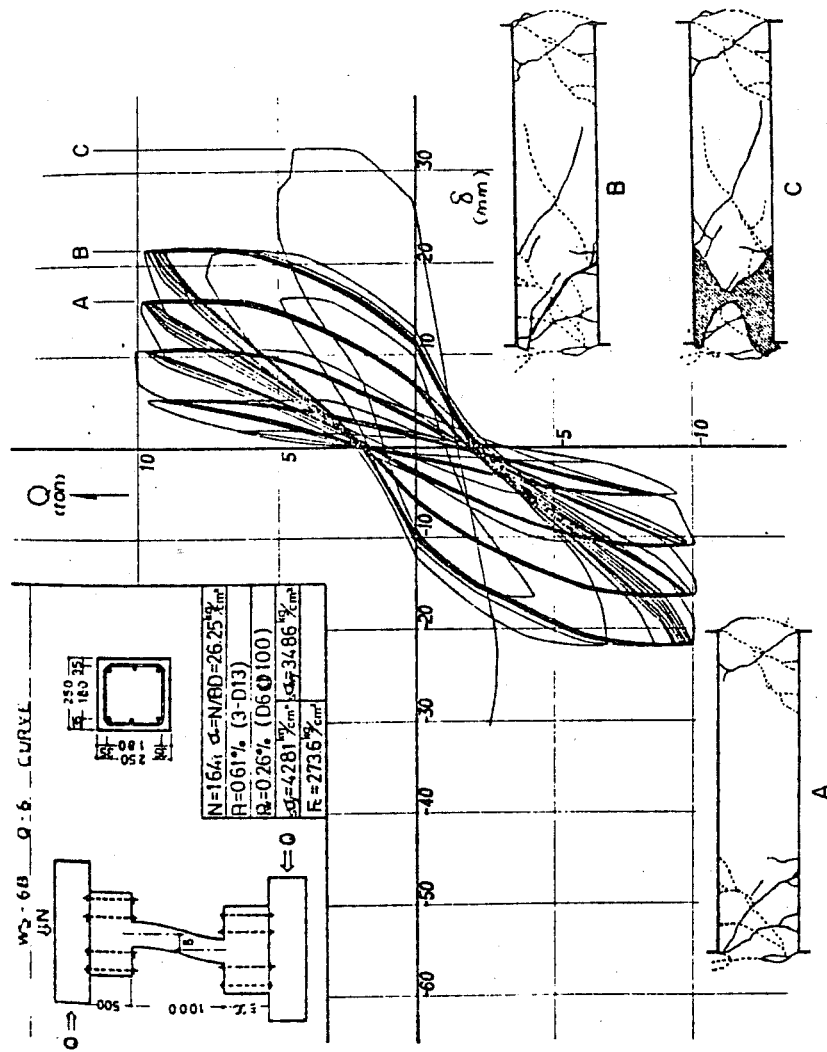


Fig. 6.29 Load-deflection curves and crack patterns, Specimen WS6B [58]

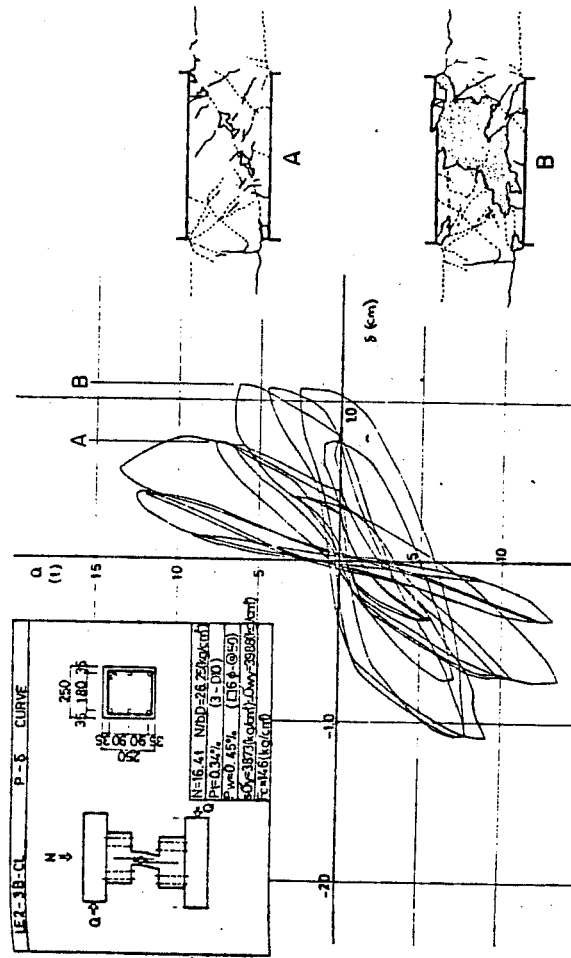


Fig. 6.30 Load-deflection curves and crack patterns, Specimen LE23BCL [60]

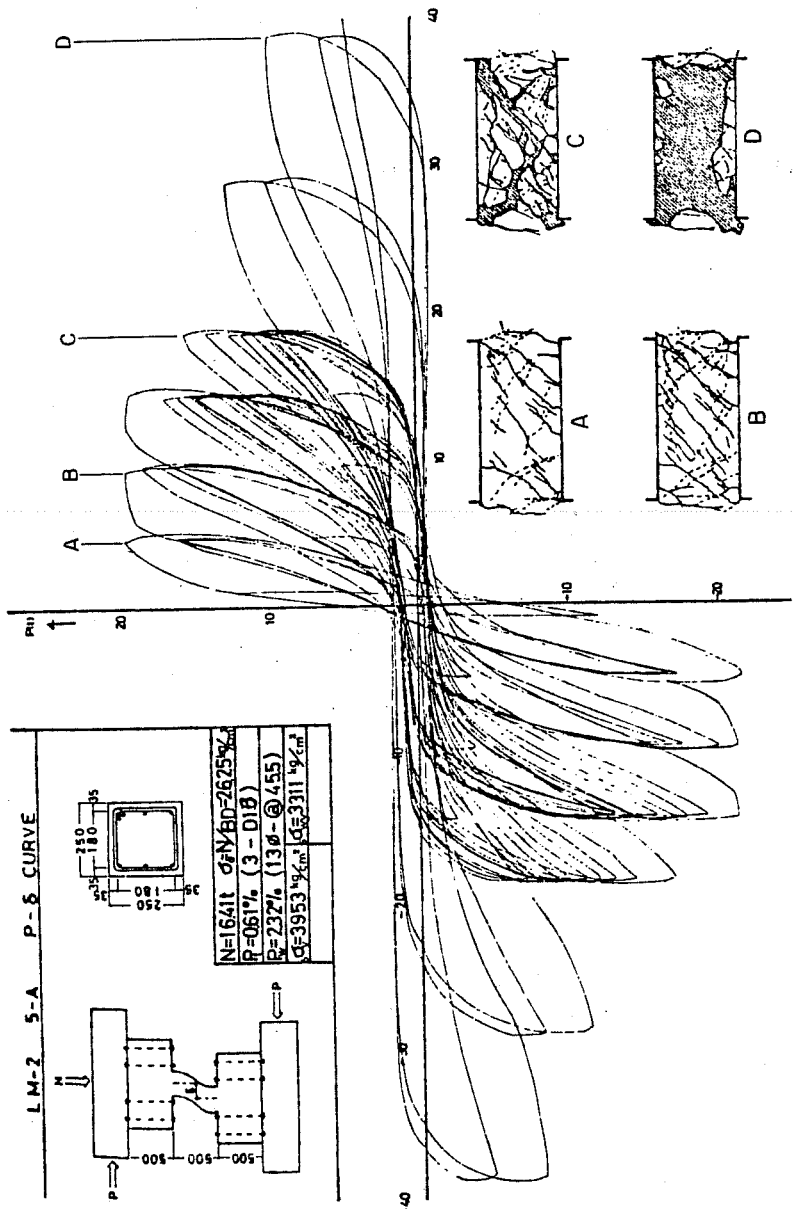


Fig. 6.31 Load-deflection curves and crack patterns, Specimen LM25A [58]

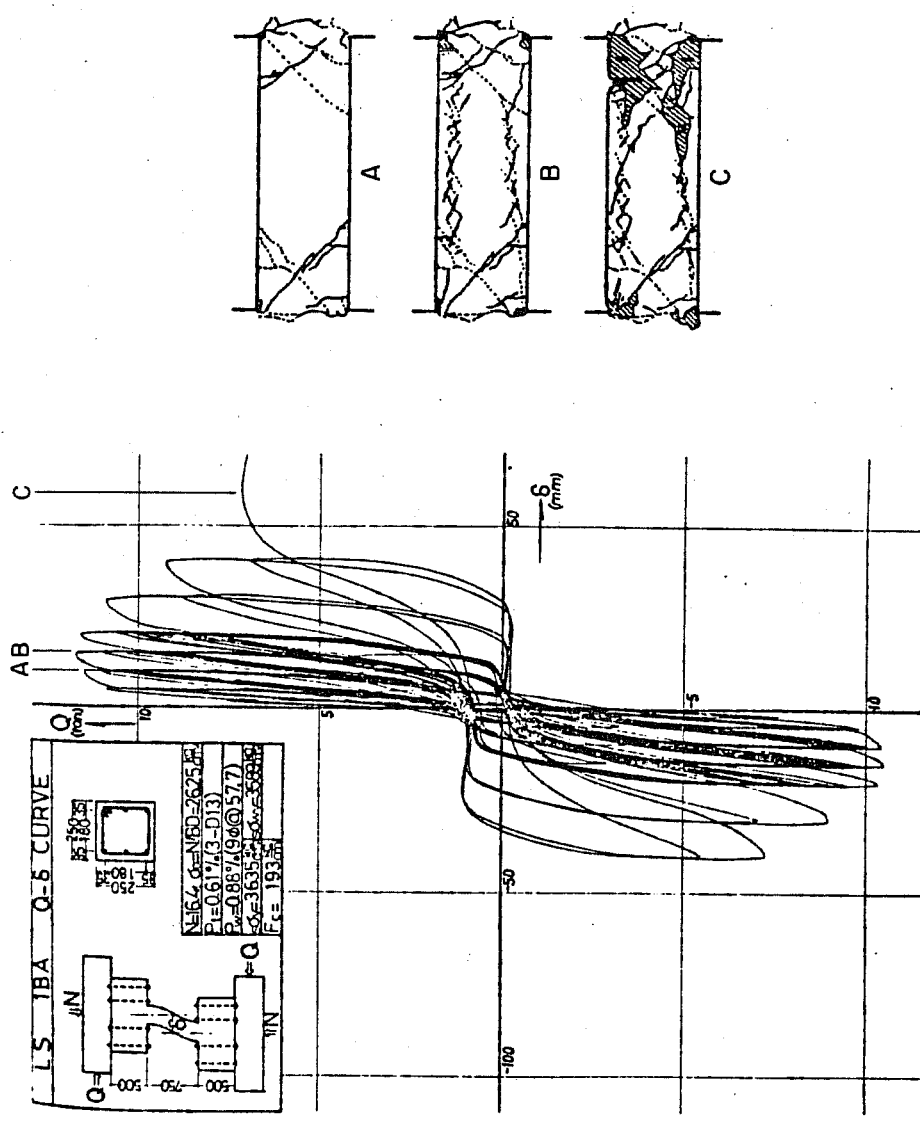


Fig. 6.32 Load-deflection curves and crack patterns, Specimen LS1BA [60]

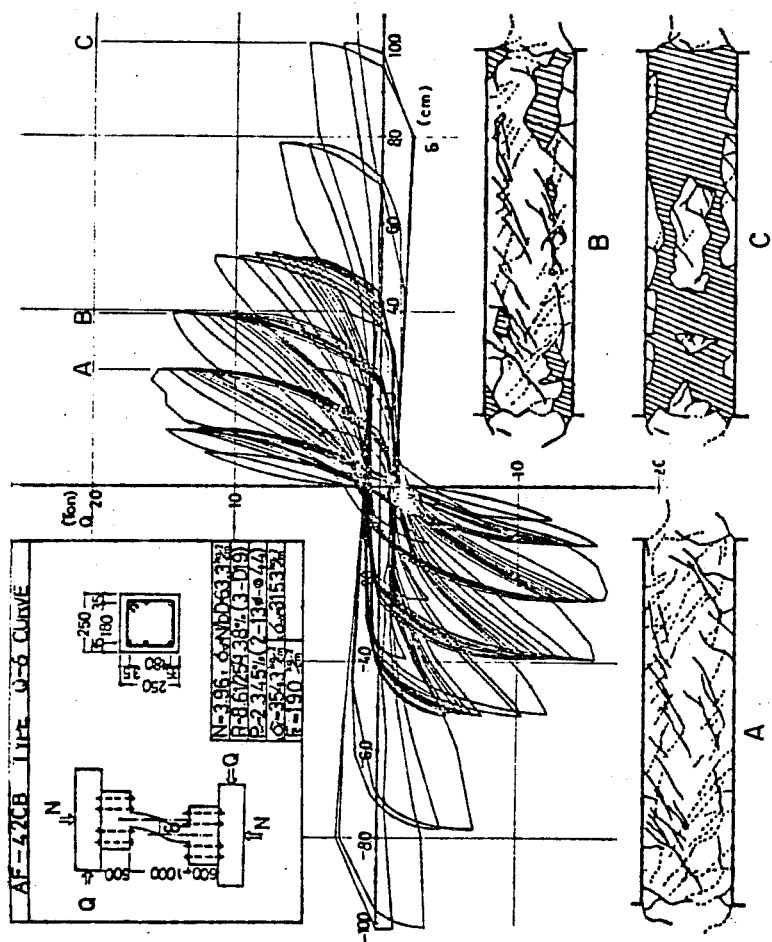


Fig. 6.33 Load-deflection curves and crack patterns, Specimen AF42CB [60]



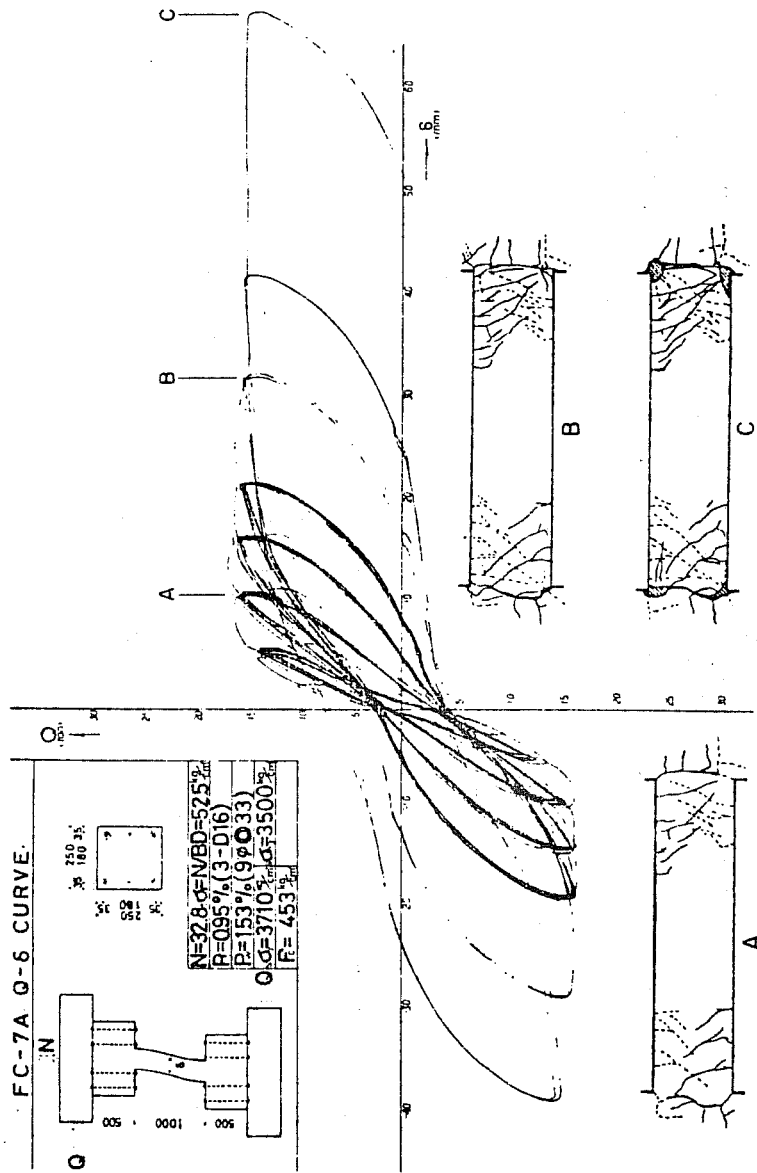


Fig. 6.34 Load-deflection curves and crack patterns, Specimen FC7A [58]

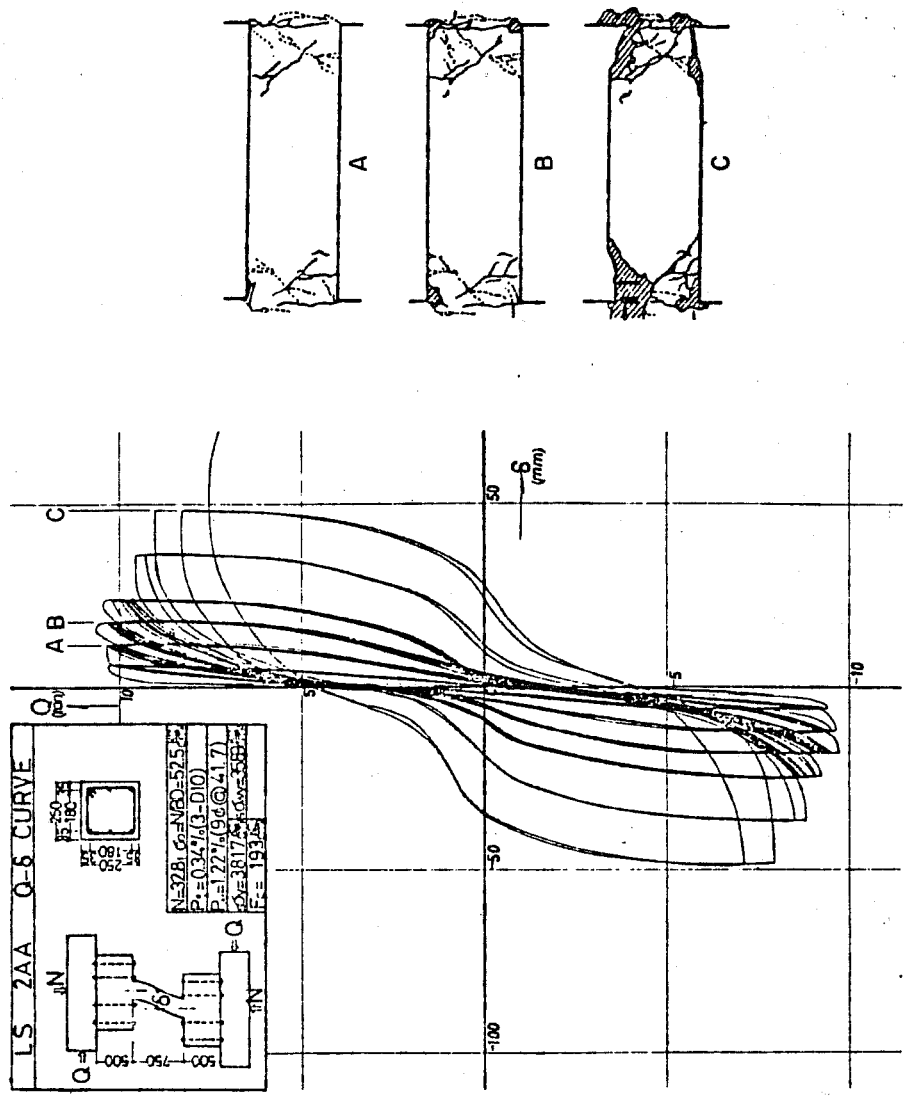


Fig. 6.35 Load-deflection curves and crack patterns, Specimen LS2AA [60]

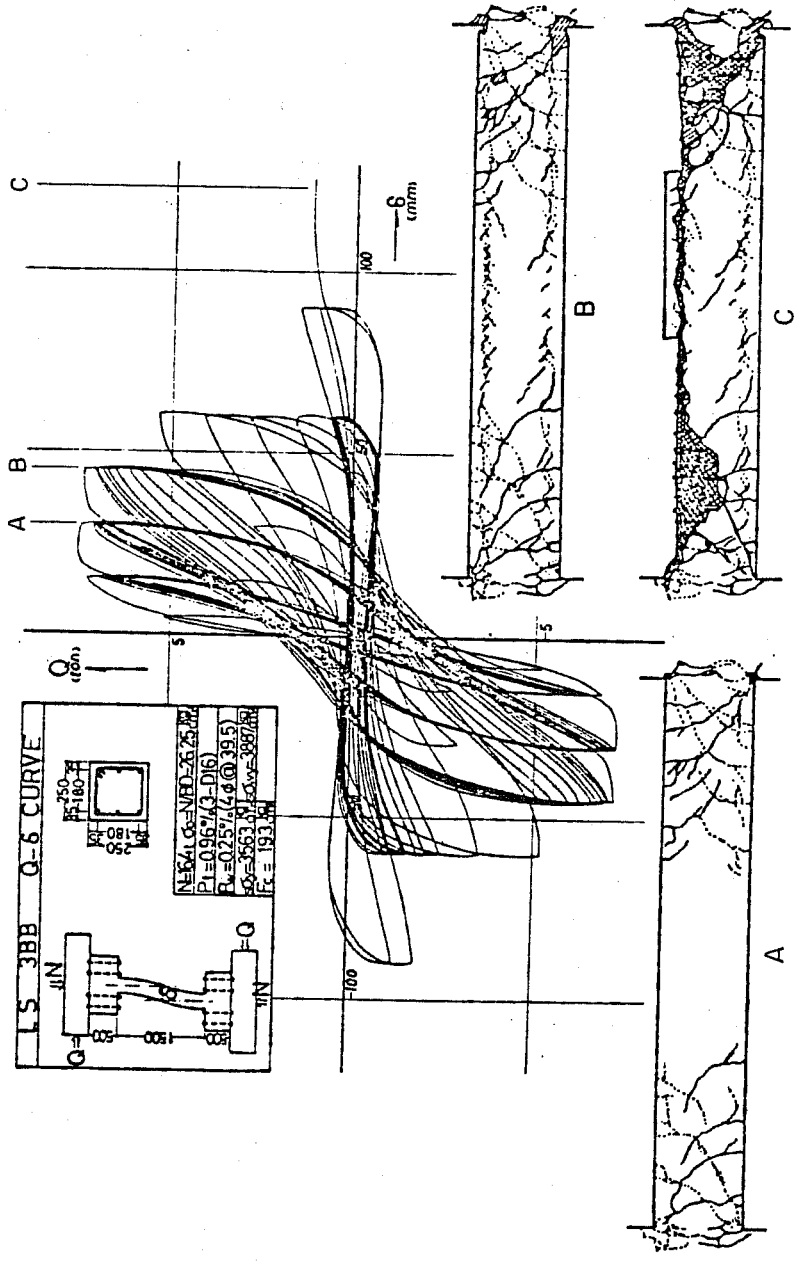


Fig. 6.36 Load-deflection curves and crack patterns, Specimen LS3BB [60]

Figure 6.29 clearly illustrates the rapid degradation of the hysteretic loops and the large diagonal crack on specimen LE23BCL.

Minimum Transverse Reinforcement--If the ratio of  $V_{csc}$  to  $V_{rf}$  is at least 1.0, then the behavior is flexure-dominated. It is necessary to provide a minimum amount of transverse reinforcement even for flexure-dominated behavior, because of the effect that cyclic reversed loading has on a column. Concrete has an extremely low tensile strain limit. Under cyclic deformations, flexure-shear cracks will widen and with continued cycling will eventually cause deterioration of the section. The transverse reinforcement restrains the cracks to prevent a rapid breakdown. In Japanese tests in which the ratio of  $V_{acc}$  to  $V_{rf}$  is greater than 0.5 no specimen exhibited degradation of the hysteretic loops. Therefore, the minimum amount of transverse reinforcement is specified by requiring the ratio of  $V_{acc}$  to  $V_{rf}$  to be at least equal to 0.5. If the ratio is less than 0.5, a premature degradation of the column behavior may occur as a result of excessive crack widths and core degradation. It is not possible to determine the point in the loading history at which degradation may occur and it is possible that under moderate loading degradation due to insufficient transverse reinforcement may not occur. For this reason, the NO branch of the  $V_{acc}$  to  $V_{rf}$  comparison rejoins the YES branch. An example of a flexurally dominated behavior that changed as a result of insufficient transverse reinforcement is shown in the results of specimen WS6B, for which load-deflection curves are shown in Fig. 6.30. Notice that the hysteretic loops are stable for a large number of cycles until there is rapid drop in the lateral load and stiffness. The crack patterns indicate the widening of the flexure-shear cracks and the formation of inclined cracks when the drop occurred.

The YES branch of the  $V_{acc}$  to  $V_{rf}$  comparison for shear-dominated behaviors and both branches for flexure-dominated behaviors lead to a common point in the flowchart. It is important to realize that while a behavior may be shear-dominated, the specimen may still undergo bond degradation, core loss, and longitudinal bar buckling, just as in flexure-dominated behaviors. The performance of a specimen with a large amount of transverse reinforcement may be stable because aggregate interlock can be an effective shear resisting mechanism. Even though inclined cracks may occur, the shear-dominated degradation is gradual enough to permit other degrading effects to come into play.

Secondary Branches--The criteria common to both shear or flexure-dominated behaviors are those which pertain to bond degradation, core integrity or confinement, and longitudinal bar buckling. Each of these effects can produce degradation at different points in the loading history of a short column. Depending on the severity of the loading all, none, or some of the effects may come into play. It is not possible to predict exactly when in the loading history they will occur, but it is possible to identify the columns which are susceptible to such degradation. As a result, the criteria provide guides as to the conditions which will prevent the degrading effects from being a factor. Because the effects may or may not result in degradation, the NO branch following each comparison rejoins the YES branch.

The criteria for confinement,  $Z_n < 15$ , should not be considered exact, as there is considerable uncertainty in defining the effect of confinement because it is so directly related to the role transverse reinforcement plays in inclined crack restraint.

The flowchart divides again into shear-dominated and

flexure-dominated behaviors after the comparisons are made for bond, confinement, and bar buckling. The same criterion used initially,

$$\frac{V_{csc}}{V_{rf}} \geq 1.0 \quad \text{is considered again at this point.}$$

The examples of behavior for both shear-dominated and flexure-dominated behaviors are divided into two groups. One group is columns which did not suffer from the effects of bond, core loss, or bar buckling. The other group contains examples of columns which suffered from one or more of those effects.

Shear Behavior--In shear-dominated behaviors, where none of the other effects are critical, the column will have inclined cracks distributed along its length. The hysteretic loops will be unstable and the peak lateral load cannot be maintained. The rate of degradation of the lateral load is dependent on the amount of transverse reinforcement present in the column. The more transverse reinforcement, the slower the rate of degradation. An example is specimen LM25A, shown in Fig. 6.31.

For shear-dominated behaviors, where any of the other effects are critical, the column will still have inclined cracks distributed along its length and the hysteretic loops will be unstable, but the rate of lateral load degradation will increase. If bond degradation is present, the hysteretic loops will contain less area (narrow or pinched loops near origin). If other effects are present, then increasing the amount of transverse reinforcement will not improve the behavior as much as if the other effects were not present. The effect of transverse reinforcement on the other effects is secondary compared to its effect on aggregate interlock. Two examples of shear-dominated behavior in which other effects are critical are LS1BA and AF42CB. Load-deflection

curves are shown in Figs. 6.32 and 6.33. Notice that specimen LS1BA did not develop inclined cracks along its length, but instead two large inclined cracks formed at the ends at an angle of about  $45^\circ$ , which is consistent with the assumption of crack orientation used in the development of the equation for  $V_{acc}$ . Bond cracks along the line of the longitudinal bars are present in the crack patterns for both specimens. In specimen AF42CB, which had 0.75 in. diameter longitudinal bars the effect of bond degradation is very pronounced at deflection level A. The loops are no longer stable with the onset of bond degradation.

Flexural Behavior--In flexure-dominated behaviors in which no other effects are critical, the hysteretic loops are very stable and the behavior can be characterized as a flexural hinging behavior. Generally, in this kind of behavior the cracking is limited to flexure and flexure-shear cracks. A typical example of the kind of behavior exhibited by a specimen developing flexural hinging is FC7A, shown in Fig. 6.34. The loops are pinched, but very stable even at high deflection levels. The pinching is to be expected because of sliding shear at the column ends and the phenomena is typical of the observations made by other investigators [4,5] studying cantilever beams subjected to cyclic reversed loadings.

In flexure-dominated behaviors in which other effects are critical, the hysteretic loops become unstable at some point in the test. Initially, the cracking is typical of flexure-dominated behavior without other effects, but as the deflection and number of cycles increase so does the likelihood of the other effects becoming a factor. An example of a flexure-dominated behavior in which bar buckling caused degradation is LS2AA, Fig. 6.35. It is clear that longitudinal bar buckling can have a serious

detrimental effect on stiffness and lateral load resistance. It is interesting to note that even though the bars buckled the loops remained open in shape. Specimen LS3BB exhibited bond degradation and its load-deflection curves are shown in Fig. 6.36. Note that at the deflection level B the bond cracks appeared and the hysteretic loops became unstable. With increased deflection the remaining lateral load resistance was rapidly lost.

The predictive guide illustrated in Fig. 6.27 offers a rational, unified approach to both describing the effects of various specimen parameters on behavior and predicting the probable behavior of a column subjected to cyclic reversed deformations.

#### 6.6 Predictive Guide Applied to Current Investigation

The numeric comparisons in the predictive guide presented in the last section are based primarily on the results of the Japanese tests, because a large number of short columns were tested and the results are available for study. It is felt that while the concepts embodied by the predictive guide are general, the quantitative formulations require additional study before they can be applied to all cases. In particular, the effect of load history on the various capacities is unclear except for the case of unilateral cyclic loadings.

The values of the predictive guide criteria for each of the specimens in the current investigation are listed in Table 6.3. The predicted and observed specimen behaviors are also shown. The guide generally provides a good indication as to the hysteretic behavior. In most cases, the predictive guide adequately predicts the reasons for the degradation. For the 86 series specimens with axial load, the behavior is predicted to be flexure dominated. Thus, degradation is partially attributable to excessive crack



TABLE 6.3 GUIDE CRITERIA FOR TEST SPECIMENS

Test Name	$V_{if}$ kips	$V_{csc}$ kips	$\frac{V_{csc}}{V_{if}}$	$V_{acc}$ kips	$\frac{V_{acc}}{V_{if}}$	$Z_n$	$l_d$ in.	$s_h$ in.	Predicted Behavior	Observed Behavior
0-86-32-D	64	32	0.50	46	0.72	10	20	1.125	Diagonal Tension	Degrading (S,B)
C-86-32-D	80	85	1.06	46	0.58	17	20	1.125	Degrading (B)	Degrading (S,B)
C-86-21-D	83	93	1.12	30	0.36	37	20	1.75	Degrading (I,B)	Degrading (S,B)
C-86-14-D	79	71	0.90	20	0.25	65	20	2.57	Diagonal Tension	Degrading (S,B)
C-86-09-D	83	93	1.12	13	0.16	120	20	4.0	Degrading (I,B)	Degrading (S,B)
C-86-03-D	80	98	1.23	4	0.05	420	20	12.0	Degrading (I,B)	Diagonal Tension
C-84-32-D	61	59	0.97	46	0.75	17	13	1.125	Diagonal Tension	Degrading (Bu)
C-84-21-D	58	63	1.09	30	0.52	37	13	1.75	Degrading (Bu)	Degrading (Bu)
C-84-14-D	56	73	1.30	20	0.36	65	13	2.57	Degrading (Bu)	Degrading (Bu)
0-86-14-DM	67	51	0.76	20	0.30	50	20	2.57	Diagonal Tension	Degrading (S)
C-86-14-DM	79	85	1.08	20	0.25	63	20	2.57	Degrading (I,B)	Degrading (S,B)

B - Bond      S - Shear      I - Crack Width Control      Bu - Longitudinal Bar Buckling

- $V_{if}$  - lateral load capacity based on flexure, kips
- $V_{csc}$  - concrete shear capacity, kips
- $V_{acc}$  - after cracking shear capacity, kips
- $Z_n$  - core confinement criterion
- $l_d$  - longitudinal bar development length (tension), in.
- $s_h$  - tie spacing, in.

widths due to an insufficient amount of transverse reinforcement. However, the specimens actually exhibited degradation due to excessive shear on the section. The distinction between the two behaviors is dependent on the  $V_{csc}$  to  $V_{rf}$  ratio. In the axially loaded 86 series specimens the ratios are close to 1.0 which makes the predicted behavior sensitive to the inaccuracies in either the  $V_{csc}$  or  $V_{rf}$  term. For specimen C-84-32-D, a diagonal tension failure is predicted because the ratio of  $V_{csc}$  to  $V_{rf}$  is 0.97. If the ratio had been greater than 1.0, the predicted behavior would have agreed with the observed behavior.

The predicted behavior of specimen O-86-32-D indicates that the  $V_{csc}$  term does not adequately reflect the effect axial load has on member behavior. The calculated  $V_{csc}$  term is quite low compared to the capacity the specimen achieved in flexure. The  $V_{csc}$  term overemphasizes the contribution of axial load. The reason may in part be due to the use of the area of concrete in compression as the area initially resisting shear. The area increases markedly with increasing compressive axial load. There may be a lower bound on the area actively engaged in the aggregate interlock shear resisting mechanism.

In summary, the specimens of the current investigation had capacity ratios which were close to the values determining the branches of the behavior in the predictive guide. For this reason, it was difficult to make clear predictions as to causes of behavior, but the general type of behavior could be predicted in most cases. It was clear from the comparisons that when a sufficient number of tests becomes available in which bidirectional deformations and variable load histories are applied, the quantitative criteria will have to be modified to account for loading history.

### 6.7 Implications of Guide to Design

The guide described in Fig. 6.27 is based on the criteria outlined in Fig. 6.28. The criteria are directly related to the design of columns and for this reason the implications of the criteria warrant discussion.

Naturally enough, reinforced concrete members exhibit the most desirable behavior if the member remains uncracked during any given loading history. However, it has been generally accepted for quite some time that such a requirement is unrealistic and uneconomical. Cracking of the member is accepted and with it the consequences to behavior which results, such as reduced stiffness. What is not accepted, however, is cracking which results in significant losses of load-carrying capacity. The objective of design is to design a member which carries a given load economically. Flexural cracking is accepted because by permitting it the load capacity of a reinforced concrete member is greatly increased compared to the same member uncracked. Current design practice necessitates that the design capacity of a member be maintained to provide some assurance against structural collapse and loss of life.

The criteria described in Fig. 6.28 provide the designer with a rationale which incorporates the concepts discussed in the preceding paragraph. The lateral load capacity based on flexure ( $V_{rf}$ ) uses the ultimate moment capacity of the section which is the most load the section can carry with any degree of long term stable hysteretic behavior. The ultimate moment should be calculated using reinforcement strain-hardening effects and realistic material strengths.  $V_{rf}$  is used as the design load and the other criteria provide recommendations on what must be done to avoid effects causing degradation of the load-carrying capacity of the member.

The load capacity based on the shear capacity of the concrete ( $V_{csc}$ ) gives an indication of the likelihood that inclined cracking and thus shear degradation will occur. The after cracking capacity ( $V_{acc}$ ) provides guidance to an amount of transverse reinforcement necessary to restrain the degrading effects of flexure-shear or strain capacity cracks which tend to propagate with cycling and increased deformations of the member.  $V_{rf}$ ,  $V_{csc}$ , and  $V_{acc}$  serve as the fundamental capacity criteria and ensure that for the short term the flexural load capacity of the member can be reached and maintained. However, even for flexural failures (characterized by the formation of plastic hinges) the stability of the hysteretic behavior at the hinge locations must be ensured by careful attention to detailing. The load capacity of the core concrete must be maintained through cyclic reversed loadings by an adequate amount of confinement. The effectiveness of transverse reinforcement as confining steel is indicated by the  $Z_n$  criterion. Cyclic reversed loadings have a very detrimental effect on the bond characteristics of reinforcing bars. Satisfaction of the criteria for development length will provide assurance that the degrading effects of bond loss will not occur. Buckling of the longitudinal reinforcement can have a degrading effect on load capacity and the provisions for tie spacing provide an indication of the requirements for reducing the effects of bar buckling on the load capacity of the member.

The predictive guide because it encompasses a broad range of behavior also includes the behavior most desired in seismic design. Figure 6.37 shows the path in the predictive guide which leads to a predominately flexural behavior. All other paths have been omitted to emphasize the conditions which must be satisfied in order to achieve a stable hysteretic behavior.

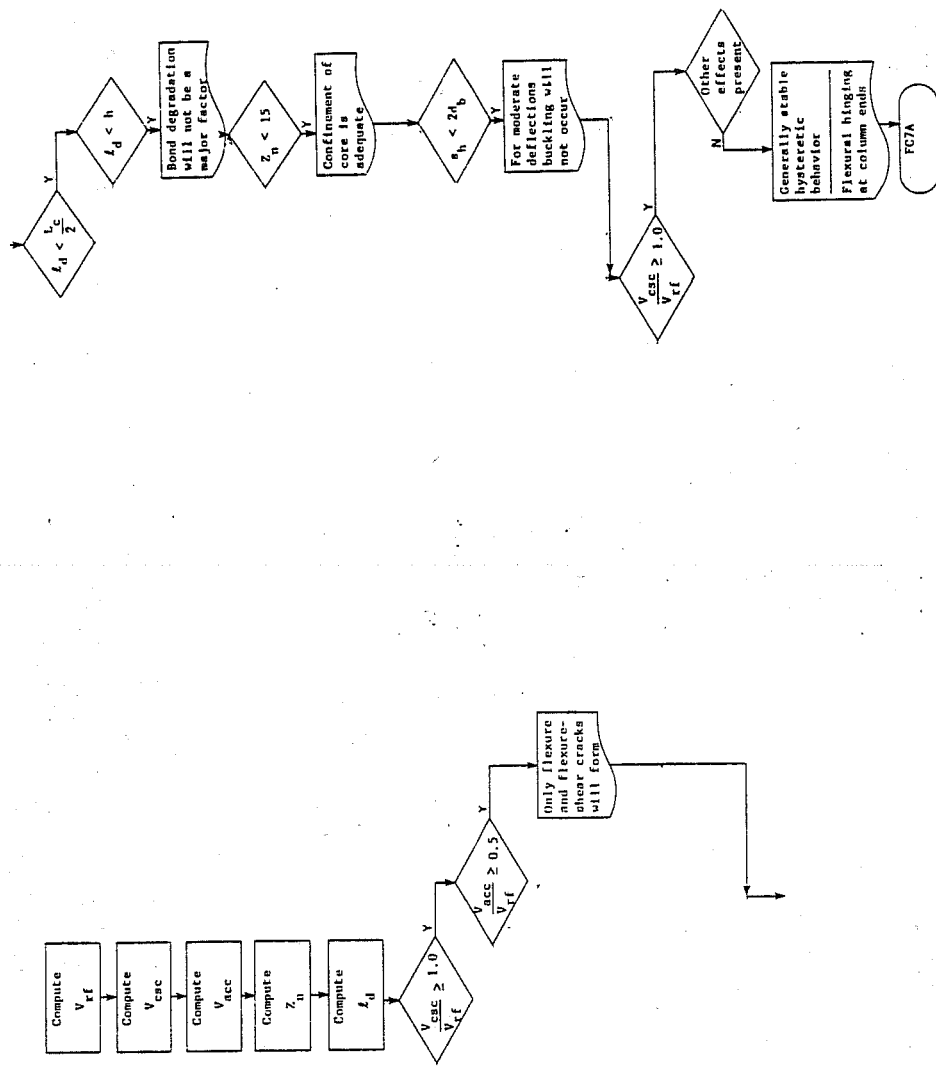


Fig. 6.37 Path to flexural behavior

In summary,  $V_{rf}$ ,  $V_{csc}$ , and  $V_{acc}$  describe the requirements to achieve the capacity based on flexure while the criteria for confinement, development length, and bar buckling provide guidance to the proper detailing to maintain the flexural capacity.

## 6.8 Summary

A quantitative predictive guide for column behavior has been developed in Chapter 6. The criteria in the guide were based on the observations from both the current investigation and numerous Japanese tests used as supplemental data. The numerical comparisons in the guide were developed by using values which best represented the trends in the large number of Japanese tests reported.

The predictive guide uses six criteria to classify behavior. They are the concrete shear capacity,  $V_{csc}$ , the flexural capacity,  $V_{rf}$ , the after cracking capacity,  $V_{acc}$ , the development length required for the longitudinal bar,  $l_d$ , a confinement index,  $Z_n$ , and the spacing of the column ties for buckling,  $s_h$ . The critical comparison is that of  $V_{csc}$  to  $V_{rf}$ , because it determines whether the column will be dominated by shear effects and exhibit a degrading behavior or whether it will be dominated by flexural effects and exhibit stable flexural behavior. The guide offered a means to evaluate the importance of various parameters such as concrete strength on the probable behavior of a column. In addition, the guide offered a unified approach to behavior classification.

The predictive guide is best suited to unilateral cyclic reversed loadings of columns subjected to imposed deflections, since these were the conditions imposed on the columns in the Japanese tests. Comparisons between the predicted behavior based on the guide and the observed behavior in the tests of the current investigation revealed that load history and deformation path seem to play a significant role in determining the column behavior.

However, there is insufficient data to quantify these effects, so they are omitted in the predictive guide.

## CHAPTER 7

### SUMMARY AND CONCLUSIONS

#### 7.1 Summary of the Investigation

The objective of the study was to develop a rationale for the classification and prediction of the behavior exhibited by reinforced concrete short columns subjected to cyclic lateral deformations. An experimental investigation was conducted on a series of short columns which provided the foundation for a further study using results reported in the literature.

7.1.1 Experimental Investigation. Eleven reinforced concrete columns were tested in the current study. The test specimens represented a column bounded by large framing members which restrained rotation. The columns were subjected to slowly applied cyclic translations of the upper end of the column relative to the bottom end to simulate the action of a building column subjected to seismic excitation.

The main variable in the test series was the ratio of shear resistance to flexural resistance of the columns. The ratio was altered in order to obtain a wide range of member behavior. Two other variables were also included in the investigation--(1) axial load and (2) loading history. The resistance ratio (shear to flexure) was varied by altering the amounts of longitudinal and transverse reinforcement relative to each other.

Test Specimen--The overall geometry of the specimen was not varied. The column was a 2/3-scale model of a prototype column 54 in. long with a cross section 18 in. x 18 in. and 1-1/2 in. clear cover. The resulting test column was 36 in. long



with a 12 in. × 12 in. cross section and a 1 in. clear cover. The longitudinal reinforcement was either eight #6 bars or eight #4 bars uniformly arranged around the section (three per face). The transverse reinforcement consisted of 6 mm perimeter ties. The tie spacing in the test series varied from 1-1/8 in. to 12 in.

The column was rotationally restrained at each end and the lower end was held stationary. The upper end of the column was translated laterally relative to the lower end in a horizontal plane producing reversed curvature conditions in the column.

Deformation Path and Loading History--The same deformation path and loading history were used to test the majority of the eleven columns. The columns were deflected along their diagonals producing bilateral column deflections and forces. Three cycles of reversed deflection were applied along each diagonal at each deflection limit. A constant 120 kip compressive axial load was applied to the column during testing. The axial load was approximately 50 percent of the axial load at balanced strain conditions.

Of the eleven columns, three were subjected to different loading conditions. Two of the three columns were cyclically deflected between a single high deflection level. One column had no applied axial load and the other the 120 kip constant compressive axial load. The third specimen had ties at the minimum spacing and was cycled using incrementally increasing deflections, but had no applied axial load.

Instrumentation--Load cells, linear potentiometers, and strain gages were used to monitor the performance of the specimen. The linear potentiometers measured the deflections imposed on the specimen both vertically and laterally. The strain gages were bonded to various locations on both the transverse and longitudinal

reinforcement.

The acquisition of data and loading of the specimen were controlled through a computer based load control system. The data were reduced using computer based software which included digital plotting capabilities.

7.1.2 Supplemental Research. Additional data for developing the predictive guide was obtained by studying numerous tests conducted in Japan. The results were from short columns similar in geometry, but with a smaller cross section than that of the column specimen used in this experimental investigation. The columns were subjected to cyclic unilateral reversed deflections. A large number of parameters were varied in the Japanese tests, making them very useful in extending the results obtained from the experimental investigation.

## 7.2 Observations--Experimental Investigation

Axial Load--The presence of a compressive axial load (less than that at balanced strain conditions) on specimens exhibiting degrading behavior with no axial load produced the following effects on the load-deflection curves:

1. The axial load increased the initial stiffness of the lateral load-deflection curves.
2. The axial load increased the maximum lateral load achieved by the column.
3. The axial load increased the rate of both load and stiffness loss with cycling at deflections equal to or greater than the deflection at which the maximum lateral load occurred.

4. The axial load increased the amount of cover spalling and caused spalling to occur at a smaller deflection than in specimens with no axial load.

The presence of an axial load had no noticeable effect on the orientation of the inclined cracks which formed along the column length.

Loading History--In columns underdesigned for shear according to the 1977 ACI Building Code [17], the effect of cyclic loading versus monotonic loading was to significantly increase the degradation of both the stiffness and the lateral load. The degradation occurred with cycling at deflections equal to or greater than the deflection at maximum lateral load. Prior to reaching the deflection at maximum load, the load capacity was unaffected by cycling, but there was a small amount of stiffness deterioration.

Transverse Reinforcement--A short column with ties at a 12 in. spacing exhibited a very brittle diagonal tension failure. The maximum lateral load attained by the specimen was taken to be a result of the concrete shear capacity only. The maximum load achieved by the column was substantially (about 3 times) higher than the concrete shear capacity predicted by the 1977 ACI Building Code Chap. 11 shear capacity equations.

The short column with ties at a 12 in. spacing had practically the same observed shear capacity as a short column with ties at 2.57 in. spacings. The observed shear capacity was 80 to 90 percent of the computed flexural capacity. Columns with smaller tie spacings (1.75 and 1.125 in.) achieved computed flexural capacity. There was only a small difference between the shear capacity of the section with negligible transverse reinforcement and the computed flexural capacity. This made

it difficult to observe the amount of shear capacity attributable to the transverse reinforcement.

The columns with smaller tie spacings exhibited a more stable hysteretic load-deflection relation. However, because of sliding shear at the ends of the column it may be extremely difficult to achieve a true flexural hysteretic behavior.

Longitudinal Reinforcement--Two different amounts of longitudinal reinforcement were used in the experimental investigation. The longitudinal reinforcement was either eight #6 bars or eight #4 bars. The most significant difference was the occurrence of bond degradation in the specimens with the #6 bars. The specimens with the #6 bars exhibited loss of concrete around the longitudinal bars primarily in the midheight region of the column.

The specimens with #6 bars exhibited more inclined cracking than the specimens with #4 bars. The increased amount of inclined cracking was the result of a higher flexural capacity. The increased flexural capacity led to a higher imposed shear force on the specimens with #6 bars as compared to the specimens with #4 bars.

The specimens with #4 longitudinal bars exhibited a more stable hysteretic behavior than the specimens with #6 bars. The load-deflection curves for the #4 bar specimens exhibited less pinching and did not exhibit the severe loss of stiffness that was common in the specimens with #6 longitudinal bars. The improved behavior was attributable to less bond degradation along the #4 bars and a lower imposed shear force on the column as the result of a smaller flexural capacity in the #4 bar specimens.

The specimens with eight #4 longitudinal bars all exhibited longitudinal bar buckling. The #4 bar specimens with ties at 1-3/4 in. and 1-1/8 in. showed a restrained degradation of the load-deflection curves. The #4 bar specimen with ties at 2.57 in. failed explosively. The longitudinal bars buckled and transferred the axial load onto the concrete section. The concrete section then reached a stage where it could no longer carry the axial load and as a result failed.

### 7.3 Needed Future Research

The study of the test data from the current investigation and research conducted elsewhere pointed to the areas which require additional study.

Loading History--The study of the effect of cycling on short column behavior needs considerable more study. The bulk of the research on member capacities have been done using monotonic loadings. The effect of cycling on capacities, especially shear and bond, requires a great deal of research in order to define the limits which cycling places on the limits which cycling places on the capacity which a member can sustain. It is clear that loading histories other than increasing incremental deflections need to be considered. An example is large deflection cycles followed by small deflection cycles.

Specimen Geometry--The short columns tested were square and doubly symmetric. The behavior of a rectangular section may not be adequately represented by the results obtained from a square section. This is especially true for the shear capacity of a rectangular section which is loaded along some arbitrary angle. There is presently no guidance as to the shear capacity of a rectangular member loaded along a skewed axis.

Axial Load--The effect of much higher axial compression loads (near the axial load at balanced strain conditions) on the hysteretic behavior of short columns requires study. Such axial loads may cause a much more severe deterioration of the section because of a higher imposed shear on the member.

Confinement--The effectiveness of transverse reinforcement as confining steel in members subjected to conditions of high imposed shear and normal forces needs additional study. The influence of such confinement on the deformation and load capacity of a member is especially important when considering cyclic reversals of loading.

Bond--Bond degradation along the longitudinal bars was an important cause of degrading hysteretic behavior in short columns. The development length required by a bar subjected to load reversals requires additional study. Such effects as peak stress in the bar, confinement of the surrounding concrete, and bending of the bar in conjunction with an axial load all need further study in order to reflect the conditions in a short column.

Shear Capacity--The manner in which a short column resists shear forces seems to differ from that suggested for beams. The effect of the loading condition needs further study in order to determine its influence on the shear resisting mechanism. The shear capacity of columns loaded along an arbitrary axis requires further study to determine the effect of loading direction on capacity.

#### 7.4 Conclusions

The following conclusions are based on the experimental investigation of eleven short reinforced concrete columns. The columns had a clear height-to-depth ratio of 3. The columns were

cyclically deflected along their diagonals. All but two of the columns had an applied compressive axial load.

1. In columns with degrading hysteretic behavior without an axial load, the presence of a compressive axial load less than the axial load at balanced strain conditions increases both the initial stiffness of the column and the maximum lateral load attained by the column. However, the axial load significantly increases the degradation of both column stiffness and strength if the specimen is deflected past the deflection at which the maximum lateral load occurred.
2. The transverse reinforcement must be designed to resist the additional shear force introduced onto the member by the application of a compressive axial load. A compressive axial load increases the concrete contribution to shear capacity, but after inclined cracking the axial load causes a higher stress condition in the transverse reinforcement. Unless accounted for, the combination of axial load and shear force can cause the transverse reinforcement to yield and drastically reduce the shear resistance of the short column.
3. In short columns exhibiting a degrading behavior under monotonic loading, cycling of deformations results in a significant increase in the rate of degradation of both the lateral load and stiffness of the column.
4. In the short columns tested, there was a lower limit on the amount of transverse reinforcement which was required before an increase in the maximum lateral load of the column was observed. Varying the amount of transverse

reinforcement while still below the limit did not cause a proportionate increase in the shear capacity of the short columns.

5. The shear capacity of a short column is most dependent on the capacity of the concrete to resist shear before inclined cracking. After cracking, the shear resistance of the column is strongly related to the effectiveness of aggregate interlock along the inclined cracks. The primary function of the transverse reinforcement is to control the widths of the inclined cracks so as to maintain the effectiveness of the aggregate interlock.
6. The concrete contribution to the shear capacity of a short column is conservatively estimated by the shear provisions of the 1977 ACI Building Code [17]. The shear provisions of the Code give a conservative estimate of the ultimate shear capacity of the short columns. However, the calculated values from the shear provisions do not follow the trend of the short column test data.
7. The flexural capacity of the short columns computed using actual material strengths gave a reliable upper bound on the maximum lateral load that the columns can reach.
8. Bond degradation along the longitudinal bars is strongly affected by the boundary and loading conditions imposed on the test specimen. Double curvature and the lack of positive restraint to the sides of the member seemed to have a detrimental effect on bond conditions. Bond degradation has a significant detrimental effect on the short column load-deflection hysteresis loops.



9. Buckling of the longitudinal reinforcement is likely when the bars have repeated cycles of both tension and compression yielding. Small diameter bars are most susceptible to this condition because of the usually small flexural capacity associated with columns reinforced with small diameter bars. Buckling is difficult to prevent as shown by the buckling of #4 bars restrained by ties at 1-1/8 in.
10. No single parameter uniquely determines the behavior a member will exhibit, but there does seem to be a hierarchy of parameters which do define the member behavior.
11. In columns which exhibit degrading hysteretic behavior, the degradation begins with cycling at the deflection where the maximum lateral load is achieved and continues with both cycling and increased deflections.
12. In cyclically loaded columns which exhibit shear distress or serious bond degradation, increasing the deflection of the column does not necessarily cause the load-deflection curves to reach the monotonic load-deflection curve.

#### 7.5 Predictive Guide

The guide to column behavior classification and prediction (predictive guide) is the culmination of the current study. It is primarily directed to columns which are subjected to cyclic reversed deformations. The guide is based on the observations and conclusions from both the current experimental investigation and the results of tests conducted in Japan (Secs. 7.2 and 7.4).

The predictive guide is in the form of a flowchart and presents an orderly, rational approach to defining the types of

behavior a column may exhibit and the parameters which most directly affect the kind of behavior exhibited. The guide encompasses a broad range of behaviors from stable flexural hinging mechanisms to brittle diagonal tension failures. Effects of bond degradation and bar buckling are also included.

The guide is composed of criteria which can be compared to each other or to a given limit to determine behavior characteristics of the column. The criteria included in the predictive guide reflect the concrete shear capacity of the section, the flexural capacity of the section, the effect of transverse reinforcement on shear capacity and core confinement and the susceptibility of the longitudinal bars to bond degradation and buckling.

The guide is both a research tool and a design tool. For researchers it provides guidance on the effect of certain parameters on behavior. For designers the criteria provide checks or limits that may be used to ensure that the column will exhibit the desired stable flexural hysteretic behavior.

A P P E N D I C E S

- A. REVIEW OF RELEVANT RESEARCH
- B. FLEXURAL CAPACITY COMPUTER PROGRAM
- C. TRANSVERSE REINFORCEMENT CALCULATIONS
- D. MATERIAL PROPERTIES
- E. GEOMETRY CORRECTION

## A P P E N D I X A

### REVIEW OF RELEVANT RESEARCH

#### A.1 Shear

The shear resisting mechanism in a reinforced concrete member is a very complex phenomenon dependent on many inter-related variables. Most of the past investigations of shear capacity have been on simply supported beams monotonically loaded to failure and so the bulk of the following review will reflect those conditions.

Monotonic Tests--Hognestad, in his excellent paper [19], traces the historical development of shear capacity equations from before 1900 to about 1950. The most interesting points are the early recognition of key variables and the adoption of a design philosophy for shear still used in the current design recommendations of the ACI Building Code. However, it was in the 1950's that the systematic investigation of shear capacity of reinforced concrete beams began.

The bulk of the tests conducted in the period 1950-1960 was simply supported beams with either one or two point loadings on the compression faces of the beam. There were, however, some notable exceptions.

Clark [20] was the first investigator to systematically vary the shear span of the beams. In addition, he studied the effect of the concrete strength, percentage of longitudinal reinforcement, and the percentage of transverse (web) reinforcement. Clark's primary contribution was the recognition of shear span as a major parameter in the shear capacity of a section. Like later investigators, Clark adopted the expression

$$\frac{V}{bjd} \quad (A.1)$$

where  $b$  is the beam width and  $jd$  is the internal moment arm as a representation for the diagonal tension stress in a beam and used it in the development of his proposed design recommendation. Hognestad states that the form of Eq. A.1 was originally proposed by Mörsch [19]. Talbot [20] adopted Eq. A.1 and offered the justification that if diagonal tension stress is the criterion of cracking and the concrete is assumed to carry no longitudinal tension stress, then the result of the formula for principal stress is simply

$$\sigma_t = v \quad (A.2)$$

where  $v$  is the shear stress and  $\sigma_t$  is the diagonal tension. Talbot then suggests that  $v$  can be taken as

$$\frac{V}{bd'} \quad (A.3)$$

where  $V$  is the shear force,  $b$  is the beam width, and  $d'$  is the internal moment arm.

Laupa [21] suggested that the criterion for shear capacity is crushing of the concrete compressive block. He based this idea on the assumption that shear can only be resisted by the concrete surfaces in contact in the compressive block. Laupa also presented the conclusion that diagonal tension cracks were responsible for failure because they caused a reduction in the depth of the compression block. Other investigators continued Laupa's line of reasoning [22,23] but modified it to apply only to shear compression failures which were classified as crushing failures of the compressive block in combination with diagonal tension cracks.

Moody, et al. [24,25,26,27] reported an extensive series of tests on simply supported beams. Their results pointed to percentage

of longitudinal reinforcement, percentage of transverse reinforcement, concrete strength, and shear span as being the most important variables affecting shear capacity. They reported, as did Clark previously, an increase in the load at first diagonal tension cracking with decreasing shear span and noted that the beams with small shear spans carried shears greater than that which caused first diagonal cracking, while beams with large shear spans failed suddenly with the formation of the first diagonal tension crack. An interesting observation was made to the effect that web reinforcement did not affect the load at which diagonal tension cracking first occurred, but did increase the shear carried after formation of the crack.

Baron and Siess [23] continued the work started by Laupa by looking at the effect of compressive axial load on shear capacity. They reported that axial load increased the diagonal tension strength, but that the increase was small in beams with a high steel percentage or long shear span.

Ferguson [28] in a series of beam tests investigated the effect of shear span ratio to determine the influence of boundary conditions. This paper convincingly pointed out that the major reason for the importance of shear span ratios in beam tests was the method of support and load application. Ferguson found that the significant increase in shear capacity with decreasing shear span was the result of applying loads through bearing plates on the compression face of the beam. In tests where the load was transferred to the beam through side stubs, Fig. A.1, he found that the effect of the shear span ratio was not significant.

Viest and Morrow [29] conducted a series of tests on knee beams and center stub beams, Fig. A.2. No web reinforcement was used in any of the beams. The knee beams were a way of introducing axial loads into the beam. The authors suggested that

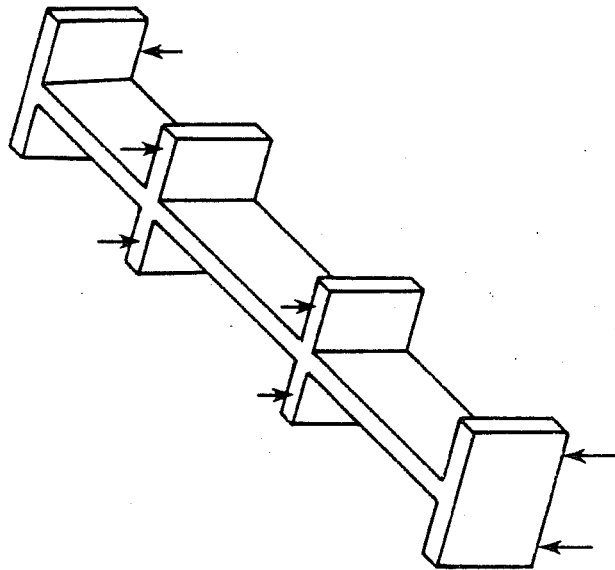


Fig. A.1 Indirect beam loading method used by Ferguson

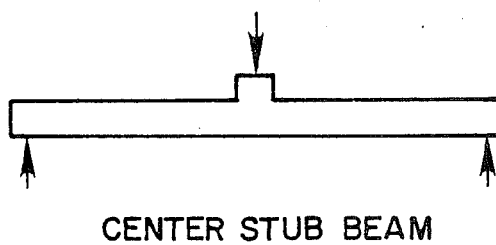
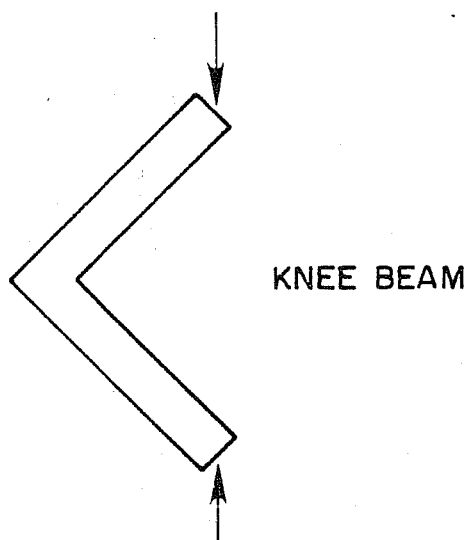


Fig. A.2 Knee beam and center stub beam



$$2 \sqrt{f'_c} \quad (\text{A.4})$$

represented a lower bound to the shear stress capacity of a section, shear stress being computed in the manner of Eq. A.3. The authors proposed that axial load only affects the diagonal tension strength of a member insofar as it affects the static equilibrium of the member. The axial load does not increase the capacity by changing the properties of the material itself.

Taub and Neville [30,31,32,33,34] in their investigation of shear capacity reported that the effect of  $\rho$ , percentage of tension reinforcement, was to increase the shear strength in beams with shear span ratios greater than 3. If the shear span ratio was less than 3,  $\rho$  did not seem to affect the strength. The authors suggested that beams differing only in the percentage of web reinforcement exhibit the same diagonal tension cracking load. An interesting point made by the authors was that while spacing of the ties was a significant factor the diameter was not.

Taylor [35] reported on the results of his investigation of beams without shear reinforcement using both indirect and direct loading. Indirect loading was applied in a manner similar to that used by Ferguson while direct loading was the conventional direct bearing on the compression face. He found that indirectly loaded beams failed with occurrence of the first diagonal tension crack, while directly loaded beams could attain a higher load than that at first diagonal cracking. The tests had shear span ratios between 1.5 and 5.5.

The report in 1962 of the ACI-ASCE Committee 326 [36] was a comprehensive review of the past investigations on shear and diagonal tension in reinforced concrete members. The recommendations that developed from the review formed the basis for the shear

provisions of the 1963 ACI Building Code [37] and current ACI Building Codes. Since the shear provisions of the ACI Building Codes were used as a guide to the design of the shear reinforcement in the University of Texas investigations, a closer examination of the specifications is warranted. ACI-ASCE Committee 326 adopted the truss analogy to represent the action of the shear reinforcement. The truss analogy for a reinforced concrete beam transforms the beam into a truss, Fig. A.3, where the compression chord of the truss is the concrete compressive block, the tension chord is the tension reinforcing steel in the beam, the posts are the transverse reinforcement, and the compression diagonals are compressive concrete struts. The shear resistance of the beam can then be determined using yielding of the transverse reinforcement as the upper limit on capacity. It did so primarily because (1) it was easy to use, and (2) it seemed to reflect the trend of the experimental data. However, it was suggested that the truss analogy be adjusted to include a contribution to shear capacity due exclusively to the concrete. By doing this, better agreement was found with the experimental data. The concrete contribution was taken to be the amount of shear carried by a beam at the formation of the first diagonal tension crack. This is a conservative assumption, since only in beams with medium to long shear spans would the first diagonal tension crack represent a failure condition. At the limit, a beam without any web reinforcement should be able to carry at least the load required to cause diagonal tension cracking.

The concrete capacity equation presented by ACI-ASCE Committee 321 was primarily developed by Viest, based on the work by Morrow. The final form of the equation was the same equation as in the current ACI Building Code.

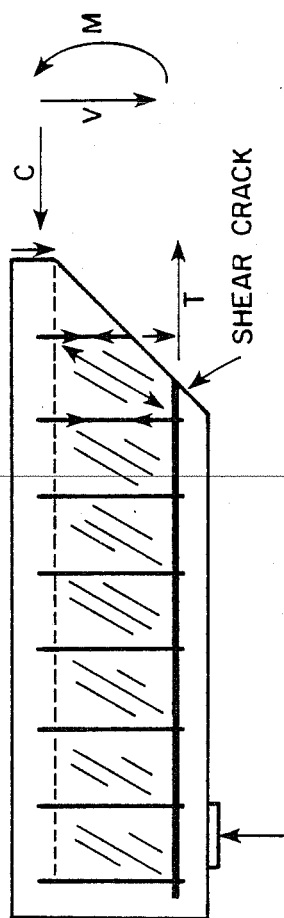


Fig. A.3 R/C beam truss analogy

$$\frac{v_c}{bd \sqrt{f'_c}} = 1.9 + 2500 \frac{\rho V d}{M \sqrt{f'_c}} \leq 3.5 \quad (\text{A.5})$$

The general form of the equation was derived on the basis of a maximum principal tensile stress criterion. A modification to Eq. A.5 was necessary if an axial load was acting on the section. The modification to the equation was a simple reflection of the altered stress state in the beam as a result of the axial load. The term

$$N \left( \frac{h}{2} - \frac{d}{8} \right) \quad (\text{A.6})$$

was subtracted from the moment acting on the section. In Eq. A.6,  $N$  is the applied compressive axial load,  $h$  is the total depth of the section, and  $d$  is the effective depth of the section. Effective depth is the distance from the extreme compression fiber to the centroid of the tension reinforcement.

The final form of the shear equation presented by the Committee was

$$\frac{V}{bd} = Krf_y + v_c \quad (\text{A.7})$$

where  $Krf_y$  was the contribution of the shear reinforcement based on the truss analogy,  $v_c$  was the contribution of the concrete,  $b$  was the total width of the section, and  $d$  was the effective depth.

Moe [38] in his discussion of the ACI-ASCE Committee 326 report first introduced a contribution to shear resistance by aggregate interlock along the flexural crack. He mentioned this effect when he suggested that the reason the ratio of shear span to effective depth ( $a/d$ ) had an effect on shear strength was that it affected the width of the flexural cracks. The width of flexural cracks influenced the effectiveness of aggregate interlock to transfer shear.

Based on the results of twelve beam tests, Bresler and Scordelis [39] questioned the use of the simple addition of the web reinforcement term in Eq. A.7. They suggested  $2\sqrt{f'_c}$  as a simple replacement for the more complicated equation for the concrete shear capacity,  $v_c$ , presented by Committee 326. This was found to be a lower bound to the concrete shear stress capacity in experimental tests.

Fenwick and Paulay [40] concentrated on identifying the mechanisms by which shear was resisted in beams without web reinforcement. They proposed that the principal shear resisting mechanisms were aggregate interlock along the flexural and diagonal tension cracks, dowel action of tension reinforcement, and the flexural resistance of concrete cantilevers between cracks. These three elements are shown in Fig. A.4. Based on their investigation, the authors proposed that the contribution to the total shear resistance by each element was about 60 percent, 20 percent, and 10 percent, respectively. The remaining 10 percent was not specifically related to any particular mechanism. The importance of this paper was the recognition that shear stresses were transferred across cracks. The mechanism of aggregate interlock was not included in shear strength considerations previously.

Haddadin, et al. [41] reported on the results of an investigation into the effect of axial load on the capacity of shear reinforcement. The authors concluded that the effectiveness of web reinforcement was unaffected by the presence of either a compressive or tensile axial load. The authors also suggested that while the shear provisions expressed in the 1963 ACI Building Code were conservative, they did not accurately represent the trends of behavior observed as the parameters were varied. The shear provisions of the 1977 ACI Building Code were almost identical to the 1963 ACI Building Code for the calculation of the concrete shear capacity term.

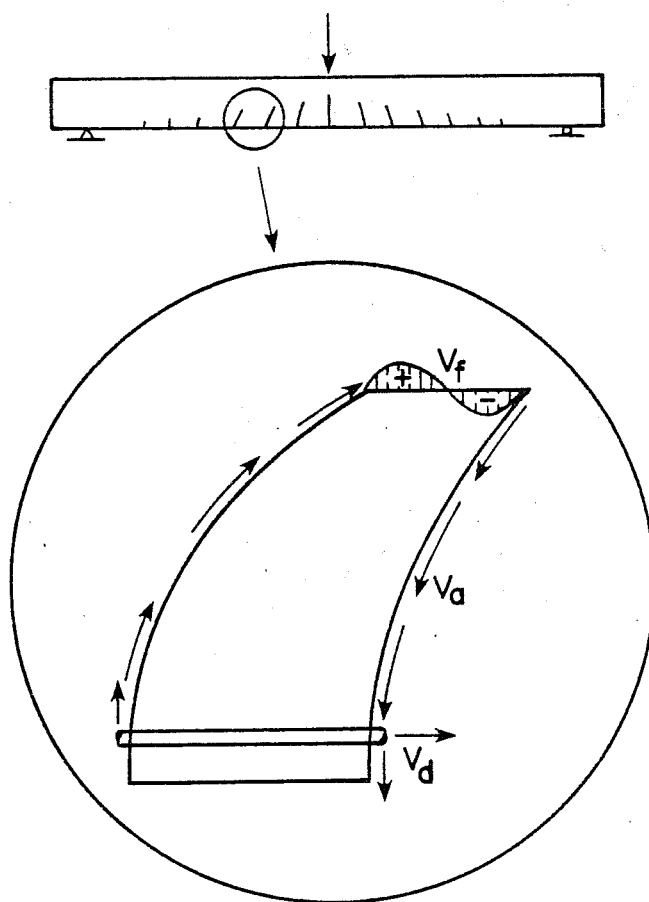


Fig. A.4 Contributing actions to beam shear resistance

Zsutty [42,43] in his two statistical analyses of existing experimental data suggested a different form of the equation for the diagonal tension cracking strength of beams. He divided the beams into two categories based on loading conditions and shear span ratios because such a division gave the best correlation with the experimental data. Zsutty proposed that for beams with a shear span ratio greater than 2.5 or any beam loaded indirectly, such as done by Ferguson, the diagonal tension cracking stress was

$$v_c = \frac{V_c}{bd} = 60 \left( f'_c \rho \frac{d}{a} \right)^{1/3} \quad (\text{A.8})$$

where  $v_c$  = concrete shear stress capacity, psi  
 $V_c$  = concrete shear force capacity, lbs  
 $b$  = total width of member, in.  
 $d$  = effective depth of member, in.  
 $f'_c$  = concrete compressive strength, psi  
 $\rho$  = tension reinforcement ratio,  $A_s/bd$   
 $A_s$  = area of tension reinforcement, sq. in.  
 $a$  = shear span, in.

For directly loaded beams with a shear span to effective depth ratio ( $a/d$ ) less than 2.5, Zsutty proposed that

$$v_c = \frac{V_c}{bd} = 150 (f'_c \rho)^{1/3} (d/a)^{4/3} \quad (\text{A.9})$$

Nielsen, et al. [44] and Thürlimann [45] presented formulations based on plasticity theory for the shear capacity of a beam. The equations presented by Nielsen, et al. required calibration with experimental test results. The approach offered by Thürlimann appears promising but requires additional research to increase its generality. Along the same line is the solution offered by Rabbat [46], which presented a rationale using a variable angle space truss to model the action of reinforcement and concrete. It

was developed primarily for torsion and has not been fully extended to the case of just vertical shear.

Additional sources which proved helpful to the understanding of the present philosophy of the shear resisting mechanisms were papers by Bresler and MacGregor [47], MacGregor and Hanson [48], and the report of the ACI-ASCE Committee 426 [49]. The ACI-ASCE Committee 426 report is a comprehensive review of the research in the area of reinforced concrete shear resistance.

Review of Monotonic Tests--Thus far, the review of previous studies has been devoted to investigations of simply supported beams which provided the experimental basis for the current shear recommendations of the ACI Building Code. In these tests, primarily in the decade between 1950 and 1960, monotonic static loadings to failure were applied. A few of the major points of interest to this study were:

1. Effect of boundary conditions such as method of loading on the shear capacity of a section.
2. Acceptance of the truss analogy despite the physical discrepancies between observed failures and assumed action of the truss analogy.
3. Aggregate interlock along crack surfaces resisting a major part of the shear in beams with no web reinforcement.
4. Suggestions that the equation for concrete capacity in the ACI Building Code did not properly reflect the trend of behavior.

Cyclic Tests--The study of shear failures in members subjected to cyclic reversed loadings has not been of much interest in the United States. Primarily because the design philosophy discourages reliance on a shear failure and stresses the desirability of flexural failures characterized by the formation of plastic



hinges which have stable load capacity at high deformations and the ability to absorb a large amount of strain energy. The result has been a relatively modest effort to observe the effect of high shear on the hysteretic behavior, but little emphasis on developing a predictive behavioral model to describe the phenomena.

Brown and Jirsa [4] in one of the first investigations in the United States on the effect of high shear stresses described the adverse effect on the hysteretic behavior. They concluded that the degradation was initiated by shear forces which led to large shear deformations as a result of sliding along vertical cracks not crossed by stirrups. Their specimen was a cantilever beam with no applied axial load and the cyclic loading was unilaterally applied between quite high deformation limits.

Wight and Sozen [50] in a later study also used cantilever beams, but applied an axial compressive load to the beam as well. The authors presented the following observations:

1. The shear resisting mechanism changed at the onset of spalling cracks in the compressed concrete.
2. Progressive strength and stiffness degradation occurred unless the transverse reinforcement was designed to carry all of the shear.
3. Compressive axial load slowed the degradation in strength and stiffness with cycling.

The authors suggested that the spacing of stirrups not exceed one-fourth of the effective depth, but pointed out that, even so, shear failures may still occur in members subjected to large load reversals.

Tests conducted at the University of California at Berkeley [5,6,51] on cantilever beams concluded that in order to prevent degradation of hysteretic behavior the shear stress in the beam

must be less than  $3.5 \sqrt{f_c}$ . In addition, they emphasized the need for closely spaced ties and the importance of properly restraining the longitudinal bars by having each bar enclosed by a bend in a tie. Special methods of web reinforcing were suggested to better resist the effects of shear stresses.

The emphasis in the Japanese investigations has been on short columns and the prevention of shear failures and other degrading type failures. The emphasis was prompted by the column shear failures in the 1968 Tokachi-Oki earthquake in Japan.

Ohno, et al. [52] reported the results of an investigation on short columns in a two-story, one-bay frame shown in Fig. A.5. They observed that the crack pattern in axially loaded specimens was no different than that of specimens with no axial load. Also, the cracking was generally limited to the end regions of the column until failure, when a large diagonal crack formed in the midheight region of the columns.

Higashi and Ohkubo [53] reported that the behavior of short columns could be determined simply by considering the clear height-to-depth ratio ( $L_c/h$ ). This was the primary variable in their tests, shown in Fig. A.6. The authors reported that for  $L_c/h$  less than 2 the failures were primarily diagonal tension, for  $L_c/h$  between 2 and 4 the failures were a combination of shear and flexure, while for  $L_c/h$  greater than 4 the failures were flexural. The authors also compared dynamic to static loading and found that the hysteretic characteristics were similar.

Kokusho and Ogura [54] presented the results of cyclic tests which were demonstrative of the effects of certain parameters. In Fig. A.7, the load-deflection curves for specimens identical except for the amount of longitudinal steel illustrated the impact of increasing the flexural capacity of a section while holding the shear capacity approximately the same. The specimen with a longitudinal column reinforcing ratio ( $\rho$ ) of 1.94 percent, Fig. A.7 (b),

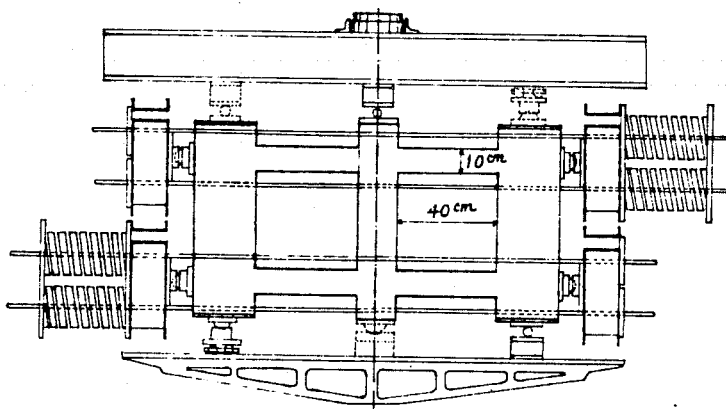


Fig. A.5 Test setup of Ohno, et al. [52]

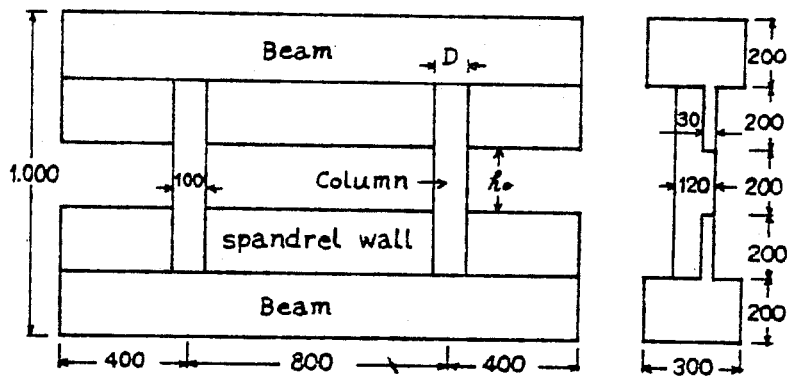


Fig. A.6 Test specimen used by Higashi and Ohkubo [53]

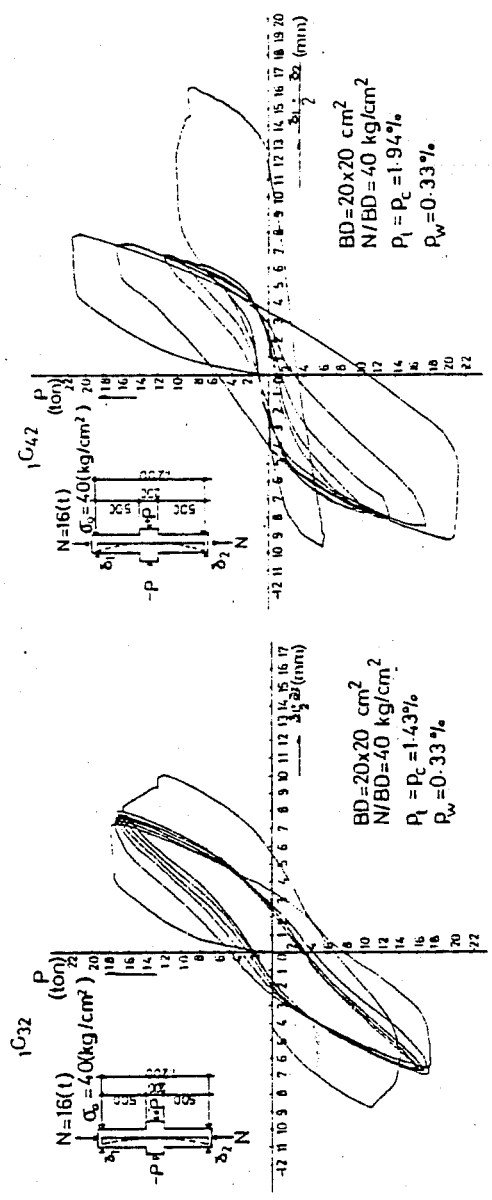
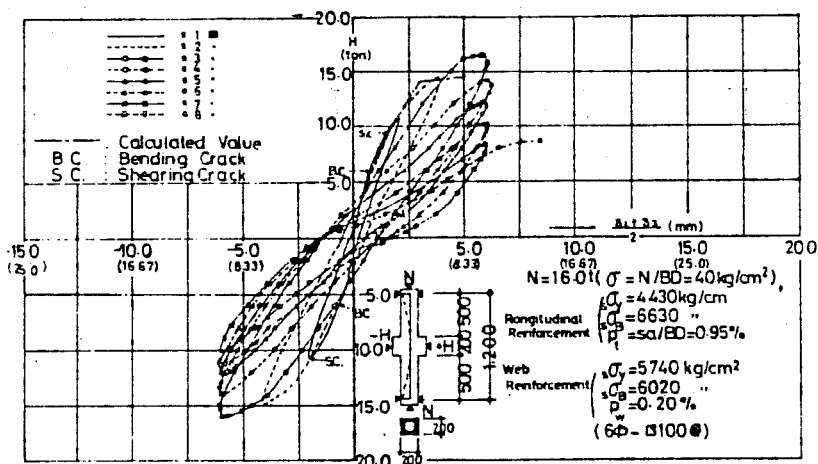


Fig. A.7 Effect of longitudinal reinforcement ratio (Kokusho and Ohura) [54]

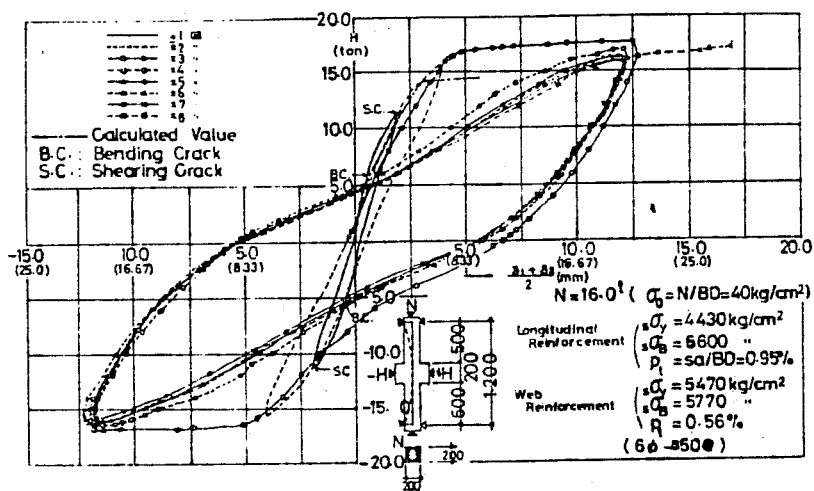
suffered a rapid degradation in lateral load capacity with cycling, while the specimen with 1.43 percent, Fig. A.7(a), did not. Figure A.8 showed the difference in the hysteretic behavior for specimens with different amounts of transverse reinforcement. The specimen shown in Fig. A.8(b) had twice the amount of transverse steel as the specimen in Fig. A.8(a), and demonstrated stable hysteretic loops, while the specimen in Fig. A.8(a) exhibited degrading hysteretic loops. The effect of axial compressive load versus no axial load was demonstrated by the specimens in Fig. A.9. Figure A.9(a) shows the results for a specimen with no axial load and Fig. A.9(b) for a specimen with axial load. Notice that the loops for the specimen with no axial load were more pinched toward the origin than those with axial load.

Minami and Wakabayashi [55] tested specimens shown in Fig. A.10. The authors were particularly interested in the effect of beam stiffness on the column behavior, but they also varied the amount of web reinforcement, the axial load, and the  $L_c/h$  ratio. The authors reported that increased compressive axial load increased the maximum strength of the frame, but it also caused much more deterioration of the load capacity after attainment of the maximum capacity. The authors reported that increased beam stiffness resulted in an increased amount of energy absorbing capacity.

Yamada [56] proposed that reinforced concrete member behavior could be classified into two principal types, one being predominantly shear in short members and the other being predominantly bending in long members. He suggested that the parameter which best determined the kind of behavior a member would exhibit was shear span ratio. Yamada presented an equation which indicates the shear span ratio at which the transition between predominantly shear and predominantly flexure dominated behavior occurs. The variables in the equation were primarily axial load and the amount of longitudinal steel in the section.

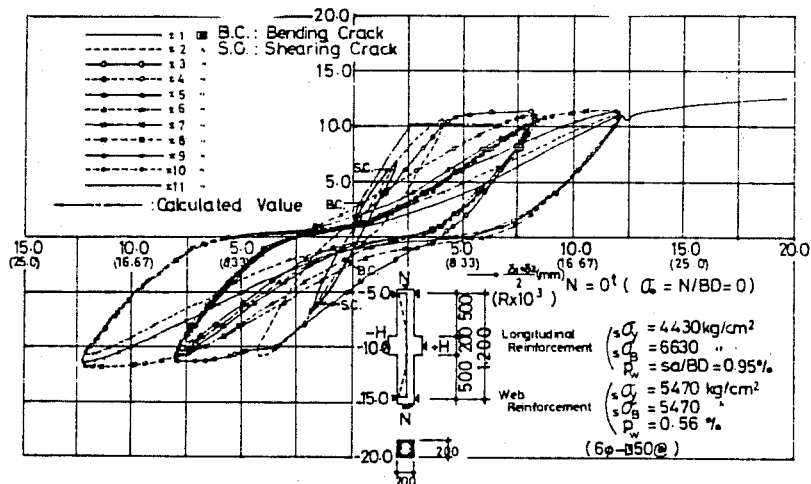


(a)  $\rho_s = 0.0020$

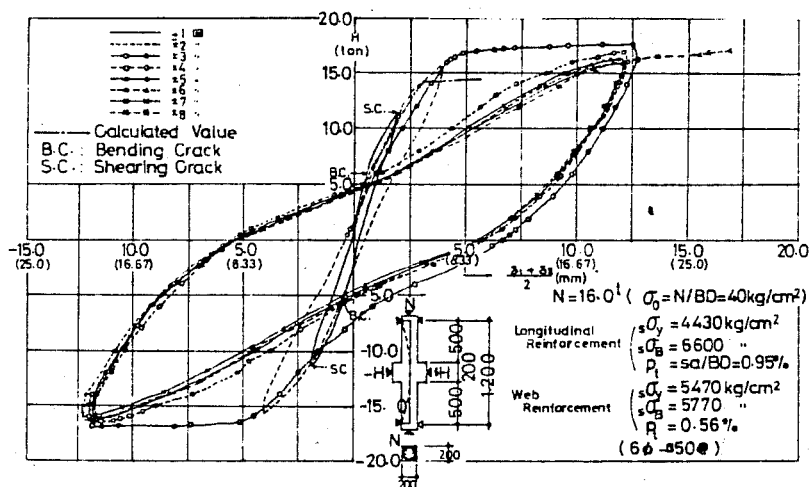


(b)  $\rho_s = 0.0056$

Fig. A.8 Effect of transverse reinforcement ratio (Kokusho and Ogura) [54]

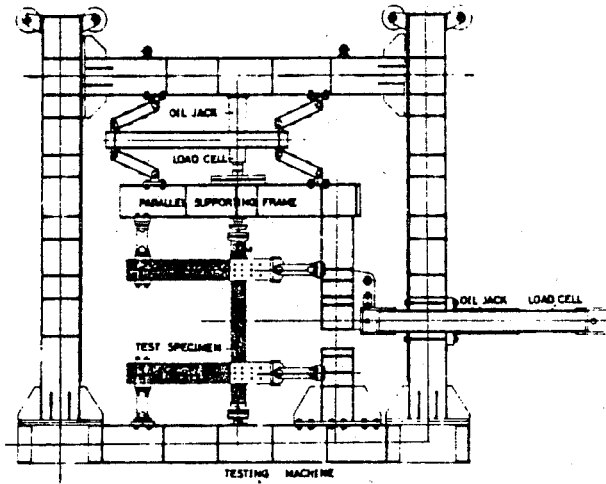


(a) N = 0 kips

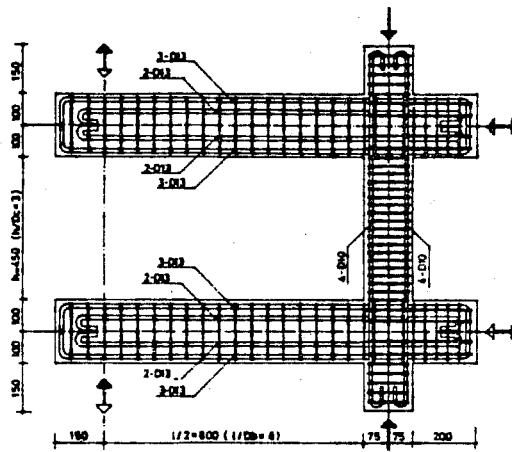


(b) N = 32 kips

Fig. A.9 Effect of axial load  
(Kokusho and Ogura) [54]



(a) Loading system



(b) Test specimen

Fig. A.10 Test used by Minami and Wakabayshi [55]

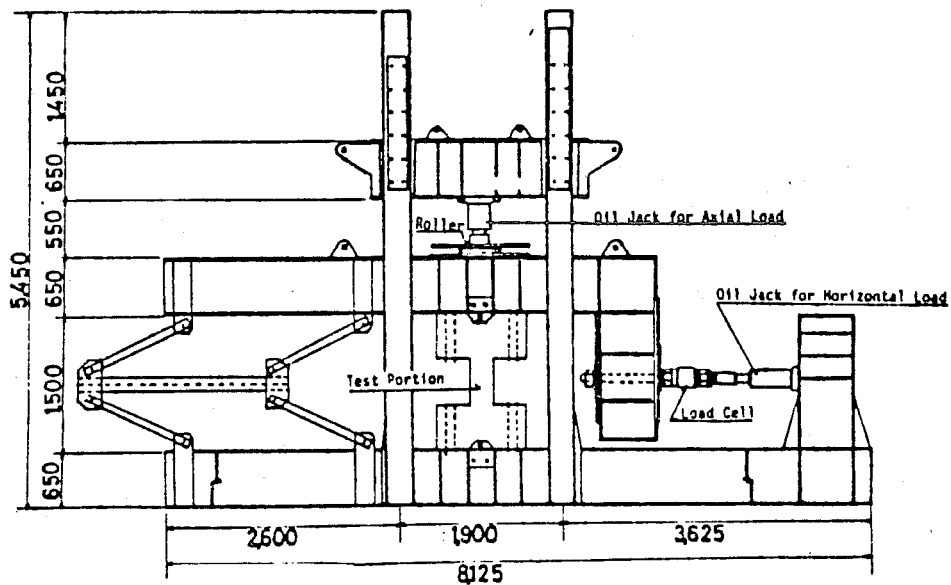


Hirosawa, et al. [57] reviewed a large experimental research program on reinforced concrete columns conducted in Japan. The authors described the loading system and test specimen developed for the investigation at the Building Research Institute of Japan, Figs. A.11(a) and A.11(b), respectively. Little data were presented but the authors concluded that if the shear stress in the column was more than 425 psi the column would fail in a brittle manner despite heavy web reinforcement.

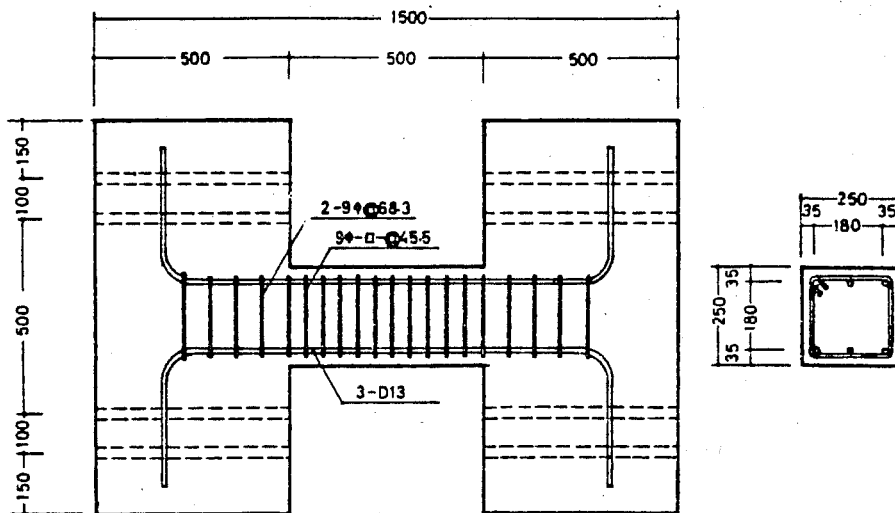
References 58, 59, and 60 provide a valuable source of experimental data on short columns subjected to cyclic reversed lateral loadings. The material in the references are load-deflection curves and crack patterns from a number of unidirectional short column tests. The tests were done at several Japanese research facilities. No conclusions or descriptions of particular tests were presented.

The two investigations in The University of Texas at Austin research program which preceded the present investigation were unique in that they were the first to investigate short columns (or columns under high shear stresses) subjected to cyclic bidirectional deformations. In addition, much of the loading system, test apparatus, and test specimen configuration used in the current investigation was developed in these studies.

In both investigations the same specimen, Fig. A.12, and loading system, Fig. A.13, was used. The specimen was purposely designed to have a shear capacity less than that required to develop full plastic hinging at the ends. The effect of high shear stresses on behavior would then be more apparent. The general shape of the specimen and loading system were modeled on those used by the Building Research Institute in Japan, except that the current loading system can apply bidirectional deformations as well as an axial load.



(a) Loading system



(b) Test specimen

Fig. A.11 B.R.I. loading system and test specimen [58]

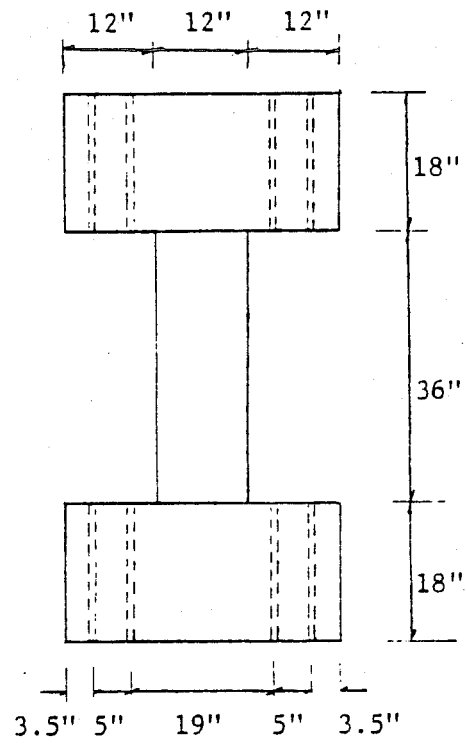


Fig. A.12 Specimen used by  
Maruyama and Ramirez

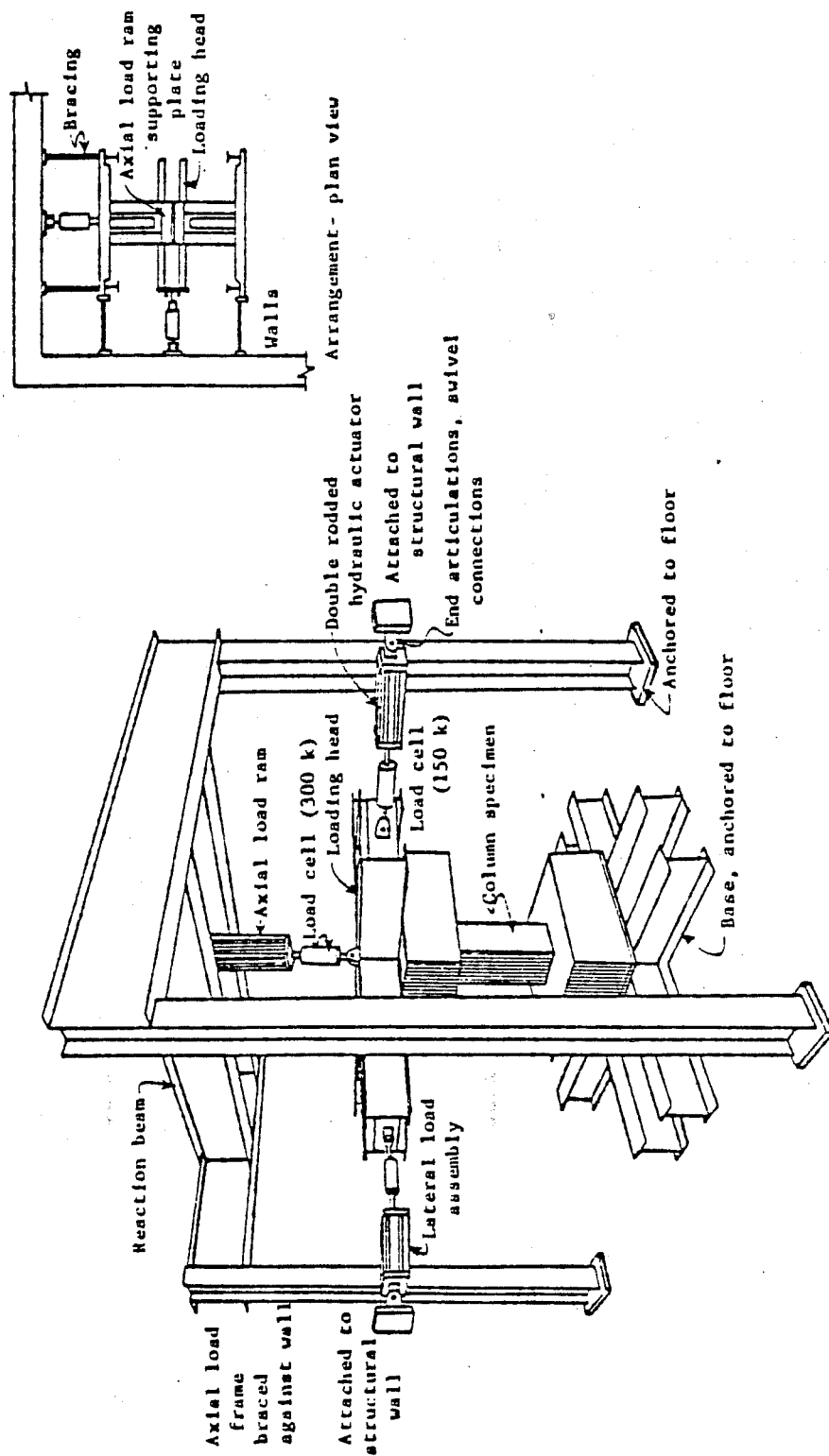


Fig. A.13 Loading system used by Maruyama and Ramirez [15]

Maruyama [14] conducted a series of tests in which the only variable was the deformation path imposed on the specimens. Some of the deformation paths are shown in Fig. A.14 in schematic form. Figure A.14 shows the paths of the top of the specimen (in a horizontal plane) as seen from above the specimen. The loading history consisted of the deformation path repeated three times at each deflection level. A typical loading history is shown in Fig. A.15 (case (a) in Fig. A.14). Based on a series of ten tests, the following conclusions were presented:

1. Deformation path was relatively unimportant as long as the deflection level imposed on the specimen was less than the deflection at which the maximum shear capacity was reached in a monotonic test.
2. Deformation paths which involved reversals along the same line such as cases c and d in Fig. A.14 caused the same response if the axes of the load and deflection measurements were along the line of deflection.
3. Deformation paths which involved a grinding motion on the column, case e in Fig. A.14, caused severe and rapid degradation of the lateral load capacity of the column.

Ramirez [15] investigated the effect of both compressive and tensile axial load on the behavior of short columns. Two deformation paths were used, one unidirectional and the other bidirectional (cases a and c in Fig. A.14). One value of axial compression was used, but three different tensile axial loads were used corresponding to  $1/4$ ,  $1/2$  and full tensile yielding. In addition, tests using an alternating tension and compression axial load were conducted. Based on a series of ten tests, Ramirez presented the following conclusions:

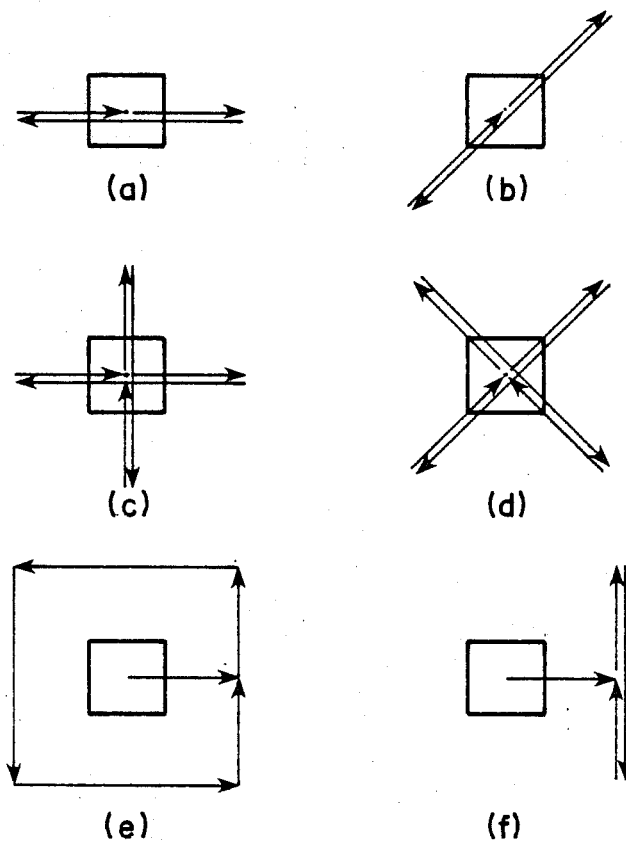


Fig. A.14 Deformation paths used by Maruyama

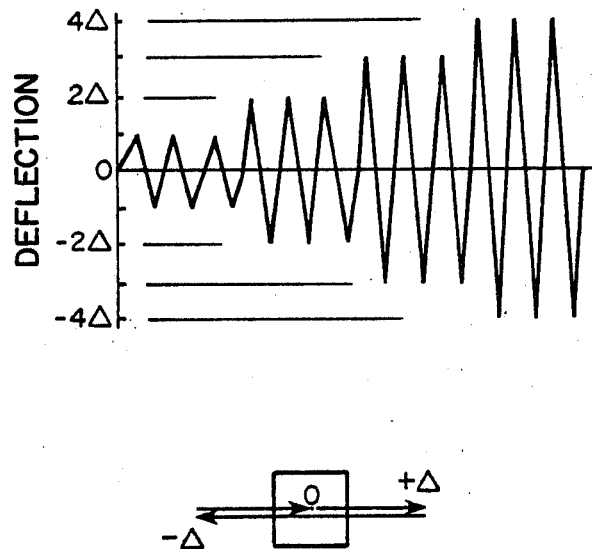


Fig. A.15 Typical loading history  
(Maruyama and Ramirez)

1. Constant compressive axial load accelerated shear degradation and reduced the energy dissipation capacity of the column.
2. Constant tensile axial load drastically reduced the maximum shear capacity of the column, but the deterioration of the capacity was reduced.
3. The confinement and shear strength provided by the ties dictated the overall response of the column.
4. Lateral deflections applied in an orthogonal direction, cycling, and compressive axial load all tended to reduce the efficiency of the ties to confine the core.

Shear Friction Concept--A supplemental mechanism for resisting shear is shear friction or the ability to transfer shear across a crack in concrete. The concept comes into play for both the contribution of aggregate interlock to the shear resistance of beams and the shear resistance across construction joints in walls and other primarily vertical elements.

Birkeland and Birkeland [61] presented a discussion on shear friction as a possible analytical tool for the proper design of connections such as corbels. The authors presented the following equation for the ultimate shear capacity at a section:

$$V_u = T_u \tan\phi = A_s f_y \tan\phi \quad (\text{A.10})$$

where  $A_s$  = total cross-sectional area of reinforcing across interface

$f_y$  = yield strength of reinforcing ( $\leq 60$  ksi)

$\tan\phi = 1.7$  for monolithic concrete

$\tan\phi = 1.4$  for artificially roughened construction joints

$\tan\phi = 0.8$  to  $1.0$  for ordinary construction joints and for concrete to steel interfaces

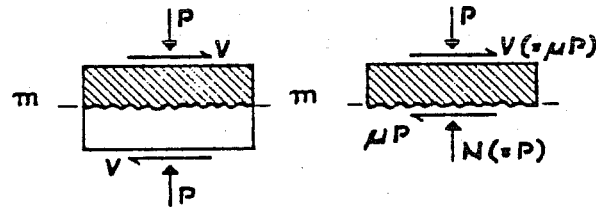


The form of the equation is very similar to the equation adopted by the ACI Building Code in its provisions for shear-friction. The concept of shear-friction is straight-forward and is described in Fig. A.16, taken from Ref. 61. In the absence of reinforcement across the crack, the shear which can be transferred is a function of the externally applied compressive axial load. The stress transfer concept is identical to Newtonian friction. If reinforcement crosses the crack and the two surfaces move laterally, the surfaces separate as they ride over the roughened surface. The separation elongates the reinforcement, stressing it and thus applying the normal compressive force on the cracked surface.

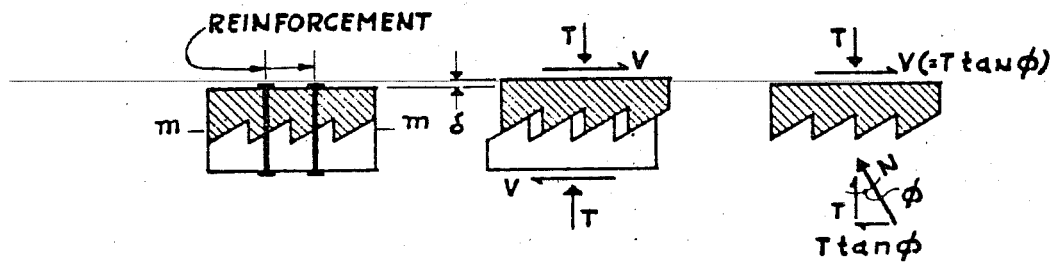
Hofbeck, et al. [62] reported an experimental investigation of the shear transfer capacity across cracked and uncracked concrete planes. The specimen used in the investigation is shown in Fig. A.17. The authors found reasonable agreement between the test results and the general concept outlined by Birkeland and Birkeland, though the authors gave more substantiated recommendations as to the limits on the equation than did Birkeland and Birkeland.

Mattock and Hawkins [63] continued and expanded the work done by Hofbeck, et al. Three types of specimens, Fig. A.18, were used in the investigation to more fully explore the effect of both parallel and normal external stresses on the shear transfer capacity of the cracks. A hypothesis for the behavior was presented and a more general equation for the ultimate shear transferable across the section was given. The equation included both the effects of externally applied compressive stresses and reinforcement crossing the crack.

The preceding papers were concerned with the monotonic ultimate shear capacity of cracked concrete. Obviously, these conditions do not directly reflect the conditions imposed on the test specimens of the current investigation. Laible, et al. [64]



(a) Without reinforcement



(b) With reinforcement

Fig. A.16 Shear-friction concept [61]

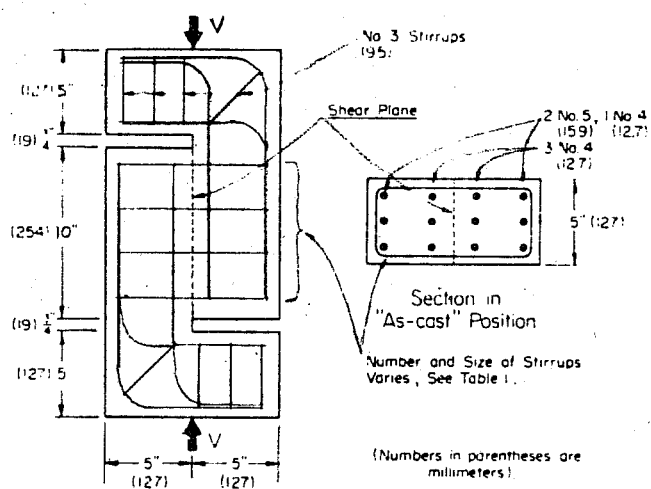


Fig. A.17 Shear-friction test specimen used by Hofbeck, et al. [62]

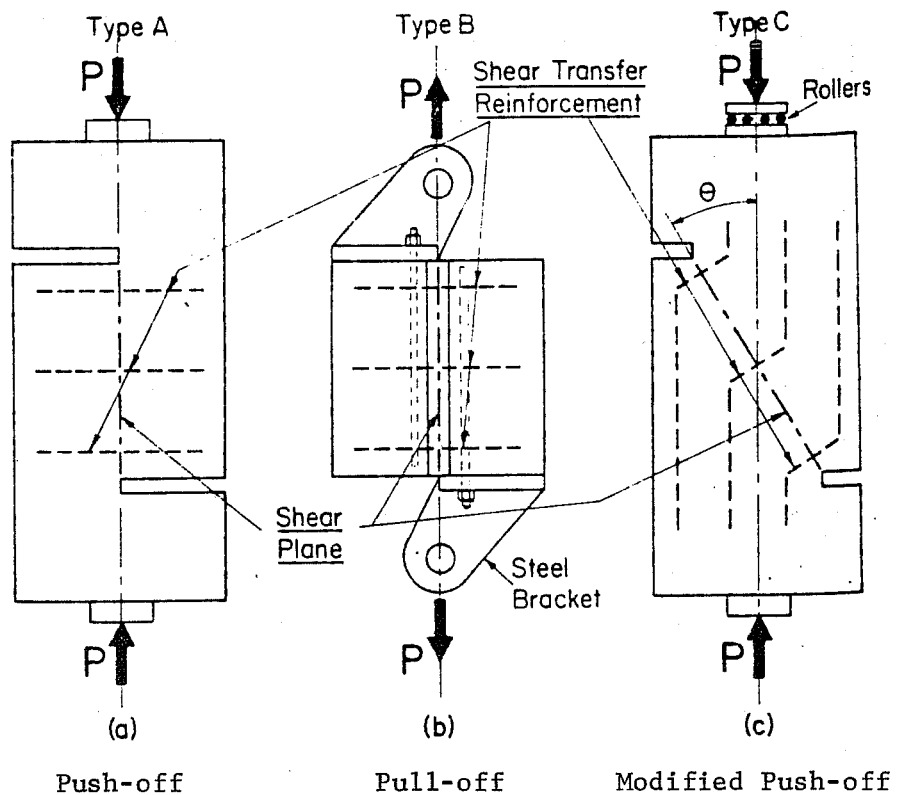


Fig. A.18 Shear-friction specimens used by Mattock and Hawkins [63]

reported a study of the effect of cycling on the shear transfer capacity across a crack. Other parameters were varied, but for the current investigation the effect of cycling is the most important. The specimen and loading system is shown in Fig. A.19. The concrete test block was cast monolithically and then prior to testing a crack was formed by using wedges in v-notches on the sides of the block. One-half of the block was then moved across the other during loading. Axial compression was applied to the block through external restraining rods to simulate the action of reinforcing steel crossing the crack. The observed behaviors were highly dependent on a number of variables, such as initial crack width, but the effect of cycling was to cause rapid degradation of both the stiffness and shear capacity. The specimens in the investigation were cycled between shear stress levels rather than between deflection levels, but an indication of the effect of cycling is given in Fig. A.20, which shows a typical shear stress versus slip curve.

1.4.2 Flexure. The computation of the flexural capacity of a column for a static, monotonic loading is well-documented and no discussion of it will be given. Any reference on reinforced concrete design (such as by Park and Paulay [65]) will provide a satisfactory approach to the problem. The flexural mechanism, unlike the shear mechanism, is a relatively well-understood phenomenon. Because the flexural capacity is well-defined and reliable, it has generally been used as the controlling capacity in design for both monotonic and cyclic loading conditions. The flexural capacity is used because it can be made stable even at high member deformations as typified by a bilinear or trilinear moment-curvature relation for a reinforced concrete section.

Numerous research projects have been reported in which the flexural characteristics of the hysteretic loops of reinforced

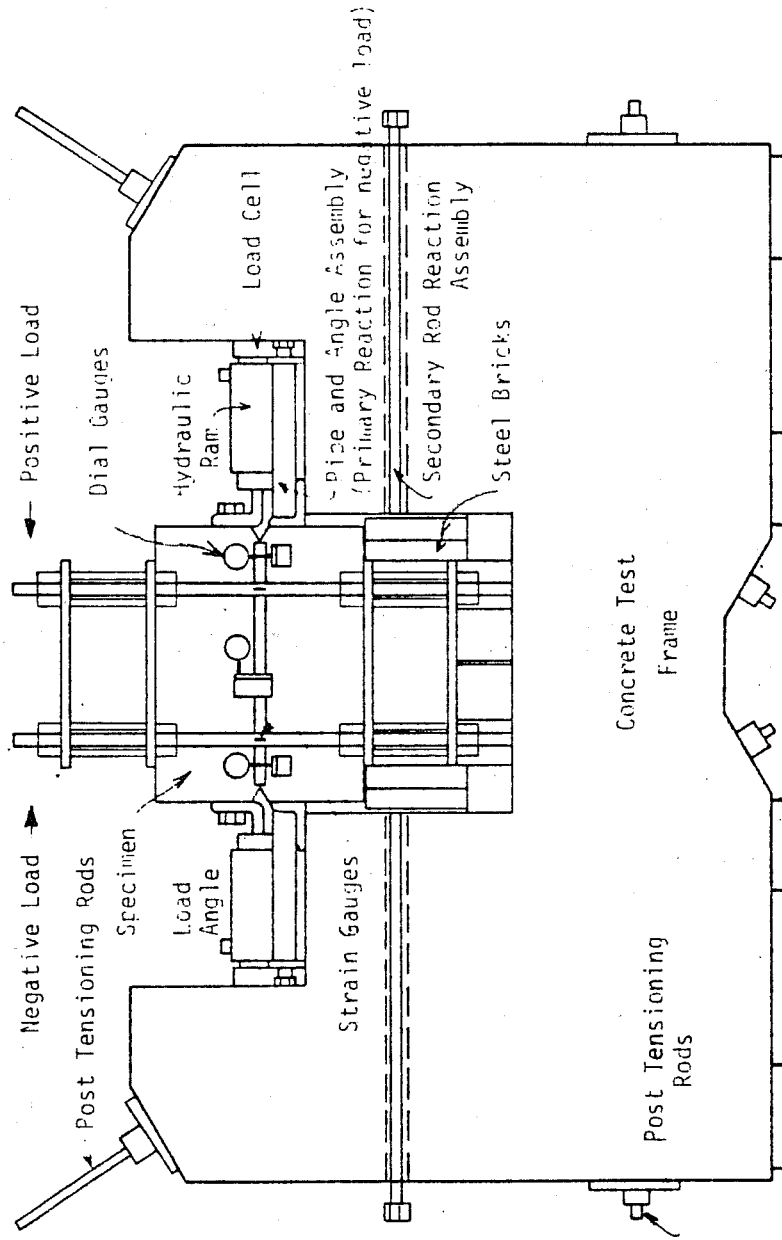


Fig. A.19 Test setup used by Laible, et al. [64]

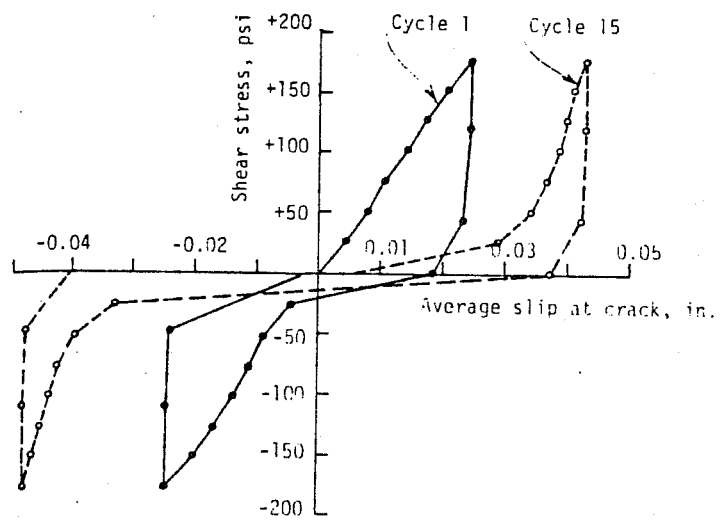


Fig. A.20 Shear stress versus slip across crack [64]

concrete members subjected to cyclic reversed loadings were examined. Generally, the investigations studied the development of an hysteretic model or the examination of the effect of variable changes on the behavior for the purpose of developing design recommendations.

Takeda, et al. [7] conducted a series of tests on medium length cantilever beams representing columns. The main thrust of the experimental research was to provide data on which a hysteretic model could be developed. The test specimens, Fig. A.21, were subjected to quasi-static load reversals. The analytical hysteretic model was based on a trilinear skeleton curve and subsequent loadings and unloadings were described by a set of empirical rules. The skeleton curve and an example of an analytical hysteretic curve are shown in Fig. A.22. A major consideration in the analytical model was that while provisions were included to model the experimentally observed stiffness degradation, it was assumed that the curve would always reach the skeleton curve at the peak displacement. There was no provision for load degradation because in a specimen dominated entirely by flexure, such load losses were very small.

Penzien, et al. [66] discussed the results of a test program which examined several aspects of cyclic behavior in reinforced concrete members. The authors reported that in a doubly reinforced symmetric beam, cyclic reversed loadings reduced the instantaneous stiffness of the beam, but the ultimate strength, curvature, ductility, and energy absorption were increased compared with a nonreversing cyclic loading. The desirable nature of such flexural hysteretic characteristics is illustrated in Fig. A.23. The authors suggest that in critical regions under reversed cyclic loading beyond initial yielding, the behavior was controlled by the mechanical characteristics of the reinforcing steel and that



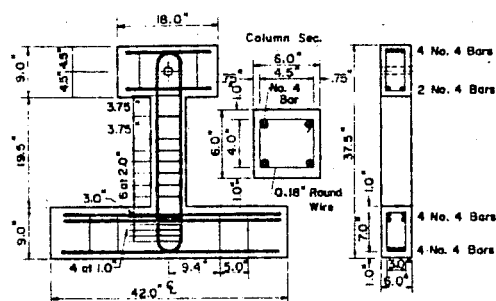


Fig. A.21 Takeda's test specimen [7]

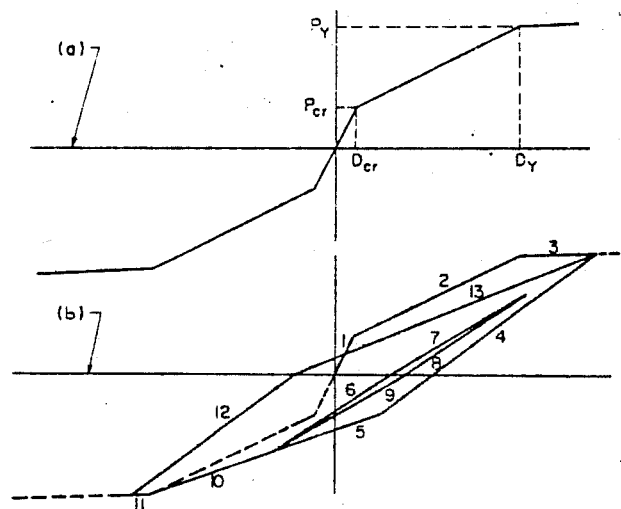


Fig. A.22 Example hysteresis curve using Takeda's model [7]

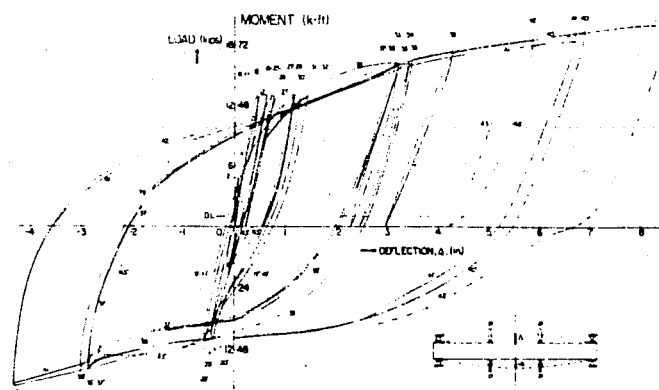


Fig. A.23 Flexural hysteresis loops [66]

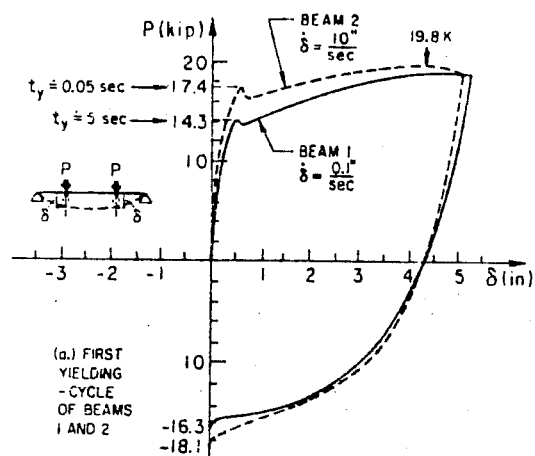


Fig. A.24 Effect of strain rate on load-deflection relation [66]

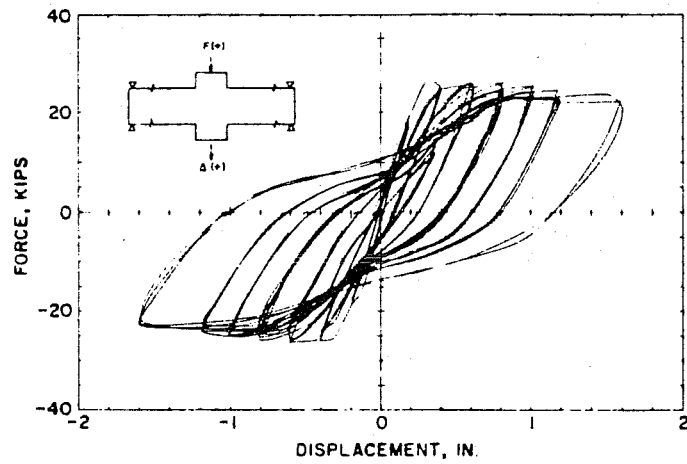
changes in these characteristics result from Bauschinger's effect and bond deterioration between the flexural cracks.

Figure A.24 depicted the first half-cycle of two beams loaded at different rates. The authors concluded that increased rates of loading only had a significant effect on the characteristics at and prior to first yielding of the reinforcement.

Figure A.25 illustrated the observed effect of compressive axial load. Figure A.25(a) had a lower level of axial load than the specimen in Fig. A.25(b). The effect of higher axial load was to increase the initial stiffness and peak load capacity, but to cause a deterioration in behavior at high displacement levels. Figure A.26 depicted the effect of shear span ratio on the observed behavior with the load-deflection curves shown in Fig. A.26(a) for a specimen having a higher shear span ratio than the one in Fig. A.26(b). The effect seems to be a significant pinching of the hysteretic loops.

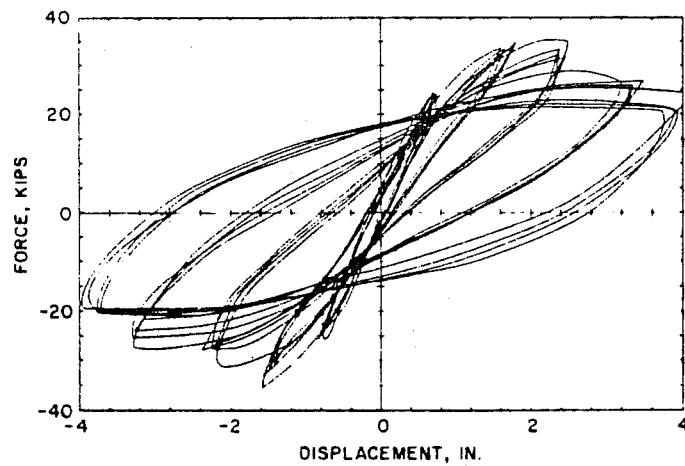
Atalay and Penzien [67] presented an analytical model for the hysteretic characteristics of reinforced concrete members which included provisions for load degradation with cycling. An example of the results of their model is shown in Fig. A.27. Notice the degrading skeleton curve and the reduction in load capacity with cycling at the point marked A on the curve. The authors reported good agreement between their model and test results obtained using a center stub beam subjected to reversed loadings. The authors did not discuss the reason for degradation. It should be noted that the beams tested were quite long to limit shear stresses and only one beam configuration was used.

Otani, et al. [68] reported a series of tests on cantilever beams subjected to cyclic bilateral loadings. The beams exhibited a flexural failure mode and the authors concluded that a degrading trilinear model gave analytical hysteretic curves which fairly closely modeled the observed hysteretic loops.



Hysteretic behavior - Specimen No. 3,  
Axial load =  $60^k$ , Lateral reinforcement  
spacing = 3 inches.

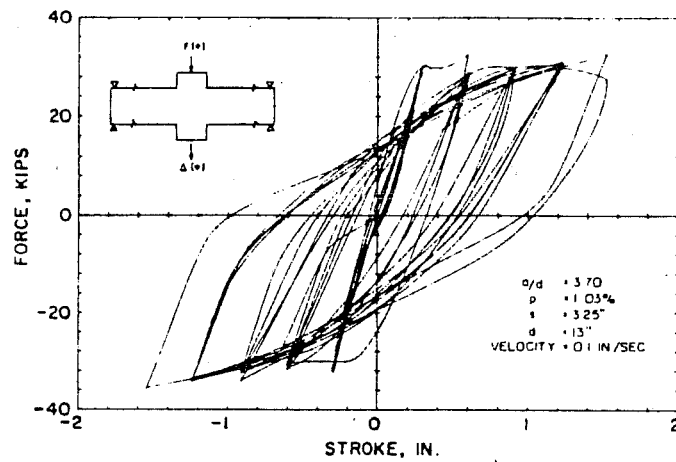
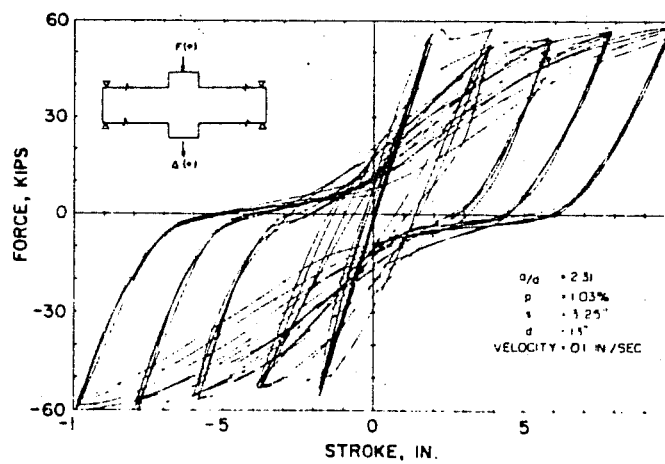
(a)  $N = 60$  kips



Hysteretic behavior - Specimen No. 9  
Axial load =  $180^k$ , Lateral reinforcement  
spacing = 3 inches.

(b)  $N = 180$  kips

Fig. A.25 Effect of axial load  
(Penzien, et al.) [66]

(a)  $a/d = 3.70$ (b)  $a/d = 2.31$ Fig. A.26 Effect of shear span ratio  
(Penzien, et al.) [66]

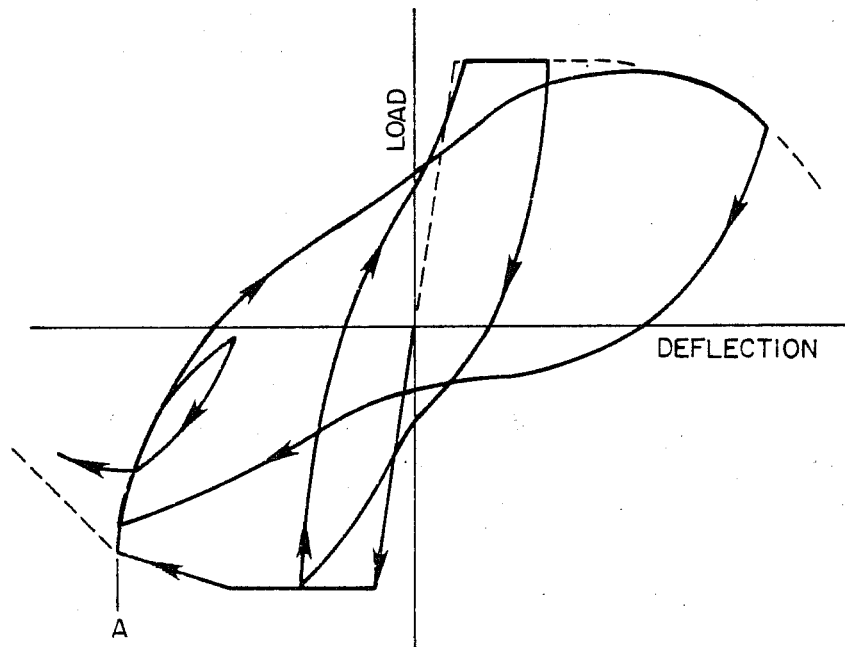
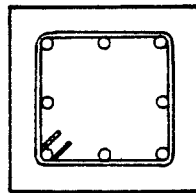


Fig. A.27 Degrading hysteresis model  
Atalay and Penzien [67]

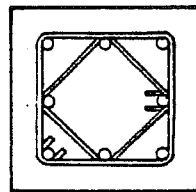
1.4.3 Confinement. A number of investigators have studied the effect of confinement on the behavior of reinforced concrete members [69,70,71,72,73,74,75,76]. Most of these investigations studied prisms or short members subjected to a concentric monotonically applied axial compressive load. A few have studied the effect of web reinforcement on the rotational capacity of the compression block in a monotonically loaded beam. Research into the effect of confinement on members similar to those used in the current investigation which involves both axial loading and bending is limited.

The research to date has been somewhat contradictory regarding the effect of confining steel. All investigators agree that confinement significantly improves the deformation capacity of concrete; however, there is disagreement as to whether confinement increases the compressive strength of concrete. Sheikh [69] presented an extensive review of the literature on confinement in addition to reporting on his own investigation on concentrically loaded columns. He suggested that many of the discrepancies in previous test results came from the fact that widely varying specimen types were used in the investigations. He especially pointed to specimens which were quite small and specimens without cover as reasons for the differences in conclusions. Sheikh proposed that confinement increases the compressive strength of concrete above the value obtained from cylinder tests,  $f'_c$ . He proposed that confinement is a function of both the longitudinal steel and the transverse steel and that single ties were not nearly as effective as multiple ties (shown in Fig. A.28) because single ties did not effectively restrain the center longitudinal bars on each face.

Kent and Park [77] suggested a stress-strain curve for concrete in flexural members based on experimental investigations of confinement by rectangular ties. The form of the curve is shown in Fig. A.29. The curve accounts for confinement by adjusting the



SINGLE TIE



MULTIPLE TIE

Fig. A.28 Tie arrangement



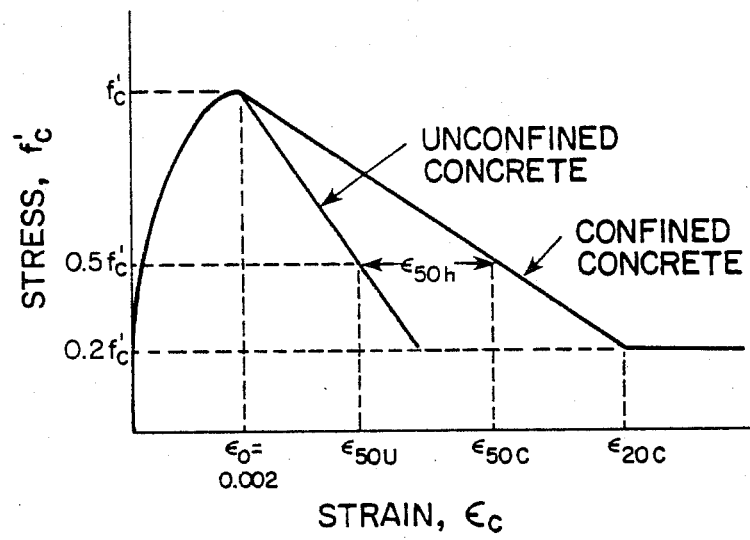


Fig. A.29 Kent and Park's concrete stress-strain curve [77]

slope of the descending branch of the curve and setting a minimum value of concrete stress equal to 20 percent of the concrete compressive strength. The slope of the descending branch is primarily related to the percentage of transverse reinforcement.

Sheikh [69], based on a detailed review of previous data and the results of his own investigation, proposed a stress-strain curve similar to that shown in Fig. A.30. The quantitative expressions which define the curve are fairly complex and account for a larger number of variables than other stress-strain curves. The maximum stress attainable by the section can be greater than the value of  $f'_c$  and depends on the amount of confinement provided. Sheikh reported good correlation between test and computed results, but he considered only concentrically loaded axial specimens.

1.4.4 Buckling of Reinforcement. The buckling of reinforcement has been a fairly common occurrence in cyclic reversed loading tests. The recommendations for preventing it usually have been empirical, though some analytical justification is sometimes offered.

Ruiz and Winter [78] discussed bar buckling in their report on a test series of cyclically loaded simply supported beams. The approach used by the authors was to consider the stability of the bar neglecting any restraint of concrete above the bar. The bar was modeled as an axially loaded continuous strut with the stirrups acting as elastic supports. The authors assumed buckling could only occur outwards and used an energy method to find the buckling load. The result of their study was that buckling could not be predicted using the above approach and the authors concluded that random variations in tie and concrete restraint must have been responsible for bar buckling.

Brown [79] used a similar approach to Ruiz and Winter except that he used the tangent modulus theory to predict buckling

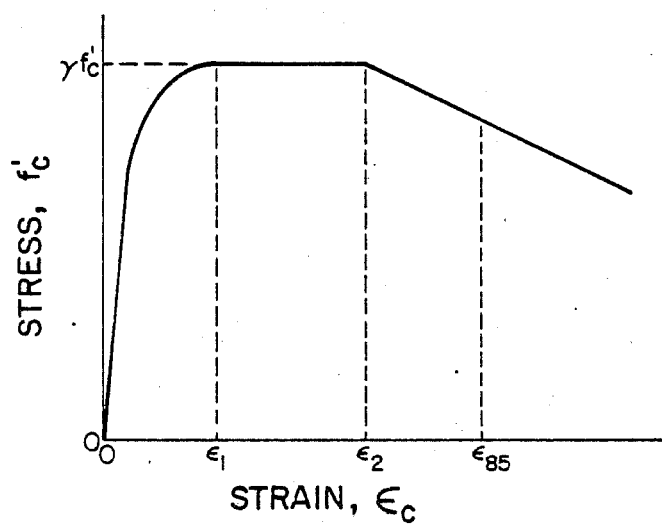


Fig. A.30 Sheikh's concrete stress-strain curve

and assumed that buckling of the bar would occur in the first mode between two ties. No comparisons were made between the test results and the predictive equation.

Bertero and Collins [80] based on observations of failures and analytical studies not described suggested that the spacing of the lateral support (ties) should be no more than 6 to 8 diameters of the bar being restrained.

It is clear that there is no reliable criterion which will assure the designer that buckling will not occur. The previous investigations have generally looked at the elastic solution to buckling making a number of simplifying assumptions.

#### 1.4.5 Bond.

Monotonic Tests--Lutz [81] investigated the mechanism of bond both experimentally and analytically using a finite element method. In addition, he reviewed and incorporated the experimental results of past investigations on bond. A brief summary of the major points presented by Lutz are listed below:

1. While the ultimate bond capacity of a deformed bar was not independent of bar diameter, it was not a linear function of bar diameter as assumed in the 1963 ACI Building Code.
2. The bar diameter influenced the ultimate bond capacity in about the same proportion as longitudinal tension steel affects shear capacity of a beam without web reinforcement.
3. Transverse binding reinforcement around the bars significantly improved the bond strength.

In a state of the art paper, ACI Committee 408 [82] reviewed the results of research prior to 1966. The paper stated that in

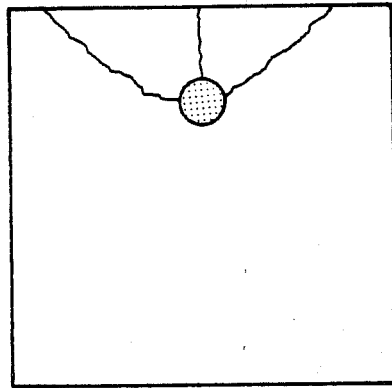


Fig. A.31 Bond splitting

pullout tests using deformed bars the failure was almost always a splitting failure where the concrete developed cracks radially outward from the bar which split the concrete into two or more sections. An example of splitting is shown in Fig. A.31. The exceptions were usually small diameter and top bars where the failure was shearing of the concrete by the bar lugs. In discussing splitting, Committee 408 stated that clear cover over a bar and stirrups were significant parameters in the ultimate bond capacity. In beams, Committee 408 reported that the stirrups must be in excess of the amount necessary for shear reinforcement before they improve the ultimate bond strength.

Orangun, et al. [83], in their examination of existing test data, developed an equation for development length which has been incorporated into a recommendation for the ACI Building Code by ACI Committee 408 [84]. In the paper by Orangun, et al., the basis for the current equation for development length was described as being an adoption of the ultimate bond stresses in ACI 318-63, with the assumptions that the bond stress was uniform along the bar and the bar had to develop at least 125 percent of the yield stress of the bar. The authors found poor agreement between the results of the ACI Building Code equation and the test results. The authors presented an equation which accounted for cover around the bar, the number of bars in a layer, and the effect of reinforcement crossing the splitting cracks. Primarily, the development of the equation was based on experimentally observed crack patterns at failure, shown in Fig. A.32, taken from Ref. 83. The equation proposed by the authors for bars with a nominal yield of 60 ksi was:

$$l_d = \frac{10200d_b}{\sqrt{f'_c} \phi (1 + 2.5C/d_b + K_{tr})} \quad (A.11)$$

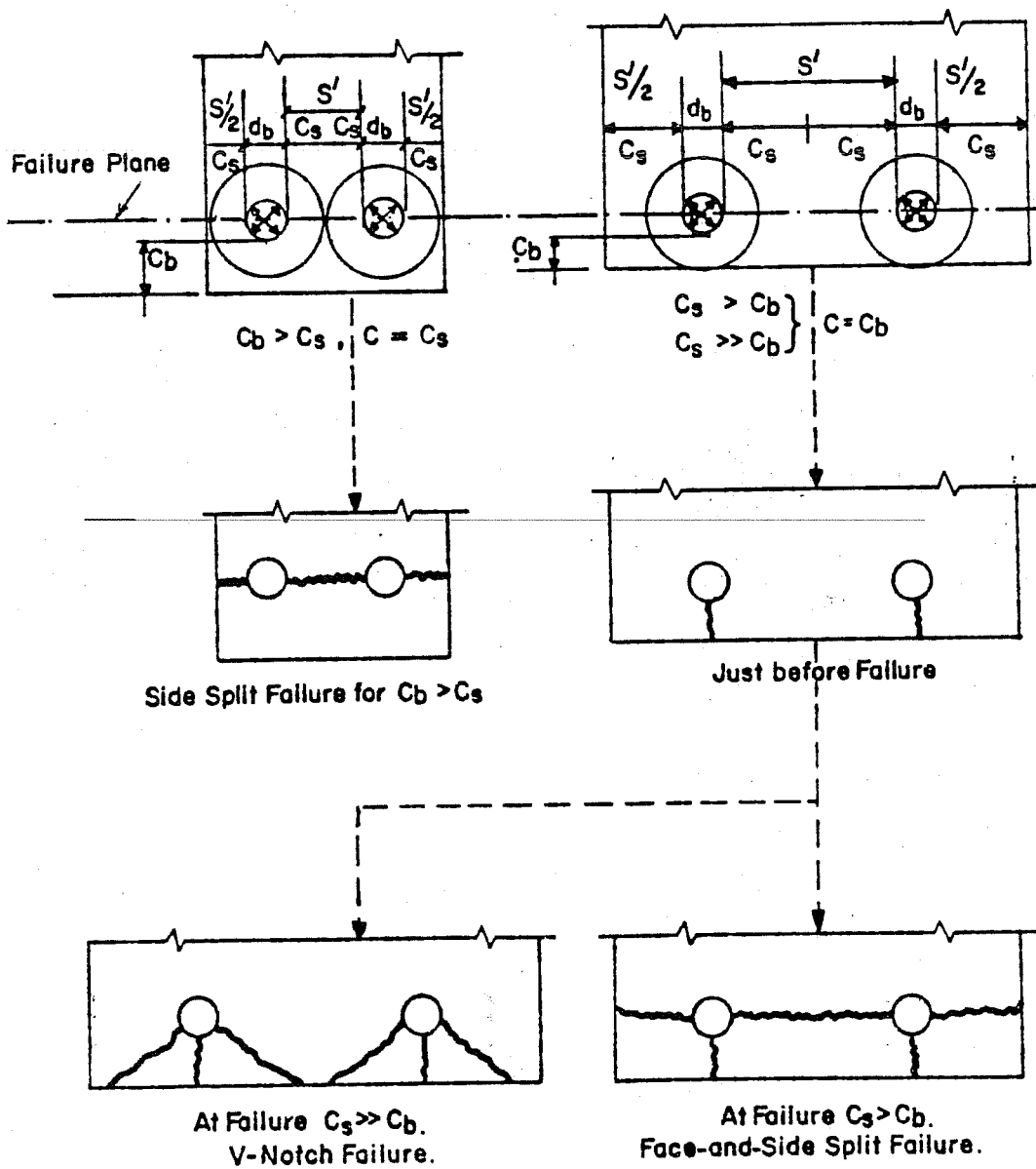


Fig. A.32 Bond failure patterns [83]

where  $l_d$  = development length of the bar (tension), in.  
 $d_b$  = nominal diameter of bar, in.  
 $f'_c$  = concrete compressive strength, psi  
 $C$  = the smaller of  $C_b$  or  $C_s$ , in.  
 $C_b$  = clear bottom cover to main reinforcement, in.  
 $C_s$  = half clear spacing between bars or splices or half available concrete width per bar or splice resisting splitting in the failure plane, in.  
 $K_{tr}$  = an index of the transverse reinforcement provided along the anchored bar,  $A_{tr} f_{yt} / 500s d_b$   
 $A_{tr}$  = area of transverse reinforcement normal to the plane of splitting through the anchored bars, sq. in.  
 $f_{yt}$  = yield strength of transverse reinforcement, psi  
 $s$  = spacing of transverse reinforcement, center-to-center, in.  
 $\phi$  = reduction factor

The authors recommended that  $C/d_b$  be less than 2.5 and  $l_d$  be at least 12 in.

Cyclic Tests--The recommendations made above were based on monotonic tests of pullout specimens and beams. The effect of cyclic reversed loading has been widely reported to create severe bond conditions leading to bond degradation [52,57,80,85,86,87,88,89]. Hassan and Hawkins [90] reported the results of a test series in which reinforcing bars were loaded cyclically. Figure A.33 shows the testing method which they employed and was taken directly from the reference. The authors concluded from the experimental investigation that:

1. There was progressive bond deterioration in bars subjected to cyclic reversed loadings.
2. Loading history was a significant parameter in bond degradation.



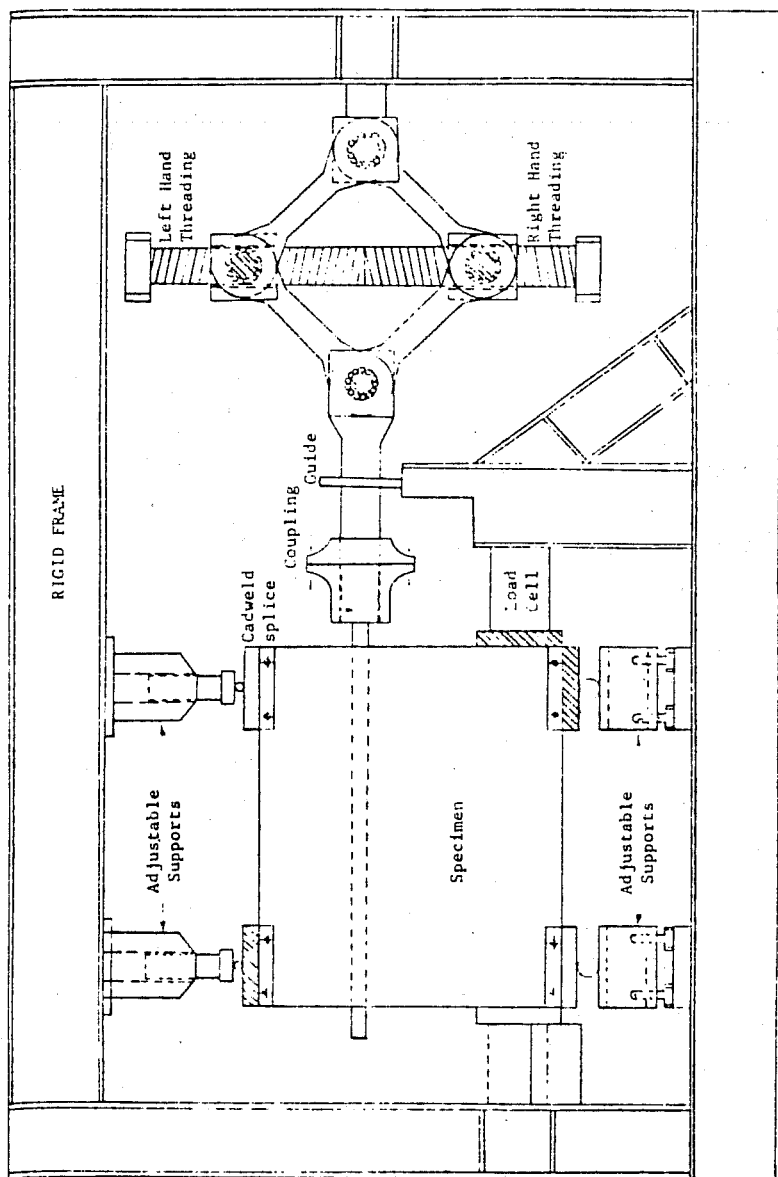


Fig. A.33 Test setup of Hassan and Hawkins [90]

3. Cycles with equal displacements in both directions caused significantly more bond degradation than cycles with larger displacements in one direction than the other.

## A P P E N D I X B

### FLEXURAL CAPACITY COMPUTER PROGRAM

A computer program was developed to analyze the axial load and moment capacities of reinforced concrete sections for any imposed linear strain profile. The neutral axis can be translated and rotated to any given location.

The program divides the section into a number of elements and assumes that the strain at the centroid of the element is uniform over the element. The stress on the element is determined on the basis of user defined stress-strain relationships for both the concrete and reinforcing steel. The force on each element is summed to calculate the axial load. The force times a moment arm for each element is summed to calculate the moment.

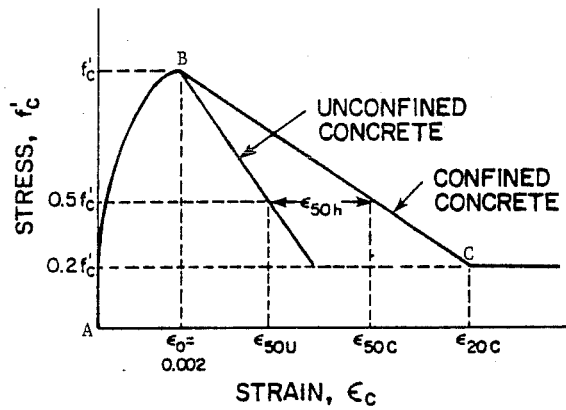
The stress-strain relationship for concrete used by the program is the Kent and Park [77] stress-strain curve for confined concrete. It is shown in Fig. B.1. A bilinear stress-strain curve is used for the reinforcing steel.

The results obtained from the program agree reasonably well with the Portland Cement Association (PCA) design charts [13] for bilaterally loaded columns. An example is given below for a column section identical to an 86 series column with a 120 kip compressive axial load and nominal strengths of 5000 psi for the concrete compressive strength and 60000 psi for the steel yield stress.

PCA : Unilateral M = 1380 kip-in.  
Bilateral (45°) M = 1210 kip-in.

Program : Unilateral M = 1355 kip-in.  
Bilateral (45°) M = 1245 kip-in.

The differences are most likely the result of discretization methods and assumed concrete stress-strain relations.



Region AB

$$f_c = f'_c \left[ \frac{2\epsilon_c}{0.002} - \left( \frac{\epsilon_c}{0.002} \right)^2 \right]$$

Region BC

$$f_c = f'_c [1 - Z(\epsilon_c - 0.002)]$$

$$Z = \frac{0.5}{\epsilon_{50u} + \epsilon_{50h} - 0.002}$$

$$\epsilon_{50u} = \frac{3 + 0.002f'_c}{f'_c - 1000}$$

$$\epsilon_{50h} = 0.75 \rho_s \sqrt{\frac{b''}{s_h}}$$

- $f_c$  - concrete stress, psi       $b''$  - width of confined core  
 (out-to-out of hoops)  
 $\epsilon_c$  - concrete strain, in./in.  
 $f'_c$  - concrete compressive strength, psi  
 $\rho_s$  - ratio of volume of transverse reinforcement to volume  
 of confined core (out-to-out of hoops)  
 $s_h$  - spacing of hoops

Fig. B.1 Kent and Park's concrete stress-strain relation

## A P P E N D I X C

### TRANSVERSE REINFORCEMENT CALCULATIONS

#### C.1 Shear

Section A.5.9 of the 1977 ACI Building Code [17] requires that the web reinforcement be designed to resist the shear produced by moments acting at the ends of the member. The moments are taken to be the ultimate moment capacity of the section. The system described by Section A.5.9 is shown in Fig. C.1. The shear force is

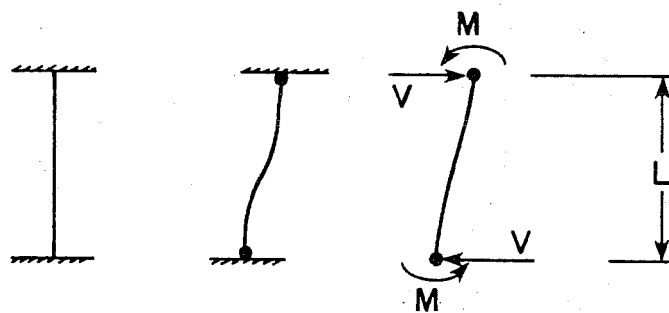
$$V = \frac{2M}{L} \quad (C.1)$$

The column length is taken as the clear height of the test specimen which is 36 in. The test specimen is deflected along its diagonal and the ultimate moment capacity is taken from the bilateral axial load-moment interaction curve (Fig. 2.5). The axial load is 120 kips (compression). The ultimate moment capacity of an 86 series column based on a concrete strength of 5000 psi and a reinforcement yield strength of 60 ksi is 1245 kip-in. The shear force is

$$V = \frac{2(1245 \text{ kip-in.})}{36 \text{ in.}} \quad (C.2)$$

$$V = 69 \text{ kips}$$

The ACI Building Code equation for the transverse reinforcement contribution to shear resistance is based on the truss analogy (described in the review of past research, Appendix A).



$$V = \frac{2M}{L}$$

Fig. C.1 Column hinging mechanism

The equation is

$$V_s = \frac{A_v f_y d}{s} \quad (C.3)$$

- where
- $V_s$  = the shear force carried by the transverse reinforcement, lbs.
  - $A_v$  = area of shear reinforcement within a distance  $s$ , sq. in.
  - $f_y$  = yield strength of transverse reinforcement, psi
  - $d$  = distance from extreme compression fiber to centroid of longitudinal tension reinforcement, in.
  - $s$  = spacing of transverse reinforcement in direction parallel to longitudinal reinforcement, in.

The equation is based on a member whose transverse reinforcement is parallel to the direction of loading as shown in Fig. C.2a. The application of the equation to a section oriented as shown in Fig. C.2b (diagonally loaded) is uncertain and there are no reported shear tests on members loaded diagonally.

Equation C.3 was applied to the diagonally loaded member in the following manner. The location of the neutral axis at ultimate moment conditions (peak compressive strain of 0.003) for the diagonally loaded member was found using the computer program described in Appendix B. The neutral axis location (distance  $c$  in Fig. C.2b) showed that the five shaded bars in Fig. C.2b were in tension. The distance to the centroid of the tension reinforcement for the diagonally loaded column ( $d'$ ) was computed to be 10.96 in. The value of  $d'$  was used in Eq. C.3 in place of the value of  $d$ . Figure C.3 shows an idealized cracked section where the transverse reinforcement has a force of  $T_v$  acting along its axis. The vertical component of the tie force ( $T'_v$ ) is taken as  $T_v/\sqrt{2}$ .  $T_v$  is taken to be the yield force



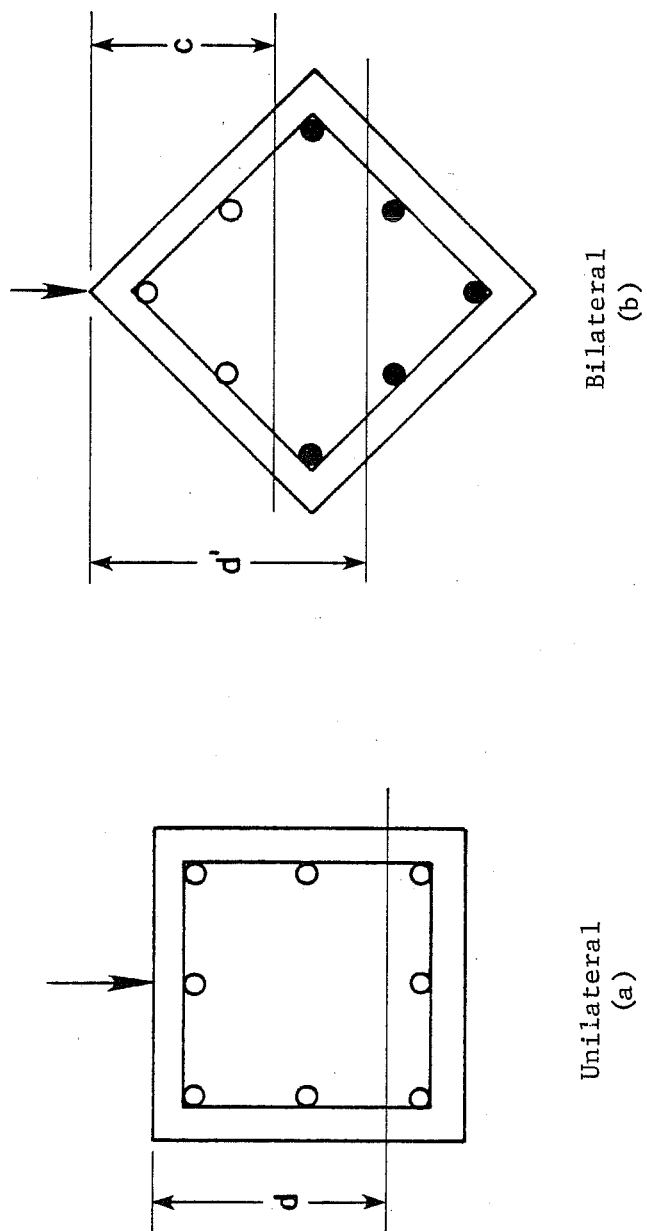


Fig. C.2 Loading Orientations

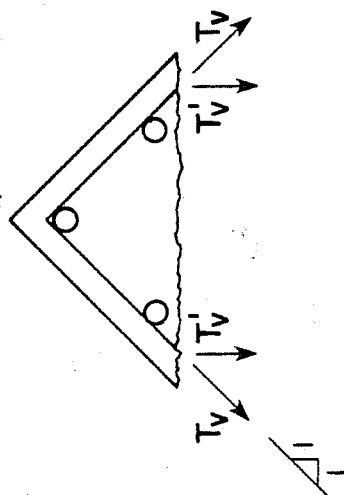


Fig. C.3 Bilateral shear reinforcement action

of the bar

$$T_v = \frac{A_v f_y}{2} \quad (C.4)$$

and so

$$T'_v = \frac{A_v f_y}{2\sqrt{2}} \quad (C.5)$$

where  $A_v$  = area of two legs of a perimeter tie, sq. in.  
 $f_y$  = yield strength of perimeter tie, psi.

The final form of the equation for the transverse reinforcement contribution to the shear resistance of a diagonally loaded column is

$$V'_s = \frac{2T'_v d'}{s} \quad (C.6)$$

$$V'_s = 2 \frac{A_v f_y}{2\sqrt{2}} \frac{d'}{s} \quad (C.7)$$

$$V'_s = \frac{A_v f_y d'}{s\sqrt{2}} \quad (C.8)$$

The shear force to be resisted (Eq. C.2) is 69 kips. The area of the transverse reinforcement is based on two legs of a 6 mm bar and is 0.088 sq. in. The yield strength is assumed to be 60 ksi. The value of  $d'$  is 10.96 in. The required transverse reinforcement spacing to resist 69 kips is computed by rearranging Eq. C.8. The required spacing is

$$s = \frac{(0.088 \text{ sq. in.})(60 \text{ ksi})(10.96 \text{ in.})}{(69 \text{ kips})\sqrt{2}} \quad (C.9)$$

$$s = 0.59 \text{ in.}$$

## C.2 Confinement

Section A.6.5 of the 1977 ACI Building Code [17] requires that if the ratio of applied compressive axial load to the axial load at balanced strain conditions is greater than 0.4 then confinement of the core must be provided. The ratio for the test specimens is 0.46 (120 kips / 260 kips).

The transverse reinforcement required for confinement is given in Sec. A.6.5.3 of the ACI Code.

$$A_{sh} = \frac{l_h \rho_s s_h}{2} \quad (C.10)$$

where  $A_{sh}$  = area of transverse hoop bar  
(one leg), sq. in.

$l_h$  = maximum unsupported length of rectangular hoop  
measured between perpendicular legs of hoop or  
supplementary cross ties, sq. in.

$\rho_s$  = ratio of volume of spiral reinforcement to total  
volume of core (out-to-out of spirals)

$s_h$  = center-to-center spacing of hoops, in.

$\rho_s$  is the volumetric ratio required by Sec. A.6.5.2, which is

$$\rho_s = 0.45 \left( \frac{A_g}{A_c} - 1 \right) \frac{f'_c}{f_y} \quad (C.11)$$

$$\text{or } \rho_s \geq 0.12 f'_c / f_y \quad (C.12)$$

Equation C.11 gives  $\rho_s$

$$\rho_s = 0.45 \left( \frac{12 \text{ in.} (12 \text{ in.})}{10 \text{ in.} (10 \text{ in.})} - 1 \right) \frac{5 \text{ ksi}}{60 \text{ ksi}}$$

$$\rho_s = 0.0165$$

Equation C.12 gives  $\rho_s$

$$\rho_s \geq (0.12) \frac{5 \text{ ksi}}{60 \text{ ksi}}$$

$$\geq 0.0100$$

$$\rho_s = 0.0165$$

Rearranging Equation C.10 gives

$$s_h = \frac{2 A_{sh}}{l_h \rho_s}$$

$$s_h = \frac{2(0.044 \text{ sq. in.})}{(10 \text{ in.})(0.0165)}$$

$$s_h = 0.53 \text{ in.}$$

The tie spacing cannot exceed 0.53 in. in order to meet the requirements of Sec. A.6.5 (confinement) of the ACI Code.

## A P P E N D I X D

### MATERIAL PROPERTIES

#### Concrete

The concrete for each cast was obtained from the same local ready mix plant. To minimize concrete strength variations, two specimens were cast at a time. Three cubic yards of concrete were ordered for each cast. The mix proportions as ordered from the plant were:

Water	250 #/cu. yd.
Cement	517 #/cu. yd.
Fine Aggregate	1500 #/cu. yd.
Coarse Aggregate (max. size 5/8")	1800 #/cu. yd.
Airsene L (water reducer)	25 oz/cu. yd.
5-1/4 sacks of cement per cu. yd.	

A relatively high slump concrete was necessary because of congestion of reinforcement in the form and the need to ensure proper placement of the concrete without excessive vibration. The concrete was purposely ordered with a slump less than the desired 7 in. and water was added on site prior to casting to achieve the required slump.

Six standard 6 in. X 12 in. control cylinders for were cast for each specimen. The cylinders were tested on the day of testing to determine the compressive strength of each specimen. Table D.1 lists the compressive strengths obtained for each specimen. The compressive strengths are averages of at least five cylinder tests.

### Reinforcing Steel

Three sizes of reinforcing steel were used in the fabrication of the column cages: #6 bars, #4 bars, and 6 mm deformed bars. Two different lots of both #6 bars and 6 mm bars were used.

Specimens were taken from bars in each lot and tested to determine yield stress, ultimate stress, and the stress-strain relationships. The #6 and #4 bars were tested using an electronic extensometer which automatically plotted the stress-strain curve on an x-y recorder. Average stress-strain curves for the #6 and #4 bars are shown in Fig. D.1. The stress-strain curves for the 6 mm bars were obtained using the load indicator on the test machine and monitoring a strain gage bonded to the test coupons. The curves for the two lots of 6 mm bars are shown in Fig. D.2. The yield stresses and ultimate stresses are listed in Table D.2. The lot number of the bars used in each specimen is listed in Table D.1.

TABLE D.1 SPECIMEN CONCRETE STRENGTHS

Test Specimen	Date Cast	Date Tested	$f'_c$ * psi	Slump in.	#6 bar lot	6mm bar lot
O-86-14-DM	10/23/78	12/12/78	5950	5	1	1
C-86-14-DM	2/ 8/79	3/30/79	5250	8	2	2
O-86-32-D	12/11/78	3/ 3/79	4550	8	1	1
C-86-32-D	11/27/78	1/11/79	5400	8	1	1
C-86-21-D	1/30/79	3/29/79	5750	7	1	1
C-86-14-D	12/11/78	3/ 7/79	4650	8	1	2
C-86-09-D	1/30/79	3/17/79	5750	7	1	2
C-86-03-D	10/23/78	12/22/78	6100	5	1	1
C-84-32-D	1/18/79	3/ 9/79	4850	7	-	1
C-84-21-D	1/18/79	3/13/79	4850	7	-	1
C-84-14-D	11/27/78	1/27/79	5450	8	-	1
O-86-14-D**	3/31/78	5/ 5/78	5050	8	3	1

\* Average of at least 5 cylinder tests.

\*\* Tested by Maruyama [14].



TABLE D.2 REINFORCEMENT PROPERTIES

Bar	Nominal Bar Area sq in.	Yield Stress ksi	Ultimate Stress ksi
6mm - 1	0.044	73	102
6mm - 2	0.044	74 <sup>*</sup>	131
<del>#4</del>	<del>0.20</del>	<del>70</del>	105
#6 - 1	0.44	70	101
#6 - 2	0.44	66	110
#6 - 3 <sup>**</sup>	0.44	65	109

\* Taken as the proportional limit.

\*\* Used only in specimen 0-86-14-D  
tested by Maruyama [14].

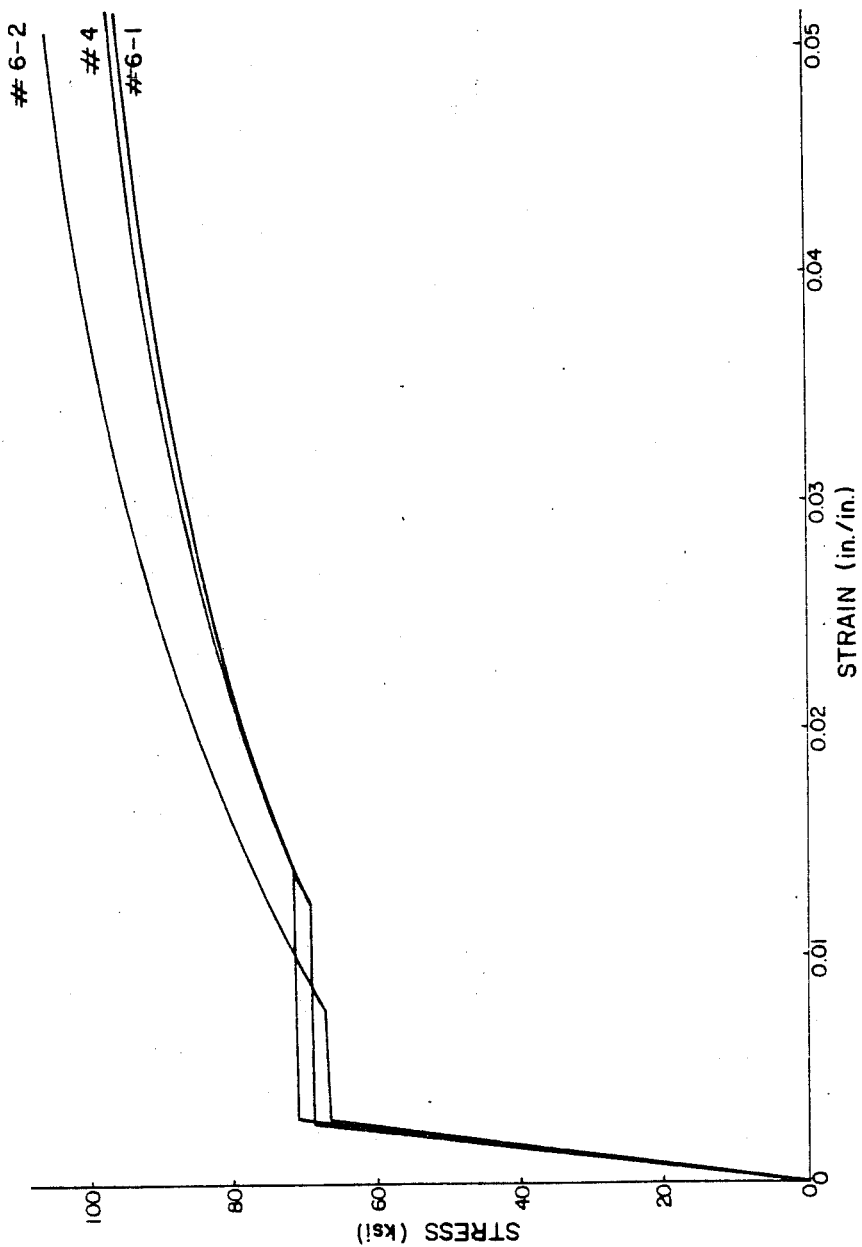


Fig. D.1 Stress-strain curves for #6 and #4 bars

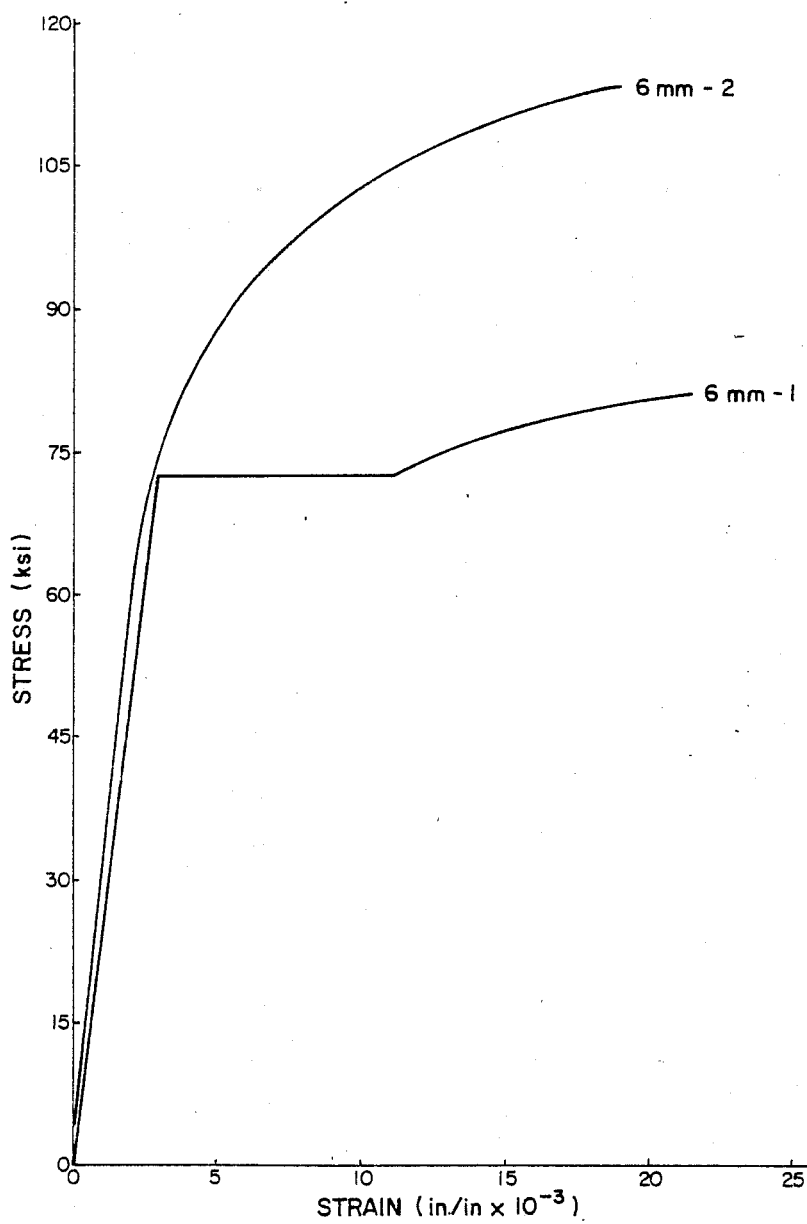


Fig. D.2 Stress-strain curves for  
6 mm bars

## A P P E N D I X E

### GEOMETRY CORRECTION

The deflection measuring devices (potentiometers) monitor the movement of the specimen along the north-south, east-west, and vertical axes of the specimen. The orientation of the potentiometers does not vary during the test. The load cells, however, are attached to the rams so that they measure load along the axes of the rams. During movement of the specimen, the axes of the rams also move. Thus, the load values read from the load cells are not oriented along axes coincident with the axes of deflection measurement. In order to have values of load which act along the axes of deflection measurement, the load cell readings are adjusted to account for the geometry change of the loading system. The method is to simply break the load cell reading into components along the desired axes and then sum the components in each direction to obtain the corrected value of load.

The process is straightforward, but because it must be done three-dimensionally, it is somewhat difficult to visualize. Figure E.1 shows a coordinate system in which the original position of the specimen is shown as point O. A movement of the specimen shifts its position to point O'. The components of deflection are  $\Delta_S$  along the north-south axis,  $\Delta_E$  along the east-west axis, and  $\Delta_V$  along the vertical axis. Figure E.2 shows the components of load for each of the load cells. The values of load as measured by the load cells are denoted by  $N_M$ ,  $H_{SM}$ , and  $H_{EM}$  for the axial load cell, south lateral ram load cell, and east lateral ram load cell, respectively. The components of load for each load cell are

shown as well as the original length of the rams  $L_V$ ,  $L_S$ , and  $L_E$  (axial, south lateral, and east lateral). The resolution of the load cell readings to their components is quite simple and the equations are presented in Fig. E.3. The final step is the algebraic sum of the components with due regard to sign conventions.

The geometry correction was applied to each test and all reported values of load include the correction. An example of the effect the correction had on load-deflection curves is illustrated in Fig. E.4, which is the resultant load versus resultant deflection of a monotonic test with a compressive axial load.

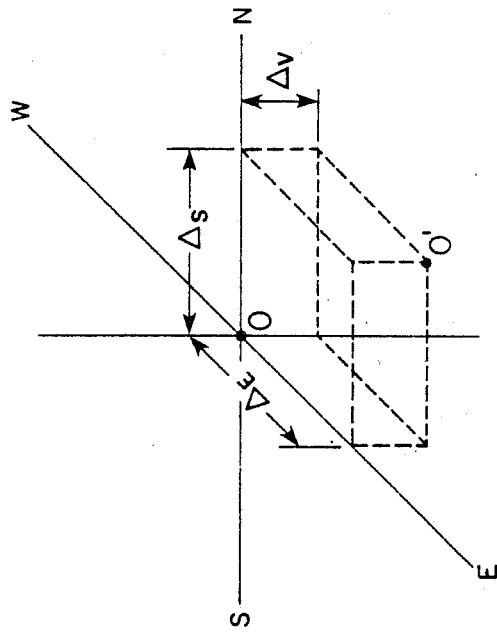
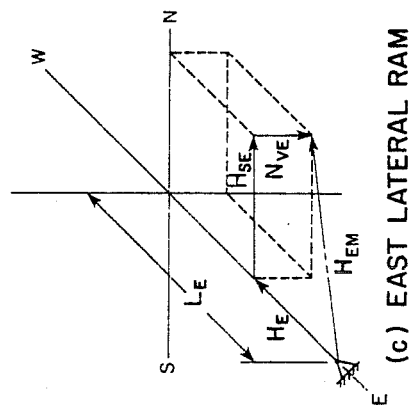
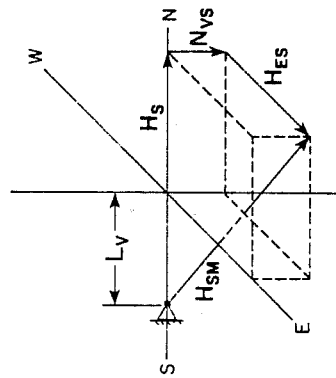


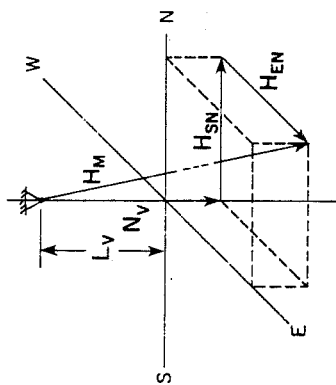
Fig. E.1 Coordinate system



(c) EAST LATERAL RAM



(b) SOUTH LATERAL RAM



(a) AXIAL RAM

Fig. E.2 Load components

AXIAL RAM	SOUTH LATERAL RAM	EAST LATERAL RAM
$N_V = \frac{N_M (L_V + \Delta_V)}{\sqrt{(L_V + \Delta_V)^2 + \Delta_E^2 + \Delta_S^2}}$	$N_{VS} = \frac{H_{SM} \Delta_V}{\sqrt{(L_S + \Delta_S)^2 + \Delta_V^2 + \Delta_E^2}}$	$N_{VE} = \frac{H_{EM} \Delta_V}{\sqrt{(L_E + \Delta_E)^2 + \Delta_V^2 + \Delta_S^2}}$
$H_{EN} = \frac{N_M \Delta_E}{\sqrt{(L_V + \Delta_V)^2 + \Delta_E^2 + \Delta_S^2}}$	$H_{ES} = \frac{H_{SM} \Delta_E}{\sqrt{(L_S + \Delta_S)^2 + \Delta_V^2 + \Delta_E^2}}$	$H_E = \frac{H_{EM} (L_E + \Delta_E)}{\sqrt{(L_E + \Delta_E)^2 + \Delta_V^2 + \Delta_S^2}}$
$H_{SN} = \frac{N_M \Delta_S}{\sqrt{(L_V + \Delta_V)^2 + \Delta_E^2 + \Delta_S^2}}$	$H_S = \frac{H_{SM} (L_S + \Delta_S)}{\sqrt{(L_S + \Delta_S)^2 + \Delta_V^2 + \Delta_E^2}}$	$H_{SE} = \frac{H_{EM} \Delta_S}{\sqrt{(L_E + \Delta_E)^2 + \Delta_V^2 + \Delta_S^2}}$

Fig. E.3 Equations for load components



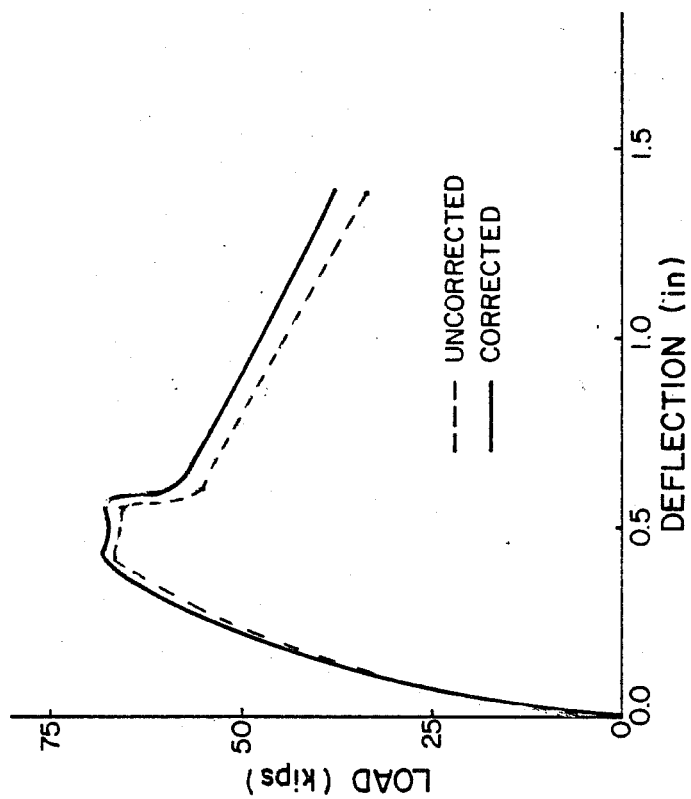


Fig. E.4 Effect of geometry correction

## REFERENCES

1. Pecknold, D., and Sozen, M., "Calculated Inelastic Structural Response to Uniaxial and Biaxial Earthquake Motions," Fifth World Conference on Earthquake Engineering, Preprint Paper 223, Session 5B: Response of Structures to Ground Shaking, Rome, 1973.
2. Pecknold, D., and Suharwardy, M., "Effects of Two-Dimensional Earthquake Motion on Response of R/C Columns," Earthquake-Resistant Reinforced Concrete Building Construction, Proceedings of a Workshop Held at The University of California, Berkeley, California, July 1977, Volume II, Technical Papers, University of California, University Extension, Berkeley, California, June 1978, pp. 950-959.
3. Selna, L., and Lawder, J., "Biaxial Inelastic Frame Seismic Behavior," Reinforced Concrete Structures in Seismic Zones, American Concrete Institute, SP-53, Detroit, 1973, pp. 439-462.
4. Brown, R., and Jirsa, J., "Reinforced Concrete Beams under Load Reversals," Journal of the American Concrete Institute, Proc. V. 68, No. 5, May 1971, pp. 380-390.
5. Bertero, V., Popov, E., and Wang, T., "Hysteretic Behavior of Reinforced Concrete Flexural Members with Special Web Reinforcement," Report No. EERC 74-9, University of California, Berkeley, California, August 1974.
6. Ma, S., Bertero, V., and Popov, E., "Experimental and Analytical Studies on the Hysteretic Behavior of Reinforced Concrete Rectangular and T-Beams," Report No. EERC 76-2, University of California, Berkeley, California, May 1976.
7. Takeda, T., Sozen, M., and Nielsen, N., "Reinforced Concrete Response to Simulated Earthquakes," Journal of the Structural Division, ASCE, Vol. 96, No. ST12, December 1970, pp. 2557-2564.
8. Paulay, T., "Simulated Seismic Loading of Spandrel Beams," Journal of the Structural Division, ASCE, Vol. 97, No. ST3, March 1971, pp. 2407-2422.

9. Barney, G., et al., "Earthquake Resistant Structural Walls-- Tests of Coupling Beams," Report to National Science Foundation, Portland Cement Association, Construction Technology Laboratories, Skokie, Illinois, January 1978.
10. Aoyama, H., et al., "A Study on the Cause of Damage to the Hachinohe Technical College due to 1968 Tokachi-Oki Earthquake (Part 1)," Proceedings of the U.S.-Japan Seminar on Earthquake Engineering with Emphasis on the Safety of School Buildings, Sendai, Japan, September 1970, The Japan Earthquake Engineering Promotion Society, Tokyo, Japan, 1971, pp. 199-212.
11. Wright, R., and Kramer, S., "Building Performance in the 1972 Managua Earthquake," Center for Building Technology, Institute for Applied Technology, National Bureau of Standards, Washington, D.C., November 1973.
12. Okada, T., et al., "Analysis of the Hachinohe Library Damaged by '68 Tokachi-Oki Earthquake," Proceedings of the U.S.-Japan Seminar on Earthquake Engineering with Emphasis on the Safety of School Buildings, Sendai, Japan, September 1970, The Japan Earthquake Engineering Promotion Society, Tokyo, Japan, 1971, pp. 172-189.
13. "Biaxial and Uniaxial Capacity of Rectangular Columns," Advanced Engineering Bulletin, No. 20, Portland Cement Association, Skokie, Illinois, 1967.
14. Maruyama, K., "Behavior of Reinforced Concrete Short Columns under Bidirectional Lateral Loadings," unpublished Ph.D. dissertation, The University of Texas at Austin, Texas, 1979.
15. Ramirez, H., "Effect of Axial Loads on the Behavior of Reinforced Concrete Short Columns under Cyclic Lateral Deformations," unpublished Ph.D. dissertation, The University of Texas at Austin, Texas, 1979.
16. ACI Committee 318, Building Code Requirements for Reinforced Concrete (ACI318-71), American Concrete Institute, Detroit, 1971.
17. ACI Committee 318, Building Code Requirements for Reinforced Concrete (ACI318-77), American Concrete Institute, Detroit, 1977.
18. Uniform Building Code, International Conference of Building Officials, 1976 Edition, Whittier, California, 1976.

29. Viest, I., and Morrow, J., "Shear Strength of Reinforced Concrete Frame Members without Web Reinforcement," Journal of the American Concrete Institute, Proc. V. 53, No. 9, March 1957, pp. 833-869.
30. Taub, J., and Neville, A., "Resistance to Shear of Reinforced Concrete Beams. Part 1 - Beams without Web Reinforcement," Journal of the American Concrete Institute, Proc. V. 57, No. 2, August 1960, pp. 193-220.
31. Taub, J., and Neville, A., "Resistance to Shear of Reinforced Concrete Beams. Part 2 - Beams with Vertical Stirrups," Journal of the American Concrete Institute, Proc. V. 57, No. 3, September 1960, pp. 315-336.
32. Neville, A., and Taub, J., "Resistance to Shear of Reinforced Concrete Beams. Part 3 - Beams with Bent-up Bars," Journal of the American Concrete Institute, Proc. V. 57, No. 4, October 1960, pp. 443-463.
33. Neville, A., and Taub, J., "Resistance to Shear of Reinforced Concrete Beams. Part 4 - Behavior of Beams with Different Types of Web Reinforcement," Journal of the American Concrete Institute, Proc. V. 57, No. 5, November 1960, pp. 517-532.
34. Taub, J., and Neville, A., "Resistance to Shear of Reinforced Concrete Beams. Part 5 - Anchorage and Bond," Journal of the American Concrete Institute, Proc. V. 57, No. 6, Part One, December 1960, pp. 715-730.
35. Taylor, R., "Some Shear Tests on Reinforced Concrete Beams without Shear Reinforcement," Magazine of Concrete Research, Vol. 12, No. 36, November 1960, pp. 145-154.
36. ACI-ASCE Committee 326, "Shear and Diagonal Tension," Journal of the American Concrete Institute, Proc. V. 59, No. 1, January 1962, pp. 1-30; Vol. 59, No. 2, February 1962, pp. 277-333; Vol. 59, No. 3, March 1962, pp. 353-396.
37. ACI Committee 318, Building Code Requirements for Reinforced Concrete (ACI 318-63), American Concrete Institute, Detroit, 1963.
38. Moe, J., Discussion of a paper by ACI-ASCE Committee 326, "Shear and Diagonal Tension," Journal of the American Concrete Institute, Proc. V. 59, No. 9, September 1962, pp. 1341-1347.

19. Hognestad, E., "What Do We Know About Diagonal Tension and Web Reinforcement in Concrete? A Historical Study," University of Illinois Bulletin, Vol. 49, No. 50, University of Illinois, Urbana, Illinois, March 1952.
20. Talbot, A., "Tests of Reinforced Concrete Beams, Series of 1906," University of Illinois Engineering Experiment Station Bulletin, Vol. IV, No. 30, August 1907.
21. Laupa, A., "The Shear Strength of Reinforced Concrete Beams," Report No. CESRS 62, University of Illinois, Urbana, Illinois, September 1953.
22. Feldman, A., and Siess, C., "Effect of Moment-Shear Ratio on Diagonal Tension Cracking and Strength in Shear of Reinforced Concrete Beams," Report No. CESRS 107, University of Illinois, Urbana, Illinois, June 1955.
23. Baron, M., and Siess, C., "Effect of Axial Load on the Shear Strength of Reinforced Concrete Beams," Report No. CESRS 121, University of Illinois, Urbana, Illinois, June 1956.
24. Moody, K., Viest, I., Elstner, R., and Hognestad, E., "Shear Strength of Reinforced Concrete Beams. Part 1 - Tests of Simple Beams," Journal of the American Concrete Institute, Proc. V. 51, No. 4, Part One, December 1954, pp. 317-332.
25. Moody, K., Viest, I., Elstner, R., and Hognestad, E., "Shear Strength of Reinforced Concrete Beams. Part 2 - Tests of Restrained Beams without Web Reinforcement," Journal of the American Concrete Institute, Proc. V. 51, No. 5, January 1955, pp. 417-436.
26. Elstner, R., Moody, K., Viest, I., and Hognestad, E., "Shear Strength of Reinforced Concrete Beams. Part 3 - Tests of Restrained Beams with Web Reinforcement," Journal of the American Concrete Institute, Proc. V. 51, No. 6, February 1955.
27. Moody, K., and Viest, I., "Shear Strength of Reinforced Concrete Beams. Part 4 - Analytical Studies," Journal of the American Concrete Institute, Proc. V. 51, No. 7, March 1955, pp. 697-730.
28. Ferguson, P., "Some Implications of Recent Diagonal Tension Tests," Journal of the American Concrete Institute, Proc. V. 53, No. 2, August 1956, pp. 157-172.

39. Bresler, B., and Scordelis, A., "Shear Strength of Reinforced Concrete Beams," Journal of the American Concrete Institute, Proc. V. 60, No. 1, January 1963, pp. 51-72.
40. Fenwick, R., and Paulay, T., "Mechanisms of Shear Resistance of Concrete Beams," Journal of the Structural Division, ASCE, Vol. 94, No. ST10, October 1968, pp. 2325-2350.
41. Haddadin, M., et al., "Stirrup Effectiveness in Reinforced Concrete Beams with Axial Force," Journal of the Structural Division, ASCE, Vol. 97, No. ST9, September 1971, pp. 2277-2297.
42. Zsutty, T., "Beam Shear Strength Prediction by Analysis of Existing Data," Journal of the American Concrete Institute, Proc. V. 65, No. 11, November 1968, pp. 943-951.
43. Zsutty, T., "Shear Strength Prediction for Separate Categories of Simple Beam Tests," Journal of the American Concrete Institute, Proc. V. 68, No. 2, February 1971, pp. 138-143.
44. Nielsen, Braestrup, Jensen, and Bach, Concrete Plasticity, Beam Shear - Shear in Joints - Punching Shear, Special Publication, Danish Society for Structural Science and Engineering, Copenhagen, Denmark, October 1978.
45. Thürlimann, B., "Shear Strength of Reinforced and Prestressed Concrete Beams--CEB Approach," Concrete Design: U.S. and European Practices, American Concrete Institute, SP-59, Detroit, 1979, pp. 93-116.
46. Rabbat, B., "A Variable Angle Space Truss Model for Structural Concrete Beams," Doctoral thesis, Department of Civil Engineering, University of Toronto, 1975.
47. Bresler, B., and MacGregor, J., "Review of Concrete Beams Failing in Shear," Journal of the Structural Division, ASCE, Vol. 91, No. ST5, October 1965, Part 1, pp. 19-42.
48. MacGregor, J., and Hanson, J., "Proposed Changes in Shear Provisions for Reinforced and Prestressed Concrete Beams," Journal of the American Concrete Institute, Proc. V. 66, No. 4, April 1969, pp. 276-288.

49. ACI-ASCE Committee 426, "The Shear Strength of Reinforced Concrete Members," Journal of the Structural Division, ASCE, Vol. 99, No. ST6, June 1973, pp. 1091-1187; Vol. 100, No. ST8, August 1974, pp. 1543-1591.
50. Wight, J., and Sozen, M., "Strength Decay of RC Columns under Shear Reversals," Journal of the Structural Division, ASCE, Vol. 101, No. ST5, May 1975, pp. 1053-1065.
51. Bertero, V., and Popov, E., "Hysteretic Behavior of Ductile Moment-Resisting Reinforced Concrete Frame Components," Report No. EERC 75-16, University of California, Berkeley, California, April 1975.
52. Ohno, K., Shibata, T., and Hattori, T., "An Experimental Study on the Failure of Columns," Proceedings of the U.S.-Japan Seminar on Earthquake Engineering with Emphasis on the Safety of School Buildings, Sendai, Japan, September 1970, The Japan Earthquake Engineering Promotion Society, Tokyo, Japan, 1971, pp. 145-151.
53. Higashi, Y., and Ohkubo, M., "Static and Dynamic Loading Tests of Reinforced Concrete Frames with Thin Spandrel or Wing Walls," Proceedings of the U.S.-Japan Seminar on Earthquake Engineering with Emphasis on the Safety of School Buildings, Sendai, Japan, September 1970, The Japan Earthquake Engineering Promotion Society, Tokyo, Japan, 1971, pp. 225-231.
54. Kokusho, S., and Ogura, K., "Shear Strength and Load Deflection Characteristics of Reinforced Concrete Members," Proceedings of the U.S.-Japan Seminar on Earthquake Engineering with Emphasis on the Safety of School Buildings, Sendai, Japan, September 1970, The Japan Earthquake Engineering Promotion Society, Tokyo, Japan, 1971, pp. 364-381.
55. Minami, K., and Wakabayashi, M., "Seismic Resistance of Reinforced Concrete Beam-and-Column Assemblages with Emphasis on Shear Failure of Column," Preprints, Sixth World Conference on Earthquake Engineering, Vol. 11, New Delhi, India, 1977, pp. 11-111 - 11-116.
56. Yamada, M., "Shear Strength, Deformation and Explosion of Reinforced Concrete Short Columns," Shear in Reinforced Concrete, American Concrete Institute, SP-42, Detroit, 1974, pp. 617-638.

57. Hirosawa, M., Ozaki, M., and Wakabayashi, M., "Experimental Study on Large Models of Reinforced Concrete Columns," Fifth World Conference on Earthquake Engineering, Preprint Paper 96, Session 2D: Dynamic Behavior of Structural Elements, Rome, 1973.
58. The Establishment of Detailing Practice for Current Building Design in Japan - Papers about the Ductility of Reinforced Concrete Columns under Large Deflections (In Japanese), The Architectural Institute of Japan, March 1974.
59. Umemura, H., Aoyama, H., and Noguchi, H., "Experimental Studies on Reinforced Concrete Members and Composite Steel and Reinforced Concrete Members" (In Japanese), Vol. 2, Department of Architecture, The University of Tokyo, December 1977.
60. A List of Experimental Results on Deformation Ability of Reinforced Concrete Columns under Large Deflections (No. 3) (In Japanese), Building Research Institute, Ministry of Construction, Japan, February 1978.
61. Birkeland, P., and Birkeland, H., "Connections in Precast Concrete Construction," Journal of the American Concrete Institute, Proc. V. 63, No. 3, March 1966, pp. 345-368.
62. Hofbeck, J., Ibrahim, I., and Mattock, A., "Shear Transfer in Reinforced Concrete," Journal of the American Concrete Institute, Proc. V. 66, No. 2, February 1969, pp. 119-128.
63. Mattock, A., and Hawkins, N., "Shear Transfer in Reinforced Concrete," Journal of the Prestressed Concrete Institute, Vol. 17, No. 2, March/April 1972, pp. 55-76.
64. Laible, J., White, R., and Gergely, P., "Experimental Investigation of Seismic Shear Transfer Across Cracks in Concrete Nuclear Containment Vessels," Reinforced Concrete Structures in Seismic Zones, American Concrete Institute, SP-53, Detroit, 1977, pp. 203-226.
65. Park, R., and Paulay, T., Reinforced Concrete Structures, John Wiley and Sons, New York, 1975.
66. Penzien, J., Bertero, V., and Atalay, B., "Inelastic Cyclic Behavior of Reinforced Concrete Flexural Members," Proceedings of the Review Meeting, U.S.-Japan Cooperative Research Program in Earthquake Engineering with Emphasis on the Safety of School Buildings, August 1975, Honolulu, Hawaii, The Japan Earthquake Engineering Promotion Society, Tokyo, Japan, 1976, pp. 52-74.



67. Atalay, B., and Penzien, J., "Inelastic Cyclic Behavior of Reinforced Concrete Flexural Members," Preprints, Sixth World Conference on Earthquake Engineering, Vol. 11, New Delhi, India, 1977, pp. 11-61 - 11-66.
68. Otani, S., Cheung, V., and Lai, S., "Behavior and Analytical Models of Reinforced Concrete Columns under Biaxial Earthquake Loads," Preprint, Canadian National Conference on Earthquake Engineering, Montreal, Canada, June 1979.
69. Sheikh, S., "Effectiveness of Rectangular Ties as Confinement Steel in Reinforced Concrete Columns," Doctoral thesis, Department of Civil Engineering, University of Toronto, June 1978.
70. Chan, W., "The Ultimate Strength and Deformation of Plastic Hinges in Reinforced Concrete Frameworks," Magazine of Concrete Research, Vol. 7, No. 21, November 1955, pp. 121-132.
71. Pfister, J., "Influence of Ties on the Behavior of Reinforced Concrete Columns," Journal of the American Concrete Institute, Proc. V. 61, No. 5, May 1964, pp. 521-537.
72. Base, G., and Read, J., "Effectiveness of Helical Binding in the Compression Zone of Concrete Beams," Journal of the American Concrete Institute, Proc. V. 62, No. 7, July 1965, pp. 763-781.
73. Corley, W., "Rotational Capacity of Reinforced Concrete Beams," Journal of the Structural Division, ASCE, Vol. 92, No. ST5, October 1966, pp. 121-146.
74. Soliman, M., and Yu, C., "The Flexural Stress-Strain Relationship of Concrete Confined by Rectangular Transverse Reinforcement," Magazine of Concrete Research, Vol. 19, No. 61, December 1967, pp. 223-238.
75. Somes, N., "Compression Tests on Hoop-Reinforced Concrete," Journal of the Structural Division, ASCE, Vol. 96, No. ST7, July 1970, pp. 1495-1509.
76. Shah, S., and Rangan, B., "Effects of Reinforcements on Ductility of Concrete," Journal of the Structural Division, ASCE, Vol. 96, No. ST6, June 1970, pp. 1167-1184.
77. Kent, D., and Park, R., "Flexural Members with Confined Concrete," Journal of the Structural Division, ASCE, Vol. 97, No. ST7, July 1971, pp. 1969-1990.

78. Ruiz, W., and Winter, G., "Reinforced Concrete Beams under Repeated Loads," Journal of the Structural Division, ASCE, Vol. 95, No. ST6, June 1969, pp. 1189-1211.
79. Brown, R., "Reinforced Concrete Cantilever Beams under Slow Cyclic Loadings," Ph.D. dissertation, Rice University, Houston, Texas, April 1970.
80. Bertero, V., and Collins, R., "Investigation of the Failures of the Olive View Stairtowers during the San Fernando Earthquake and Their Implications on Seismic Design," Report No. EERC 73-26, University of California, Berkeley, California, December 1973.
81. Lutz, L., "The Mechanics of Bond and Slip of Deformed Reinforcing Bars in Concrete," Report No. 324, Cornell University, Ithaca, New York, August 1966.
82. ACI Committee 408, "Bond Stress--The State-of-the-Art," Journal of the American Concrete Institute, Proc. V. 63, No. 11, November 1966, pp. 1161-1190.
83. Orangun, C., Jirsa, J., and Breen, J., "The Strength of Anchored Bars: A Reevaluation of Test Data on Development Length and Splices," Center for Highway Research, Report No. 154-3F, The University of Texas at Austin, January 1975.
84. ACI Committee 408, "Suggested Development, Splice, and Standard Hook Provisions for Deformed Bars in Tension," Concrete International, Design and Construction, Vol. 1, No. 7, July 1979, pp. 44-46.
85. Zagajeski, S., Bertero, V., and Bouwkamp, J., "Hysteretic Behavior of Reinforced Concrete Columns Subjected to High Axial and Cyclic Shear Forces," Report No. UCB/EERC - 78/05, University of California, Berkeley, California, April 1978.
86. Gosain, N., and Jirsa, J., "Bond Deterioration in Reinforced Concrete Members under Cyclic Loads," Preprints, Sixth World Conference on Earthquake Engineering, Vol. 11, New Delhi, India, 1977, pp. 11-61 - 11-66.
87. Higashi, Y., Ohkubo, M., and Ohtsuka, M., "Influences of Loading Excursions on Restoring Force Characteristics and Failure Modes of Reinforced Concrete Columns," Preprints, Sixth World Conference on Earthquake Engineering, Vol. 11, New Delhi, India, 1977, pp. 11-135 - 11-140.

88. Hayashi, S., Kokusho, S., Teramoto, E., and Osanai, T., "Study of the Bending Behavior of Reinforced Concrete Columns under Changing Axial Force," AICAP-CEB Symposium, Structural Concrete under Seismic Actions, Vol. II, Rome, 1979, pp. 37-44.
89. Umemura, H., Hirosawa, M., and Endo, T., "Experimental Research on Ductility of Reinforced Concrete Columns," U.S.-Japan Seminar on Earthquake Engineering with Emphasis on Safety of Reinforced Concrete Structures, Berkeley, California, September 1973.
90. Hassan, F., and Hawkins, N., "Analysis of Reinforcing Bars for Seismic Forces," Reinforced Concrete Structures in Seismic Zones, American Concrete Institute, SP-53, Detroit, 1977, pp. 387-416.
91. Taraboulsi, M., "A Comparative Study between a Tied and a Spiral Column under Bidirectional Lateral Loading," unpublished Master's report, The University of Texas at Austin, May 1979.
92. Jirsa, J., Maruyama, K., and Ramirez, H., "Development of Loading System and Initial Tests--Short Columns under Bidirectional Loading," CESRL Report No. 78-2, The University of Texas at Austin, September 1978.
93. Maruyama, K., and Jirsa, J., "Shear Behavior of Reinforced Concrete Members under Bidirectional Reversed Lateral Loading," CESRL Report No. 79-1, The University of Texas at Austin, August 1979.
94. Woodward, K., and Jirsa, J., "Design and Construction of a Floor-Wall Reaction System," CESRL Report No. 77-4, The University of Texas at Austin, December 1977.
95. Longwell, J., Unfinished Master's thesis, The University of Texas at Austin, 1979.
96. Arakawa, S., and Takeda, H., "Shear Reinforcement in Reinforced Concrete Structures, The Effect of Shear Reinforcement on Columns and Beams," (In Japanese), Journal of the Japanese Concrete Institute, Vol. 17, No. 6, June 1979.

97. Sozen, M., et al., "Engineering Report on the Caracas Earthquake of 29 July 1967," Prepared for the Committee on Earthquake Engineering Research, Division of Engineering-National Research Council, National Academy of Engineering, Washington, D.C., 1968.

## VITA

Kyle Andrew Woodward was born in Athens, Texas, on September 4, 1954, the son of Mary Rusk Woodward and Andrew Lee Woodward. He entered The University of Texas at Austin in 1972 and received the degree of Bachelor of Science in Civil Engineering in May 1976. While earning the degree he worked as an Engineering Cooperative Student for Houston Lighting and Power in Houston, Texas. In June of 1976, he entered the Graduate School of The University of Texas at Austin. He was awarded the degree of Master of Science in December 1977 with a major in Civil Engineering. During and since his study for the Master of Science degree he has been employed as a Research Assistant in the Department of Civil Engineering at The University of Texas at Austin.

Permanent address: 333 Mulberry  
Uvalde, Texas 78801

This dissertation was typed by Maxine DeButts.

